

*Neuronal control of sleep in
Caenorhabditis elegans*

Dissertation

for the award of the degree

“Doctor rerum naturalium”

(Dr. rer. nat.)

of the Georg-August-Universität Göttingen

within the doctoral program *Systems Neuroscience*
of the Georg-August University School of Science (GAUSS)

submitted by

Inka Busack

from Berlin

Göttingen 2020

Thesis Committee Members

Prof. Dr. Henrik Bringmann

(1st Reviewer)

Department of Animal Physiology/

Neurophysiology

Philipps-Universität Marburg

Prof. Dr. Tim Gollisch

(2nd Reviewer)

Department of Ophthalmology

University Medical Center Göttingen

Prof. Dr. Ralf Heinrich

Department of Cellular Neurobiology

Georg-August-Universität Göttingen

Examination Board Members

Prof. Dr. Nils Brose

Department of Molecular Neurobiology

MPI for Experimental Medicine, Göttingen

Prof. Dr. Martin Göpfert

Department of Cellular Neurobiology

Georg-August-Universität Göttingen

MD/PhD Arezoo Pooresmaeili

Research Group Perception and Cognition

European Neuroscience Institute,

Göttingen

Date of oral examination: 27.10.2020

Affidavit

I herewith declare that this thesis titled *Neuronal control of sleep in Caenorhabditis elegans* was produced entirely by myself and that I have only used sources and materials cited. The thesis has not been submitted to any other examination board for any other academic award.

Inka Busack

Abstract

Sleep is crucial for all organisms with a nervous system. Amongst other functions, it is required for energy allocation, higher brain functions and the control of physiological processes. Sleep-active neurons have previously been identified in many species. These neurons act as the motor of sleep as their depolarization causes inhibition of wakefulness circuits and leads to sleep induction. However, how these sleep-active neurons get regulated and how exactly they are involved in molecular pathways for the benefits of sleep remains unclear. In this study I focused on the neuronal component of sleep regulation in the model organism *Caenorhabditis elegans*. In *C. elegans* the ring interneuron RIS functions as single sleep active neuron.

First, I aimed to identify a neuronal circuit that regulates RIS activity. I found that RIS is controlled by the command interneuron PVC through a positive feedback loop. The interneurons PVC and RIM act together to activate RIS and sleep is most likely induced at the transition from forward to reverse locomotion. While RIS activity and hence sleep gets regulated by the nervous system, I could also show through pan-neuronal imaging that the control is reciprocal and RIS depolarization directly inhibits nervous system activity.

Next, I intended to design a stand-alone device for optogenetic long-term experiments: the OptoGenBox. Optogenetics is a method in which through genetically knocked-in actuators and light, for instance, individual neurons can get de- or hyperpolarized. Implementation of the OptoGenBox was successful and I could show that long-term optogenetic sleep inhibition by hyperpolarization of RIS leads to a reduced longevity of arrested first larval stage worms.

Lastly, I investigated the functions of sleep in *C. elegans*. Selected health span assays and investigation of synaptic changes did not reveal further functions of sleep. To better assess sleep benefits, strains, in which RIS was either constantly de- or hyperpolarized through genetically knocked-in ion channels, were generated and characterized. Constant de- as well as hyperpolarization of RIS led to a reduction in sleep but diverging longevity effects in the arrested first larval stage.

In conclusion, sleep in *C. elegans* is highly controlled by the nervous system and sleep induction is not only dependent on sleep-active neurons but furthermore wake-active circuits that activate sleep neurons. As sleep is evolutionary conserved, these circuits are most likely also existent in organisms with more complex nervous systems such as mammals. The OptoGenBox as well as the here presented new RIS manipulated worm strains present potent tools to further investigate neuronal circuits and protective pathways downstream of the sleep neuron RIS.

Contents

Affidavit	i
Abstract	iii
Contents	v
Acknowledgements	ix
Table of Figures	xi
Abbreviations	xiii
1. Introduction	1
1.1. Importance of sleep	1
1.2. Characteristics of sleep	1
1.3. Regulation of sleep	3
1.4. <i>Caenorhabditis elegans</i> as a model organism	7
1.5. Sleep in <i>Caenorhabditis elegans</i>	9
1.5.1. Sleep in lethargus	9
1.5.2. Starvation-induced sleep in L1 arrested animals.....	10
1.6. RIS - the motor of sleep in <i>Caenorhabditis elegans</i>	10
1.7. Optogenetics	12
2. Thesis Aims	13
3. Methods	15
3.1. <i>Caenorhabditis elegans</i> maintenance	15
3.2. New strain generation	18
3.2.1. Cloning	18
3.2.2. Microparticle Bombardment	18
3.2.3. Crosses.....	18
3.3. Imaging	20
3.3.1. Cameras and Software	20
3.3.2. Imaging in agarose microchambers	20
3.3.3. Differential Interference Contrast (DIC) and bright field imaging	20
3.3.4. Calcium imaging	21
3.3.5. L1 arrest imaging.....	21
3.3.6. Pre- and post-synaptic marker imaging	21
3.3.7. mKate expression imaging	22

3.3.8. Optogenetic experiments	22
3.4. Imaging Analysis	23
3.4.1. Analysis of calcium imaging data	23
3.4.2. Normalization of calcium imaging data	24
3.4.3. Analysis of DIC images.....	24
3.4.4. Sleep bout analysis	25
3.4.5. Sleep bout alignment	25
3.4.6. Forward and reverse locomotion data	25
3.4.7. RIM peak detection	25
3.5. Behavioral assays.....	26
3.5.1 Cold stress assay	26
3.5.2 Habituation assay.....	26
3.5.3. Pumping assay	26
3.5.4. Lifespan and recovery assays	27
3.5.4.1. Lifespans in the OptoGenBox	27
3.5.4.2. Lifespan of L1 arrested worms in M9 buffer	27
3.5.4.3. Recovery of L1 arrested worms in M9 buffer	27
3.5.5. Inhibition of AVA	28
3.6. Statistics.....	28
4. Results.....	29
4.1. Aim 1 - How the nervous system regulates sleep in <i>C. elegans</i>.....	29
4.1.1. Publication I.....	29
4.1.2. Command interneurons regulate the sleep neuron RIS	98
4.1.2.1. Locomotion regulating command interneurons additionally regulate starvation induced sleep.....	98
4.1.2.2. Loss of function of AMPA and NMDA type glutamate receptors does not cause a sleep phenotype.....	100
4.1.2.3. Sleep affects forward and reverse locomotion equally.....	102
4.1.2.4. Disturbance of the command interneuron circuit can cause ectopic sleep bouts outside of lethargus	102
4.1.2.5. AVB activates in lethargus during motion bouts, prior to sleep bouts	104
4.1.3. How sleep dampens the nervous system in <i>C. elegans</i>	105
4.1.4. Optogenetic manipulation of the sleep neuron RIS directly influences the overall nervous system activity	107
4.2. Aim 2 - Implementation of the OptoGenBox: a device to conduct optogenetic long-term experiments in <i>C. elegans</i>	109
4.2.1. Publication II	109
4.3. Aim 3 - Functions of sleep in <i>Caenorhabditis elegans</i>.....	144
4.3.1. No found evidence for synaptic homeostasis to be a function of sleep in <i>C. elegans</i>	144

4.3.2. Early adult stage worms can form a memory during a habituation assay for at least 15min, which is independent of sleep	147
4.3.3 Feeding behavior and recovery from coldness as read outs for health span are not affected by sleeplessness	150
4.3.4. Genetic manipulations of RIS	151
4.3.4.1. Expression of ion channels in RIS and their consequences on the neuronal potential	151
4.3.4.2. Constant de- and hyperpolarization of a sleep neuron both lead to a reduced amount of sleep	157
4.3.4.3. Changing the potential of RIS impacts survival of arrested first larval stage worms	160
4.3.4.4. Activity of the nervous system is wake-like in constantly RIS activated worms	161
4.3.4.5. RIM peaks wild-type-like in constantly RIS depolarized worms.....	164
5. Discussion and Outlook.....	168
5.1. Command interneurons regulate RIS activity and homeostasis	168
5.2. The OptoGenBox	170
5.3. No found evidence for the synaptic homeostasis hypothesis or sleep improving health in arrested first larval stage <i>C. elegans</i>	171
5.4. Ion channels expressed in RIS allow for behavioral manipulations and the discovery of pathways for sleep benefits	172
5.5. Pan-neuronal imaging to investigate the regulation and benefits of sleep.	175
5.6. Conclusion	176
6. Appendix.....	177
6.1. Sequences of CRISPR strains generated by Sunybiotec.....	177
6.2. Recurrently used MATLAB scripts.....	183
6.2.1. Extract individual neuron intensities	183
6.2.2. Bout detection.....	185
6.2.3. Calculation of the direction of movement from the wormtracker data	186
6.2.4. Sleep bout alignment including sleep fraction and time in sleep	186
References.....	189

Acknowledgements

Many people have contributed to this PhD thesis in one way or another and I would like to take this opportunity to express my gratitude.

First, I would like to say a special word of thanks to my supervisor Prof. Henrik Bringmann. He took me in as a PhD student when I planned to apply to a Master's program. His door was always open to discuss scientific problems and ideas and the amount of scientific advice and support I got from him is incredible. Thank you for your trust and guidance! Next, I would also like to thank my committee members Prof. Tim Gollisch and Prof. Ralf Heinrich for supporting my projects. The committee meetings always included fruitful discussions. Thank you for your great ideas.

Of course, I am very grateful for my collaborators. Together, we were able to generate hopefully impactful publications. Many thanks to Elisabeth Maluck, Judith Besseling and Florentin Masurat for the cooperation on the RIS circuit paper. Furthermore, a big thank you to Florian Jordan and Peleg Sapir for their work on the OptoGenBox.

I had the pleasure to work with several undergraduate students during my PhD. A big thank you goes to Laura Kircke, my student assistant, who helped with crossings and worm maintenance for one year. I would furthermore like to thank my interns Chantal Schmidt, Moataz Nouredine and Jasmina Bier, who conducted valuable experiments.

Throughout my PhD studies I was lucky to work with fantastic colleagues, who were always keen to discuss scientific questions and provide ideas. The working atmosphere was so collaborative thanks to you Yang Hu, Jan Konietzka, Anastasios Koutsoumparis, Byoungjun Park, Gill Pollmeier, Marina Sinner and Yin Wu! A special appreciation goes to Judith Besseling for introducing me to the wonderful world of *C. elegans* research at the beginning of my PhD. I would also like to thank Gill, Marina, Tasos and Judith for each proofreading a section of this thesis.

Different lab technicians supported me by providing reagents and by cleaning lab supplies. For this, I would like to thank Silvia Gremmler, Sabine König, Sigrid Stöhr, Regina Löchel and Gabor Szerencsi.

Last but not least, I want to thank the GGNB and Systems Neuroscience for interesting classes and travel grants, the CGC for many worm strains and the *C. elegans* research community for offering such a cooperative and inspiring scientific environment.

Table of Figures

Figure 1. The specific sleep posture as a characteristic to identify sleep.	3
Figure 2. The wake-sleep flip-flop switch in mammals.	4
Figure 3. The evolution of sleep-active neurons.	5
Figure 4. The life cycle of <i>C. elegans</i> .	8
Figure 5. Wiring diagram of RIS and its presynaptic neurons.	11
Figure 6. Automated detection of neuron intensities.	24
Figure 7. Command interneuron ablation in L1 lethargus and L1 arrest.	99
Figure 8. AMPA and NMDA type receptors are not necessary for sleep induction.	101
Figure 9. Sleep affects forward and reverse locomotion.	102
Figure 10. Reverse command interneuron ablation can cause ectopic sleep bouts before lethargus.	103
Figure 11. AVB activity measurements during lethargus.	104
Figure 12. Sleep dampens the nervous system.	106
Figure 13. Optogenetic depolarization of RIS inhibits nervous system activity.	108
Figure 14. A comparison of presynaptic active zones reveals only a small influence of sleep on synaptic homeostasis.	145
Figure 15. A post-synaptic marker shows a differently timed peaking post-synaptic strength between <i>aptf-1(gk794)</i> and wild-type worms.	146
Figure 16. Sleeplessness does not affect habituation and memory in adult <i>C. elegans</i> .	149
Figure 17. Sleep is not required for recovery from coldness or feeding behavior.	151
Figure 18. Maximum intensity z-projection of mKate expression of different genetic tools in RIS.	153
Figure 19. Ion channels expressed in RIS can cause constant de- or hyperpolarization of RIS.	155
Figure 20. RIS shows little transients and is hyperpolarized in worms expressing EGL-23 in RIS.	156
Figure 21. Constant RIS hyper- as well as depolarization cause decreased sleep in L1 arrested worms.	158
Figure 22. Ion-channels expressed in RIS influence the amount of sleep in lethargus.	159
Figure 23. Changes in RIS activity influence the lifespan of <i>C. elegans</i> in L1 arrest.	161
Figure 24. A lack of sleep bouts leads to an overall neuronal activity increase in worms in the <i>aptf-1(gk794)</i> background.	163
Figure 25. RIM peaks more frequently but with less amplitude in an <i>aptf-1(gk794)</i> background in L1arrest.	166

Abbreviations

AMPA:	α -amino-3-hydroxy-5-methyl-4-isoxazolepropionic acid
AMPK:	5' adenosine monophosphate-activated protein kinase
ArchT:	archaerhodopsin; green light-activated outward rectifying proton pump
ATR:	all-trans retinal
CLOCK:	circadian locomotor output cycles kaput
co:	codon optimized
CRISPR:	clustered regularly interspaced short palindromic repeats
CRY:	cryptochrome
DIC:	Differential Interference Contrast
DNA:	deoxyribonucleic acid
DR:	dorsal raphe nucleus
EEG:	electroencephalography
EGF:	epidermal growth factor
EM gain:	Electron-Multiplying gain
FLP:	FMRF-Like Peptide
GABA:	γ -aminobutyric acid
GCaMP:	genetically-encoded calcium indicator; fusion of GFP, calmodulin, and M13(peptide sequence from myosin light chain kinase)
gf:	gain-of-function
GFP:	green fluorescent protein
ICE:	interleukin-1 β -converting enzyme
L1 - L4:	larval stage 1 - larval stage 4
LC:	locus coeruleus
LDT:	laterodorsal tegmental nucleus
LED:	light-emitting diode
MnPO:	median preoptic nucleus
NGM:	Nematode Growth Medium
NMDA:	N-methyl-D-aspartic acid
PB:	parabrachial nucleus
PC:	precoeruleus area
PCR:	polymerase chain reaction

PER:	period
PPT:	pedunculo pontine tegmental nucleus
ReaChR:	red-shifted variant of channelrhodopsin
REM:	rapid eye movement
ROI:	region of interest
SCN:	suprachiasmatic nucleus
SEM:	standard error of the mean
SKI LODGE:	single-copy knock-in loci for defined gene expression
TMN:	tuberomammillary nucleus
TTL:	transistor-transistor logic
UNC:	uncoordinated
UTR:	untranslated region
UV:	ultraviolet
VLPO:	ventrolateral preoptic nucleus
vPAG:	ventral periaqueductal gray

1. Introduction

1.1. Importance of sleep

Humans (*Homo sapiens*) sleep an average of 8 hours in one day, which is one third of their time. African elephant (*Loxodonta africana*) matriarchs are currently the animals with the known shortest amount of time in sleep. They only sleep for 2 hours within 24 hours. On the other side of the spectrum are little brown bats (*Myotis lucifugus*), which are asleep for approximately 20 hours each day (1–4). However, not only mammals sleep but also species from other classes such as zebrafish (*Danio rerio*), which sleep for 9.5 hours within one day and fruit flies (*Drosophila melanogaster*), which sleep for 16.5 hours (5, 6). Sleep is a state of quiescence and vulnerability, yet it is evolutionary conserved (7). There is currently no convincing evidence for a species with a nervous system that does not sleep (8). One could hypothesize that a nervous system either requires or enables sleep, or eventually even both. The prevalence of sleep in all animals with a nervous system points to one or several existential functions.

Indeed, studies have shown the importance of sleep for organisms. Energy is conserved and allocated during sleep (2, 9–11) and physiological processes such as the metabolism or DNA repair are controlled by sleep (10, 12–18). In mammals sleep is required for higher brain functions as for example synaptic downscaling and memory formation (19–24). Sleep deprivation in humans comes with health impairments as for instance an increased risk of obesity, cardiovascular disease, type 2 diabetes (T2D), cancer, infections, anxiety and depression (4, 25–28). While functions of sleep and effects of sleep deprivation have been identified, it is still not clear if sleep serves one primary purpose with added-on secondary functions or if several functions are of equal importance.

1.2. Characteristics of sleep

Sleep is commonly defined as a state of behavioral quiescence. In humans and other mammals it can be characterized via electroencephalography (EEG). With this method, voltage changes of neuronal groups within one location of the cortex are measured

through electrodes (29–31). Two sleep phases can be distinguished with EEG recordings. Rapid eye movement (REM) phases get their name from the active eye muscles (32). Most other body muscles are paralyzed in that phase. REM sleep is further characterized by a high frequency and small amplitude electroencephalogram in the cortex, similarly to wake phases (33). The second type of sleep in mammals is named non-REM sleep. Very characteristic for non-REM sleep are slow-waves, which means that EEG recordings are slowly oscillating (34, 35). Non-REM sleep can be further categorized into three (previously four) different stages. These stages are defined by the sleep depth, so by how easily the sleeping organism can be woken up. The first stage is most similar to wakefulness and one can easily apply a waking stimulus. On the contrary, organisms in phase three are much more difficult to be woken up by an arousing stimulus (36, 37). The two types of sleep, REM and non-REM sleep, are cycling (38, 39). Humans spend 75-80% of their time asleep in non-REM stages (37).

However, EEG measurements cannot be recorded for all organisms because of anatomical differences between nervous systems (4). Hence, behavioral criteria have been defined for the identification of sleep (3):

- Sleep is manifested in a specific sleep posture. This posture may vary across species (Figure 1).
- Sleeping organisms can be woken up. Sleep is reversible.
- Responsiveness to stimuli is reduced in sleep compared to the wake state.
- A homeostatic and/or circadian regulation underlies sleep.

For an individual organism to count as sleeping, all criteria have to be fulfilled.

More recent research has identified increased chromosome dynamics as potential molecular marker for sleep (17). However, in practice, molecular markers for sleep identification are not yet established in the scientific community. Currently, sleeping organisms are identified by the given behavioral criteria.

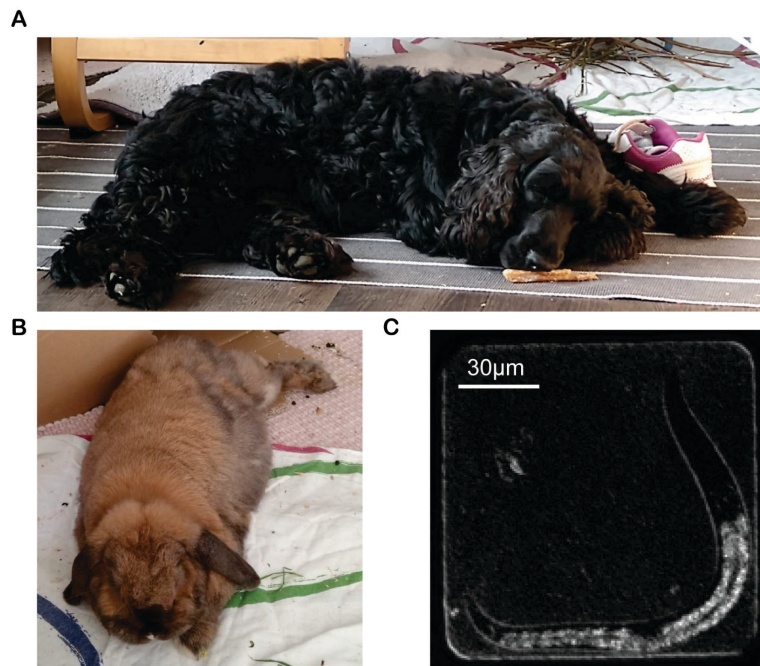


Figure 1. The specific sleep posture as a characteristic to identify sleep.

Depicted are (A) a sleeping dog (*Canis familiaris*), (B) a sleeping European rabbit (*Oryctolagus cuniculus*) and (C) a sleeping nematode (*Caenorhabditis elegans*). Photos from A and B by Karo Thiele printed with her permission.

1.3. Regulation of sleep

The nervous system is a key regulator of sleep. Sleep-promoting, sleep-active neurons have been found in many different species. These neurons are typically active at sleep onset and release for example neuropeptides and γ -aminobutyric acid (GABA). These neurotransmitters can inhibit wake-promoting neurons and induce sleep (8, 40). Contrary, arousing, wake-promoting, wake-active neurons can inhibit sleep-active neurons, which ensures the reversibility of sleep for example upon a threatening stimulus. This so-called flip-flop switch has been well described in mammals (Figure 2). Here, the wake-promoting brain areas laterodorsal tegmental nucleus, pedunculopontine tegmental nucleus, locus coeruleus, parabrachial nucleus, precoeruleus area, dorsal raphe nucleus, ventral periaqueductal gray and tuberomammillary nucleus (LDT, PPT, LC, PB, PC, DR, vPAG, TMN) are mostly located in the upper brainstem and activated by orexin neurons in the lateral hypothalamus. These wake-promoting regions can get inhibited by the ventrolateral

(VLPO) and median (MnPO) preoptic nuclei, which act as major sleep-active and sleep-promoting regions in mammals. Reversely, the wake-promoting areas can inhibit the VLPO to form the flip-flop switch between wake- and sleep-promoting neurons (8, 41, 42).

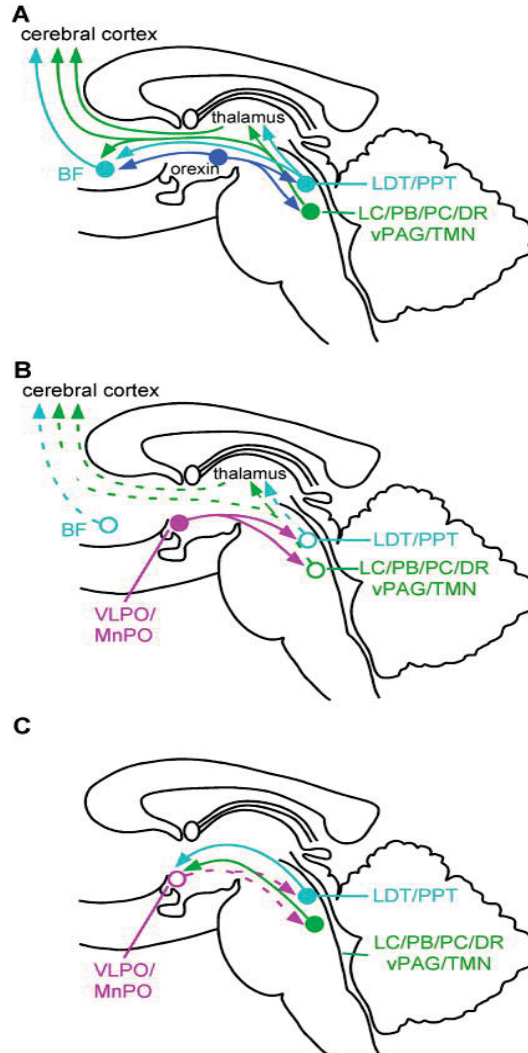


Figure 2. The wake-sleep flip-flop switch in mammals.¹

(A) Wake-promoting brain regions of mammals are mostly found in the upper brainstem. These cholinergic (turquoise) laterodorsal tegmental nucleus (LDT) and pedunculopontine tegmental nucleus (PPT) and monoaminergic, probably glutamatergic areas (dark green) locus coeruleus (LC), parabrachial nucleus (PB), precoeruleus area (PC), dorsal raphe nucleus (DR), ventral periaqueductal gray (vPAG) and tuberomammillary nucleus (TMN) present the major wake- and arousal-promoting areas. Orexin neurons (blue) are found in the lateral hypothalamus. On the one hand, they reinforce the wake-promoting regions in the upper brainstem; on the other hand, they can directly promote arousal in for example the BF. (B) The ventrolateral (VLPO)

¹ Reprinted from Neuron, Vol 68/6, Saper, Fuller, Pedersen, Lu, Scammell, Sleep State Switching, 1023-1042, Copyright (2010), with permission from Elsevier.

and median (MnPO) preoptic nuclei could be identified as sleep-promoting regions in mammals. They can inhibit wake-promoting areas. (C) Additionally, wake-promoting areas can inhibit sleep-promoting areas, thus forming a flip-flop switch between wake and sleep-promoting neurons (41).

Sleep-promoting neurons have not only been found in mammals but also other non-mammalian species (8). In zebrafish, a subtype of glutamatergic neurons expressing neuropeptides of the RFamide (Arg-Phe-NH₂ motif at their C-terminus) family called QRFP have been identified as sleep-promoting (43). Currently, there are four known sleep-promoting brain regions in *Drosophila* (8, 44). Neuronal populations in the mushroom body (MB) (44–46), a single pair of GABAergic and serotonergic medial neurons (47), peptidergic neurons in the PI (48) and ExF12 neurons (49, 50) have all been classified as sleep-promoting in the fruit fly. While sleep-promoting neurons are central to the regulation of sleep, their organizational complexity varies between species, which is likely due to evolutionary divergences (Figure 3).

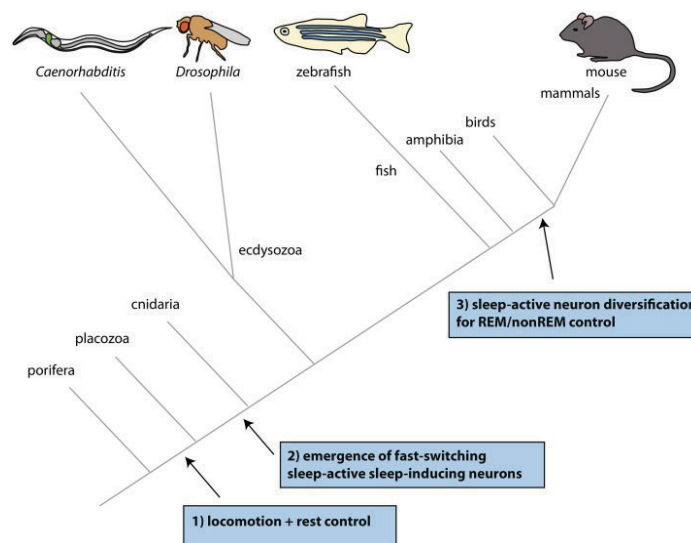


Figure 3. The evolution of sleep-active neurons.²

(1) With the evolution of locomotion there was a need for rest control. This was probably accomplished through endocrine regulation. (2) The second key step consists of sleep-active, sleep-inducing neurons required for fast switching between sleep and wake states once the nervous system had evolved. (3) Higher brain functions required another set of sleep-active neurons that could regulate REM (Rapid Eye Movement) and non-REM sleep (8).

² Reprinted from Genetics, Vol 208/4, Bringmann, Sleep-Active Neurons: Conserved Motors of Sleep, 1279-1289, Copyright (2018), with permission from Genetics Society of America.

Upstream of sleep-promoting neurons for sleep regulation are other pathways and timers as for example the circadian clock (8). In many organisms, sleep is regulated by a circadian rhythm. This means that sleep is dependent on the time of the day. Humans for example are usually asleep at night, whereas rabbits are nocturnal, meaning they mostly sleep during the day and are awake at night. The circadian rhythm is determined by a master oscillator in the suprachiasmatic nucleus (SCN) (51, 52). The SCN synchronizes individual cells and tissues, some of them having their own circadian patterns when isolated from the SCN (53–56). Circadian control in mammals still functions in the absence of daylight rhythms, yet the SCN has to get recalibrated by sunlight every day through photoreceptors in the eyes in order to maintain the 24 hour cycle (56–58). The SCN determines the synthesis of the hormone melatonin, which has been shown to be sleep-promoting by for example inhibiting orexin neurons (59–61). In mammals, circadian regulation consists of a transcriptional feedback loop. The transcription factor CLOCK (Circadian Locomotor Output Cycles Kaput) plays a key role. Bound to BMAL1 (encoded by gene ARNTL, Aryl Hydrocarbon Receptor Nuclear Translocator Like), the heterodimer initiates the transcription of PER (Period) and CRY (Cryptochrome) proteins, which then inhibit CLOCK:BMAL1 and therefore their own transcription (62–65).

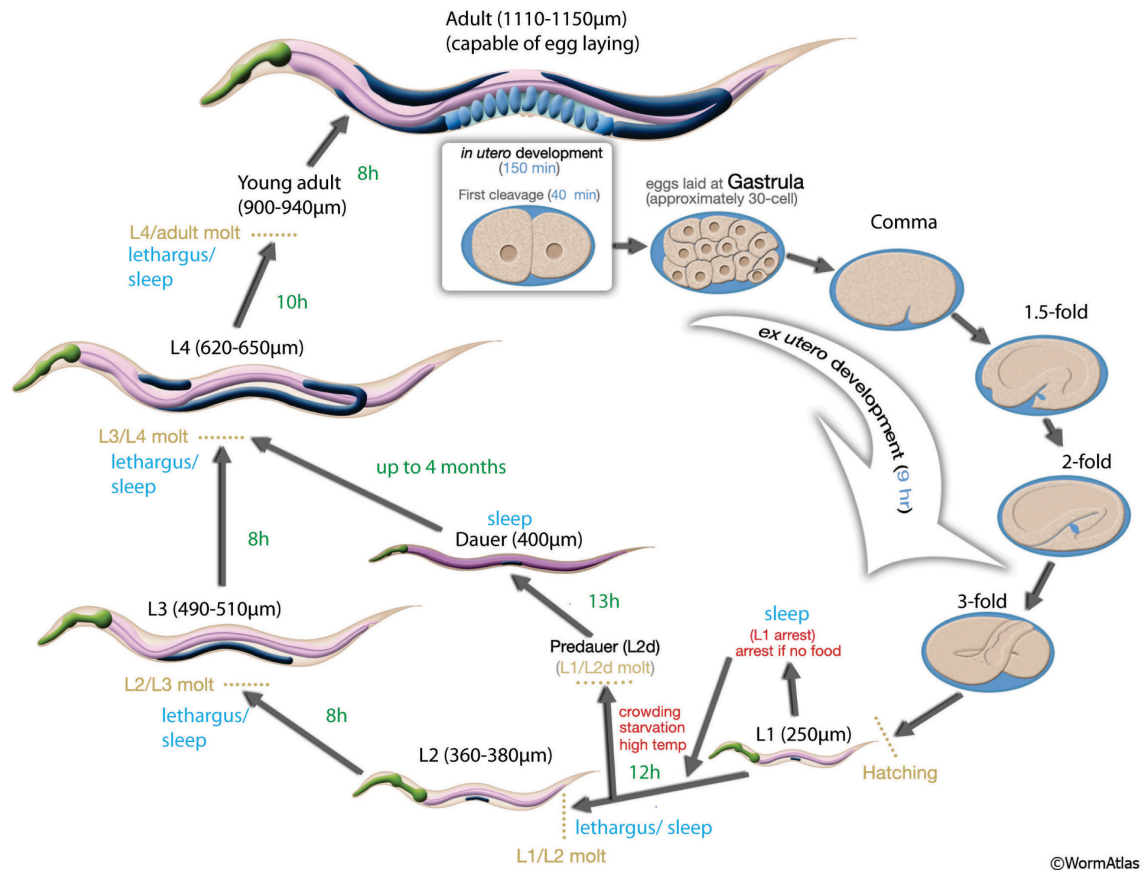
One key characteristic of sleep is its homeostatic regulation (3). Homeostasis is important to control for sleep time and sleep depth. Sleep pressure builds up during wakefulness. This sleep pressure was proposed to partly consist of somnogens, sleep-promoting molecules (8). The longer the organism is awake for, the more somnogens get accumulated and the stronger is the sleep pressure. Hence, long wake phases are followed by long and deep sleep phases whereas short wake phases are preceded by short and less deep sleep bouts. An example for a somnogen in mammals is extracellular adenosine (66, 67). Extracellular adenosine gets accumulated during the wake state and can inhibit neuronal activity in most wake-promoting brain areas (68–70). It is furthermore proposed to be activating sleep-promoting brain areas (71). Astrocytes have been linked to sleep homeostasis and might be involved in extracellular adenosine accumulation (8, 72, 73). Other mechanisms that have been suggested to play a role in sleep homeostasis are the sustenance of cellular homeostasis (18, 74, 75), energy allocation (76, 77) and synaptic strength regulation (78, 79). However, for a more detailed understanding of homeostatic sleep control, further research is needed.

1.4. *Caenorhabditis elegans* as a model organism

Caenorhabditis elegans (*C. elegans*) are up to 1mm long nematodes that present themselves as an ideal model organism for sleep research due to several features. In nature, they can be found at most places in the world on rotten plant material. In the laboratory, they are grown on agar plates and feed on the bacterial strain *Escherichia coli* (*E. coli*) OP50 (80, 81). After careful study to find an ideal model organism to investigate development, Sydney Brenner introduced *C. elegans* as research model organism in the 1960s (82, 83). Since then, the worms have been widely studied and nowadays a research community consisting of more than 1400 laboratories (registered on wormbase on the 28th of July 2020) shares their knowledge through many open access sources such as the websites wormbase and wormatlas. This open access and collaborative environment has allowed for a fast characterization of the model organism *C. elegans*.

One of *C. elegans*' many advantages is the determined life cycle and short generation time. At a temperature of 20° Celsius the worms can develop from egg to adulthood within approximately 3 days (84). Throughout their development the animals undergo four larval stages before they finally become adults. Each larval stage is completed by a molt (Figure 4). The cell lineage of *C. elegans* is entirely known and invariant. This means that the cell development within individuals follows a deterministic pattern. Adult hermaphrodite *C. elegans* have 959 somatic cells (85, 86).

With 83% of their ~20.000 protein-coding genes having human homologs, *C. elegans* are well suited for fundamental discoveries (87). *C. elegans* are diploid with five autosomal chromosomes. Hermaphrodites have an additional two X sex chromosomes whereas males lack one X chromosome and therefore have the genotype XO. Meiotic non-disjunction of the X chromosome hence leads to males. This happens rarely spontaneously (0.1% of animals). However, 50% of offspring through mating are males. One hermaphrodite can produce up to 300 progeny through self-fertilization. Homozygous hermaphrodites generating homozygous offspring is very useful for research since it allows for a high genetic control. Males are rarely experimentally investigated but very useful for strain generation via crossing (84).



©WormAtlas

Figure 4. The life cycle of *C. elegans*.³

Worms go through four larval stages (L1-L4) before they reach the adult state. At the end of each larval state is a developmentally regulated phase called lethargus in which the worms sleep. Following lethargus, the larval state is completed with a molt. Without food, hatching worms arrest in the first larval stage. L1 worms enter the Dauer state upon crowding and starvation. Sleep is present in L1 arrest as well as the Dauer state (84).

An advantage of *C. elegans* for imaging and behavioral analysis is the model organism's transparency. Furthermore, *C. elegans* have a relatively accessible nervous system. The nervous system of a hermaphrodite consists of only 302 neurons. Males have an additional 83 neurons to allow for a more complex mating behavior (88). The hermaphrodite nervous system is comprised of a small pharyngeal nervous system (20 neurons) and a large somatic nervous system (282 neurons). The two systems are distinct and independent and only communicate via a single interneuron pair (89). In comparison, fruit flies have a central nervous system of around 200 000 neurons and humans of approximately 100 billion neurons (90, 91). This illustrates the relative

³ Adapted from wormatlas.org.

simplicity of the *C. elegans* nervous system, which makes it very suitable for neuroscientific studies such as the identification of neuronal circuits.

Additionally, all neuronal connections (chemical and electrical synapses) have been identified in *C. elegans* (92–94). Even though the nature of many connections - if they are inhibitory or activatory - has not been discovered yet, knowing the connectome of a relatively small nervous system allows for straightforward testing of such properties and for the analysis of neuronal circuits.

1.5. Sleep in *Caenorhabditis elegans*

Sleep is widely present in *C. elegans*' life. It can be a behavioral response to stresses such as starvation, a high temperature or UV light (15, 95–99). Furthermore, worms show satiety quiescence upon ingestion of high quality food (100, 101). Sleep can also be developmentally regulated and is present in the developmental stage called lethargus (102, 103). While sleep as a behavioral response is identical in all previously mentioned sleep states, upstream pathways that trigger sleep vary. EGF signaling (104, 105), insulin signaling (99, 106) and developmental signaling (107) can all make a worm fall asleep. This thesis focuses on two types of sleep: sleep during lethargus and starvation-induced sleep in L1 arrested animals.

1.5.1. Sleep in lethargus

Throughout its life, *C. elegans* molts four times until it finally reaches adulthood. Each molt is preceded by a time of behavioral quiescence and suppressed feeding called lethargus. The duration of lethargus varies depending on the larval stage and even within one stage between individual animals. However, on average lethargus lasts two hours (108). During lethargus the worm cycles between sleep and motion bouts (109).

A circadian clock does not regulate sleep in *C. elegans*. Instead, lethargus is developmentally regulated. Interestingly, some of these developmental genes regulating sleep have homologues to mammalian circadian genes. The oscillating gene *lin-42* is an ortholog of the mammalian *period* and controls the timing of development and hence lethargus in *C. elegans*. LIN-42 regulates for example the sleep-inducing neuropeptide NLP-22, which is expressed in the RIA interneurons (107, 110). A total of 520 genes

oscillate within the molting cycle of *C. elegans* and it is possible that a subset of these genes might be involved in the developmental regulation of lethargus and sleep (111). A non-oscillating gene that has been reported to be involved in the regulation of sleep in lethargus is the cGMP-dependent protein kinase (PKG) gene *egl-24*. EGL-24 is sleep inducing when expressed in sensory neurons (112).

1.5.2. Starvation-induced sleep in L1 arrested animals

Sleep can also be triggered in *C. elegans* as a response to starvation (99). Worms that are not supplied with sufficient food upon hatching cannot undergo regular development but arrest in the first larval stage. This starvation-dependent arrest is termed L1 arrest. In this state, worms show cyclic sleep and motion bouts. The fraction of sleep increases with prolonged starvation (106). Sleep in L1 arrest is regulated by insulin-like signaling pathways (99). AMP-activated kinase and FoxO, which are also known regulators of longevity and developmental arrest, were found to be sleep-inducing. Sleep seems to be of utmost importance in L1 arrest, since sleep-deficient worms have a strongly reduced survival compared to wild-type worms (106).

1.6. RIS - the motor of sleep in *Caenorhabditis elegans*

For all different types of sleep in the nematode *C. elegans*, the single ring interneuron RIS has been identified to play a key role. RIS is located in the head of the worm on the right side of the ventral ganglion. It depolarizes at sleep onset, its activation leads to sleep induction and it is homeostatically regulated. These characteristics allow for RIS to be termed the motor of sleep in *C. elegans* (8, 113, 114). RIS is GABAergic and peptidergic and it induces sleep through release of the neuropeptide FLP-11 (115). FLP-11 is transcriptionally regulated by APTF-1, an AP2 transcription factor (113). A loss of APTF-1 as in *aptf-1(gk794)* mutants leads to a loss of transcription of FLP-11 in RIS. Hence, *aptf-1(gk794)* are non-sleeping and present a potent tool to investigate effects of genetic sleep deprivation in *C. elegans* (4, 113).

Thanks to previous research and an established connectome (92–94), the upstream neurons of RIS have already been identified. The sensory CEP and URY neurons have each a connection onto RIS. Furthermore, the RIM motor and interneurons project a

process onto RIS. Interneurons AVJ, PVC and SDQ are additionally upstream of RIS. RIS forms gap junctions with RIM and AVJ (Figure 5). Knowing RIS's upstream neurons facilitates the investigation of a neuronal circuit for RIS regulation and hence sleep homeostasis.

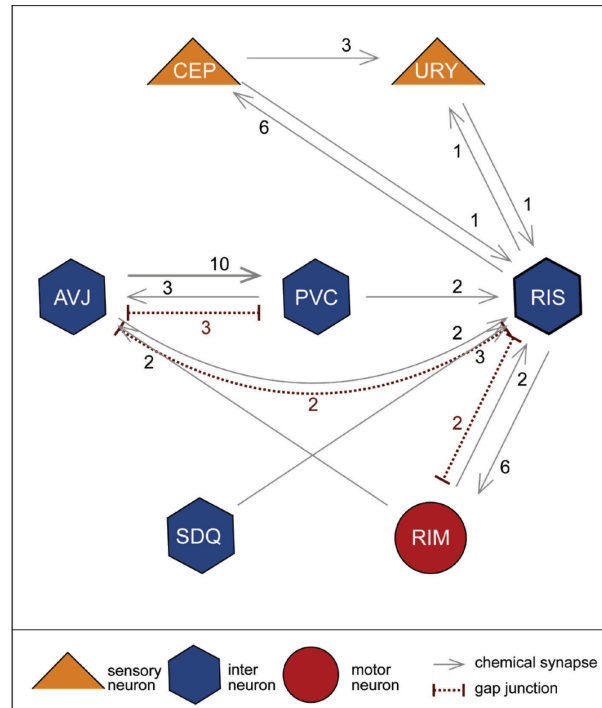


Figure 5. Wiring diagram of RIS and its presynaptic neurons.⁴

Neurons are shown that project one or more chemical synapses onto the sleep neuron RIS. SDQ has 3 synapses onto RIS. PVC, RIM and AVJ form each 2 synapses onto RIS. CEP and URY only project one synapse onto RIS. RIS has additional electrical synapses with RIM and AVJ (92, 116).

⁴ Designed with the online tool from the Database of Synaptic Connectivity of *C. elegans* for Computation, which utilizes data from White et al. 1986 (92, 116).

1.7. Optogenetics

Optogenetics is a method to actively manipulate biochemical reactions or neuronal activity (117). Upon expression of a light-sensitive actuator, a specific cell as for example a neuron can get activated or inhibited by light. Common tools for activation are the light-gated ion channels channelrhodopsins, which were first discovered in algae (118, 119). Light-gated ion pumps, which originate from halobacteria are commonly utilized for neuronal inhibition (120).

The method optogenetics was first established in *C. elegans* (119, 121) and it became soon clear that *C. elegans* presents an excellent model organism for optogenetic studies (121, 122). Its transparency allows for non-invasive optogenetic experiments (121). Red-shifted channelrhodopsin (ReaChR) is very suitable for neuronal depolarization in the nematodes (123). For inhibition, the outward proton pump ArchT presents a great means (124). Yellow to orange light (585-605nm) can be utilized to activate these genetic tools.

There are at least two main categories of experiments for which optogenetics can be applied. First, optogenetics is very useful in the identification of neuronal circuits. Here, a presynaptic neuron gets optogenetically activated or inhibited and the response of the post-synaptic neuron recorded (114). Secondly, one can induce or inhibit a specific behavior through optogenetic manipulations. Activation of the sleep neuron RIS for instance induces sleep in *C. elegans* (113, 114) and activation of the escape response neuron ASH causes an escape locomotion of the worm (106, 114).

2. Thesis Aims

When this project was started, the foundation for sleep research in *C. elegans* had just been laid. The concept of *C. elegans* sleeping and not just having sleep-like states had recently become accepted in the scientific community (125). Previous studies had identified the interneuron RIS to be the sleep neuron, which releases the neuropeptide FLP-11 to induce sleep (113, 115). FLP-11 was found to be regulated by the AP2 transcription factor APTF-1 and a non-sleeping *aptf-1(gk794)* mutant was characterized (113). These findings allowed for a further investigation of different aspects of sleep in *C. elegans*. With the known connectome and RIS presenting a single sleep neuron in *C. elegans*, one was able to take a closer look into neuronal mechanisms and circuits of sleep control and sleep homeostasis. The *aptf-1(gk794)* mutant, in which RIS is non-functional, presents a potent tool to investigate the functions of sleep.

All my PhD projects served one purpose: to better understand the regulation and functions of sleep in *C. elegans*. To approach this rather broad topic from different perspectives, I defined the following aims:

Aim 1 – How the nervous system regulates sleep in *C. elegans*

The sleep neuron RIS is essential for sleep induction and homeostasis in *C. elegans*. I aimed to characterize the regulation of RIS and found a neuronal circuit that controls RIS and is hence responsible for its homeostatic regulation. An unexpected key finding of mine was the positive feedback loop between RIS and PVC, a wake-active command interneuron. Results of this project were published in Publication I. Through pan-neuronal imaging I could test for the reciprocal control of RIS on the nervous system by showing that RIS activation and sleep directly suppress nervous system activity.

Aim 2 – Development of a device for optogenetic long-term experiments to test for effects of optogenetic sleep deprivation

I implemented a device to conduct long-term optogenetic experiments in *C. elegans* – the OptoGenBox. With this device I could show that optogenetic sleep deprivation of starved first larval stage animals leads to a reduced survival compared to wild-type worms. The results of this project were published in Publication II.

Aim 3 – Test for benefits of sleep in *Caenorhabditis elegans*

I conducted different experiments to investigate the benefits of sleep. First, I tested for the synaptic homeostasis hypothesis in *C. elegans* by comparing wild-type worms to non-sleeping *aptf-1(gk794)* mutants. Then, I also conducted experiments to investigate the health span of genetically sleep-deprived worms. However, these tests did not give conclusive results. To find further functions of sleep and how they are coupled to the activation of the sleep neuron RIS, I investigated new mutants. These mutants expressed ion channels in RIS through CRISPR genome editing. I found that worms, in which RIS was constantly depolarized, and worms, in which RIS was constantly hyperpolarized, showed a highly reduced amount of sleep in L1 arrest and lethargus. However, even though constant RIS activation led to a reduction of sleep, these worms survived longer in L1 arrest compared to wild type. In contrast, RIS hyperpolarization led to a reduced survival. I could hence show that it is possible to uncouple immobility as a key behavioral characteristic of sleep from sleep benefits for longevity. The new genetic knock-in strains present potent tools to further investigate pathways downstream of RIS that are responsible for the benefits of sleep.

3. Methods

Methods for published experiments can be found in the corresponding publications. Methods for all other experiments in this thesis are stated here.

3.1. *Caenorhabditis elegans* maintenance

Worms were maintained on nematode growth medium (NGM) plates. They were fed with the *Escherichia coli* (*E. coli*) strain OP50 (82). Growing worms were kept at 15-25°C. A list of all utilized strains can be found here:

AML18	<i>wtfIs3(rab-3p::NLS::GFP, rab-3p::NLS::tagRFP)</i> . (126)
AML32	<i>wtfIs5(rab-3p::NLS::GCaMP6s, rab-3p::NLS::tagRFP)</i> . (126)
CX14845	<i>kyEx4863(rig-3p::HisC11:sl2mCherry)</i> . (127)
HBR227	<i>aptf-1(gk794)</i> II. (113)
HBR507	<i>flp-11(tm2706)</i> X. (115)
HBR560	<i>goels120(tdc-1p::SL1-GCaMP3.35-SL2::mKate2-unc-54-3'utr, unc119(+))</i> . (114)
HBR1361	<i>goels304(flp-11p::SL1-GCaMP3.35-SL2::mKate2-unc-54-3'UTR, unc119(+))</i> . (106)
HBR1753	<i>wtfIs5(rab-3p::NLS::GCaMP6s, rab-3p::NLS::tagRFP)</i> . Generated for this study by outcrossing AML32 twice with N2.
HBR1777	<i>goels384(flp-11p::egl-1::SL2-mkate2-flp-11-3'utr, unc119(+))</i> . (106)
HBR1883	<i>goels403(flp-11p::ReaChR::mkate2-flp-11-3'utr)</i> . Generated for this study.
HBR1937	<i>aptf-1(gk794)</i> II; <i>goels121(tdc-1p::SL1-GCaMP3.35-SL2::mKate2-unc-54-3'utr, unc119(+))</i> . (114)
HBR2091	<i>nmr-1(ak4)</i> II ; <i>glr-1(n2461)</i> III. Generated for this study by crossing KP4 and VM487.
HBR2092	<i>aptf-1(gk794)</i> II; <i>jsIs821(mec-7p::GFP::RAB-3)</i> . Generated for this study by crossing HBR227 and NM2689.

HBR2141	<i>aptf-1(gk794)</i> II; <i>nuIs25 (glr-1p::glr-1::GFP, lin-15(+))</i> . Generated for this study by crossing HBR227 and KP1148.
HBR2260	<i>aptf-1(gk794)</i> II; <i>akIs11(nmr-1p::ICE)</i> . Generated for this study by crossing HBR227 and VM4770.
HBR2340	<i>flp-11(syb1445[flp-11-SL2-unc-58(L428F)-linker-mKate2])</i> X. Generated for this study by outcrossing PHX1445 with N2.
HBR2369	<i>flp-11(syb2146[flp-11-SL2-egl-23(n601)-linker(GSGSG)-mKate2])</i> X; <i>goeIs304(fl p-11p::SL1-GCaMP3.35-SL2::mKate2-unc-54-3'UTR, unc-119(+))</i> . Generated for this study by crossing HBR1361 with PHX2146.
HBR2370	<i>flp-11(syb2193[flp-11-SL2(gpd-2)-mKate2-linker-twk-18(e1913)])</i> X; <i>goeIs304(fl p-11p::SL1-GCaMP3.35-SL2::mKate2-unc-54-3'UTR, unc-119(+))</i> . Generated for this study by crossing HBR1361 with PHX2193.
HBR2371	<i>flp-11(syb1445[flp-11-SL2-unc-58(L428F)-linker-mKate2])</i> X; <i>goeIs304(fl p-11p::SL1-GCaMP3.35-SL2::mKate2-unc-54-3'UTR)</i> . Generated for this study by crossing HBR1361 with HBR2340.
HBR2420	<i>aptf-1(gk794)II</i> ; <i>flp-11(syb1445[flp-11-SL2-unc-58(L428F)-linker-mKate2])</i> X; <i>otIs672(rab-3p::NLS::GCaMP6s, arrd-4p::NLS::GCaMP6s)</i> . Generated for this study by crossing OH15265 with PHX1445.
HBR2421	<i>flp-11(syb1445[flp-11-SL2-unc-58(L428F)-linker-mKate2])</i> X; <i>otIs672(rab-3p::NLS::GCaMP6s, arrd-4p::NLS::GCaMP6s)</i> . Generated for this study by crossing OH15265 with HBR2340.
HBR2446	<i>flp-11(syb1445[flp-11-SL2-unc-58(L428F)-linker-mKate2])</i> X; <i>goeIs120(tdc-1p::SL1-GCaMP3.35-SL2::mKate2-unc-54-3'utr, unc119(+))</i> . Generated for this study by crossing HBR560 and PHX1445.
HBR2447	<i>aptf-1(gk794)</i> II; <i>flp-11(syb1445[flp-11-SL2-unc-58(L428F)-linker-mKate2])</i> X; <i>goeIs121(tdc-1p::SL1-GCaMP3.35-SL2::mKate2-unc-54-3'utr, unc119(+))</i> . Generated for this study by crossing HBR1937 and PHX1445.
HBR2467	<i>otIs672(rab-3p::NLS::GCaMP6s, arrd-4p::NLS::GCaMP6s)</i> , <i>lgc-38(syb2346[flp-11p::dpy-10 site::flp-11 3'UTR], syb2493[ReaChR-linker-mKate2])</i> . Generated for this study by crossing OH15265 and PHX2493.
KP1148	<i>nuIs25(glr-1p::glr-1::GFP, lin-15(+))</i> . (128)
KP4	<i>glr-1(n2461)</i> III. (129)
N2	wild type (Bristol) (82)

NM2689	<i>jsIs821(mec-7p::GFP::RAB-3)</i> . (130)
OH15265	<i>otIs672(rab-3p::NLS::GCaMP6s, arrd-4p::NLS::GCaMP6s)</i> . (131)
OS4976	<i>nsEx2846(pept-3p::TeTX, elt-2p::mCherry)</i> . (132)
PHX1433	<i>flp-11(syb1433[flp-11-SL2-egl-23cDNA(A383V)-linker-mKate2])</i> X. Generated by Sunybiotec according to Henrik Bringmann's design for this study.
PHX1445	<i>aptf-1(gk794)II; flp-11(syb1445)[flp-11-SL2-unc-58(L428F)-linker-mKate2]</i> X. Generated by Sunybiotec according to Henrik Bringmann's design for this study.
PHX1464	<i>flp-11(syb1464[flp-11-SL2-egl-23cDNA(L229N)-linker-mKate2])</i> X. Generated by Sunybiotec according to Henrik Bringmann's design for this study.
PHX2146	<i>flp-11(syb2146[flp-11-SL2-egl-23(n601)-linker(GSGSG)-mKate2])</i> X. Generated by Sunybiotec according to Henrik Bringmann's design for this study.
PHX2193	<i>flp-11(syb2193[flp-11-SL2-mKate2-linker-twk-18(e1913)])</i> X. Generated by Sunybiotec according to Henrik Bringmann's design for this study.
PHX2493	<i>lgc-38(syb2346[flp-11p::dpy-10 site::flp-11 3'UTR], syb2493[ReaChR-linker-mKate2])</i> III. Generated by Sunybiotec according to Henrik Bringmann's design for this study.
VM4770	<i>akIs11(nmr-1p::ICE)</i> . (133)
ZIM498	<i>mzmEx324(sra-11p::mCherry, sra-11p::GCaMP5K)</i> . (134)

3.2. New strain generation

3.2.1. Cloning

The MultiSite Gateway system (Invitrogen, California) was utilized for cloning. The LR reactions were done with pCG150 (Addgene plasmid #17247) as destination vector. For the reaction, the protocol in the MultiSite Gateway User Manual was followed (135).

The following constructs were generated for this study:

K354 pflp-11::glr-1(A/T)::SL2mKate2 unc-54 3' UTR, (unc-119+)
K364 pZK673.11::ArchT::SL2mKate2 unc-54 3' UTR, (unc-119+)

3.2.2. Microparticle Bombardment

A previously described protocol was followed for microparticle bombardment (136). *unc-119(ed3)* mutants were bombarded and an *unc-119* rescue served as selection marker (137).

3.2.3. Crosses

For *C. elegans* crosses, males were either generated via heat shock based on standard protocol or maintained by a continuation of crossings of worms of the same genotype (138). Selection was based on phenotype or fluorescent markers whenever possible. Mutants and non-visible transgenes were checked through a PCR.

The following primers were used to validate genotypes upon crossing or for Sanger sequencing:

aptf-1(gk794)

CGACAATCTTCCCAAAGACC
CGGATCGATTGCTAGAGAGG
GCTTGGACGGCTTTAGTTGA

egl-1::SL2-mKate2

CAACGGACCAGTCATGCAAA
AGTGACCTGTTCGTTGCAAC

flp-11(syb1445)

ACGAGGAAGACTTTGCTCCA
AAACTCGCAAAAACGAGGAA
GACACCAATCAAATTCTAGACAGC

flp-11p::SL2::egl-23(n601)

AGCTCACCTCAAGAAGTCC
TTGGCACGGATGAAGTTTGG

flp-11p::SL2::unc-58(L428F)

GACCACATGCACGACCTTTT
ATGACTTTCTCCTGCCGTGA

glr-1(n2461)

CTAAAATTGCCAAGTTGATATGATCCTCCC
AATGCGACACCTTTCGGCTCCGATTT
GCAGCCAACATTGAAATGACCATAACCAC
TGCGGAAGGAATTGAAAGAGTTCGAAGT

ICE

CCGAGCTTTGATTGACTCCG
AGTCATGTCCGAAGCAGTGA

lgc-38(syb2346)

ATGGCGATGTCATTTTCATGTT
AGACCACCTACCGTTCCAAG
ATCCCAGTTGTTTGACGGTT

mKate

GGGGACAAGTTTGTACAAAAAAGCAGGCTATGTCCGAGCTCATCAAG
GGGGACCACTTTGTACAAGAAAGCTGGGTTTAACGGTGTCCGAGCTT

nmr-1(ak4)

TGCTGGTGACTIONTATGAGCCT
TGCTGGCGATCTTACTGGAA
CAACACCGATGCAGAGCTC

3.3. Imaging

3.3.1. Cameras and Software

For imaging I used the Nikon cameras DS Qi2 ($4,908 \times 3,264$ pixels) (Nikon, Tokyo) and the back-illuminated sCMOS camera Photometrics Prime 95B ($1,200 \times 1,200$ pixels) (Nikon, Tokyo), or the Andor cameras iXon EMCCD (512×512 pixels) (Andor Technology Ltd., Belfast), and iXon Ultra EMCCD ($1,024 \times 1,024$ pixels) (Andor Technology Ltd., Belfast). The EM gain of the EMCCDs was usually set to 200, occasionally to 150. The camera read-out was set to 10, 20 or 30MHz at 14- or 16-bit depending on the utilized camera when filming with NIS. For image acquisition I set the exposure time between 5-800ms. The imaging experiments were conducted using the software NIS Elements 5 (Nikon, Tokyo) or Andor IQ 2 or Andor IQ 3 (Andor Technology Ltd., Belfast).

3.3.2. Imaging in agarose microchambers

Worms were filmed in microfluidic chambers as previously described (*139, 140*). In summary, box-shaped indentations were cast in a hydrogel through a PDMS mold. The hydrogel was made of either 3% diluted agarose in S-Basal (Figures 7-12 and 17) or 5% agarose diluted in M9 buffer (Figures 13, 19-22, 24 and 25). For different experiments, differently sized chambers were utilized. For L1 lethargus chambers and L1 arrest experiments from Figure 7, $190 \times 190 \times 15 \mu\text{m}$ chambers were made. L1 arrest experiments in Figures 17, 19-22, 24 and 25 utilized chambers of size $110 \times 110 \times 10 \mu\text{m}$.

3.3.3. Differential Interference Contrast (DIC) and bright field imaging

Differential interference contrast (DIC) and bright field imaging were done with a standard 100W halogen lamp and an infrared filter (Semrock Brightline HC 785/62) (IDEX Health and Science, New York). Continuous DIC images were acquired with a frame rate of 0.2Hz (Figure 7A-C, 8, 9, 21 and 22) or 0.1Hz (Figure 7D-E, 10 and 11). The worms were filmed with either a 40x (Figure 9), 20x (Figure 7, 8, 10, 11 and 22) or a 10x objective (Figure 21). When the 20x objective was utilized an additional 0.7 lens was added.

3.3.4. Calcium imaging

Calcium imaging was conducted with a 480nm LED and a standard GFP filter set (EGFP, Chroma). The EMCCD camera TTL signal triggered the LED. The 490nm intensities were set to 0.71mW/mm² (Figure 11), 0.23mW/mm² (Figure 19), 1.1mW/mm² (Figure 12,13 and 20), 0.09mW/mm² (Figure 24) or 0.51mW/mm² (Figure 25). Either a 10x (Figure 19 and 24) or a 20x objective (Figure 11, 12, 13, 20 and 25) was utilized. The imaging set-up in Figure 19 included an additional 1.5 lens. The lethargus experiments included an additional 0.7 lens. The exposure time was set to either 5ms (Figure 12, 13, 24 and 25) or 50ms (Figure 11, 19 and 20).

To compare neuronal activations between different strains, an additional mKate signal was recorded. This was done with a 585nm LED and a set of standard Texas red filters (Chroma). The 585nm LED intensities were set to 0.11mW/mm² (Figure 19), 0.39mW/mm² (Figure 20) or 0.15mW/mm² (Figure 25). The camera exposure time was set to 5ms (Figure 25), 50ms (Figure 19) or 100ms (Figure 20). Worms were calcium and mKate imaged with a frame rate of 0.1 Hz.

3.3.5. L1 arrest imaging

They were starved for 48h at 25°C except for the experiment in Figure 7. There, the worms were starved for 24h at 25°C. DIC images and in some experiments also GCaMP images were taken with a frame rate of 0.2Hz (Figures 7A-C and 21) or 0.1Hz (Figures Figure 7D-E, 19, 20, 24 and 25).

3.3.6. Pre- and post-synaptic marker imaging

Worms were first synchronized by bleaching according to standard protocol (82). Upon bleaching, *C. elegans* worms were kept in 1.5ml microcentrifuge tubes in M9 buffer. The tubes were placed in a rotator to allow for sufficient oxygen supply. The rotator stood in a 20°C incubator. For imaging, worms were pipetted from the tubes onto a 3% agarose pad with 5µl 25mM levamisole. This way, a paralysis of the worms was ensured. The worms were filmed through a spinning disc confocal microscope. The 490nm laser was used. The iXon Ultra camera (Andor Technology Ltd., Belfast) exposure time was set to 204ms and the EM gain to 200. Worms were filmed through a

100x objective. 91 z-planes encompassing 18 μ m were filmed with the piezo z-stage NanoScanZ 100 (Prior Scientific Instruments Ltd, Cambridge). The 490nm laser was set to an intensity of 0.04mW/mm².

The analysis of the synaptic marker images was conducted in ImageJ and MATLAB. The pre-synaptic sites in the nerve ring were manually defined as ROIs in ImageJ and numbers of synapses, mean intensities and areas extracted. For the post-synaptic marker, the five brightest post-synaptic areas were defined manually as ROIs and the mean intensity as well as area of each ROI was extracted.

3.3.7. mKate expression imaging

Fixed worms were imaged on a 3% agarose pad. The agarose was solved in S-Basal. 25mM levamisole (Sigma Aldrich) was added to the worms for fixation. An Andor Revolution disc system (Andor Technology Ltd.) and a CSU-X1 spinning disc head (Yokogawa) were utilized for spinning disc imaging. The 561nm laser light intensity was set to 0.14mW/mm². The worms were imaged through a 100x oil objective. An EM gain of 200 was included and the camera read-out time was set to 30MHz. The *C. elegans* strains PHX2146 and PHX2193 were imaged with an exposure time of 500ms. The strains HBR2340 and PHX1445 were imaged with an exposure time of 800ms. A z-stack spanning a total of 10 μ m (21 planes, 0.5 μ m distance between planes) was acquired. The maximum intensity z-projection was calculated for representation.

3.3.8. Optogenetic experiments

For the optogenetic RIS activation experiment in L1 lethargus, a time sequence was repeated all 20min. First, 20 DIC images with a frame rate of 2Hz were recorded to detect the pumping state of the worm. Then, for 3min, a baseline of GCaMP images was recorded with a frame rate of 0.33Hz. This was followed by a stimulation phase of 1min, in which again GCaMP images were acquired with a frame rate of 0.33Hz. In between the images, 585nm LED light with an intensity of 0.17mW/mm² was triggered in by the software for 1s. After the stimulation period, a recovery period of 3min was imaged, in which GCaMP images were acquired with a frame rate of 0.33Hz. The 490nm LED intensities for imaging were set to 0.76mW/mm².

10mM all-trans-retinal (ATR, Sigma Aldrich) was supplemented to the chambers for optogenetic manipulations. Control worms did not receive ATR treatment.

3.4. Imaging Analysis

3.4.1. Analysis of calcium imaging data

When only one neuron expressed GCaMP, a custom-written MATLAB script detected the location and calculated the speed and mean intensity of that neuron in each frame. In the case of a wider GCaMP expression, the location of the neuron of interest was manually identified and the speed and mean intensity of the neuron was automatically calculated. When GCaMP was expressed in several neurons and the intensity of all neurons together was of interest, several neurons were considered as a blob and automatically tracked as if they were a large single neuron. The logic of the MATLAB script was to first read in the image (Figure 6A), secondly, to use an intensity threshold for the background and create a binary (Figure 6B). The in-built MATLAB function *regionprops* could then detect all connected components in the binary image. The component with the largest area usually presented the signal (unless for example another marker was expressed by the worm then the second largest component could be identified as signal). The location of center of mass of the largest component was then transferred to the original image and a square cut out around it (Figure 6C). Depending on the function input arguments, a percentage of brightest pixels in the cut out square were averaged as signal and a percentage of low intensity pixels within the square was averaged as background. The written MATLAB function hence needed four input arguments: the length of one side of the square which was cut out around the signal, an intensity threshold for the background, the number of signal pixels within the cut out square and finally how many seconds were between two acquired images. The center of mass was then utilized to calculate the speed of the worm. The GCaMP intensities in Figure 20 were too faint to be automatically tracked. However, in this experiment the mKate signal could be tracked and the position of center of mass from the mKate images was utilized to identify the GCaMP signal of the same time point.

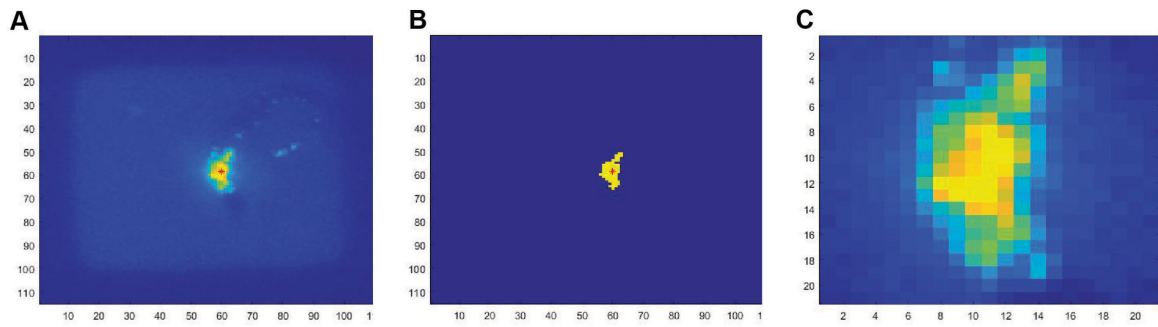


Figure 6. Automated detection of neuron intensities.

(A) The image is read in. (B) Based on an intensity threshold a binary is created and the center of mass of the largest connected component gets extracted. (C) The location of the center of mass is then applied to the original image and a square cut out around it. From this square the brightest pixels are averaged as signal and the darkest pixels utilized for background correction. Here, the pan-neuronal signal of the strain OH15265 is presented as example.

3.4.2. Normalization of calcium imaging data

When only GCaMP data was recorded continuously, a baseline was found by averaging the 21st to 40th lowest mean values. The extracted mean intensity values of each frame were then normalized by first subtracting the baseline and then dividing over the baseline.

For comparisons of neuronal activations between different strains, the GCaMP signal was normalized for each image by dividing over the mKate signal, which was taken in the same time loop.

In optogenetic experiments, the intensity average during the baseline period was used for normalization in each time sequence.

3.4.3. Analysis of DIC images

Movement of *C. elegans* worms was analyzed from DIC images by image subtraction (141). The matrix of intensity values of the preceding image was subtracted from the matrix of intensity of the current image. All values of the difference matrix were then averaged to attain a mean smoothed image subtraction value, which represents the movement of the worm.

3.4.4. Sleep bout analysis

Sleep bouts were detected by first smoothing speed or image subtraction values. This was done over 20 time points using the in-built MATLAB function *smooth*, which calculates a first-degree polynomial local regression model. The smoothed data was then normalized between 0 and 1. A percentage of the maximum speed was determined as threshold. Only times during which the normalized speed was below this threshold were counted as sleep bouts. The threshold varied for different experiments between 10-40% to account for strain variability and different chamber sizes. However, in lethargus the threshold was usually 10% (Figure 8 and 11) and for L1 arrested animals the threshold was usually 20% (Figure 19-21) or 10% (Figure 24 and 25). In addition to the speed threshold, a time threshold was implemented so that sleep bouts had to last at least for a minimum duration of the given time threshold. Depending on the experiment and therefore sleep state, this time threshold was 1, 2 or 3 minutes.

3.4.5. Sleep bout alignment

Speeds and GCaMP intensities were aligned to the start of sleep bouts, which had been detected with the sleep bout analysis. Sleep bouts were only counted for the alignment when the worm was awake throughout 3min prior to the sleep bout onset. This alignment was done with a custom-written MATLAB script.

3.4.6. Forward and reverse locomotion data

To analyze forward and reverse locomotion in *C. elegans*, worms were DIC imaged in 190x190x15 μ m microfluidic chambers with a 40x objective all 5s. The images were then analyzed with an automated program (142) to extract the locations of the nose and the centroid (grinder). From these positions, the direction of movement was calculated through a custom-written automated MATLAB script.

3.4.7. RIM peak detection

RIM peaks were found by first smoothing the normalized neuronal activity with the in-built MATLAB function *smooth* over 5 time points. Then, the peaks with minimum

amplitude of 2 were detected with the in-built MATLAB function *islocalmax*. From the number of peaks in wake bouts as well as the duration of wake bouts, the peak frequency was calculated for different worm strains.

3.5. Behavioral assays

3.5.1 Cold stress assay

Larval 4 stage worms that grew at 20°C were picked onto fresh NGM plates and placed in a 4°C refrigerator. One plate hosted between 4 and 10 worms. After 6h at 4°C, the worms were moved back to room temperature and observed through a stereo microscope (Leica, Wetzlar). The time was measured until they started moving on the plate.

3.5.2 Habituation assay

Worms were synchronized for the habituation assay by bleaching according to the standard protocol (82). The assay was conducted with adult worms on different days. Day 1, 2 and 3 adult worms were pooled as early stage adult worms. Day 12, 13 and 15 adult worms were counted as late stage adult worms. Worms were prepicked for isolation. Worms were not reutilized on different days. Upon prepicking, there was at least a 30min recovery time before the start of the habituation assay. Tapping was conducted with either a platinum pick or hair. The tap was given to the side of the worm behind the pharynx (143). A total of 20 taps were given in one trial with 5s of rest in between. Each worm underwent three trials. One initial trial, a second after 2 minutes of recovery time and a third after a total of 15 min recovery time from the first trial.

3.5.3. Pumping assay

Eggs were picked into 190x190x15µm microfluidic chambers without food and starved for 24 hours at 20°C. The L1 arrested worms were then filmed via bright field and a 20x objective for one minute. The frame rate was set to as fast as possible, which is approximately 35Hz. The number of pumps was counted manually for each worm with a clicker.

3.5.4. Lifespan and recovery assays

3.5.4.1. Lifespans in the OptoGenBox

C. elegans worms were kept in microfluidic devices of the size 110x110x10µm similarly to other L1 arrest experiments. There were between 29 and 45 worms in one device, kept in individual chambers. Devices were replenished with 10µl of 10mM all-trans-retinal (ATR, Sigma Aldrich) every 3-4 days for optogenetic manipulation. Control chambers did not receive ATR. 20µl of 10µg/ml nystatin was pipetted to each chamber 2-4 times throughout the lifespan to avoid fungal contamination. Furthermore, 20µl of sterile water was added every other day until day 15 of the lifespan and then each day to counteract the agarose drying out over time. In the earlier days of the lifespan experiment, worms were counted every second day. Later, they were counted every single day. If a worm didn't move for 2 min under stimulation with a blue light LED, it was counted as dead.

3.5.4.2. Lifespan of L1 arrested worms in M9 buffer

Worms were synchronized by bleaching according to standard protocol (82). Worms on 1-2 well grown NGM plates with a diameter of 6cm were bleached per genotype. The day of bleaching was counted as day 0. The next day was counted as day 1 of the lifespan. After bleaching, the worms were kept in 1ml M9 buffer in a 1.5ml Eppendorf tube and placed in a rotator located in the 25°C incubator. For counting, 4x2µl of the worms in M9 buffer were pipetted onto fresh plates. A few hours later (at least 2 hours) the alive and dead worms were counted manually with the help of a clicker.

3.5.4.3. Recovery of L1 arrested worms in M9 buffer

For the recovery assay, worms that survived from the lifespan assay were checked and counted for development into L4 larvae or adulthood 1-5 days post pipetting.

3.5.5. Inhibition of AVA

Histamine (HA, Sigma Aldrich, St. Louis, MO, 10mM) was supplemented to NGM plates as has previously been documented (127). For experimentation, young adult worms expressing an AVA specific HA chloride channel, were picked onto NGM plates the evening before. The next morning, microfluidic chambers were prepared with eggs and *E. coli* bacteria from the NGM HA plates (139, 140). The chambers were then imaged through DIC imaging.

3.6. Statistics

Internal controls were included in the experiments whenever possible. If this was not possible, the experimental condition was alternated with the control. The habituation experiments from chapter 4.3.2. and lifespan experiments from chapter 4.3.4.3 were blinded. Experiments, in which an automated analysis was conducted, were not blinded. The utilized statistical tests and respective p-values are declared in the figure captions. The conducted statistical test for speeds and GCaMP intensities as well as tapping responses within the same strain was the Wilcoxon signed rank test. Either the Welch test or the Kosmogorov-Smirnov test was conducted to compare data from different strains. For the statistical analysis of contingency tables as for example sleep fractions or lifespans and survival in liquid culture at a certain time point, the Fisher's exact test was used. To correct for multiple testing, experiments with four or more genotypes were corrected by the Benjamini-Hochberg procedure with a 5% false discovery rate. The graphs show the mean \pm SEM unless otherwise stated. Box plots include the individual data points. Depicted are the interquartile range and the median. The 10th-90th percentile is portrayed by the whiskers.

4. Results

4.1. Aim 1 - How the nervous system regulates sleep in *C. elegans*

4.1.1. Publication I

Maluck E,* **Busack I***, Besseling J, Masurat F, Turek M, et al. (2020) A wake-active locomotion circuit depolarizes a sleep-active neuron to switch on sleep. PLOS Biology 18(2): e3000361. <https://doi.org/10.1371/journal.pbio.3000361>

*equal contribution

This project was done in collaboration with Elisabeth Maluck, Judith Besseling, Florentin Masurat, Michal Turek, Emanuel Bush and Henrik Bringmann. It was published on Feb 20 2020 in Plos Biology.

I designed and performed the experiments in Figures 2A, B and D, 3, 4B-D, 6A and B, S6, S8A-F and S13. I analyzed the data from those figures and additionally the data of Figures 1A, 4A and 4E and S11A. The panels from the previously mentioned figures and additionally Figure 8A-C were illustrated by me. Furthermore, I generated the strain HBR2231. I contributed to the manuscript by writing the methods section corresponding to experiments that were conducted by me and by editing it.

RESEARCH ARTICLE

A wake-active locomotion circuit depolarizes a sleep-active neuron to switch on sleep

Elisabeth Maluck^{1,2}, Inka Busack^{1,2}, Judith Besseling¹, Florentin Masurat¹, Michal Turek¹, Karl Emanuel Busch³, Henrik Bringmann^{1,2*}

1 Max Planck Institute for Biophysical Chemistry, Göttingen, Germany, **2** University of Marburg, Marburg, Germany, **3** University of Edinburgh, Edinburgh, United Kingdom

☞ These authors contributed equally to this work.

* henrik.bringmann@biologie.uni-marburg.de



Abstract

Sleep-active neurons depolarize during sleep to suppress wakefulness circuits. Wake-active wake-promoting neurons in turn shut down sleep-active neurons, thus forming a bipartite flip-flop switch. However, how sleep is switched on is unclear because it is not known how wakefulness is translated into sleep-active neuron depolarization when the system is set to sleep. Using optogenetics in *Caenorhabditis elegans*, we solved the presynaptic circuit for depolarization of the sleep-active RIS neuron during developmentally regulated sleep, also known as lethargus. Surprisingly, we found that RIS activation requires neurons that have known roles in wakefulness and locomotion behavior. The RIM interneurons—which are active during and can induce reverse locomotion—play a complex role and can act as inhibitors of RIS when they are strongly depolarized and as activators of RIS when they are modestly depolarized. The PVC command interneurons, which are known to promote forward locomotion during wakefulness, act as major activators of RIS. The properties of these locomotion neurons are modulated during lethargus. The RIMs become less excitable. The PVCs become resistant to inhibition and have an increased capacity to activate RIS. Separate activation of neither the PVCs nor the RIMs appears to be sufficient for sleep induction; instead, our data suggest that they act in concert to activate RIS. Forward and reverse circuit activity is normally mutually exclusive. Our data suggest that RIS may be activated at the transition between forward and reverse locomotion states, perhaps when both forward (PVC) and reverse (including RIM) circuit activity overlap. While RIS is not strongly activated outside of lethargus, altered activity of the locomotion interneurons during lethargus favors strong RIS activation and thus sleep. The control of sleep-active neurons by locomotion circuits suggests that sleep control may have evolved from locomotion control. The flip-flop sleep switch in *C. elegans* thus requires an additional component, wake-active sleep-promoting neurons that translate wakefulness into the depolarization of a sleep-active neuron when the worm is sleepy. Wake-active sleep-promoting circuits may also be required for sleep state switching in other animals, including in mammals.

OPEN ACCESS

Citation: Maluck E, Busack I, Besseling J, Masurat F, Turek M, Busch KE, et al. (2020) A wake-active locomotion circuit depolarizes a sleep-active neuron to switch on sleep. *PLoS Biol* 18(2): e3000361. <https://doi.org/10.1371/journal.pbio.3000361>

Academic Editor: Paul Shaw, Washington University School of Medicine in St. Louis, UNITED STATES

Received: June 15, 2019

Accepted: January 23, 2020

Published: February 20, 2020

Peer Review History: PLOS recognizes the benefits of transparency in the peer review process; therefore, we enable the publication of all of the content of peer review and author responses alongside final, published articles. The editorial history of this article is available here: <https://doi.org/10.1371/journal.pbio.3000361>

Copyright: © 2020 Maluck et al. This is an open access article distributed under the terms of the [Creative Commons Attribution License](https://creativecommons.org/licenses/by/4.0/), which permits unrestricted use, distribution, and reproduction in any medium, provided the original author and source are credited.

Data Availability Statement: All data are available as part of this manuscript. Data used for figure

generation are provided in the [S1](#) and [S2](#) Data supplemental Excel sheets.

Funding: This work was supported by the Max Planck Society (Max Planck Research Group) to H. B., a European Research Council Starting Grant under the European Union's Horizon 2020 research and innovation program (ID: 637860; SLEEPCONTROL) to H.B., and the University of Marburg to H.B. The funders had no role in study design, data collection and analysis, decision to publish, or preparation of the manuscript.

Competing interests: The authors have declared that no competing interests exist.

Abbreviations: $\Delta F/F$, change of fluorescence over baseline; APTF-1, Activating enhancer binding Protein 2 Transcription Factor 1; ArchT, archaerhodopsin from *Halorubrum* strain TP009; ATR, all-trans-retinal; dFB, dorsal Fan-shaped Body; DIC, differential interference contrast; EEG, electroencephalogram; FLP-11, FMRF-Like Peptide 11; GCaMP, genetically encoded calcium indicator; HA, histamine; HisCl, Histamine-gated Chloride channel; ICE, Caspase-1/Interleukin-1 converting enzyme; NGM, Nematode Growth Medium; NREM, non-Rapid Eye Movement; PVC, Posterior Ventral Cord neuron of the lumbar ganglion class name; R, fluorescence of GCaMP divided by fluorescence of mKate2; R2, ring neurons of the ellipsoid body; ReaChR, Red-activatable channelrhodopsin; RIM, Ring Interneuron M class name; RIS, Ring Interneuron S class name; SDQL, Posterior lateral interneuron class name—left cell.

Introduction

Sleep is a behavior that affects many, if not all, physiological processes. Disorders and curtailment of sleep affect the lives of 10% to 30% of the adult population of modern societies. Sleep loss is associated with an increased risk of infection [1], cardiovascular disease [1], psychiatric disease (including depression [2,3]), obesity [4,5], type 2 diabetes [4,5], and cancer [1]. The high prevalence of insomnia and insufficient sleep quality thus presents a massive unmet health and economic problem [1,3–5]. To understand how sleep behavior is generated, it is crucial to solve the underlying neural circuits.

Sleep circuits require inhibitory sleep-active sleep-promoting neurons, which depolarize specifically at sleep onset and actively induce sleep by releasing inhibitory neurotransmitters, GABA and neuropeptides, to dampen arousal and the activity of wake circuits [6]. Sleep behavior induced by inhibitory sleep-active neurons includes the suppression of voluntary movements and sensory perception, reversibility, and homeostasis [7]. Inhibitory sleep-active neurons suppress wake circuits and can be rapidly suppressed by arousing stimulation to allow for quick awakening. Forced wakefulness is followed by an increase of sleep-active neuron depolarization, which leads to homeostatic sleep corrections. Thus, understanding sleep control requires comprehension of the circuit mechanisms that determine when and how much inhibitory sleep-active neurons depolarize [6,8].

Circuits control the depolarization of inhibitory sleep-active neurons. For example, wake-active wake-promoting neurons promote arousal and suppress inhibitory sleep-active neurons, whereas sleep need causes sleep-active neuron depolarization. Thus, sleep-active sleep-promoting and wake-active wake-promoting neurons form a flip-flop switch, which ensures that sleep and wake exist as discrete states. This sleep switch is under the control of arousal that favors wake and inhibits sleep through the suppression of sleep-active neurons by inhibitory wake-active neurons [6,9]. It has been proposed that sleep induction is favored by disinhibition of inhibitory sleep-active neurons [10–12]; also, excitatory sleep-active neurons exist that might perhaps present activators of inhibitory sleep-active neurons [13]. However, the forces and mechanisms that flip the sleep switch from wake to sleep when an organism gets sleepy cannot be satisfactorily explained by the present circuit models as it is unclear how sleep-active neurons are turned on when the system is set to sleep.

Sleep is under circadian and homeostatic controls that determine the timing of sleep and ensure that enough of this essential physiological state takes place [14]. Sleep homeostasis comprises multiple mechanisms that act on different timescales. On long timescales, sleep is a function of prior wakefulness, i.e., prolonged wakefulness leads to increased sleep propensity, and sleep loss triggers compensatory increases in the intensity or duration of sleep. This chronic sleep homeostasis likely is mediated by several parallel mechanisms. For example, in mammals, somnogens such as adenosine accumulate during wakefulness, leading to the inhibition of wake-promoting neurons [15,16]. In *Drosophila*, activity-dependent plasticity of sleep-promoting neurons increases during wakefulness to increase subsequent sleep [17,18]. On short timescales, acute homeostasis determines whether the system's actual state matches the system's set point and carries out corrective action if those values do not match. For example, to homeostatically maintain sleep despite disturbance, micro-arousals need to be compensated for. In humans, homeostatic sleep maintenance can be seen in electroencephalogram (EEG) recordings in the form of k-complexes, in which a spontaneous or evoked short cortical up state is followed by a down state [19–21]. Homeostatic sleep maintenance is also found during sleep in *C. elegans*, in which sleep bouts are interrupted by short motion bouts, with the length of a motion bout correlating with the length of the subsequent sleep bout [22,23]. Thus, across systems, homeostatic sleep maintenance requires constant surveillance of sleep and corrective action.

Sleep-active sleep-promoting neurons are conserved regulators of sleep and have been found both in vertebrates as well as in invertebrates [8,24]. Mammals possess several populations of sleep-active neurons, most of which are inhibitory, across the brain. These neurons reside in the anterior hypothalamus, brain stem, and cortex [6,12]. Excitatory sleep-active neurons were found in the perioctular midbrain that project to inhibitory sleep-active neurons in the anterior hypothalamus, the role of which could be to activate inhibitory sleep-active neurons [13]. Studying sleep in less complex brains facilitates sleep circuit analysis. In *Drosophila*, sleep-promoting neurons are found at several locations in the brain. A well-characterized population of sleep-promoting neurons is formed by neurons residing in the dorsal Fan-shaped Body (dFB). R2 ring neurons of the ellipsoid body accumulate homeostatic sleep pressure over time to promote activation of sleep-promoting dFB neurons, probably by an indirect mechanism [17,18]. *C. elegans* possesses a single inhibitory sleep-active neuron called RIS. Like its mammalian counterparts, RIS depolarizes at sleep onset. RIS is crucial for sleep induction because its ablation leads to a virtually complete loss of detectable sleep bouts [25–27]. The small, invariant nervous system, its mapped connectome, and the transparency of *C. elegans* facilitate neural circuit analysis [28]. However, the specific neural circuits that control RIS activity are not yet understood.

C. elegans shows sleep behavior during many stages and conditions. Here, we analyzed sleep behavior during development, also known as lethargus, the stage prior to each of the 4 molts during larval development [8,27,29–31]. We used optogenetics to dissect the neural circuits that control the activation of the sleep-active RIS neuron in *C. elegans*. We found a third and novel important element of the flip-flop switch: interneurons that are active during wakefulness and that are known to control locomotion are required for RIS activation and sleep. These findings suggest a tripartite flip-flop circuit model that can explain how arousing stimulation inhibits RIS depolarization, how RIS depolarization is homeostatically controlled, and how reduced arousal can induce RIS depolarization. Our RIS circuit model has 2 important implications for understanding sleep control: (1) it suggests that sleep control has evolved from circuits controlling locomotion; and (2) sleep induction requires an important third element, wake-active sleep-promoting neurons, which translate wakefulness into sleep when the animal is sleepy but awake.

Results

Interneurons known to govern locomotion behavior control RIS activity

RIS is crucially required for sleep and typically activates during sleep bouts (Fig 1A) [25]. However, the presynaptic driver neurons that activate and control this neuron are not known. To identify the circuits controlling RIS activation, we optogenetically tested the role of neurons that are presynaptic to RIS according to the *C. elegans* connectome [28]. The neurons called AVJL, CEPDL, URYVL, RIMR, PVCL, and SDQL have been shown to be presynaptic to RIS [28,32]. To find out how these presynaptic neurons control RIS, we activated them with ReaChR (red-activatable channelrhodopsin) and green light and followed RIS calcium activity using GCaMP (a genetically encoded calcium indicator) during and outside of lethargus. We confirmed the expression of ReaChR through a fused fluorescent reporter (mKate2). AVJ, CEPD, URYV, RIM, PVC, and SDQ each are a pair of 2 neurons, of which only one is presynaptic to RIS. Because only promoters that express in both neurons of each pair are available—and because the 2 neurons of each pair are in close proximity—we always manipulated both neurons of the neuronal pair (except for SDQL) [28,32]. Because there were no specific promoters available for the expression in SDQL and PVC, we expressed ReaChR using semi-specific promoters and selectively illuminated only the presynaptic neuron class. We used L1

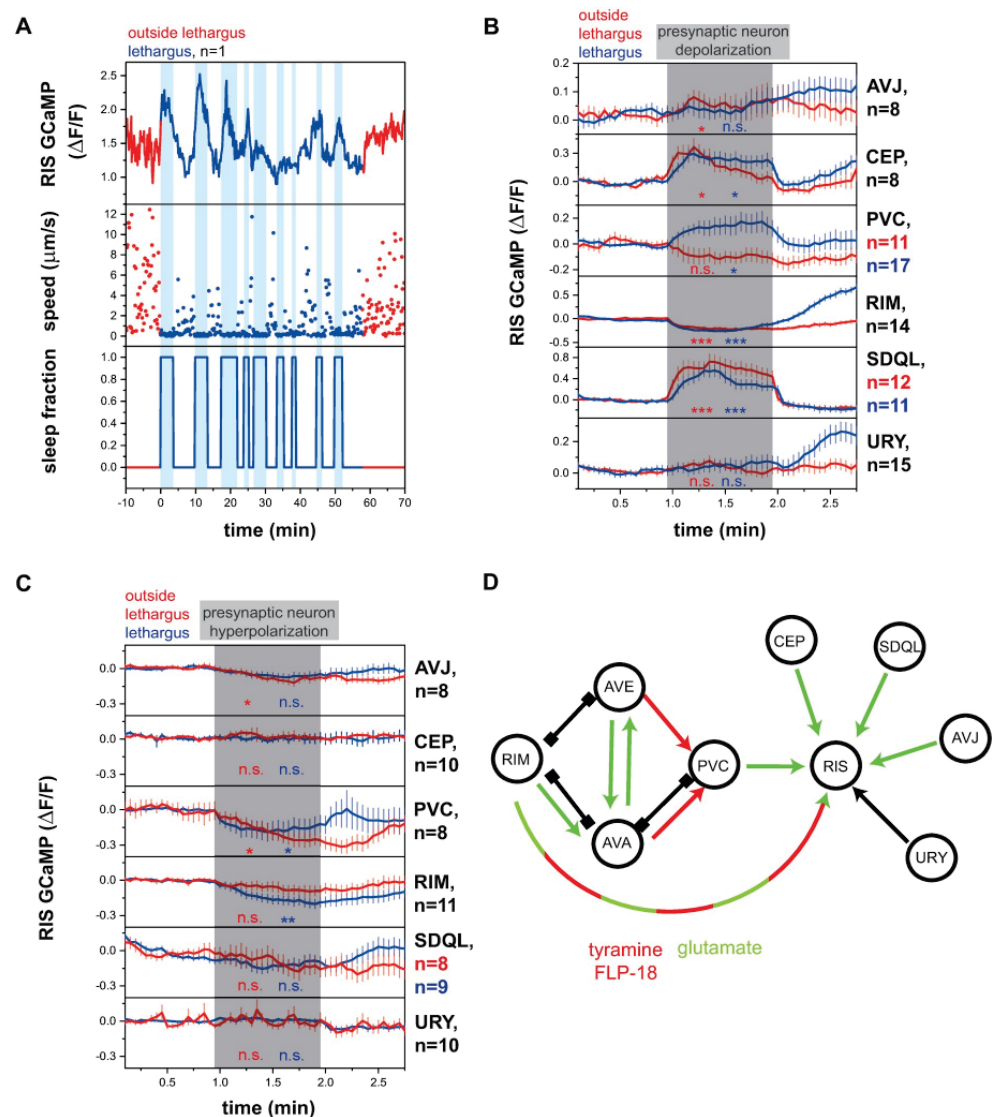


Fig 1. Presynaptic neurons control the activity of the sleep-active RIS neuron. (A) Sample trace of RIS activity and worm locomotion behavior outside of and during lethargus. RIS has no strong calcium transients outside of lethargus but shows strong activity transients during lethargus. Upon RIS activation, worms enter sleep bouts. (S1 Data, Sheet 1A). (B) Presynaptic neurons activate or inhibit RIS outside of and during lethargus. For statistical calculations, neural activities before the stimulation period (0–0.95 min) were compared to activity levels during the stimulation period (1–1.95 min). * $p < 0.05$, ** $p < 0.01$, *** $p < 0.001$, Wilcoxon signed rank test. (S1 Data, Sheet 1B). (C) RIS activity decreases upon optogenetic PVC and RIM hyperpolarization. Statistical calculations were performed as described in panel B, but in experiments in which SDQL was stimulated, baseline activity levels were calculated over the time interval from 0.6 to 0.95 min. Baseline activity levels were calculated starting from 0.6 min as baseline activity levels were unstable before that time point. * $p < 0.05$, ** $p < 0.01$, Wilcoxon signed rank test. (S1 Data, Sheet 1C). (D) Circuit model of the RIS presynaptic regulatory network. Activating synaptic input is shown as green arrows, inhibitory synaptic input is shown as red arrows, and unclear synaptic input is shown as black arrows. Gap junctions are indicated as black connections. Neurons that are presynaptic to RIS present mostly activators. PVC is essential for lethargus-specific RIS activation. RIM can inhibit RIS through tyramine and FLP-18 and can activate RIS with glutamate. $\Delta F/F$, change of fluorescence over baseline; FLP-18, FMRF-Like Peptide 18; GCaMP, genetically encoded calcium indicator; n.s., not significant; PVC, Posterior Ventral cord neuron class name; RIM, Ring Interneuron M class name; RIS, Ring Interneuron S class name; SDQL, Posterior lateral interneuron class name—left cell.

<https://doi.org/10.1371/journal.pbio.3000361.g001>

larvae for most of the optogenetic experiments to dissect the circuit. As SDQL is born postembryonically and likely is not yet functional during the L1 stage, we used L4 larvae to assay its function [33]. We compared the effects of optogenetic stimulation outside and during lethargus, defined as the period prior to the molt during which the animals do not feed [34]. Before lethargus, we measured an activation of RIS upon depolarization of AVJ, CEP, and SDQL. During lethargus, the activation of CEP, PVC, and SDQL caused RIS activation (Fig 1B and S1A Fig).

All neurons showed consistent effects on RIS depolarization except RIM. RIM is known to play complex roles in controlling behavior and is involved in seemingly opposing behaviors. For example, specific RIM activation can trigger a reversal [35], whereas RIM inhibition has been suggested to be required for reversals through an alternative circuit [36]. We performed optogenetic depolarization experiments of RIM expressing ReaChR using 2 different promoters, the *tdc-1* promoter, which is known to express strongly, and the *gcy-13* promoter, which is known to express at a lower level [37]. Activation of RIM with channelrhodopsin expressed from the *tdc-1* promoter has previously been shown to cause reversals [35], and we observed that activation of RIM using ReaChR expressed from this promoter led to RIS inhibition (Fig 1B, RIM panel). The *tdc-1* promoter expresses strongly in RIM, but also weakly in RIC [38]. To test whether the inhibitory effect of *tdc-1* promoter-driven ReaChR expression on RIS was caused by RIC, we also specifically expressed ReaChR in RIC using the *tbh-1* promoter [38]. Specific RIC activation led to RIS activation rather than inhibition (S1B Fig). Therefore, the *tdc-1::ReaChR*-mediated RIS inhibition appears to stem from RIM activation. Activating RIM with the weaker *gcy-13* promoter did not cause any net effects on RIS when all trials were averaged (S1C Fig). Visual inspection of the individual trials, however, showed that RIM activation could either inhibit or activate RIS. We therefore sorted single trials for the *gcy-13* experiment into 2 classes, in which RIM either activated or inhibited RIS function (S1D Fig). The activation or inhibition of RIS by RIM was indistinguishable during the beginning or end of lethargus (S1E Fig).

To confirm that RIM can both activate and inhibit RIS, we tested whether activation and inhibition are mediated by different neurotransmitters. We tested the effects of RIM activation on RIS in mutants, which lack transmitters that are known to be expressed in RIM. The RIM neurons are well known to inhibit downstream neurons using tyramine, which requires the *tdc-1* gene [38], and also express neuropeptides (FMRF-Like Peptide 18 [FLP-18]) encoded by the *flp-18* gene [39]. To test whether RIM can inhibit RIS using these known transmitters, we analyzed mutant worms that lack functional *flp-18* and *tdc-1*. Individual inactivation of *flp-18* and *tdc-1* reduced—and double mutation abolished—the inhibition of RIS by RIM (S2 Fig). Therefore, the transmitters tyramine and FLP-18 are together responsible for RIS inhibition by RIM. We next tested activation of RIS by RIM in *eat-4(ky5)* mutant larvae, which lack glutamatergic signaling in many neurons, including RIM [40,41]. RIS activation by RIM activation was completely gone in *eat-4(ky5)* mutant larvae (S3 Fig, we used L4 larvae for this assay as the response was more robust). Therefore, glutamate is required for RIS activation by RIM. Together, these results suggest that RIM can act both as an activator as well as an inhibitor of RIS by employing different neurotransmitters, with weaker activation allowing for RIS activation and stronger activation favoring inhibition.

The majority of synaptic inputs into RIS that we studied had activating effects; the sole inhibitory effect was observed after strong activation of RIM, whereas weaker RIM activation could also lead to RIS activation. The CEP, URY, and SDQL neurons present sensory receptors and might play a role in activating RIS in response to stimulation. For example, CEP might activate RIS as part of the basal slowing response [42,43]. The PVCs appeared to be strong activators of RIS specifically during lethargus. This suggests either that the PVC-to-RIS

connection might be specific to lethargus or that it has not yet matured during the mid-L1 stage. We therefore repeated the experiment and activated PVC in L2 larvae. PVC activated RIS both during and outside of lethargus, but the activation during lethargus was much stronger, suggesting that the activation of RIS by PVC is strongly enhanced during lethargus (S4 Fig).

To find out which presynaptic neurons are required for inhibition or activation of RIS during lethargus, we tested the effect of optogenetic inhibition of the presynaptic neurons on RIS activation. We used ArchT (archaerhodopsin from *Halorubrum* strain TP009), which hyperpolarizes neurons by pumping protons out of the cell [44,45]. As earlier, we verified the expression of ArchT in neurons of interest by using an mKate2-tagged version. As in the ReaChR experiments, we specifically illuminated each presynaptic neuron class and quantified RIS activation using calcium imaging. Before lethargus, inhibition of AVJ and PVC led to an inhibition of RIS, whereas inhibition of the other neurons tested had no acute statistically significant effect on RIS (optogenetic RIM hyperpolarization using the stronger *tdc-1* promoter in worms outside of lethargus showed a tendency to inhibit RIS function [$p = 0.0539$; $N = 11$ animals], whereas the weaker *gcy-13* promoter had no detectable effect). During lethargus, optogenetic inhibition of PVC and RIM (using the stronger *tdc-1* promoter) led to significant RIS inhibition, whereas there was no effect seen for the other neurons (Fig 1C and S5A Fig; inhibition of RIM using the weaker *gcy-13* promoter only produced a tendency but no statistically significant net effect, S5B and S5C Fig).

Absence of an effect of optogenetic inhibition of presynaptic neurons could mean either that these neurons are not required for RIS activation, that the inhibition was not strong enough, or that they may act redundantly (we did not find any evidence for redundancy, at least for CEP and URY, S5D Fig). Our optogenetic analysis revealed a complex set of presynaptic inputs for regulation of RIS activity (Fig 1D). The optogenetic depolarization experiments suggest that CEP, PVC, RIM, and SDQL present the most potent presynaptic activators of RIS. The capacity of PVC to activate RIS is strongly increased during lethargus, indicating that this neuron is involved in the lethargus-specific activation of RIS. The optogenetic hyperpolarization experiments suggest that PVC and RIM are essential presynaptic activators of RIS during lethargus. Therefore, we focused our analysis on PVC and RIM neurons.

PVC becomes resistant to inhibition during lethargus

Neuronal activation and silencing experiments revealed PVC as a main activator of RIS. These results predict that neuronal activity of PVC should correlate with RIS activation and sleep bouts. To test for such correlation, we measured the activity of both neurons simultaneously. Because the calcium transients observable in PVC are typically small [46] and could not be detected in our assays in mobile worms (data not shown), we immobilized the larvae and used RIS activation as a proxy for sleep bouts. We extracted both RIS and PVC activity and aligned all data to the RIS activation maxima. This analysis showed that PVC activated approximately 1 min earlier than RIS and reached its maximum activation approximately 1.5 min earlier than RIS. PVC activity decreased slowly during the RIS transient (Fig 2A). This result is consistent with a role for PVC in promoting RIS depolarization.

PVC inhibition reduced RIS activity in immobilized animals, but it is unclear how PVC inhibition affects behavior. To be able to test the effects of PVC inhibition on behavior without affecting the other command interneurons, we chose a more specific promoter for expression in PVC from single-cell RNA sequencing data. There was no gene in the available datasets that was expressed only in the cluster of cells containing PVC, but the previously uncharacterized gene *zk673.11* was expressed specifically in PVC and in only a few other neurons excluding

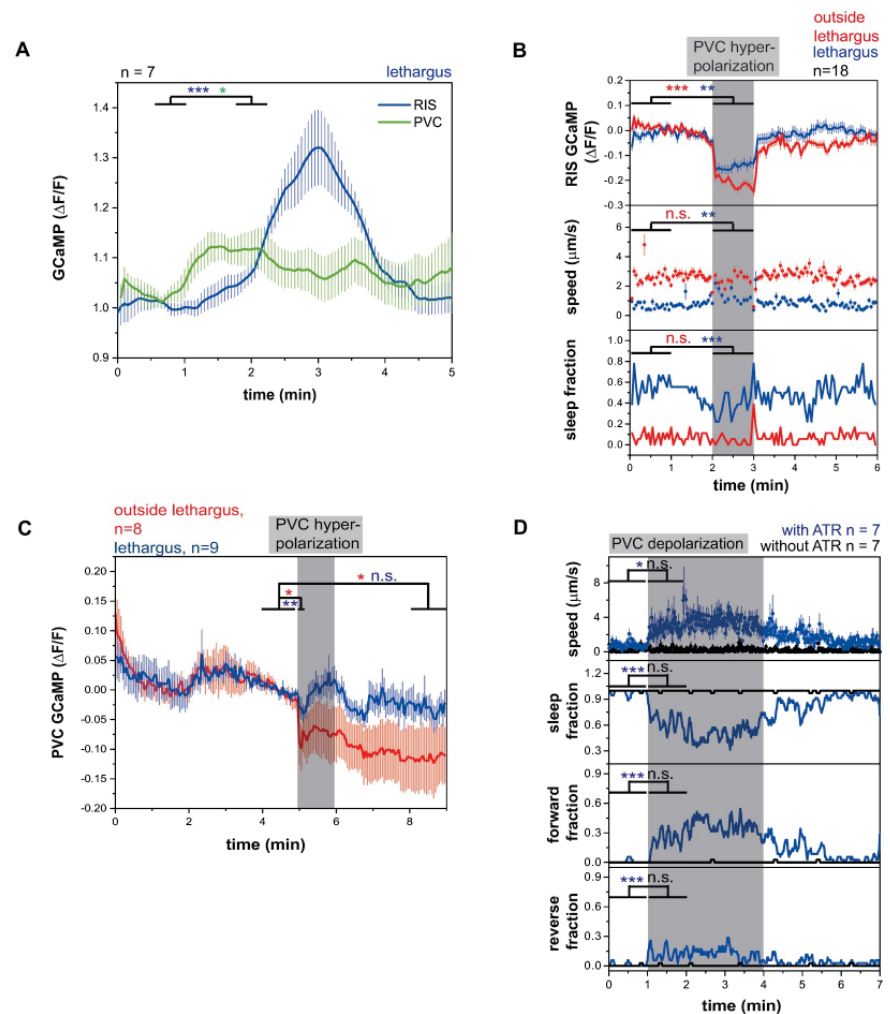


Fig 2. PVC is an RIS activator that becomes resistant to inhibition during lethargus, but PVC activation is not sufficient for sleep induction. (A) Simultaneous PVC and RIS GCaMP traces aligned to RIS peaks in fixed L1 lethargus worms. PVC activates before the RIS peak and stays active until the peak. $*p < 0.05$, $**p < 0.01$, Wilcoxon signed rank test. (S1 Data, Sheet 2A). (B) PVC hyperpolarization inactivates RIS and induces behavioral activity. PVC hyperpolarization was performed by expressing ArchT under the *zk637.11* promoter. In contrast to the *nmr-1* promoter, the *zk637.11* promoter lacks expression in head command interneurons. $**p < 0.01$, $***p < 0.001$, Wilcoxon signed rank test for GCaMP and speed, Fisher's exact test for sleep fraction. (S1 Data, Sheet 2B). (C) During lethargus, PVC becomes resistant to inhibition. Outside of lethargus, its inhibition is stronger and continues beyond the end of optogenetic stimulation. During lethargus, PVC activity levels return back to baseline already during the stimulation period. $*p < 0.05$, $**p < 0.01$, Wilcoxon signed rank test. (S1 Data, Sheet 2C). (D) PVC activation translates into mostly a forward mobilization in L1 lethargus. $*p < 0.05$, $***p < 0.001$, Wilcoxon signed rank test for Speed. Fisher's exact test for fraction of direction. (S1 Data, Sheet 2D). ArchT, archaerhodopsin from *Halorubrum* strain TP009; ATR, all-trans-retinal; $\Delta F/F$, change of fluorescence over baseline; GCaMP, genetically encoded calcium indicator; n.s., not significant; PVC, Posterior Ventral cord neuron class name; RIS, Ring Interneuron S class name.

<https://doi.org/10.1371/journal.pbio.3000361.g002>

other command interneurons [47,48] (personal communication from J. Packard to H. Bringmann; S6 Fig). Hyperpolarization of PVC using ArchT driven by the *zk673.11* promoter led to an acute inhibition of RIS, an increase in locomotion, and a reduction of sleep (Fig 2B). Hyperpolarization of PVC using ArchT also strongly inhibited RIS outside of lethargus. This experiment confirmed the role of the PVCs in activating RIS.

Hyperpolarization of PVC outside of lethargus appeared to have a stronger and longer-lasting effect on RIS inhibition compared with during lethargus (Figs 1C and 2B). This is surprising because PVC is a stronger activator of RIS during lethargus in the optogenetic activation experiments (Fig 1B). This effect could be explained if PVC responded more severely to inhibition outside of lethargus. We tested this idea by inhibiting PVC using ArchT and green light and simultaneously imaged PVC activity. PVC hyperpolarization was stronger in worms outside of lethargus, and PVC remained inhibited after the optogenetic manipulation. During lethargus, PVC was only weakly inhibited at the beginning of optogenetic stimulation and returned to baseline levels already during the stimulation (Fig 2C). We also tested whether optogenetic excitability of PVC was modulated during lethargus but could not find any differences in excitability of PVC during or outside of lethargus (S7A Fig). Thus, PVC is more susceptible to inhibition outside of lethargus but becomes resistant to inhibition during lethargus. This effect can explain the stronger hyperpolarization of RIS during PVC inhibition outside of lethargus, and this effect likely presents an important modulation of the circuit to favor PVC activation and thus RIS activation during lethargus.

PVC is known to promote forward movement upon posterior mechanical stimulation, and optogenetic stimulation of PVC in adults has been shown to promote forward locomotion [49,50]. Our data showed that PVC also activates the RIS neuron, and consistent with this observation, mechanical stimulation caused RIS activation (S7B Fig). This suggests that PVC activates RIS to modulate forward locomotion speed and to promote sleep. However, it is unclear how PVC can promote forward motion and sleep, as these are two seemingly opposing behaviors. We therefore tested whether optogenetic stimulation of PVC in larvae induces sleep behavior. We activated PVC using *nmr-1::ReaChR* in mobile L1 larvae during lethargus and specifically illuminated the tail of the animal, which contains the cell bodies of the PVC neurons but not the other *nmr-1*-expressing neurons. We quantified the speed as well as the direction of movement of the worm. During PVC activation during lethargus, the worms visibly accelerated movement and mostly crawled forward, but we could not see induction of sleep behavior during optogenetic stimulation (Fig 2D). Consistent with this finding, optogenetic PVC activation during and before lethargus always led to the activation of AVB interneurons, which are known to be premotor neurons required for forward locomotion [49] (S7C and S7D Fig). Together, these experiments showed that PVC activates prior to RIS and is required for RIS activation. However, its activation alone does not seem to be sufficient to induce sleep behavior.

RIS and PVC activate each other forming a positive feedback loop

PVC presents a major activator of RIS, but how a forward command interneuron can cause strong and state-specific activation of the RIS neuron during sleep bouts is not clear. We therefore tested how optogenetic RIS activation affects PVC activity. We selectively activated RIS using ReaChR and measured calcium activity in PVC in immobilized animals. Upon RIS stimulation, PVC immediately displayed unexpectedly strong calcium transients, which were slightly stronger during lethargus (Fig 3A and S8A Fig). These results show that PVC and RIS activate each other, thus forming a positive feedback loop. The sleep-inducing RIS neuron has so far only been shown to inhibit other neurons, making PVC the first neuron that is not

inhibited but is activated by RIS. For example, command interneurons such as AVE and AVA and other neurons are not activated but are inhibited by RIS [25].

RIS induces sleep through the release of neuropeptides with the major sleep-inducing neuropeptides encoded by the *flp-11* gene [51]. To test whether FLP-11 neuropeptides are required for RIS-induced PVC activation, we repeated the optogenetic RIS activation with simultaneous PVC calcium measurement in an *flp-11* deletion mutant. RIS-induced PVC activation was almost completely abolished in the *flp-11* deletion (reduction of transient maximum by 79% during lethargus), indicating that FLP-11 neuropeptides are required for RIS-induced PVC activation (Fig 3B).

While PVC is presynaptic to RIS, RIS is not presynaptic to PVC [28,32]. The activation of PVC by RIS could involve diffusional mechanisms or could be indirect through other neurons, perhaps mediated by the inhibition of a PVC inhibitor such as AVA/AVD/AVE. RIS has been shown to inhibit AVA/AVE [25], and RIS is presynaptic to AVE [28,32], suggesting that PVC activation involves inhibition of AVE. We therefore repeated RIS activation and PVC calcium imaging in a strain in which AVE was impaired through expression of tetanus toxin [52]. The initial PVC activation maximum after AVE impairment was reduced by 43% during lethargus, but subsequent PVC activity was increased (Fig 3C–3E). AVE is connected to other reverse command interneurons, which collectively inhibit PVC [28,53]. This circuit design suggests that AVE might play a dual role in controlling RIS activity. It should have a positive role in mediating activation of PVC through RIS and thus could promote the feedback loop, but it should also have an inhibiting role by promoting PVC inhibition. To test for a role of the arousal neurons AVE and AVA in sleep, we inhibited AVE with tetanus toxin [52] and AVA using HisCl (Histamine-gated Chloride channel) [54] and quantified sleep amount. Whereas we could not find any effect of AVA impairment on sleep amount, AVE impairment led to an average increase of sleep by 42% (Fig 3F). Together, these data suggest that PVC and RIS rely on positive feedback for their activation that involves the release of FLP-11 neuropeptides and inhibition of PVC by AVE.

If depolarization of RIS activates PVC, what consequences does hyperpolarization of RIS have on PVC activity? To answer this question, we measured the response of PVC to RIS inhibition. We hyperpolarized RIS optogenetically for 1 min using ArchT and measured the activity of PVC. Interestingly, PVC showed a small but significant activity increase during RIS inhibition, an effect that was increased during lethargus (S8B Fig). The disinhibition of PVC by RIS inactivation is likely not direct and may reflect a general increase in neuronal and behavioral activity that is caused by RIS inhibition and that extends to the PVC neurons. Because PVC is a major activator of RIS, its disinhibition could be part of a homeostatic feedback regulation.

Our results suggest that there is a positive feedback from sleep induction onto RIS activation and that full RIS activation is only possible when sleep is successfully induced, explaining the strong correlation of RIS depolarization and sleep-bout induction [27]. This model would predict that RIS transients are dampened if RIS is not able to induce sleep bouts. To test this idea, we analyzed RIS calcium transients in *aptf-1(-)* mutant worms in which RIS still shows depolarization transients during lethargus but cannot efficiently induce quiescence [25,51]. In *aptf-1(-)* mutant animals, calcium transient maxima were reduced by about 35% (Fig 3G–3I). A major function of APTF-1 (Activating enhancer binding Protein 2 Transcription Factor 1) is the expression of FLP-11 neuropeptides that are required for quiescence induction [51]. To test whether FLP-11 neuropeptides play an essential role in shaping RIS transients, we measured RIS calcium transients in mutant worms carrying a deletion of *flp-11*. These mutant animals showed only a reduced number of long RIS transients that were of reduced size (Fig 3G–3I). *flp-11(-)* showed, however, many short RIS transients (S8C–S8F Fig) that were not

associated with sleep bouts but may reflect attempts to induce sleep bouts. These results are consistent with the idea that sleep induction is a self-enforcing process in which RIS-mediated inhibition of brain activity through FLP-11 neuropeptides promotes long RIS calcium transients (Fig 3).

We next tested what feedback interaction exists between RIM and RIS neurons. We optogenetically depolarized or hyperpolarized RIS and measured RIM activity. RIS activation did not significantly change RIM activity, but there was a small inhibitory trend (S8G Fig). RIS inhibition led to an activation of RIM (S8H Fig). These results show that, while RIM can activate as well as inhibit RIS, RIS is an inhibitor of RIM.

RIM can activate RIS, but its activation is not sufficient for sleep induction

A second important activator of RIS is RIM. We therefore asked whether RIM, similar to PVC, also is active prior to RIS depolarization and sleep bouts. We measured RIM activity by imaging GCaMP in moving worms. All sleep bouts were extracted, and RIM activity was aligned to sleep-bout onset. Averaged RIM activity peaked approximately 30 s before the beginning of the sleep bout (Fig 4A). This finding is consistent with a function for RIM in RIS activation. We then asked whether RIM is required for sleep induction. We ablated RIM through expression of *egl-1* under the *tdc-1* promoter. We quantified lethargus sleep in RIM-ablated worms. RIM-ablated larvae showed a normal fraction of sleep, a slightly increased frequency of sleep bouts, and a normal length of sleep bouts (Fig 4B–4D). In analogy to the PVC experiments, we analyzed the effect of optogenetic RIM depolarization on behavior. We first tested behavior caused by activation of RIM with ReaChR driven by the strong *tdc-1* promoter on the locomotion of worms. Consistent with previous findings [35] and our observation that RIS is inhibited under these conditions, RIM activation during lethargus caused mobilization, and larvae crawled mostly backwards (Fig 4E). We next tested for the effects of weaker RIM activation using the *gcy-13* promoter. Activation of RIM caused increased mobility when RIS was inhibited. In trials in which RIM activation led to RIS activation, there was no significant change of speed of the worms (S1D Fig). We next wanted to test whether excitability of RIM is altered during the lethargus state. We therefore activated RIM strongly using the *tdc-1* promoter and measured RIM activity. Outside of lethargus, RIM was strongly excited. During lethargus, however, excitability was strongly reduced (Fig 4F and 4G). In summary, RIM activation is not sufficient to induce sleep. RIM could, however, contribute to strong RIS activation and sleep induction by acting in concert with other neurons. Reduced excitability of RIM during lethargus could favor the activating effect of RIM on RIS while dampening the inhibiting effects of RIM on RIS.

Interneurons regulating locomotion act in concert to activate RIS

Separate activation of PVC or RIM neurons caused moderate RIS activation but not the strong activation of RIS that is typically associated with sleep bouts. Thus, hypothetically, multiple neurons act in concert to cause strong RIS activation. Our earlier presynaptic neuron analysis suggests that this hypothetical set of neurons should include PVC and RIM interneurons but could also include additional neurons. Our analysis of RIM and PVC points to neurons of the command interneuron circuit for RIS activation, and thus we tested the effects of ablation of a large fraction of the interneurons controlling locomotion. The *nmr-1* promoter expresses in AVA, AVE, AVD, and PVC command interneurons as well as in second-layer RIM neurons [55]. We used a strain that ablates these locomotion-controlling interneurons by expressing the pro-apoptosis regulator ICE (Caspase-1/Interleukin-1 converting enzyme) from the *nmr-1* promoter [55] and measured sleep and RIS activation. Command interneuron ablation

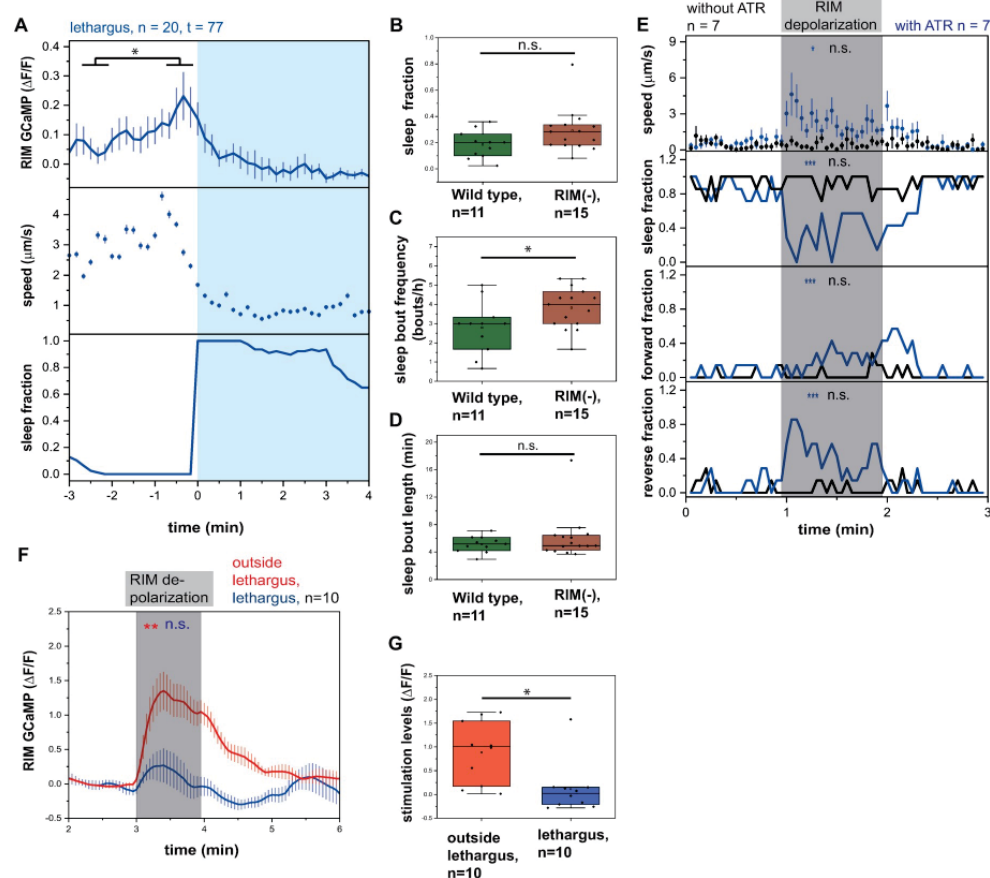


Fig 4. RIM activity peaks prior to sleep bouts, but RIM activation is not sufficient for sleep induction. (A) RIM activates prior to sleep bouts. $*p < 0.05$, Wilcoxon signed rank test (S1 Data, Sheet 4A). (B–D) RIM-ablated worms have an increased sleep-bout frequency, while the sleep fraction and bout duration are not significantly changed during L1 lethargus. RIM was genetically ablated by expressing *egl-1* under the *tdc-1* promoter. $*p < 0.05$, Kolmogorov-Smirnov test (S1 Data, Sheet 4B–D). (E) RIM depolarization leads to increased mobility and reverse motion. $*p < 0.05$, $***p < 0.001$, Wilcoxon signed rank test for speed. Fisher's exact test for fraction of direction (S1 Data, Sheet 4E). (F–G) During lethargus, RIM becomes resistant to activation. RIM was optogenetically activated using ReaChR expressed under the *tdc-1* promoter. Outside of lethargus, its activation is stronger (F). Activity levels during the stimulation period were quantified by subtracting baseline activity levels from levels during the stimulation period (G). $*p < 0.05$, $**p < 0.01$, Wilcoxon signed rank test for GCaMP and Kolmogorov-Smirnov test for quantification of stimulation levels (S1 Data, Sheet 4F–G). ATR, all-trans-retinal; $\Delta F/F$, change of fluorescence over baseline; GCaMP, genetically encoded calcium indicator; n.s., not significant; ReaChR, red-activatable channelrhodopsin; RIM, Ring Interneuron M class name.

<https://doi.org/10.1371/journal.pbio.3000361.g004>

reduced sleep bouts during lethargus by about 76% (Fig 5A), and RIS activation was reduced by 63% (S9A Fig). The movement of command interneuron-ablated worms also was slower (S9B Fig). Quiescence bouts did not occur at the beginning of the lethargus phase as defined by cessation of feeding and were only observed around the middle of the lethargus phase (S9C Fig). An independently generated strain that ablates command interneurons using *egl-1* expression—also by using the *nmr-1* promoter—caused a reduction of sleep by 81% (Fig 5A).

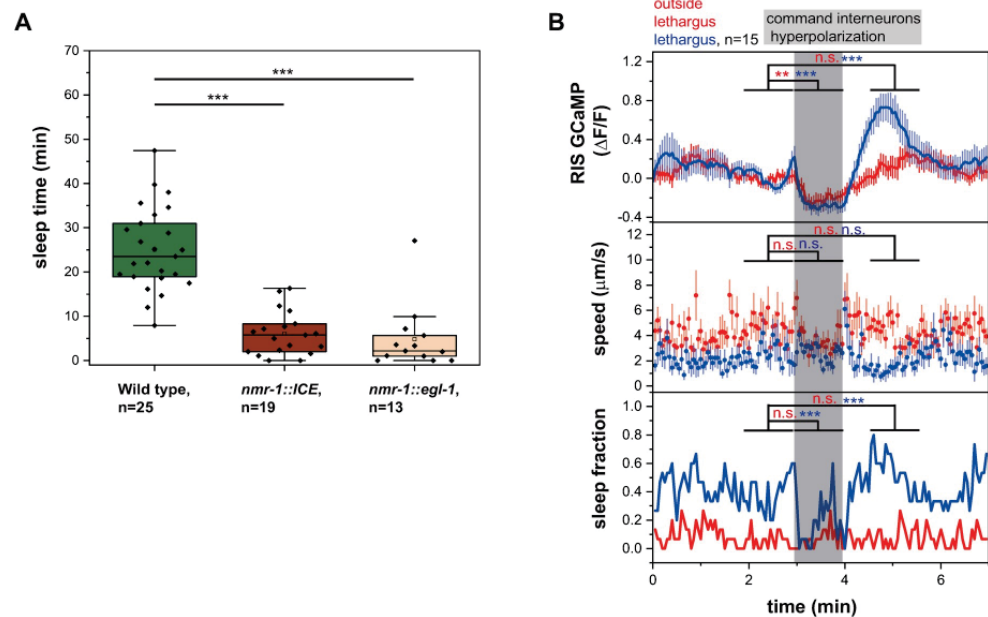


Fig 5. The locomotion interneuron circuit controls RIS activation and sleep. (A) Command interneurons are responsible for the majority of sleep. Command interneurons were genetically ablated by expressing ICE or *egl-1* under the *nmr-1* promoter. Command interneurons-ablated worms display a massive loss-of-sleep phenotype. $***p < 0.001$, Welch test (S1 Data, Sheet 5A). (B) Hyperpolarization of command interneurons causes RIS inhibition and suppresses sleep. During lethargus, the hyperpolarization is followed by a strong post-stimulation activation of RIS. $**p < 0.01$, $***p < 0.001$, Wilcoxon signed rank test for GCaMP and speed, Fisher's exact test for sleep fraction (S1 Data, Sheet 5B). $\Delta F/F$, change of fluorescence over baseline; GCaMP, genetically encoded calcium indicator; ICE, Caspase-1/Interleukin-1 converting enzyme; n.s., not significant; RIS, Ring interneuron S class name.

<https://doi.org/10.1371/journal.pbio.3000361.g005>

Next, we wanted to test conditional loss of function of the command interneuron circuit on RIS activity. We expressed ArchT broadly in locomotion-controlling interneurons by using the *nmr-1* promoter. We then inhibited all command interneurons using green light and simultaneously imaged the activity of RIS. Inhibition of *nmr-1*-expressing neurons strongly inhibited RIS both outside and during lethargus. Interestingly, there was a strong post-stimulus activation of RIS, which was strongly increased only during lethargus. This activation peaked at approximately 170% of the RIS baseline. Sleep was inhibited by command interneuron inhibition, and worms reached mobility speeds similar to those outside of lethargus (Fig 5B). Mosaic analysis of an extrachromosomal array carrying the *nmr-1::ArchT* transgene revealed that RIS was partially inhibited when ArchT was expressed in head neurons but not in PVC and that the effect of inhibition was substantially stronger when ArchT was not only expressed in head neurons but also expressed in PVC (S9D and S9E Fig). This experiment showed that multiple interneurons act in concert to activate RIS and induce sleep. Among the *nmr-1*-expressing interneurons, only RIM and PVC are presynaptic to RIS [28,32]. However, additional reverse command interneurons could also contribute to RIS regulation through indirect mechanisms.

Because the command interneuron circuit is controlled by glutamatergic signaling [55,56] and because RIM activation of RIS requires glutamate (S3 Fig), we also analyzed the sleep behavior of *eat-4(ky5)* mutant larvae that have impaired glutamatergic neurotransmission. In

eat-4(ky5) mutant larvae, sleep-bout duration was significantly reduced, whereas sleep bouts occurred with normal frequency. This indicates that glutamate signaling might play a role in the maintenance but not in the initiation of sleep bouts (S10A–S10D Fig). Consistent with these findings, glutamate signaling also plays a role in the maintenance of NREM (non-Rapid Eye Movement) sleep in mice [13]. *nmr-1(ak4)* glutamate receptor mutant larvae only displayed slightly reduced RIS activation transients, which indicates that additional glutamate receptors are required for sleep induction (S10E–S10I Fig). Together, these mutant phenotypes support the view that excitatory neurotransmitter systems that are associated with locomotion are important for RIS activation.

RIS inhibition causes homeostatic rebound activation

The design of the sleep circuit suggests an intimate mutual control mechanism of RIS and command interneurons that could allow homeostatic control of sleep. Arousing stimulation is known to inhibit sleep-active neurons and to increase subsequent sleep [22,23,25,27]. Consistent with these published data, we observed that the maximum RIS GCaMP intensity increased logarithmically with the length of the preceding motion bout during lethargus (S11A Fig). We thus hypothesized that stimulation inhibits RIS and leads to its subsequent depolarization, forming a homeostat that allows maintaining or reinstating sleep bouts. We tested this hypothesis by arousing the worms with a blue light stimulus (Fig 6A and 6B). During the stimulus, worms mobilized, and sleep was inhibited. In some of the trials, worms went back to sleep promptly after the stimulation and decreased their motion speed again within 3 min. Because worms did not remain mobile after the stimulation, we classified these trials as “nonmobilizing.” In these nonmobilizing trials, RIS showed a post-stimulus activation, which was 34% stronger than the baseline activity. RIS activation correlated with a significantly increased fraction of sleep. In other trials during lethargus, the worms stayed mobile for at least 3 min after stimulation and did not go back to sleep. Because worms remained mobile after the stimulation, we classified these trials as “mobilizing.” In these mobilizing trials, RIS stayed inhibited and was 16% less active than the baseline before stimulation (Fig 6A). To measure global neuronal activity during the blue-light stimulation experiment, we imaged worms that expressed pan-neuronal GCaMP [57]. Trials were again divided into mobilizing and nonmobilizing trials during lethargus depending on the mobilization status after the stimulus. Nonmobilizing trials showed a global neuronal inhibition that was 93% of the baseline activity (Fig 6B). These experiments show that noxious blue-light stimulation inhibits sleep and RIS and causes a reactivation of RIS when the system returns to sleep.

In normal sleep and in the sensory stimulation experiment, periods of inactivity of RIS were always followed by periods of RIS activation. This suggested that inhibition of RIS causes its subsequent reactivation. We tested this hypothesis by optogenetically hyperpolarizing RIS and following its activity using calcium imaging. We inhibited RIS directly for 60 s by expressing the light-driven proton pump ArchT specifically in this neuron and used green light illumination to activate ArchT. We followed RIS calcium activity using GCaMP during the experiment and quantified behavior. Optogenetic hyperpolarization of RIS led to a decrease in intracellular calcium and increased behavioral activity. Approximately 1 min after the end of the inhibition, RIS showed a rebound activation transient during which calcium activity levels increased strongly and rose well above baseline levels, concomitant with a decrease in behavioral activity. Overall brain activity measurements showed that behavioral activity and brain activity correlated throughout the experiment (Fig 6C). Rebound activation was observed neither following PVC nor following RIM inhibition (Fig 2C and S11B Fig), suggesting that rebound activation is specific to RIS and is not a general property of all neurons [58].

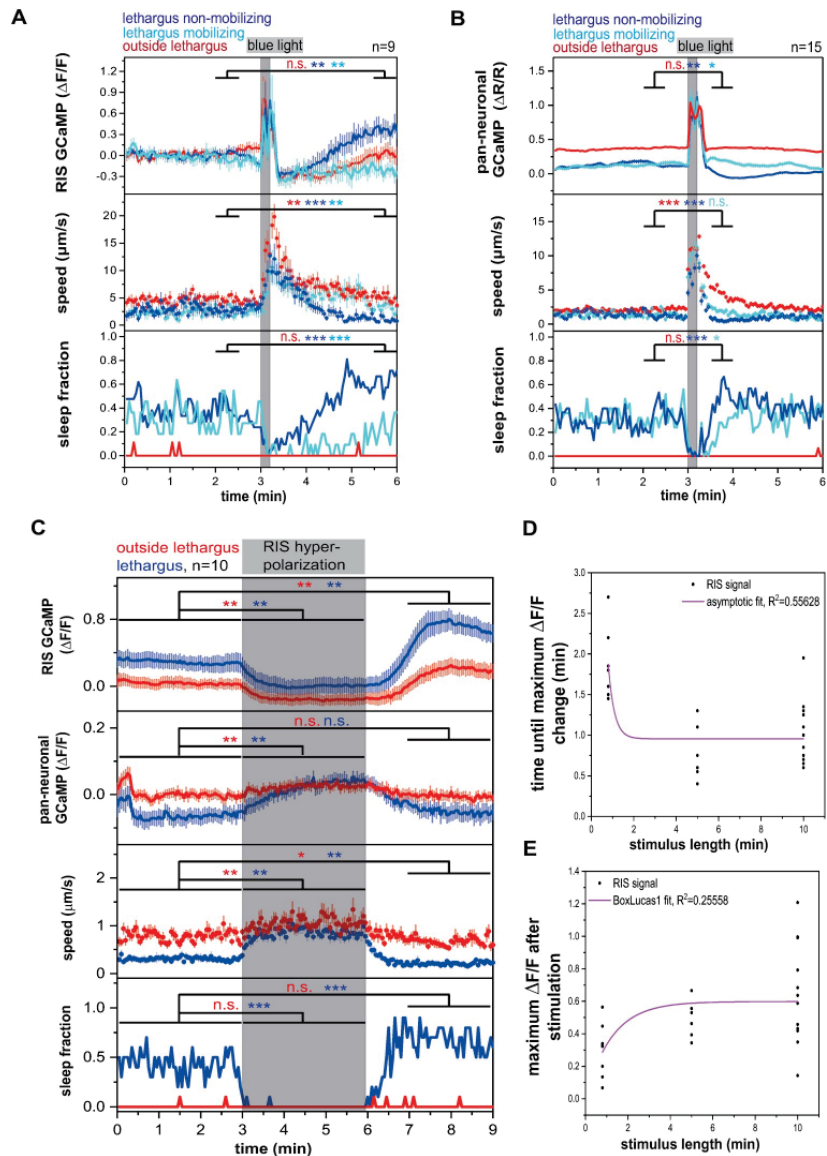


Fig 6. RIS inhibition causes homeostatic rebound activation. (A–B) A blue light stimulus leads to awakening and mobilization of *C. elegans*. Worms that go back to sleep after the stimulus show an activation rebound: pan-neuronal inhibition below baseline levels and RIS activation above baseline levels; “lethargus mobilizing” refers to animals that stayed awake and active during the post-stimulus time; “lethargus nonmobilizing” refers to animals that went back to sleep after the stimulation. * $p < 0.05$, ** $p < 0.01$, *** $p < 0.001$, Wilcoxon signed rank test for GCaMP and speed, Fisher’s exact test for sleep fraction (S1 Data, Sheet 6A and 6B). (C) RIS shows rebound activation following hyperpolarization. Behavioral and brain activity measurements correlate throughout the whole experiment. * $p < 0.05$, ** $p < 0.01$, *** $p < 0.001$, Wilcoxon signed rank test for GCaMP and speed, Fisher’s exact test for sleep fraction (S1 Data, Sheet 6C). (D–E) Dose-response curve of optogenetic RIS hyperpolarization with different stimulus lengths. RIS activation rebound transients saturate with increasing length of inhibition. Worms not showing a rebound activation transient after RIS optogenetic hyperpolarization were excluded from the analysis. Numbers of worms not responding were as follows: (1) In experiments in which RIS was optogenetically inhibited for 48 s, all worms showed an RIS

rebound activation transient. (2) In experiments in which RIS was optogenetically inhibited for 5 min, 1 out of 7 worms did not show a RIS rebound activation transient. (3) In experiments in which RIS was optogenetically inhibited for 10 min, 1 out of 13 worms did not show an RIS rebound activation transient. Curve in D was fitted as an asymptotic function, and curve in E was fitted as a BoxLucas1 function (S1 Data, Sheet 6D, E). $\Delta F/F$, fluorescence change over baseline; GCaMP, genetically encoded calcium sensor; n.s., not significant; R, fluorescence of GCaMP divided by fluorescence of mKate2; RIS, Ring Interneuron S class name.

<https://doi.org/10.1371/journal.pbio.3000361.g006>

Strikingly, while the rebound transient was also measurable outside of lethargus, the strength of the RIS rebound depolarization was 3-fold stronger during lethargus than before lethargus, indicating that the propensity for RIS rebound activation is strongly increased during lethargus.

To test whether rebound activation of RIS mediates acute or chronic homeostasis, we tested whether the strength of the rebound activation is a function of length of prior inhibition. For this experiment, we increased the length of the RIS inhibition and quantified the time it took after the end of the stimulation until the rebound transient started as well as the peak maximum of the rebound. After inhibiting RIS for 5 min, the rebound initiated immediately after the end of the stimulation and the maximum that was reached exceeded that observed after about 1 min of RIS stimulation. Inhibiting RIS for 10 min did not further increase the occurrence or strength of the rebound transient. These results show that RIS activation rebound transients rapidly saturate with increasing length of inhibition (Fig 6D and 6E and S11C–S11E Fig). Thus, RIS shows a rebound activation following inhibition. The rebound activation presents the translation of RIS inhibition into subsequently increased RIS activity and thus sleep induction. Rebound activation of RIS does not seem to constitute a chronic integrator of wake time but presents an acute homeostatic regulatory phenomenon to induce or reinstate sleep bouts.

Rebound activation of RIS could present a cell-intrinsic property or could be generated by a neural circuit. To discriminate between these hypotheses, we measured rebound activation in *unc-13(s69)* mutant animals in which synaptic signaling is globally impaired [59], or in worms that express tetanus toxin [60] specifically in RIS to abrogate synaptic transmission specifically in this neuron. Rebound activation of RIS was abolished in RIS::tetanus toxin (S11F–S11G Fig) as well as *unc-13(s69)* worms (S11F and S11H Fig). These results indicate that rebound activation of RIS is a property of the neuronal network.

In analogy to the activation rebound seen after optogenetic RIS inhibition, optogenetic RIS activation might cause a negative rebound, i.e., an inhibition of RIS inhibition below baseline levels following its optogenetic activation. Indeed, we observed such an effect. Interestingly, the negative rebound was 3-fold stronger during lethargus compared to outside of lethargus (S11I Fig). However, such a negative rebound was also present in other neurons such as PVC (S7A Fig), making it difficult to judge whether this effect is part of a specific sleep homeostatic system or rather a general response of neurons to strong depolarization [58]. In summary, RIS activity is homeostatically regulated, with its inhibition causing its reactivation. This rebound activation is strongly increased during lethargus and likely is required for inducing or reinstating sleep.

Modest dampening of brain arousal occurs upstream of RIS

Our results demonstrate that the command interneuron circuit, including PVC, plays a major role in activating RIS involving self-enforcing positive feedback, resulting in strong RIS activation and thus sleep induction. RIS calcium transients are small during development outside of lethargus, whereas transients are high during lethargus. What determines that RIS calcium transients are limited outside of lethargus but promoted during lethargus? As an important

principle of command interneuron control, forward and reverse command interneurons inhibit each other to allow discrete forward and reverse locomotion states. The AVA/AVD/AVE/RIM interneurons initiate reverse locomotion by activating premotor interneurons while inhibiting the forward command circuit including AVB/PVC. By contrast, during forward movement, reverse command interneurons are inhibited [49,56].

Small changes in arousal and activity of the command interneurons can change the equilibrium of forward and reverse command interneurons [55]. Hyperactive mutants suppress sleep across species, including *C. elegans* [61–68]. Many arousal cues trigger backwards escape movements and inhibit RIS [25,27,69]. Thus, previous studies on the command interneuron circuit together with our results suggest that arousal inhibits RIS through inhibiting PVC. This model of RIS activation would predict that there are changes during lethargus that are upstream of RIS activity that change the properties of the command circuit, leading to increased PVC and thus RIS activation.

We reasoned that it should be possible to measure these changes that occur in command interneuron activity upstream of RIS by characterizing neural activity and behavior in *aptf-1(-)* mutant worms. We quantified behavior and command interneuron calcium levels across lethargus in *aptf-1(-)* mutant worms. Wild-type animals showed successive sleep bouts and a 72% reduction in locomotion speed during lethargus. By contrast, *aptf-1(-)* mutant animals almost never showed quiescence bouts (Fig 3I), but nevertheless, locomotion speed was decreased by 20% during the lethargus phase (Fig 7). Consistent with the behavioral activity reduction, there was a significant reduction of command interneuron activity during lethargus also in *aptf-1(-)* mutant animals (Fig 7 and S12 Fig). To further characterize the neuronal changes upstream of RIS-mediated sleep induction, we imaged the activity of RIM during lethargus in *aptf-1(-)* mutants. In wild-type animals, RIM regularly showed activation transients before lethargus but did not show many transients during lethargus. RIM showed not only a change in transient frequency across the lethargus cycle but also a reduction in baseline calcium activity. In *aptf-1(-)* mutant worms, RIM continued showing calcium transients during lethargus, indicating that RIS inhibits calcium transients in RIM during sleep bouts. However, reduction of baseline calcium activity was preserved in *aptf-1(-)*, indicating that RIM activity is dampened during lethargus independently of RIS at the level of baseline calcium activity. Together, these experiments indicate that a dampening of behavioral and neural baseline activity that is independent of RIS occurs during lethargus. This neuronal baseline and behavioral dampening itself appears not to be sufficient to constitute normal sleep bouts but could hypothetically lead to an activity change and decreased mutual inhibition in command interneurons, thus promoting sleep induction [55,70].

An arousing stimulus inhibits RIS through RIM

Arousal plays a major role in inhibiting sleep, but the circuits that mediate the effect of arousing stimuli on RIS inhibition are not well understood. We therefore studied the circuit by which stimulation of a nociceptor, the ASH neurons, leads to a reverse escape response and inhibition of RIS [71]. We optogenetically stimulated ASH using ReaChR and green light and followed RIS and RIM activities. ASH activation led to a strong activation of the RIM neuron and triggered a backwards response as previously described [35,71]. Simultaneously, RIS was inhibited (Fig 8A). RIM can inhibit PVC through reverse interneurons that it synchronizes [49,72]. Furthermore, strong RIM activation can inhibit RIS more directly. To test whether ASH indirectly inhibits RIS through RIM, we ablated RIM genetically by expression of *egl-1* from the *tdc-1* promoter [35,38] and repeated the optogenetic stimulation of ASH. In RIM-ablated L4 animals, activation of ASH caused the opposite effect on RIS activity. Instead of

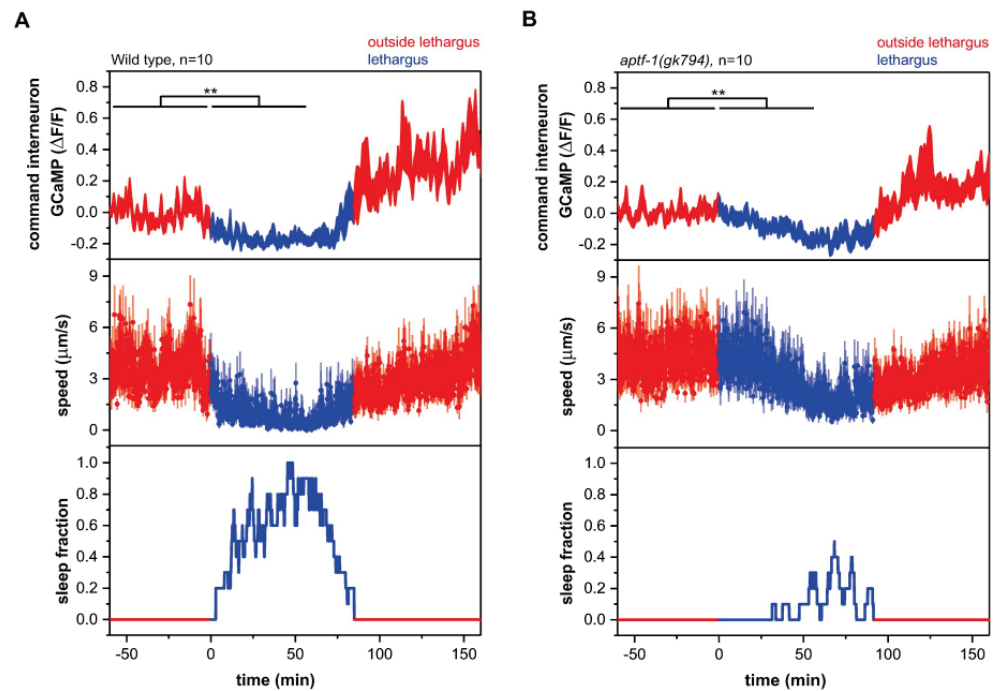


Fig 7. The dampening of neural and behavioral baseline activity levels during lethargus is independent of RIS function. Reduction of command interneuron activity levels during lethargus occurs in wild-type worms and *aplf-1(gk794)* mutants. In the wild-type condition, activity levels are reduced to -0.16 ± 0.02 . In the mutant condition, activity levels are reduced -0.08 ± 0.02 . $**p < 0.01$, Wilcoxon signed rank test (S1 Data, Sheet 7A and 7B). $\Delta F/F$, fluorescence change over baseline; GCaMP, genetically encoded calcium indicator; RIS, Ring Interneuron S.

<https://doi.org/10.1371/journal.pbio.3000361.g007>

inhibiting RIS, ASH activated RIS, while it still increased behavioral activity (Fig 8B). Consistent with our calcium imaging data, ASH stimulation after RIM ablation predominantly caused a forward locomotion response (Fig 8C). There are 2 ways ASH might inhibit RIS through RIM. One possibility is that arousal strongly activates reverse interneurons, thus inhibiting forward PVC neurons and RIS during stimulation. Consistent with this idea, gentle tail touch increased RIS activity more strongly when RIM was ablated (S13 Fig). Another option is that RIM inhibits RIS directly through tyramine and FLP-18. Both circuits might play together (Fig 8D). These results delineate a circuit model for how sensory stimulation can control RIS activation.

Discussion

A wake-active circuit that controls locomotion also controls sleep

Optogenetic activation and inhibition showed how the activity of presynaptic neurons affects RIS depolarization during developmental sleep. Several presynaptic neurons can activate RIS. RIM appears to be a potent direct inhibitor when activated strongly but can also act as an activator of RIS. Loss-of-function experiments showed that the command circuit controls activation of RIS, with PVC presenting a key activator of RIS. PVC has long been known to mediate the forward escape response by transmitting information from posterior sensory neurons to

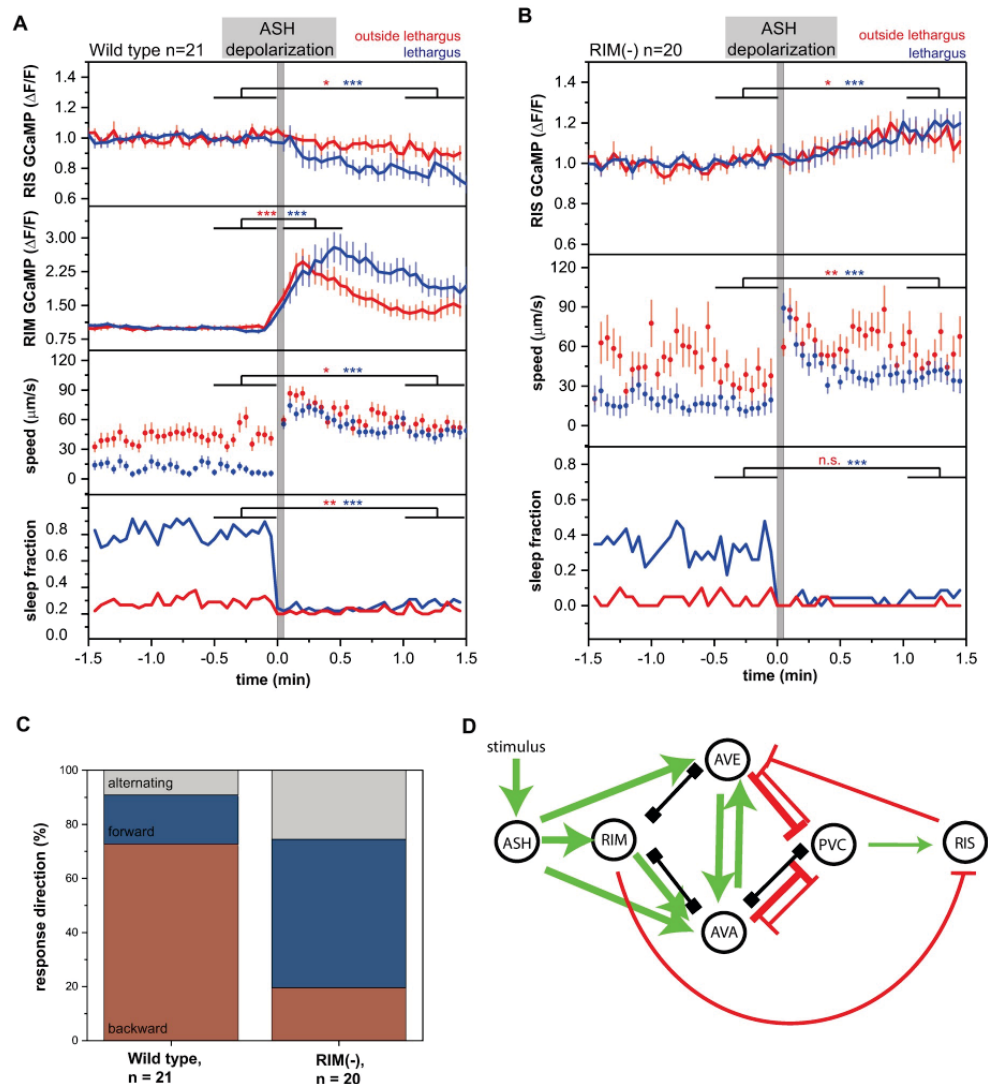


Fig 8. Arousing stimulation inhibits RIS and sleep through RIM. (A) ASH depolarization in wild-type worms leads to RIS inhibition and RIM activation, sleep suppression, and mobilization. * $p < 0.05$, ** $p < 0.01$, *** $p < 0.001$, Wilcoxon signed rank test for GCaMP and speed, Fisher's exact test for sleep fraction (S1 Data, Sheet 8A, B). (B) ASH depolarization in RIM-ablated worms leads to weaker sleep suppression, mobilization, and RIS activation. * $p < 0.05$, ** $p < 0.01$, *** $p < 0.001$, Wilcoxon signed rank test for GCaMP and speed, Fisher's exact test for sleep fraction (S1 Data, Sheet 8A, B). (C) The response direction following ASH activation in wild-type worms is predominantly reverse, while in RIM-ablated worms it is predominantly forward. *** $p < 0.001$, Fisher's exact test (S1 Data, Sheet 8C). (D) A circuit model for RIS regulation through arousal by ASH. Activating synaptic input is shown as green arrows, inhibitory synaptic input is shown as red arrows, and gap junctions are indicated as black connections. RIM could serve as a synchronizer of AVE and AVA to regulate PVC and therefore RIS inhibition. Additionally, RIM could inhibit RIS directly. ΔF/F, fluorescence change over baseline; GCaMP, genetically encoded calcium indicator; n.s., not significant.

<https://doi.org/10.1371/journal.pbio.3000361.g008>

activate AVB premotor neurons to trigger forward locomotion [46,49,50]. Consistent with promoting the forward escape response, optogenetic activation of PVC leads to an increase in forward movement [50,73] (Fig 2D). Reverse movement, in turn, is mediated by AVA, AVE, and AVD command premotor interneurons, which activate reverse motor neurons. Forward PVC and reverse AVA/AVE/AVD command interneurons are presynaptic to and mutually inhibit each other, which ensures discrete forward and reverse locomotion states analogous to a flip-flop switch [49,55,74].

Our finding that PVC and RIM neurons present key activators of RIS that act in concert suggests a model for how RIS is controlled; it also provides a potential mechanism for linking sleep induction to decreasing arousal and for homeostatically maintaining a series of sleep bouts. According to this model, during conditions of high arousal, such as during development outside of lethargus, larvae are constantly awake. The command interneuron circuit cycles between forward and reverse states, leading to the activation of forward or reverse motor programs, respectively [49,74,75]. PVC activation has been associated with the activity of forward states, and RIM has mostly been associated with the activity of reverse states. Because neither activation of only the PVC nor of the RIM neurons appears to be sufficient for sleep induction, RIS should not be activated sufficiently to induce sleep during either forward or reverse states. At the transition between forward and reverse states, locomotion pauses can occur. It has been shown that, in adult worms, RIS shows activation transients in the nerve ring during locomotion pauses. These calcium transients appear to be much smaller compared with activation transients during sleep bouts that extend to the cell soma. Locomotion pausing is reduced after RIS ablation, suggesting that weak RIS activation promotes pausing [76].

Lethargus induces a modest dampening of neuronal baseline activity that is independent of RIS and that includes the RIM neurons. The RIM neurons become less excitable, which should reduce their inhibitory effects on RIS and instead favor their activating effects. PVC becomes resistant to inhibition and more potent in its capacity to activate RIS. We hypothesize that these shifts in the properties of the interneurons of the locomotion circuit favor the activation of the RIS neuron. RIS activation appears to require concerted activation from PVC and RIM neurons (a process that is perhaps aided by other locomotion interneurons). Both PVC and RIM appear to depolarize prior to RIS activation, and both types of neurons contribute to RIS depolarization. This suggests that RIS might be activated when both PVC and RIM exert activating effects. Such an overlapping activating effect of PVC and RIM on RIS would most likely occur at the transition from forward to reverse locomotion states, where there could be an overlap of both forward and reverse neuronal activities. This would suggest that both locomotion stop and sleep bouts might be induced by locomotion control interneurons at the transition between forward and reverse locomotion states. The difference between locomotion stop and a sleep bout would be that, in the former, RIS would only be modestly activated, whereas in the latter, RIS would be strongly activated (Fig 9). Consistent with this model, sleep bouts are typically induced at the end of long forward movements, whereas the exit from the sleep bout—e.g., caused by a noxious stimulus—is often through a reverse movement [70,75,77]. Arousal promotes reverse command interneuron activity and strong RIM activation that can inhibit RIS. Locomotion control and periods of behavioral activity and rest are already present in animals that do not have a nervous system. It has therefore been hypothesized that sleep and sleep-active neurons evolved from systems controlling locomotion activity and rest [8]. The finding that a sleep-active neuron can also act as a locomotion pause neuron [76]—and the discovery presented here that the locomotion circuit controls the depolarization of a sleep-active neuron—suggests that sleep-controlling circuits might have evolved from locomotion-controlling circuits and therefore that locomotion quiescence and sleep could be regarded as homologous behaviors.

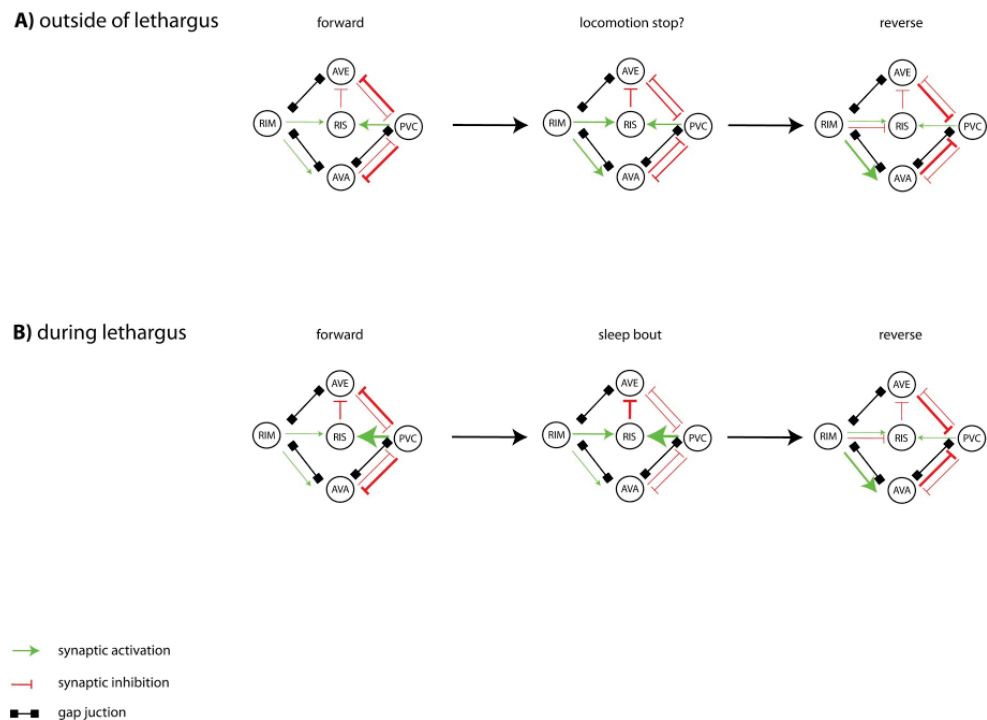


Fig 9. A circuit model for RIS activation through locomotion interneurons. (A) Activating synaptic input is shown as green arrows, inhibitory synaptic input is shown as red arrows, and gap junctions are indicated as black connections. Outside of lethargus, the nervous system cycles between forward and reverse states. RIS is not activated sufficiently to cause a sleep bout, neither during the forward state during which PVC is active nor during the reversal state during which RIM is active. The locomotion circuit activates RIS briefly to cause a locomotion pause at the transition from forward to reverse movement. Speculatively, the circuit that controls RIS during sleep also controls RIS during locomotion pauses. (B) During lethargus motion bouts, the nervous system still cycles between forward and reverse states. Baseline activity and excitability in RIM are reduced, and PVC becomes resistant to inhibition and more potent to activate RIS. These changes in locomotor interneurons shift the balance to favor strong RIS activation and induction of a sleep bout, a process that may involve simultaneous activation from multiple neurons, including RIM and PVC. Such an overlap activation of RIS by otherwise mutually exclusive neurons could occur at the transition from forward to reverse locomotion states. Perhaps, RIS activation and sleep could occur similarly at the transition from reverse to forward locomotion states.

<https://doi.org/10.1371/journal.pbio.3000361.g009>

Our model suggests that the sleep switch is tripartite and includes not only wake-active wake-promoting neurons and inhibitory sleep-active sleep-promoting neurons but also wake-active sleep-promoting neurons as mediators of switch flipping. This sleep switch acts as an amplifier that can translate a modest reduction of arousal into a massive shutdown of behavioral activity during sleep. Dampening of neural activity and altered properties of wake-active sleep-promoting locomotion neurons independently of sleep-active neurons could be interpreted as a neural equivalent of sleepiness that leads to an increased propensity to activate sleep-active neurons and to induce sleep bouts.

Mutations that increase arousal and suppress sleep increase the activity of reversal neurons, whereas conditions that decrease arousal decrease the activity of the reversal neurons and therefore increase the amount of sleep [67,68,74]. Also, the ablation of reverse command interneurons such as AVE reduces reversals and leads to ectopic quiescence, as well as increases sleep [46,52] (and this study). According to our model, increasing arousal should increase the activity of RIM and other reverse command interneurons and thus should inhibit RIS.

Conversely, reducing arousal could promote weaker RIM activation and PVC activation that should shift the equilibrium to stronger RIS activation.

What causes the termination of sleep bouts? The RIS neuron might not be able to sustain prolonged activity, leading to the spontaneous cessation of a sleep bout. The RIS activation transient and thus sleep bout can be blunted prematurely by a sensory or optogenetic arousing stimulus [25,27,70,78]. Arousing stimulation, for instance, by activating the nociceptive sensory neurons, triggers a reverse escape response through backwards command and RIM interneurons [35,72,75,79]. Strong optogenetic RIM depolarization inhibits RIS, and stimulation of the nociceptive ASH neurons causes inhibition of RIS that depends on RIM, suggesting that a main physiological role of strong RIM activation is to inhibit sleep upon arousing stimulation, perhaps by synchronizing the reverse interneurons [72]. RIM activation can inhibit sleep also in response to acute food deprivation [80,81]. Thus, RIM might present not only an activator of RIS but also an arousal module that can be activated upon sensing various external conditions that signal the need to suppress sleep.

RIS inactivation leads to disinhibition of arousal and brain activity, starting anew the cycle of locomotion interneuron activity and locomotion behavior. Depending on the arousal levels, the locomotion circuit causes RIS reactivation and thus a return to sleep either immediately or after a delay. The timing of the rebound activation can be controlled by the level of arousal—with strong arousal leading to longer wake periods before the return to sleep—whereas milder stimulations cause an immediate return to sleep [23]. Consistent with this circuit model of recurrent RIS activation, RIS activity oscillates, resulting in the typical pattern of sleep bouts that are interrupted by activity bouts [22]. This circuit design allows homeostatic sleep maintenance of a series of consecutive sleep bouts with sensory stimulation restarting the cycle of RIS activation, thus prompting an acutely increased RIS activation causing the return to sleep (Fig 6A) [23,70]. Our model predicts that RIS calcium transient strength is a function of prior behavioral activity. Consistent with this view, RIS calcium transients are stronger at the beginning and end of lethargus, when motion bouts are high, but are less pronounced in the middle of lethargus, when motion bouts are less pronounced (Fig 1A) [22,23]. Thus, the tripartite flip-flop circuit design allows an adaptation of RIS activity to the strength required to induce sleep bouts at a given behavioral activity level.

Here, we have identified a circuit controlling sleep-active neuron depolarization in *C. elegans*. This work built on the neural connectome and was facilitated by the small size and invariance of the nervous system as well as the transparency of the organism. While the *C. elegans* sleep circuit clearly is built from fewer cells than the mammalian sleep circuit [8,82,83], there are many conceptual similarities. For instance, in both *C. elegans* and humans, sleep is controlled by inhibitory sleep-active sleep-promoting neurons that depolarize at sleep onset to actively induce sleep by inhibiting wake circuits. A main difference is that humans have many brain centers each consisting of thousands of sleep-active neurons [12]. The single RIS neuron is the major inhibitory sleep-active neuron required for sleep induction in *C. elegans* [25]. Work in mammals revealed the general principles of wake-active wake-promoting neurons and sleep-active sleep-promoting neurons as well as their mutual inhibition. While this information explains the flip-flop nature of sleep and wake states, there is no satisfactory understanding of what flips the sleep switch, i.e., how wakefulness is detected when the system is set to sleep, prompting the activation of inhibitory sleep-active neurons [6]. Our model for the operation of the *C. elegans* sleep circuit indicates that flipping of the sleep switch can be understood if wake-active sleep-promoting neurons are added to the switch model. In this tripartite flip-flop sleep switch model, the sleep-active sleep-promoting center is activated by wake-active neurons. This activation should, however, only occur when the system is set to sleep, a state that could present a neural correlate of sleepiness.

Sleep is reversible by stimulation, and hyperarousal is the major cause for insomnia in humans [3,84,85]. Homeostatic sleep maintenance is an essential feature of sleep and is found from worms to humans [19–21,23]. R2 ring neurons in *Drosophila* present an integrator of wake time, causing subsequently increased depolarization of dFB sleep-inducing neurons, thus forming a chronic sleep homeostat [86,87]. In vertebrates, serotonergic raphe neurons are active during wakefulness and can reduce behavioral activity and increase sleep pressure [88]. Our model of a tripartite flip-flop circuit suggests that wake-active sleep-promoting neurons are an essential part of an acute sleep homeostat that translates acute brain activity into increased sleep neuron activity when the system is set to sleep. Wake-active sleep-promoting neurons measure systemic activity, i.e., they become active together with a global brain activity increase and can then activate inhibitory sleep-active neurons. Thus, the interplay of sleep-active sleep-promoting and wake-active sleep-promoting neurons form an oscillator that periodically sends out sleep-inducing pulses. Macroscopically, sleep in mammals exists as cortical oscillations of global down states, known as slow waves [89]. Micro-arousals trigger cortical up states that are followed by cortical down states, known as k-complexes [19–21]. Both slow-wave activity as well as k-complexes could be hypothetically generated by wake-active sleep-promoting neurons.

Materials and methods

Worm maintenance and strains

C. elegans worms were grown on Nematode Growth Medium (NGM) plates seeded with *Escherichia coli* OP50 and were kept at 15 °C to 25 °C [90]. Crossed strains were genotyped through Duplex PCR genotyping of single worms [91]. The primer sequences that were used for Duplex PCR can be found subsequently. To confirm the presence of transgenes after crossings, fluorescent markers were used. All strains and primers that were used in this study can be found in [S1 Text](#) and [S1 Table](#).

Strain generation

DNA constructs were cloned with the 3-fragments Gateway System (Invitrogen, Carlsbad, CA) into pCG150 to generate new strains [92]. The *ArchT*, the *ReaChR*, and the *egl-1* genes were expression optimized for *C. elegans* [93]. The *tdc-1::egl-1* transgene specifically expresses the apoptosis-inducing protein EGL-1 in RIM and RIC. Therefore, RIM and RIC are genetically ablated in worms carrying this transgene. The ablation is probably incomplete in L1 worms. The *nmr-1::egl-1* transgene leads to the expression of *egl-1* in all command interneurons causing their genetic ablation. Similar to the *tdc-1::egl-1* transgene, ablation might be incomplete in L1 worms. In both lines, *egl-1* was co-expressed with *mKate2*, which was used to verify the genetic ablations. Transgenic strains were generated by microparticle bombardment or by microinjection. For microparticle bombardment, *unc-119(ed3)* was used. The rescue of the *unc* phenotype was therefore used as a selection marker [94,95]. The transgenes were backcrossed twice against N2 wild-type worms to remove the *unc-119(ed3)* background. Extrachromosomal arrays were generated by DNA microinjection. DNA was injected in wild-type, mutant, or transgenic worms. For injection, DNA was prepared as follows: construct 30–100 ng/μl, co-injection marker 5–50 ng/μl, and pCG150 up to a concentration of 100 ng/μl if required. Positive transformants were selected according to the presence of co-injection markers. A table of all plasmids and a list of all constructs that were generated for this study can be found in [S2 Table](#) and [S2 Text](#).

Generation of gene modifications using CRISPR

The following allele was designed by us in silico and was generated by SunyBiotech. Correctness of the alleles was verified by using Sanger sequencing.

PHX816: *flp-11(syb816 [SL2::mKate2::linker(GSGSG)::tetanustoxin_LC]) X*

The coding sequences of tetanus toxin light chain and mKate2 were codon optimized and intronized as described previously and were synthesized [93]. The final sequence can be found in [S3 Text](#).

Imaging

Cameras and software. All imaging experiments were conducted using either an iXon EMCCD (512 × 512 pixels) (Andor Technology Ltd., Belfast, UK), an iXon Ultra EMCCD (1,024 × 1,024 pixels) (Andor Technology Ltd.), a Photometrics Prime 95B back-illuminated sCMOS camera (1,200 × 1,200 pixels) (Nikon, Tokyo, Japan), or a Nikon DS Qi2 (4,908 × 3,264 pixels) (Nikon). For the iXon cameras, the EM Gain was set between 100 and 200. The exposure times used were between 5 and 30 ms. Andor IQ 2 and 3 (Andor Technology Ltd.) and NIS Elements 5 (Nikon) were used for image acquisition.

Illumination systems. A standard 100-W halogen lamp together with an infrared filter (Semrock Brightline HC 785/62) (IDEX Health and Science, New York) were used for differential interference contrast (DIC) microscopy or bright-field imaging. For calcium imaging and blue light stimulation, an LED illumination (CoolLED) with a 490-nm LED and standard GFP filter set (EGFP, Chroma) were used. Optogenetic stimulations and RFP imaging were performed with an LED illumination (CoolLED) with a 585-nm LED and standard TexasRed filter set (Chroma Technology Corp., Bellows Falls, VT).

Agarose microchamber imaging

Long-term imaging experiments were conducted in agarose microchambers as previously described [96,97]. To summarize, a PDMS mold was used to cast box-shaped indentations in a hydrogel, which consisted of 3% or 5% agarose dissolved in S-Basal [98]. Two different sizes were used. We imaged L1 larvae in 190 × 190 × 15 μm microchambers, and L4 larvae were imaged in 370 × 370 × 25 μm microchambers. Depending on the developmental state of the worm that was imaged, either pretzel-stage eggs or L3 larvae were picked into the chambers with OP50 bacteria. Before imaging, worms were kept at either 20 °C or 25 °C.

For time-lapse calcium imaging experiments, L1 worms were filmed every 5 s (Figs 1A, 3H–3J, 4B–4D, 5A, S8C–S8F and S11A Figs), every 8 s (Fig 7, S9A, S9C and S10 Figs), or every 10 s (Figs 3F and 4A) with DIC or bright-field imaging and widefield fluorescence. The DIC and bright-field light source was left on continuously, filtered through an infrared filter, and was blocked by a shutter during fluorescence image acquisition. LED illumination was triggered by the EMCCD camera using the TTL exposure output of the camera. An objective with 20× magnification, an LED with 480 nm (light intensity was between 0.15 and 2 mW/mm²), and EM gain of 100–200 was used. With the 20× objective and a 0.7 lens, 4 worms could be imaged simultaneously in one field. One to four fields could be filmed in parallel in one experiment. These image sequences gave measurable neuronal calcium transients and clear DIC or bright-field images to identify pumping or nonpumping phases.

During the continuous experiments in Figs 3F, 4B–4D and 5A, only DIC or bright-field images were taken.

AVA inhibition experiment

NGM plates were prepared with histamine (HA; Sigma Aldrich, St. Louis, MO, 10 mM) as previously described [54]. Young adult worms expressing a HA chloride channel in AVA and control worms were picked onto NGM HA plates the night before the experiments. The next morning, eggs together with *E. coli* bacteria from the NGM HA plates were picked into microfluidic chambers and DIC imaged as previously described [96,97].

Optogenetic experiments

Optogenetic experiments were either conducted in agarose microchambers as described previously, or the worms were immobilized. For immobilization experiments, the agarose was solved in S-Basal. We used the following 3 methods of immobilization for optogenetic experiments:

1. Immobilization on a 3% agarose pad with 25 mM Levamisole (Sigma Aldrich) (S6 Fig)
2. Immobilization on a 10% agarose pad with 0.1 μm Polybead microspheres (Polysciences, Warrington, PA) [99] (Fig 1B/ SDQL, Fig 1C/ SDQL, Fig 3B–3D, S1A Fig/SDQL, S5A Fig/ SDQL, S4 and S8A Figs)
3. Immobilization on a 10% agarose pad with 0.1 μm Polybead microspheres [99] and 25 mM Levamisole (Fig 1B/PVC, Fig 1C/PVC, Figs 2A, 2C, 3B–3D, 4F–4G, S1A Fig/PVC, S5A Fig/ PVC, S7A, S7C, S7D, S8B and S8H Figs)

Worms were imaged within 30 min of immobilization. A 100 \times oil objective was used for illumination and imaging in most experiments. For images in S6A and S6B Fig, a 1.5 lens was added (S6A and S6B Fig). The imaging in Fig 2A was done using a 40 \times objective.

ReaChR for neuronal depolarization or ArchT for hyperpolarization was utilized. For optogenetic stimulation, a 585-nm LED and a standard TexasRed filter set were used.

For optogenetic experiments with L1 larvae, either L4-stage worms or young adult worms were prepicked onto NGM plates with all-trans-retinal (ATR; Sigma Aldrich) and grown at 20 $^{\circ}\text{C}$ or 25 $^{\circ}\text{C}$. During the 2 d after exposure to ATR, pretzel-stage eggs or L1 worms were taken from this plate for optogenetic experiments. For optogenetic experiments with L4 larvae, an agar chunk containing a mixed population of growing worms was added to NGM plates containing ATR. Worms for optogenetic experiments were taken from this plate within the next 2 d.

Calcium imaging was conducted with an interval of 3 s and with an exposure time of 5–200 ms. A standard optogenetic protocol included calcium imaging during a baseline. This was followed by a stimulation time, in which the worms were optogenetically stimulated. The 585-nm light exposure was continuous except for brief interruptions during the time calcium imaging was conducted. After the optogenetic stimulation, calcium images were acquired during a recovery period.

In mobile worms, this standard protocol was preceded by 20 DIC frames that were taken every 500 ms to determine whether the worm was pumping. The overall protocol was repeated every 15 to 30 min. L1 mobile worms were imaged with a 20 \times objective and a 0.7 lens. Mobile L4 worms were imaged with either a 10 \times objective (Fig 8A–8C) or a 20 \times objective (Fig 1B/ CEP, Fig 1C/URY, S1A Fig/CEP, S5A Fig/URY and S3 Fig). Fixed worms were usually imaged between 1 and 4 trials. A delay preceded the standard protocol to allow the worm to recover from immobilization and between trials. To specifically manipulate PVC and SDQL in Fig 1B/ PVC, Fig 1B/SDQL, Fig 1C/PVC, Fig 1C/SDQL, Fig 2D, S1A Fig/PVC, S1A Fig/SDQL, S4 Fig, S5A Fig/PVC, S5A Fig/SDQL, and S7C and S7D Fig, the stimulating illumination was

restricted to the neuronal areas. This was achieved by reducing the size of the field aperture of the fluorescence illumination. To activate a specific neuron, it was moved into the illuminated area by using an automated stage. To image RIS, this neuron was moved into the illuminated area by the automated stage, while the optogenetic light stimulus was switched off and imaging light was switched on. The details for optogenetic experiments can be found in [S3 Table](#).

Behavioral imaging during PVC activation

Worms were prepared on retinal plates and picked into microchambers as described previously. A 20× objective was utilized for imaging. The entire chamber was imaged through bright-field imaging. For tail-specific illumination, the LED blend was adjusted to illuminate a circular area with a radius of 58 μm. The 580-nm LED was manually turned on after 1 min of imaging and off after 4 min of imaging. A Prior XY stage (Prior Scientific, Cambridge, UK) was manually operated to keep specifically the tail of the worm in the by the LED-illuminated area during stimulation. Worms were imaged with a frame rate of 8 Hz. Only every eighth image was used for analysis.

Activity measurements of command interneurons

GCaMP3.3 was expressed in command interneurons using the *glr-1* promoter [100]. L1 larvae were placed in microfluidic chambers and were imaged using a time-lapse protocol. One DIC and one GFP image was taken every 8 s using a 20× objective and a 0.7 lens. The 490-nm intensity for GFP imaging was set to 0.15 mW/mm². Intensity values of all command interneurons located in the head of worms were extracted manually and analyzed as one entity.

Pan-neuronal activity measurements

GCaMP6s and RFP were pan-neuronally expressed under the *rab-3* promoter [101]. As in the activity measurements of command interneurons, L1 lethargus was imaged in microfluidic devices. For the optogenetic experiment ([Fig 6C](#)), every 30 min, 20 DICs were taken first in order to determine lethargus. This was followed by GFP images that were taken all 5.8 s for 9 min. The 490-nm intensity was set to 0.07 mW/mm². In the blue light stimulation experiment, additional RFP images were taken. A custom-written MATLAB code detected the mean intensity of all head neurons in each GFP and RFP frame. The head neurons were thus analyzed as one entity.

Blue-light stimulation experiments

L1 worms were placed in microfluidic chambers for blue light stimulation experiments. The protocol was repeated every 15 min. First, 20 DIC pictures were taken every 500 ms to determine whether the worm was pumping or not. Next, baseline GCaMP was imaged for 3 min, the stimulation phase then lasted 18 s, and a recovery phase was imaged for 3 min. The 490-nm intensity for calcium imaging was 0.07 mW/mm². The 490-nm intensity for stimulation was set to 1.01 mW/mm² with a 20× objective. The same LED was used for calcium imaging and stimulation. The intensity levels were controlled with Andor IQ2 software.

The RFP signal of the pan-neuronal strain was imaged in addition to the GCaMP signal during the protocol every 3 s with 585-nm LED illumination, which was set to 0.17 mW/mm².

Mechanical stimulation using dish tapping

The mechanical tapping set up was described previously [67,102]. L1 larvae were imaged in microfluidic chambers using a 20× objective and a 0.7 lens. Microfluidic chambers were put in

a specialized dish. The dish was tapped by a piston driven by an electromagnet. The piston and the electromagnet were held in a homemade aluminum frame as described previously [102] (model used was Kuhnke, product number H2246). The voltage used for stimulus application was 5 V; the tapping stimulus was applied between image acquisition using TTL triggering to avoid blurring. Imaging was controlled with Andor IQ2 software. The imaging protocol was repeated every 15 min. First, 20 DIC pictures were taken with a frequency of 2 pictures per second to determine the status of worms. Throughout all following steps, GCaMP measurements were taken every 3 s. The 490-nm intensity for calcium imaging was 0.15 mW/mm^2 . Baseline GCaMP was measured over 3 min. Following the tap, GCaMP was measured for 3 min. This experiment was initially planned to be combined with optogenetic stimulation, therefore a weak green light stimulus was applied, starting 15 s before and ending 45 s after the tapping stimulation. The part of the experiment during which a green light stimulus was applied was selected for presentation in this study. Green light (585 nm) for stimulation was set to 0.17 mW/mm^2 . Because we did not see any noticeable changes upon applying green light, we presume that it does not strongly affect the experiment.

Simultaneous calcium imaging of RIS and PVC

In order to simultaneously image RIS and PVC, L1 lethargus worms were transferred from a growing plate using a platinum wire worm pick and were fixed on 10% agarose pads with $0.1 \mu\text{m}$ Polybead microspheres [99] and 25 mM Levamisole. The worms were then imaged through a $40\times$ oil objective with an image taken every 3 s for 30 min with 490-nm light of 1.35 mW/mm^2 to image GCaMP. Fluorescence intensities for PVC and RIS were cropped by using a region of interest. A custom-written MATLAB script then detected all RIS peaks. For this, the GCaMP data were first smoothed over 30 values through the in-built function “smooth,” which is a first-degree polynomial local regression model. Through the in-built MATLAB function “islocalmax,” and a minimum prominence value of 0.2, the locations of RIS peaks were detected. The data of RIS as well as PVC GCaMP intensity were aligned to the detected RIS peak location.

Spinning disc confocal microscopy

L4 worms were fixed with Levamisole. Spinning disc imaging was done with an Andor Revolution disc system (Andor Technology Ltd.) using a 488-nm (0.34 mW/mm^2) and a 565-nm (0.34 mW/mm^2) laser and a Yokogawa (Japan) CSU-X1 spinning disc head. Worms were imaged through a $100\times$ oil objective. In *S6A* and *S6B Fig*, an additional 1.5 lens was used. z-Stacks with z-planes $0.5 \mu\text{m}$ apart spanning a total distance of $10 \mu\text{m}$ were taken, and a maximum intensity projection was calculated in ImageJ (developed by Wayne Rasband, open source).

Tail-touch experiment

L4 worms were grown and filmed on NGM plates with OP50 bacteria at 20°C . An eyelash was used to gently touch the tail of the worms during L4 lethargus. The time from tail touch until the worms were immobile again was measured with a timer. If worms did not mobilize upon tail touching, the time was counted as zero. For GCaMP intensities, worms were imaged before and after tail touch each second for a total of 30 s. They were illuminated with a Leica EL6000 LED (Leica, Wetzlar, Germany).

Image analysis

Image sequences for analysis were selected either based on lethargus or molting time points. Lethargus was determined through DIC or bright-field images as the nonpumping phase before molting. Time points were classified to be in or outside of lethargus. Typically, the entire lethargus time and 2 h before lethargus were analyzed. Worms that were immobilized during the measurements were classified according to their pumping behavior on NGM plates directly before imaging. Two parameters were extracted from the image sequences, as follows.

1. Calcium signals were extracted automatically or manually with custom-written MATLAB codes. These codes extracted defined regions of each image and detected intensity and position data. Extracted regions were chosen slightly bigger than the sizes of measured neurons. From these extracted regions, a certain percentage of highest-intensity pixel was taken as signal. The remaining pixels were taken as background. From the signal, the background was subtracted. For the pan-neuronal and interneuron activity measurements, the signal in the head was treated as one large neuron and analyzed in the same way as single neurons. All head neurons expressed under the *rab-3* promoter were included in the pan-neuronal GCaMP measurements. For all stimulation experiments (optogenetic and blue light stimulation experiments), the baseline measurement of each time point was utilized for signal normalization and $\Delta F/F$ generation, except for Fig 6C. In Fig 6C, a mean of all baseline intensities for all wake time points for each worm was calculated. The mean was then utilized for normalization for all time points for each worm to better show the different RIS activities during wake and sleep. The pan-neuronal signal in Fig 6B was normalized over the measured RFP signal to retrieve $\Delta R/R$. For the transient alignments in Fig 3G, peaks and corresponding speeds were extracted through a custom-written MATLAB script and aligned as time point zero.
2. The speeds of the worms were calculated from the positions of the tracked neuron, except for experiments in which no GCaMP intensity was measured. To analyze these experiments, frame subtraction of DIC or bright-field images was done with a custom-written MATLAB routine instead.

Baseline extraction

In S12A and S12C Fig, the baseline of RIM GCaMP data was extracted by excluding the 95th- to 100th-percentile range for wild type and by excluding the 75th- to 100th-percentile range for *aptf-1(gk794)* mutants. The baseline was smoothed through a second-degree polynomial local regression model and with weighted linear least squares. Zero weight was assigned to data points 6 means outside the absolute deviation. The number of data points used for smoothing was 3%.

Sleep-bout analysis

Sleep bouts were extracted from selected parts of the time-lapse movies. Dependent on the experiment, a specific period of the movie sequence was selected and processed:

1. The lethargus period (Figs 3F–3J, 4A, 5A, 7, S9A, S9C, S10E–S10I and S12 Figs)
2. The period from 2 h before lethargus up to the end of lethargus (Fig 1A)

3. Either 3 h (Fig 4B–4D and S8C–S8F Fig) or 4 h (S10A–S10D Fig) before shedding of the cuticle

To extract sleep bouts, speeds and subtraction values were first smoothed. In Figs 1A, 3G–3J, 4A–4D, 5A, S8C–S8F, S10, and S12 Figs, speeds were smoothed through a first-degree polynomial local regression model over 20 time points. Other experiments were smoothed through a second-degree polynomial local regression model and with weighted linear least squares. Zero weight was assigned to data points 6 means outside the absolute deviation. Data were smoothed either over 3% of all data (Figs 3H–3J, 7 and S9C–S9F Fig) or over 40 data points (S9A, S9C, S12A and S12C Figs). This was achieved with the “smooth” function in MATLAB. Smoothed speeds were normalized between 0 and 1, with 0 representing the lowest and 1 the highest smoothed speed value of each worm. In order to be scored as a sleep bout, the normalized speed had to be under a defined percentage threshold of the normalized speed for a minimum time. The exact speed and time thresholds were adjusted empirically to represent the worms’ behavior [103]. In Fig 3G–3I and S8C–S8F Fig, worms had to have a speed below 5% of their maximum smoothed speeds for at least 2 min in order to be counted as sleeping. For all other experiments, the speed threshold was 10%, and the time threshold was 2 min. The 2-min time threshold was implemented to exclude short pauses of the worm that may not represent sleep bouts. It was determined empirically. The sleep-bout analysis was carried out with a custom-written MATLAB script.

For stimulation experiments, the baseline and recovery time measurements were too short to include a minimum time threshold in the sleep-bout analysis. Therefore, immobility was used as a proxy for sleep. A mean of the wake speeds was calculated for each worm. Depending on the strain used, the worms were counted as sleeping when they were below a threshold of 5% to 30% of their mean wake speed. In most experiments, a worm was counted as sleeping when its speed was below 10% of the calculated mean of the wake speeds. To account for different locomotor behavior of the worms, in S11B Fig, the threshold was adjusted to 5%; in S8G Fig, to 20%; in S7B Fig, to 25%; in Fig 6C, S1C, S2A–S2C, S3, S5B, S9D, S9E, and S11I Figs, to 30%; and in S11C–S11E Fig, to 50%. RIS signals and speeds of wild type and mutants were aligned to sleep-bout onset for comparison in Figs 3H and 4A, S8F, S9A, S10D and S10H Figs. RIM signals and speeds were aligned to sleep-bout onset in Fig 4A. For GCaMP normalization, 10 data points before sleep-bout onset were taken as baseline in order to calculate $\Delta F/F$. In S11A Fig, motion bouts were assigned whenever there was no detected sleep bout.

RIS peak alignment

For RIS wide peak detection (Fig 3G–3H), first the normalized GCaMP data were smoothed over 60 time points with the in-built MATLAB function “smooth.” Wide peaks were then detected with the in-built MATLAB function “findpeaks” and a minimum peak prominence threshold of 0.15. GCaMP intensities, speeds, and sleep fractions were then aligned to the detected peak maxima. Analysis for narrow peaks was conducted similarly; only 2 aspects were changed (S8C–S8F Fig). To find narrow peaks, smoothing was limited to only 5 time points, and a minimum peak prominence threshold was set to 0.2.

Detection of direction of movement

The direction of movement was analyzed with a custom-written MATLAB script. This MATLAB script took 2 points, the nose and the pharynx, to calculate the direction. For 2 consecutive images, the distance of the nose in the first image to the pharynx in the first image was compared to the distance of the nose in the second image to the pharynx of the first image. If

the distance increased, the worm was counted as moving forward; if it decreased, it was counted as moving in reverse. If the worm was below a threshold of $2\ \mu\text{m/s}$, it was counted as sleeping in experiments Figs 2D and 4E. The position of nose and pharynx were detected manually (Figs 2D and 4E). For correction of the stage movement while manually tracking PVC (Fig 2D), the position of a corner of the stage was used.

Fitting

The data in Fig 6D were fitted to an asymptote, and the data in Fig 6E were fitted to a BoxLucasFit1 with Origin software. The data in S11A Fig were fitted to a logistic regression using Origin software (OriginLab Corporation, Northampton, MA). Exact functions and R^2 values can be found in the respective Figures.

Statistics

Sample sizes were determined empirically based on previous studies. If possible, experiments were carried out with internal controls. If this was not possible, control and experimental condition were alternated. Researchers were not blinded to the genotype for data analysis, as data analysis was performed by automated routines. Sample exclusion is described in the respective Methods sections. To compare GCaMP intensities and speeds of one sample group at different time points, the Wilcoxon signed rank test was utilized. The Fisher's exact test was used to compare the sleep fractions of one sample group at different time points. The entirety of the baseline was compared to the entirety of the stimulation period unless otherwise stated through significance bars. Data from different strains were compared with either the Kolmogorov-Smirnov test or the Welch test. The p -values can be taken from the respective Figure descriptions. Depicted in the graph is the mean \pm SEM unless otherwise stated. The box in the box plots represents the interquartile range with the median. The whiskers show the 10th- to 90th-percentile range, and the individual data points are plotted on top of the box.

Supporting information

S1 Fig. Weak optogenetic RIM depolarization using the *gcy-13* promoter can induce RIS activation or inhibition. (A) Control experiments. Optogenetic depolarization of RIS presynaptic neurons without the addition of ATR. For statistical calculations, baseline neural activities (0–0.95 min) were compared to neural activity levels during the stimulation period (1–1.95 min). * $p < 0.05$, ** $p < 0.01$, Wilcoxon signed rank test for GCaMP (S2 Data, Sheet S1A). (B) Optogenetic RIC depolarization induced an RIS activity increase outside of and during lethargus. An average of all responsive trials is shown in this figure. Trials were classified as responsive or nonresponsive. In responsive trials, an RIS activity increase correlated with the onset of the stimulation period. In nonresponsive trials, no change in RIS activity levels could be seen. “n” represents the number of animals tested, and “r” represents the number of trials. For statistical analysis, RIS baseline activity levels (0–0.95 min) were compared to activity levels during (1–1.95 min) and after (2–2.95 min) the stimulation. * $p < 0.05$, ** $p < 0.01$, *** $p < 0.001$, Wilcoxon signed rank test for GCaMP and speed, Fisher's exact test for sleep fraction (S2 Data, Sheet S1B). (C) Depolarization of RIM using ReaChR expressed under the *gcy-13* promoter had no net effect on RIS function. Neural baseline activity levels (0–0.95 min) were compared to neuronal levels during the stimulation (1–1.95 min) and after the stimulation (2–2.95 min). * $p < 0.05$, ** $p < 0.01$, *** $p < 0.001$, Wilcoxon signed rank test for GCaMP and speed, Fisher's exact test for sleep fraction (S2 Data, Sheet S1C-E). (D) RIM optogenetic depolarization using ReaChR expressed under the *gcy-13* promoter induced either RIS activation or inhibition. Single trials were classified as activating if an activity increase in RIS

correlated with onsets of optogenetic stimulation periods. Trials were classified as inhibitory if an activity decrease in RIS correlated with onsets of optogenetic stimulation periods. “n” represents the number of animals tested, and “r” represents the number of trials. For statistical testing, baseline neural activities (0–0.95 min) were compared to neural activity levels during the stimulation period (1–1.55 min). * $p < 0.05$, ** $p < 0.01$, *** $p < 0.001$, Wilcoxon signed rank test for GCaMP and speed, Fisher’s exact test for sleep fraction (S2 Data, Sheet S1C-E). (E) Percentage of RIS activation and inhibition following optogenetic RIM activation in different lethargus phases. Lethargus of each individual worm was split into 3 phases of comparable size (lethargus onset, middle of lethargus, and lethargus end). In each interval, for all worms tested the amount of trials showing an RIS activation or RIS inhibition were compared to the total amount of trials in this interval (S2 Data, Sheet S1C-E). (TIF)

S2 Fig. RIM inhibition of RIS requires tyramine and FLP-18. Optogenetic RIM manipulations in these experiments were all performed with ReaChR expressed from the *tdc-1* promoter. (A) Optogenetic RIM depolarization in *flp-18(db99)* single mutants. Outside of lethargus, RIS inactivation caused by RIM optogenetic depolarization was reduced to 37% of wild-type inhibition levels. During lethargus in *flp-18(db99)* mutants, animal inhibition levels were only 25% of wild-type level. Neuronal activity levels before (0–0.95 min), during (1–1.95 min), and after (2.5–2.95 min) optogenetic RIM depolarization were compared. * $p < 0.05$, ** $p < 0.01$, *** $p < 0.001$, Wilcoxon signed rank test for GCaMP and speed, Fisher’s exact test for sleep fraction (S2 Data, Sheet S2A). (B) Optogenetic RIM depolarization in *tdc-1(n3420)* single mutants. Outside of lethargus, optogenetic RIM depolarization in *tdc-1(n3420)* single mutants no longer induced changes in RIS activity levels. During lethargus, inhibition levels during the stimulation period only reached 40% of wild-type levels. Neuronal activity levels before (0–0.95 min), during (1–1.95 min), and after (2.5–2.95 min) optogenetic RIM depolarization were compared. * $p < 0.05$, ** $p < 0.01$, *** $p < 0.001$, Wilcoxon signed rank test for GCaMP and speed, Fisher’s exact test for sleep fraction (S2 Data, Sheet S2B). (C) Optogenetic RIM depolarization in *flp-18(db99)* and *tdc-1(n3420)* double mutants had no effect on RIS function. Neuronal activity levels before (0–0.95 min), during (1–1.95 min), and after (2.5–2.95 min) optogenetic RIM depolarization were compared. * $p < 0.05$, ** $p < 0.01$, *** $p < 0.001$, Wilcoxon signed rank test for GCaMP and speed, Fisher’s exact test for sleep fraction (S2 Data, Sheet S2C). (D) Quantification of inhibition strength. RIS activity levels during optogenetic RIM depolarization in *flp-18(db99)*, *tdc-1(n3420)* and *flp-18(db99)*, and *tdc-1(n3420)* double mutants were compared to wild-type levels. Wild-type data are depicted in Fig 1B, RIM panel. Inhibition strength was calculated by subtracting RIS activity levels before the stimulation (0–0.95 min) from activity levels during the stimulation (1–1.95 min). Samples were tested for normal distribution using the Shapiro-Wilk test. Wild type and mutants were compared with a Welch test. *** $p < 0.001$ (S2 Data, Sheet S2D-E). (E) Quantification of RIS activity levels following RIM optogenetic depolarization. Activity levels in *flp-18(db99)*, *tdc-1(n3420)* and *flp-18(db99)*, and *tdc-1(n3420)* double mutants were compared to wild-type levels. Wild-type data are depicted in Fig 1B in the RIM panel. For statistical calculations, RIS activity levels before the stimulation (0–0.95 min) were subtracted from activity levels after the stimulation (2.5–2.95 min). Samples were tested for a normal distribution using the Saphiro-Wilk test. To compare genotypes, a Welch test was performed for all conditions, except for the comparison of activity levels between wild type and *tdc-1(n3420)* single mutants during lethargus. The *tdc-1(n3420)* data were not normally distributed, and thus a Kolmogorov-Smirnov test was used. *** $p < 0.001$ (S2 Data, Sheet S2D-E). (TIF)

S3 Fig. RIM activation of RIS requires glutamatergic signaling. (A) RIM optogenetic depolarization using ReaChR expressed under the *gcy-13* promoter induced robust RIS activation in L4 larvae. In the L4 larvae, RIS activation by RIM optogenetic depolarization was more robust compared with the same experiment in L1 larvae. No trial selection was required. For statistical analysis, RIS baseline activity levels (0–0.95 min) were compared to activity levels during (1–1.95 min) and after (2–2.95 min) the stimulation. * $p < 0.05$, ** $p < 0.01$, *** $p < 0.001$, Wilcoxon signed rank test for GCaMP and speed, Fisher's exact test for sleep fraction (S2 Data, Sheet S3A). (B) The activating input of RIM optogenetic depolarization on RIS was almost completely abolished in *eat-4(ky5)* mutants. For statistical analysis, RIS baseline activity levels (0–0.95 min) were compared to activity levels during (1–1.95 min) and after (2–2.95 min) the stimulation. * $p < 0.05$, ** $p < 0.01$, *** $p < 0.001$, Wilcoxon signed rank test for GCaMP and speed, Fisher's exact test for sleep fraction (S2 Data, Sheet S3B). (TIF)

S4 Fig. Activation of RIS by PVC is strongly enhanced during lethargus. Optogenetic PVC depolarization in L2 larvae led to RIS activation outside of and during lethargus. RIS activation during lethargus was strongly enhanced. Plotted data represent the average over all experimental trials. Neural activity levels before the stimulation (0–0.95 min) were compared to activity levels during the stimulation (1–1.95 min). * $p < 0.05$, ** $p < 0.01$, Wilcoxon signed rank test (S2 Data, Sheet S4). (TIF)

S5 Fig. Optogenetic hyperpolarization experiments. (A) Control experiments. Optogenetic hyperpolarization of RIS presynaptic neurons without the addition of ATR. For statistical calculations, baseline neural activities (0–0.95 min) were compared to neural activity levels during the stimulation period (1–1.95 min). * $p < 0.05$, ** $p < 0.01$, Wilcoxon signed rank test for GCaMP (S2 Data, Sheet S5A). (B) Hyperpolarization of RIM using ArchT expressed under the *gcy-13* promoter had no net effect on RIS function. Neural baseline activity levels (0–0.95 min) were compared to neuronal levels during the stimulation (1–1.95 min) and after the stimulation (2–2.95 min). * $p < 0.05$, ** $p < 0.01$, *** $p < 0.001$, Wilcoxon signed rank test for GCaMP and speed, Fisher's exact test for sleep fraction (S2 Data, Sheet S5B, C). (C) RIM optogenetic hyperpolarization using ArchT expressed under the *gcy-13* promoter caused a decrease in RIS activity levels in selected trials. Single trials were classified as activating if an activity increase in RIS occurred at the onset of the optogenetic stimulation period. Trials were classified as inhibitory if an activity decrease in RIS occurred at the onset of the optogenetic stimulation period. “n” represents the number of animals tested, and “r” represents the number of trials. For statistical calculations, neural baseline activity levels (0–0.95 min) were compared to levels during the stimulation period (1–1.75 min). * $p < 0.05$, ** $p < 0.01$, *** $p < 0.001$, Wilcoxon signed rank test for GCaMP and speed, Fisher's exact test for sleep fraction (S2 Data, Sheet S5B, C). (D) Simultaneous optogenetic hyperpolarization of CEP and URY neurons does not induce changes in RIS activity levels. For statistical testing, baseline neural activities (2–2.95 min) were compared to neural activity levels during the stimulation period (3–3.95 min) and after the stimulation (6–6.95 min). ** $p < 0.01$, *** $p < 0.001$, Wilcoxon signed rank test for GCaMP and speed, Fisher's exact test for sleep fraction (S2 Data, Sheet S5D). (TIF)

S6 Fig. *zk673.11* is expressed in PVC, RID, and cholinergic motor neurons. (A–B) Expression of *nmr-1* and *zk673.11* only overlaps in PVC in the tail. (C–D) Expression of *nmr-1* and *zk673.11* does not overlap in head neurons. (TIF)

S7 Fig. PVC has multiple functions. (A) PVC excitability remained unchanged during lethargus. Experiments were performed in immobilized L1 larvae to ensure PVC-specific green light illumination. A long baseline of 10 min was used to achieve stable baseline conditions. Activity levels of PVC during optogenetic depolarization were indistinguishable outside and during lethargus. PVC displayed a negative rebound transient after optogenetic depolarization. However, there was no difference in the amount of negative rebound outside and during lethargus (S2 Data, Sheet S7A). (B) RIS showed a rebound after mechanical stimulation. This rebound was stronger in worms during lethargus, and only during lethargus was the RIS rebound accompanied by a strongly increased immobilization of worms. $**p < 0.01$, $***p < 0.001$, Wilcoxon signed rank test for GCaMP and speed, Fisher's exact test for sleep fraction (S2 Data, Sheet S7B). (C–D) Effects of PVC stimulation on AVB activity. L1 larvae were immobilized for optogenetic experiments to ensure cell-specific stimulation of PVC. AVB activated upon optogenetic PVC depolarization with the same response strength during and outside of lethargus. AVB displayed an oscillatory activity pattern in 44% of all trials in worms outside of lethargus. AVB activity oscillated in 70% of all trials during lethargus. $*p < 0.05$, $**p < 0.01$, Wilcoxon signed rank test for GCaMP (S2 Data, Sheet S7C–D). (TIF)

S8 Fig. Effects of optogenetic RIS activation and inhibition on PVC and RIM activity. (A) RIS depolarizes during optogenetic activation in fixed animals. As controls, experiments were performed in the absence of ATR. $***p < 0.001$, Wilcoxon signed rank test (S2 Data, Sheet S8A). (B) RIS hyperpolarization led to a weak PVC depolarization outside and during lethargus. For statistical calculations, neural activities before the stimulation period (0–1 min) were compared to activity levels during the stimulation period (1–2 min). $*p < 0.05$, $**p < 0.01$, compared before and during stimulation, Wilcoxon signed rank test (S2 Data, Sheet S8B). (C–D) Sample trace of RIS activity and worm locomotion behavior 3 h before shedding of the cuticle of *aptf-1(gk794)* and *flp-11(tm2706)* mutants (S2 Data, Sheet S8C and S8D). (E–F) *flp-11(tm2706)* mutants have a significantly increased number of short RIS peaks that do not correlate with sleep. (E) $**p < 0.01$, $***p < 0.001$, Welch test. (F) $**p < 0.01$, Kolmogorov-Smirnov test (S1 Data, Sheet 3G–I). (G) Optogenetic RIS depolarization has no effect on RIM activity outside of and during lethargus. Neuronal activity levels before (0–0.95 min) and during (1–1.95 min) the stimulation period were compared. $*p < 0.05$, $**p < 0.01$, $***p < 0.001$, Wilcoxon signed rank test for GCaMP and speed, Fisher's exact test for sleep fraction (S2 Data, Sheet S8G). (H) Optogenetic RIS hyperpolarization induced increased RIM activity both outside of and during lethargus. Measurements were performed in immobilized L1 larvae to reduce measurement noise. Activity levels during baseline measurements (0–0.95 min) were compared to levels during optogenetic RIS manipulation (1–1.95 min). $*p < 0.05$, Wilcoxon signed rank test for GCaMP (S2 Data, Sheet S8H). (TIF)

S9 Fig. Command interneurons are required for RIS activation and sleep induction. (A) RIS activation in sleep bouts was strongly reduced in command-interneuron-ablated worms. Samples were tested for normal distribution using the Shapiro-Wilk test. $*p < 0.05$, Welch test (S2 Data, Sheet S9A–C). (B) Command-interneuron-ablated worms moved much slower than wild-type worms. Command interneurons were genetically ablated by expressing ICE from the *nmr-1* promoter. Samples were tested for normal distribution using the Shapiro-Wilk test. $***p < 0.001$, Welch test for the wake condition and Kolmogorov-Smirnov test for the sleep condition (S2 Data, Sheet S9A–C). (C) Sample traces of RIS activity levels and worm locomotion behaviors outside of and during lethargus in command-interneuron-ablated worms and wild-type worms. In command-interneuron-ablated worms, quiescence bouts occurred only

around the middle of the lethargus period (S2 Data, Sheet S9A–C). (D–E) Mosaic analysis of worms expressing an extrachromosomal array of *nmr-1::ArchT*. Worms were selected that expressed the transgene only in head neurons (D) or head neurons and PVC (E). Neuronal activity levels before (2–2.95 min) and during (3–3.95 min) the stimulation period was compared. * $p < 0.05$, ** $p < 0.01$, *** $p < 0.001$, Wilcoxon signed rank test for GCaMP and speed, Fisher's exact test for sleep fraction (S2 Data, Sheet S9D and S9E). (TIF)

S10 Fig. Glutamatergic signaling is required for sleep induction. (A–D) Sleep-bout analysis of *eat-4(ky5)* mutant larvae. *eat-4(ky5)* animals lacked significant RIS activation at sleep-bout onset. Consistent with this finding, mutant worms displayed a strong reduction in quiescence during lethargus. Samples were tested for a normal distribution using the Shapiro-Wilk test. ** $p < 0.01$, *** $p < 0.001$, Welch test for comparisons of sleep-bout lengths, sleep-bout frequencies, and sleep fractions. Wilcoxon signed rank test for quantifications of RIS activity levels in sleep bouts (S2 Data, Sheet S10A–D). (E–I) Sleep-bout analysis of *nmr-1(ak4)* mutant animals. RIS activity levels in sleep bouts were slightly reduced in the mutant. *nmr-1(ak4)* mutants did not show a reduced amount of quiescence during lethargus. Samples were tested for a normal distribution using the Shapiro-Wilk test. * $p < 0.05$, Welch test for comparisons of sleep-bout frequencies, sleep fractions, maximum RIS activity levels in sleep bouts, and RIS activity levels at the end of sleep bouts. Kolmogorov-Smirnov test for the comparison of sleep-bout lengths (S2 Data, Sheet S10E–I). (TIF)

S11 Fig. RIS rebound activation following optogenetic hyperpolarization requires synaptic transmission. (A) RIS GCaMP transient intensities in wild-type worms are correlated with the length of the preceding motion bout. The longer the preceding motion bout, the stronger the RIS activation (S2 Data, Sheet S11A). (B) RIM was inhibited during and post hyperpolarization. * $p < 0.05$, ** $p < 0.01$, *** $p < 0.001$, Wilcoxon signed rank test for GCaMP and speed, Fisher's exact test for sleep fraction (S2 Data, Sheet S11B). (C) RIS was optogenetically hyperpolarized with stimuli lasting for 48 s (C), 5 min (D), or 10 min (E). Worms not showing a rebound activation transient were excluded from the analysis, which was no worm for 48 s-, 1 out of 7 worms for 5 min-, and 1 out of 13 worms for 10-min stimulation experiments. Data from these plots were used to generate a dose-response curve of optogenetic RIS hyperpolarization (Fig 6D and 6E). * $p < 0.05$, ** $p < 0.01$, *** $p < 0.001$, Wilcoxon signed rank test for GCaMP and speed, Fisher's exact test for sleep fraction (S1 Data, Sheet 6D,E). (F–H) Following optogenetic hyperpolarization, RIS displayed strong rebound activation during lethargus (F). Rebound activation was abolished in a strain that is deficient for neurotransmission specifically in RIS (*flp-11::TetX*). (G) Rebound activation was abolished also by a mutation that impaired global synaptic transmission (*unc-13(s69)*). (H) * $p < 0.05$, ** $p < 0.01$, Wilcoxon signed rank test (S2 Data, Sheet S11F–H). (I) RIS showed a negative rebound following its own optogenetic depolarization. The strength of the negative rebound transient depended on the lethargus status of the worm. Worms during lethargus displayed a 3-times-stronger negative rebound compared to worms outside of lethargus. * $p < 0.05$, ** $p < 0.01$, *** $p < 0.001$, Wilcoxon signed rank test for GCaMP and speed, Fisher's exact test for sleep fraction (S2 Data, Sheet S11I). (TIF)

S12 Fig. RIM baseline activity levels are dampened during lethargus independently of RIS. (A) Sample traces of RIM transient frequencies, RIM baseline activities, and worm locomotion behaviors outside of and during lethargus in wild-type worms and *aptf-1(gk794)* mutants (S2

Data, Sheet S12). (B) Wild-type worms, but not *aptf-1(gk794)* mutant worms, display changes in RIM transient frequencies across lethargus. Transient frequencies were assessed manually. To be counted as a transient, RIM activity levels had to be at least twice as high as baseline activity levels. *** $p < 0.001$ Kolmogorov-Smirnov test for wild-type condition, Welch test for mutant condition (S2 Data, Sheet S12). (C) The reduction of RIM baseline activity levels during lethargus is preserved in *aptf-1(gk794)* mutants. ** $p < 0.01$, Wilcoxon signed rank test (S2 Data, Sheet S12). (TIF)

S13 Fig. Assaying gentle tail touch reveals an inhibitory role of RIM on RIS. (A) RIM ablation increases the reinstating of immobility following gentle tail touch during lethargus. * $p < 0.05$, Kolmogorov-Smirnov test (S2 Data, Sheet S13A). (B) RIM ablation increases RIS activation in response to gentle tail touch. ** $p < 0.01$, Kolmogorov-Smirnov test (S2 Data, Sheet S13B). (TIF)

S1 Text. A list of strains that were used during this study.
(DOCX)

S2 Text. A list of generated constructs during this study.
(DOCX)

S3 Text. Sequence of the strain PHX816, which was generated during this study.
(DOCX)

S1 Table. List of primers that were used during this study.
(DOCX)

S2 Table. List of plasmids that were used during this study.
(DOCX)

S3 Table. Experimental details of all optogenetic experiments conducted during this study.
(DOCX)

S1 Data. Raw data for all experiments from the main figures (Figs 1–9).
(XLSX)

S2 Data. Raw data for the experiments from the supporting figures (S1–S13 Figs).
(XLSX)

Acknowledgments

We are grateful to Jonathan Packer and Robert Waterson for suggesting the use of the *zk673.11* promoter. We thank Cori Bargmann, Andrew M. Leifer, Andres Mariqc, Shai Shaham, Yun Zhang, Manuel Zimmer, and the Caenorhabdis Genetics Center for strains. The strain PHX816 was generated by SunyBiotech. We are grateful to Kaveh Ashrafi, Ithai Rabino-witch, and Yoshinori Tanizawa for plasmids.

Author Contributions

Conceptualization: Henrik Bringmann.

Data curation: Elisabeth Maluck, Inka Busack, Judith Besseling, Florentin Masurat.

Formal analysis: Elisabeth Maluck, Inka Busack, Judith Besseling, Florentin Masurat.

Funding acquisition: Henrik Bringmann.

Investigation: Elisabeth Maluck, Inka Busack.

Methodology: Elisabeth Maluck, Inka Busack, Judith Besseling, Florentin Masurat.

Project administration: Henrik Bringmann.

Resources: Elisabeth Maluck, Inka Busack, Judith Besseling, Florentin Masurat, Michal Turek, Karl Emanuel Busch.

Supervision: Henrik Bringmann.

Writing – original draft: Henrik Bringmann.

Writing – review & editing: Elisabeth Maluck, Inka Busack, Karl Emanuel Busch.

References

1. Irwin MR. Why sleep is important for health: a psychoneuroimmunology perspective. *Annu Rev Psychol.* 2015; 66:143–72. Epub 2014/07/26. <https://doi.org/10.1146/annurev-psych-010213-115205> PMID: 25061767.
2. McEwen BS, Karatsoreos IN. Sleep Deprivation and Circadian Disruption: Stress, Allostasis, and Allostatic Load. *Sleep medicine clinics.* 2015; 10(1):1–10. Epub 2015/06/10. <https://doi.org/10.1016/j.jsmc.2014.11.007> PMID: 26055668.
3. Drake CL, Roehrs T, Roth T. Insomnia causes, consequences, and therapeutics: an overview. *Depression and anxiety.* 2003; 18(4):163–76. Epub 2003/12/09. <https://doi.org/10.1002/da.10151> PMID: 14661186.
4. Knutson KL, Spiegel K, Penev P, Van Cauter E. The metabolic consequences of sleep deprivation. *Sleep medicine reviews.* 2007; 11(3):163–78. Epub 2007/04/20. <https://doi.org/10.1016/j.smrv.2007.01.002> PMID: 17442599.
5. Van Cauter E, Spiegel K, Tasali E, Leproult R. Metabolic consequences of sleep and sleep loss. *Sleep Med.* 2008; 9 Suppl 1:S23–8. Epub 2008/12/17. [https://doi.org/10.1016/S1389-9457\(08\)70013-3](https://doi.org/10.1016/S1389-9457(08)70013-3) PMID: 18929315.
6. Saper CB, Fuller PM, Pedersen NP, Lu J, Scammell TE. Sleep state switching. *Neuron.* 2010; 68(6):1023–42. Epub 2010/12/22. <https://doi.org/10.1016/j.neuron.2010.11.032> PMID: 21172606.
7. Campbell SS, Tobler I. Animal sleep: a review of sleep duration across phylogeny. *Neurosci Biobehav Rev.* 1984; 8(3):269–300. Epub 1984/01/01. [https://doi.org/10.1016/0149-7634\(84\)90054-x](https://doi.org/10.1016/0149-7634(84)90054-x) PMID: 6504414.
8. Bringmann H. Sleep-Active Neurons: Conserved Motors of Sleep. *Genetics.* 2018; 208(4):1279–89. Epub 2018/04/06. <https://doi.org/10.1534/genetics.117.300521> PMID: 29618588.
9. Lu J, Sherman D, Devor M, Saper CB. A putative flip-flop switch for control of REM sleep. *Nature.* 2006; 441(7093):589–94. Epub 2006/05/12. <https://doi.org/10.1038/nature04767> PMID: 16688184.
10. Morairty S, Rainnie D, McCarley R, Greene R. Disinhibition of ventrolateral preoptic area sleep-active neurons by adenosine: a new mechanism for sleep promotion. *Neuroscience.* 2004; 123(2):451–7. Epub 2003/12/31. <https://doi.org/10.1016/j.neuroscience.2003.08.066> PMID: 14698752.
11. Saper CB, Scammell TE, Lu J. Hypothalamic regulation of sleep and circadian rhythms. *Nature.* 2005; 437(7063):1257–63. Epub 2005/10/28. <https://doi.org/10.1038/nature04284> PMID: 16251950.
12. Weber F, Dan Y. Circuit-based interrogation of sleep control. *Nature.* 2016; 538(7623):51–9. Epub 2016/10/07. <https://doi.org/10.1038/nature19773> PMID: 27708309.
13. Zhang Z, Zhong P, Hu F, Barger Z, Ren Y, Ding X, et al. An Excitatory Circuit in the Pericolomotor Midbrain for Non-REM Sleep Control. *Cell.* 2019; 177(5):1293–307 e16. Epub 2019/04/30. <https://doi.org/10.1016/j.cell.2019.03.041> PMID: 31031008.
14. Borbely AA. A two process model of sleep regulation. *Human neurobiology.* 1982; 1(3):195–204. Epub 1982/01/01. PMID: 7185792.
15. Frank MG. Astroglial regulation of sleep homeostasis. *Curr Opin Neurobiol.* 2013; 23(5):812–8. Epub 2013/03/23. <https://doi.org/10.1016/j.conb.2013.02.009> PMID: 23518138.
16. Krueger JM, Frank MG, Wisor JP, Roy S. Sleep function: Toward elucidating an enigma. *Sleep medicine reviews.* 2016; 28:46–54. Epub 2015/10/09. <https://doi.org/10.1016/j.smrv.2015.08.005> PMID: 26447948.

17. Donlea JM, Pimentel D, Miesenbock G. Neuronal machinery of sleep homeostasis in *Drosophila*. *Neuron*. 2014; 81(4):860–72. Epub 2014/02/25. <https://doi.org/10.1016/j.neuron.2013.12.013> PMID: 24559676.
18. Pimentel D, Donlea JM, Talbot CB, Song SM, Thurston AJ, Miesenbock G. Operation of a homeostatic sleep switch. *Nature*. 2016; 536(7616):333–7. Epub 2016/08/04. <https://doi.org/10.1038/nature19055> PMID: 27487216.
19. Halasz P. Hierarchy of micro-arousals and the microstructure of sleep. *Neurophysiologie clinique = Clinical neurophysiology*. 1998; 28(6):461–75. Epub 1999/01/23. [https://doi.org/10.1016/s0987-7053\(99\)80016-1](https://doi.org/10.1016/s0987-7053(99)80016-1) PMID: 9894227.
20. Amzica F, Steriade M. Cellular substrates and laminar profile of sleep K-complex. *Neuroscience*. 1998; 82(3):671–86. Epub 1998/03/04. [https://doi.org/10.1016/s0306-4522\(97\)00319-9](https://doi.org/10.1016/s0306-4522(97)00319-9) PMID: 9483527.
21. Cash SS, Halgren E, Dehghani N, Rossetti AO, Thesen T, Wang C, et al. The human K-complex represents an isolated cortical down-state. *Science*. 2009; 324(5930):1084–7. Epub 2009/05/23. <https://doi.org/10.1126/science.1169626> PMID: 19461004.
22. Iwanir S, Tramm N, Nagy S, Wright C, Ish D, Biron D. The microarchitecture of *C. elegans* behavior during lethargus: homeostatic bout dynamics, a typical body posture, and regulation by a central neuron. *sleep*. 2013; 36(3):385–95. Epub 2013/03/02. <https://doi.org/10.5665/sleep.2456> PMID: 23449971.
23. Nagy S, Tramm N, Sanders J, Iwanir S, Shirley IA, Levine E, et al. Homeostasis in *C. elegans* sleep is characterized by two behaviorally and genetically distinct mechanisms. *eLife*. 2014; 3:e04380. Epub 2014/12/05. <https://doi.org/10.7554/eLife.04380> PMID: 25474127.
24. Joiner WJ. Unraveling the Evolutionary Determinants of Sleep. *Curr Biol*. 2016; 26(20):R1073–R87. Epub 2016/10/26. <https://doi.org/10.1016/j.cub.2016.08.068> PMID: 27780049.
25. Turek M, Lewandrowski I, Bringmann H. An AP2 transcription factor is required for a sleep-active neuron to induce sleep-like quiescence in *C. elegans*. *Curr Biol*. 2013; 23(22):2215–23. Epub 2013/11/05. <https://doi.org/10.1016/j.cub.2013.09.028> PMID: 24184105.
26. Bennett HL, Khoruzhik Y, Hayden D, Huang H, Sanders J, Walsh MB, et al. Normal sleep bouts are not essential for *C. elegans* survival and FoxO is important for compensatory changes in sleep. *BMC neuroscience*. 2018; 19(1):10. Epub 2018/03/11. <https://doi.org/10.1186/s12868-018-0408-1> PMID: 29523076.
27. Wu Y, Masurat F, Preis J, Bringmann H. Sleep Counteracts Aging Phenotypes to Survive Starvation-Induced Developmental Arrest in *C. elegans*. *Curr Biol*. 2018; 28(22):3610–24.e8. Epub 2018/11/13. <https://doi.org/10.1016/j.cub.2018.10.009> PMID: 30416057.
28. White JG, Southgate E, Thomson JN, Brenner S. The structure of the nervous system of the nematode *Caenorhabditis elegans*. *Philos Trans R Soc Lond B Biol Sci*. 1986; 314(1165):1–340. Epub 1986/11/12. <https://doi.org/10.1098/rstb.1986.0056> PMID: 22462104.
29. Raizen DM, Zimmerman JE, Maycock MH, Ta UD, You YJ, Sundaram MV, et al. Lethargus is a *Caenorhabditis elegans* sleep-like state. *Nature*. 2008; 451(7178):569–72. Epub 2008/01/11. <https://doi.org/10.1038/nature06535> PMID: 1818515.
30. Trojanowski NF, Raizen DM. Call it Worm Sleep. *Trends in neurosciences*. 2016; 39(2):54–62. Epub 2016/01/10. <https://doi.org/10.1016/j.tins.2015.12.005> PMID: 26747654.
31. Kayser MS, Biron D. Sleep and Development in Genetically Tractable Model Organisms. *Genetics*. 2016; 203(1):21–33. Epub 2016/05/18. <https://doi.org/10.1534/genetics.116.189589> PMID: 27183564.
32. Cook SJ, Jarrell TA, Brittin CA, Wang Y, Bloniarz AE, Yakovlev MA, et al. Whole-animal connectomes of both *Caenorhabditis elegans* sexes. *Nature*. 2019; 571(7763):63–71. Epub 2019/07/05. <https://doi.org/10.1038/s41586-019-1352-7> PMID: 31270481.
33. Sulston JE, Horvitz HR. Post-embryonic cell lineages of the nematode, *Caenorhabditis elegans*. *Dev Biol*. 1977; 56(1):110–56. Epub 1977/03/01. [https://doi.org/10.1016/0012-1606\(77\)90158-0](https://doi.org/10.1016/0012-1606(77)90158-0) PMID: 838129.
34. Cassada RC, Russell RL. The dauerlarva, a post-embryonic developmental variant of the nematode *Caenorhabditis elegans*. *Dev Biol*. 1975; 46(2):326–42. Epub 1975/10/01. [https://doi.org/10.1016/0012-1606\(75\)90109-8](https://doi.org/10.1016/0012-1606(75)90109-8) PMID: 1183723.
35. Guo ZV, Hart AC, Ramanathan S. Optical interrogation of neural circuits in *Caenorhabditis elegans*. *Nat Methods*. 2009; 6(12):891–6. Epub 2009/11/10. <https://doi.org/10.1038/nmeth.1397> PMID: 19898486.
36. Piggott BJ, Liu J, Feng Z, Wescott SA, Xu XZ. The neural circuits and synaptic mechanisms underlying motor initiation in *C. elegans*. *Cell*. 2011; 147(4):922–33. Epub 2011/11/15. <https://doi.org/10.1016/j.cell.2011.08.053> PMID: 22078887.

37. Taylor SR, Santpere G, Reilly M, Glenwinkel L, Poff A, McWhirter R, et al. Expression profiling of the mature *C. elegans* nervous system by single-cell RNA-Sequencing. *bioRxiv*. 2019:737577.
38. Alkema MJ, Hunter-Ensor M, Ringstad N, Horvitz HR. Tyramine Functions independently of octopamine in the *Caenorhabditis elegans* nervous system. *Neuron*. 2005; 46(2):247–60. Epub 2005/04/26. <https://doi.org/10.1016/j.neuron.2005.02.024> PMID: 15848803.
39. Rogers C, Reale V, Kim K, Chatwin H, Li C, Evans P, et al. Inhibition of *Caenorhabditis elegans* social feeding by FMRamide-related peptide activation of NPR-1. *Nat Neurosci*. 2003; 6(11):1178–85. Epub 2003/10/14. <https://doi.org/10.1038/nn1140> PMID: 14555955.
40. Serrano-Saiz E, Poole RJ, Felton T, Zhang F, De La Cruz ED, Hobert O. Modular control of glutamatergic neuronal identity in *C. elegans* by distinct homeodomain proteins. *Cell*. 2013; 155(3):659–73. Epub 2013/11/19. <https://doi.org/10.1016/j.cell.2013.09.052> PMID: 24243022.
41. Lee RY, Sawin ER, Chalfie M, Horvitz HR, Avery L. EAT-4, a homolog of a mammalian sodium-dependent inorganic phosphate cotransporter, is necessary for glutamatergic neurotransmission in *Caenorhabditis elegans*. *J Neurosci*. 1999; 19(1):159–67. Epub 1998/12/31. <https://doi.org/10.1523/JNEUROSCI.19-01-00159.1999> PMID: 9870947.
42. Zimmer M, Gray JM, Pokala N, Chang AJ, Karow DS, Marletta MA, et al. Neurons detect increases and decreases in oxygen levels using distinct guanylate cyclases. *Neuron*. 2009; 61(6):865–79. Epub 2009/03/28. <https://doi.org/10.1016/j.neuron.2009.02.013> PMID: 19323996.
43. Sawin ER, Ranganathan R, Horvitz HR. *C. elegans* locomotory rate is modulated by the environment through a dopaminergic pathway and by experience through a serotonergic pathway. *Neuron*. 2000; 26(3):619–31. Epub 2000/07/15. [https://doi.org/10.1016/s0896-6273\(00\)81199-x](https://doi.org/10.1016/s0896-6273(00)81199-x) PMID: 10896158.
44. Han X, Chow BY, Zhou H, Klapoetke NC, Chuong A, Rajmeh R, et al. A high-light sensitivity optical neural silencer: development and application to optogenetic control of non-human primate cortex. *Frontiers in systems neuroscience*. 2011; 5:18. Epub 2011/08/04. <https://doi.org/10.3389/fnsys.2011.00018> PMID: 21811444.
45. Okazaki A, Takagi S. An optogenetic application of proton pump ArchT to *C. elegans* cells. *Neuroscience research*. 2013; 75(1):29–34. Epub 2012/10/10. <https://doi.org/10.1016/j.neures.2012.09.002> PMID: 23044183.
46. Li W, Kang L, Piggott BJ, Feng Z, Xu XZ. The neural circuits and sensory channels mediating harsh touch sensation in *Caenorhabditis elegans*. *Nat Commun*. 2011; 2:315. Epub 2011/05/19. <https://doi.org/10.1038/ncomms1308> PMID: 21587232.
47. Cao J, Packer JS, Ramani V, Cusanovich DA, Huynh C, Daza R, et al. Comprehensive single-cell transcriptional profiling of a multicellular organism. *Science*. 2017; 357(6352):661–7. Epub 2017/08/19. <https://doi.org/10.1126/science.aam8940> PMID: 28818938.
48. Packer JS, Zhu Q, Huynh C, Sivaramakrishnan P, Preston E, Dueck H, et al. A lineage-resolved molecular atlas of *C. elegans* embryogenesis at single-cell resolution. *Science*. 2019. Epub 2019/09/07. <https://doi.org/10.1126/science.aax1971> PMID: 31488706.
49. Chalfie M, Sulston JE, White JG, Southgate E, Thomson JN, Brenner S. The neural circuit for touch sensitivity in *Caenorhabditis elegans*. *J Neurosci*. 1985; 5(4):956–64. Epub 1985/04/01. <https://doi.org/10.1523/JNEUROSCI.05-04-00956.1985> PMID: 3981252.
50. Husson SJ, Costa WS, Wabnig S, Stirman JN, Watson JD, Spencer WC, et al. Optogenetic analysis of a nociceptor neuron and network reveals ion channels acting downstream of primary sensors. *Curr Biol*. 2012; 22(9):743–52. Epub 2012/04/10. <https://doi.org/10.1016/j.cub.2012.02.066> PMID: 22483941.
51. Turek M, Besseling J, Spies JP, Konig S, Bringmann H. Sleep-active neuron specification and sleep induction require FLP-11 neuropeptides to systemically induce sleep. *eLife*. 2016; 5. Epub 2016/03/08. <https://doi.org/10.7554/eLife.12499> PMID: 26949257.
52. Katz M, Corson F, Iwanir S, Biron D, Shaham S. Glia Modulate a Neuronal Circuit for Locomotion Suppression during Sleep in *C. elegans*. *Cell reports*. 2018; 22(10):2575–83. Epub 2018/03/08. <https://doi.org/10.1016/j.celrep.2018.02.036> PMID: 29514087.
53. Chalfie M, Hart AC, Rankin CH, Goodman MB. Assaying mechanosensation. *WormBook*. 2014. Epub 2014/08/06. <https://doi.org/10.1895/wormbook.1.172.1> PMID: 25093996.
54. Pokala N, Liu Q, Gordus A, Bargmann CI. Inducible and titratable silencing of *Caenorhabditis elegans* neurons in vivo with histamine-gated chloride channels. *Proc Natl Acad Sci U S A*. 2014; 111(7):2770–5. Epub 2014/02/20. <https://doi.org/10.1073/pnas.1400615111> PMID: 24550306.
55. Zheng Y, Brockie PJ, Mellem JE, Madsen DM, Maricq AV. Neuronal control of locomotion in *C. elegans* is modified by a dominant mutation in the GLR-1 ionotropic glutamate receptor. *Neuron*. 1999; 24(2):347–61. Epub 1999/11/26. [https://doi.org/10.1016/s0896-6273\(00\)80849-1](https://doi.org/10.1016/s0896-6273(00)80849-1) PMID: 10571229.

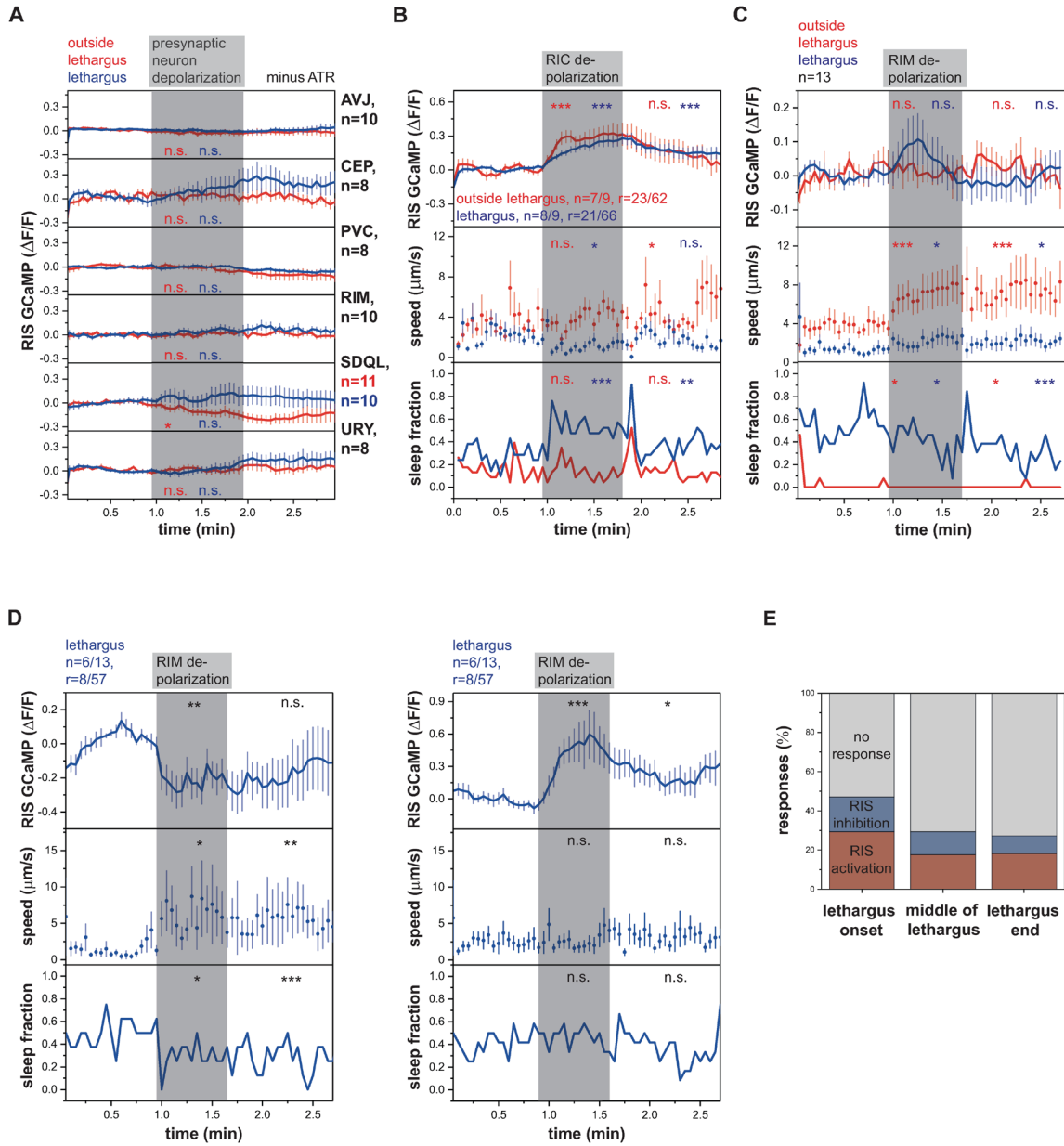
56. Brockie PJ, Mellem JE, Hills T, Madsen DM, Maricq AV. The *C. elegans* glutamate receptor subunit NMR-1 is required for slow NMDA-activated currents that regulate reversal frequency during locomotion. *Neuron*. 2001; 31(4):617–30. Epub 2001/09/08. [https://doi.org/10.1016/s0896-6273\(01\)00394-4](https://doi.org/10.1016/s0896-6273(01)00394-4) PMID: 11545720.
57. Nguyen JP, Shipley FB, Linder AN, Plummer GS, Liu M, Setru SU, et al. Whole-brain calcium imaging with cellular resolution in freely behaving *Caenorhabditis elegans*. *Proc Natl Acad Sci U S A*. 2016; 113(8):E1074–81. Epub 2015/12/30. <https://doi.org/10.1073/pnas.1507110112> PMID: 26712014.
58. Mahn M, Gibor L, Patil P, Cohen-Kashi Malina K, Oring S, Printz Y, et al. High-efficiency optogenetic silencing with soma-targeted anion-conducting channelrhodopsins. *Nat Commun*. 2018; 9(1):4125. Epub 2018/10/10. <https://doi.org/10.1038/s41467-018-06511-8> PMID: 30297821.
59. Richmond JE, Davis WS, Jorgensen EM. UNC-13 is required for synaptic vesicle fusion in *C. elegans*. *Nat Neurosci*. 1999; 2(11):959–64. Epub 1999/10/20. <https://doi.org/10.1038/14755> PMID: 10526333.
60. Davis MW, Morton JJ, Carroll D, Jorgensen EM. Gene activation using FLP recombinase in *C. elegans*. *PLoS Genet*. 2008; 4(3):e1000028. Epub 2008/03/29. <https://doi.org/10.1371/journal.pgen.1000028> PMID: 18369447.
61. Nagy S, Wright C, Tramm N, Labello N, Burov S, Biron D. A longitudinal study of *Caenorhabditis elegans* larvae reveals a novel locomotion switch, regulated by Galphas signaling. *eLife*. 2013; 2:e00782. Epub 2013/07/11. <https://doi.org/10.7554/eLife.00782> PMID: 23840929.
62. Belfer SJ, Chuang HS, Freedman BL, Yuan J, Norton M, Bau HH, et al. *Caenorhabditis*-in-drop array for monitoring *C. elegans* quiescent behavior. *sleep*. 2013; 36(5):689–98G. Epub 2013/05/02. <https://doi.org/10.5665/sleep.2628> PMID: 23633751.
63. Cirelli C, Bushey D, Hill S, Huber R, Kreber R, Ganetzky B, et al. Reduced sleep in *Drosophila* Shaker mutants. *Nature*. 2005; 434(7037):1087–92. Epub 2005/04/29. <https://doi.org/10.1038/nature03486> PMID: 15858564.
64. Koh K, Joiner WJ, Wu MN, Yue Z, Smith CJ, Sehgal A. Identification of SLEEPLESS, a sleep-promoting factor. *Science*. 2008; 321(5887):372–6. Epub 2008/07/19. <https://doi.org/10.1126/science.1155942> PMID: 18635795.
65. Kume K, Kume S, Park SK, Hirsh J, Jackson FR. Dopamine is a regulator of arousal in the fruit fly. *J Neurosci*. 2005; 25(32):7377–84. Epub 2005/08/12. <https://doi.org/10.1523/JNEUROSCI.2048-05.2005> PMID: 16093388.
66. Singh K, Ju JY, Walsh MB, Dilorio MA, Hart AC. Deep Conservation of Genes Required for Both *Drosophila melanogaster* and *Caenorhabditis elegans* Sleep Includes a Role for Dopaminergic Signaling. *sleep*. 2014; 37(9). <https://doi.org/10.5665/sleep.3990> PMID: 25142568.
67. Schwarz J, Bringmann H. Reduced sleep-like quiescence in both hyperactive and hypoactive mutants of the Galphaq Gene *egl-30* during lethargus in *Caenorhabditis elegans*. *PLoS ONE*. 2013; 8(9):e75853. Epub 2013/09/28. <https://doi.org/10.1371/journal.pone.0075853> PMID: 24073282.
68. Huang H, Hayden DJ, Zhu CT, Bennett HL, Venkatachalam V, Skuja LL, et al. Gap Junctions and NCA Cation Channels Are Critical for Developmentally Timed Sleep and Arousal in *Caenorhabditis elegans*. *Genetics*. 2018; 210(4):1369–81. Epub 2018/10/17. <https://doi.org/10.1534/genetics.118.301551> PMID: 30323068.
69. Pirri JK, Alkema MJ. The neuroethology of *C. elegans* escape. *Curr Opin Neurobiol*. 2012; 22(2):187–93. Epub 2012/01/10. <https://doi.org/10.1016/j.conb.2011.12.007> PMID: 22226513.
70. Nichols ALA, Eichler T, Latham R, Zimmer M. A global brain state underlies *C. elegans* sleep behavior. *Science*. 2017; 356(6344). Epub 2017/06/24. <https://doi.org/10.1126/science.aam6851> PMID: 28642382.
71. Kaplan JM, Horvitz HR. A dual mechanosensory and chemosensory neuron in *Caenorhabditis elegans*. *Proc Natl Acad Sci U S A*. 1993; 90(6):2227–31. Epub 1993/03/15. <https://doi.org/10.1073/pnas.90.6.2227> PMID: 8460126.
72. Gordus A, Pokala N, Levy S, Flavell SW, Bargmann CI. Feedback from network states generates variability in a probabilistic olfactory circuit. *Cell*. 2015; 161(2):215–27. Epub 2015/03/17. <https://doi.org/10.1016/j.cell.2015.02.018> PMID: 25772698.
73. Stirman JN, Crane MM, Husson SJ, Wabnig S, Schultheis C, Gottschalk A, et al. Real-time multimodal optical control of neurons and muscles in freely behaving *Caenorhabditis elegans*. *Nat Methods*. 2011; 8(2):153–8. Epub 2011/01/18. <https://doi.org/10.1038/nmeth.1555> PMID: 21240278.
74. Kawano T, Po MD, Gao S, Leung G, Ryu WS, Zhen M. An imbalancing act: gap junctions reduce the backward motor circuit activity to bias *C. elegans* for forward locomotion. *Neuron*. 2011; 72(4):572–86. Epub 2011/11/22. <https://doi.org/10.1016/j.neuron.2011.09.005> PMID: 22099460.

75. Kato S, Kaplan HS, Schrodel T, Skora S, Lindsay TH, Yemini E, et al. Global brain dynamics embed the motor command sequence of *Caenorhabditis elegans*. *Cell*. 2015; 163(3):656–69. Epub 2015/10/20. <https://doi.org/10.1016/j.cell.2015.09.034> PMID: 26478179.
76. Steuer Costa W, Van der Auwera P, Glock C, Liewald JF, Bach M, Schuler C, et al. A GABAergic and peptidergic sleep neuron as a locomotion stop neuron with compartmentalized Ca²⁺ dynamics. *Nat Commun*. 2019; 10(1):4095. Epub 2019/09/12. <https://doi.org/10.1038/s41467-019-12098-5> PMID: 31506439.
77. Skora S, Mende F, Zimmer M. Energy Scarcity Promotes a Brain-wide Sleep State Modulated by Insulin Signaling in *C. elegans*. *Cell reports*. 2018; 22(4):953–66. Epub 2018/02/02. <https://doi.org/10.1016/j.celrep.2017.12.091> PMID: 29386137.
78. Cho JY, Sternberg PW. Multilevel modulation of a sensory motor circuit during *C. elegans* sleep and arousal. *Cell*. 2014; 156(1–2):249–60. Epub 2014/01/21. <https://doi.org/10.1016/j.cell.2013.11.036> PMID: 24439380.
79. Schrodel T, Prevedel R, Aumayr K, Zimmer M, Vaziri A. Brain-wide 3D imaging of neuronal activity in *Caenorhabditis elegans* with sculpted light. *Nat Methods*. 2013; 10(10):1013–20. Epub 2013/09/10. <https://doi.org/10.1038/nmeth.2637> PMID: 24013820.
80. Gallagher T, Kim J, Oldenbroek M, Kerr R, You YJ. ASI regulates satiety quiescence in *C. elegans*. *J Neurosci*. 2013; 33(23):9716–24. Epub 2013/06/07. <https://doi.org/10.1523/JNEUROSCI.4493-12.2013> PMID: 23739968.
81. Goetting DL, Soto R, Van Buskirk C. Food-Dependent Plasticity in *Caenorhabditis elegans* Stress-Induced Sleep Is Mediated by TOR-FOXA and TGF-beta Signaling. *Genetics*. 2018. Epub 2018/06/22. <https://doi.org/10.1534/genetics.118.301204> PMID: 29925566.
82. Gaus SE, Strecker RE, Tate BA, Parker RA, Saper CB. Ventrolateral preoptic nucleus contains sleep-active, galanineric neurons in multiple mammalian species. *Neuroscience*. 2002; 115(1):285–94. Epub 2002/10/29. [https://doi.org/10.1016/s0306-4522\(02\)00308-1](https://doi.org/10.1016/s0306-4522(02)00308-1) PMID: 12401341.
83. Sherin JE, Shiromani PJ, McCarley RW, Saper CB. Activation of ventrolateral preoptic neurons during sleep. *Science*. 1996; 271(5246):216–9. Epub 1996/01/12. <https://doi.org/10.1126/science.271.5246.216> PMID: 8539624.
84. Chrousos G, Vgontzas AN, Kritikou I. HPA Axis and Sleep. In: De Groot LJ, Chrousos G, Dungan K, Feingold KR, Grossman A, Hershman JM, et al., editors. *Endotext*. South Dartmouth (MA): Endotext.org; 2016.
85. Panossian LA, Avidan AY. Review of sleep disorders. *The Medical clinics of North America*. 2009; 93(2):407–25. ix. Epub 2009/03/11. <https://doi.org/10.1016/j.mcna.2008.09.001> PMID: 19272516.
86. Liu S, Liu Q, Tabuchi M, Wu MN. Sleep Drive Is Encoded by Neural Plastic Changes in a Dedicated Circuit. *Cell*. 2016; 165(6):1347–60. Epub 2016/05/24. <https://doi.org/10.1016/j.cell.2016.04.013> PMID: 27212237.
87. Donlea JM, Pimentel D, Talbot CB, Kempf A, Omoto JJ, Hartenstein V, et al. Recurrent Circuitry for Balancing Sleep Need and Sleep. *Neuron*. 2018; 97(2):378–89 e4. Epub 2018/01/09. <https://doi.org/10.1016/j.neuron.2017.12.016> PMID: 29307711.
88. Oikonomou G, Altermatt M, Zhang RW, Coughlin GM, Montz C, Gradinaru V, et al. The Serotonergic Raphe Promote Sleep in Zebrafish and Mice. *Neuron*. 2019; 103(4):686–701 e8. Epub 2019/06/30. <https://doi.org/10.1016/j.neuron.2019.05.038> PMID: 31248729.
89. Dijk DJ. Regulation and functional correlates of slow wave sleep. *Journal of clinical sleep medicine: JCSM: official publication of the American Academy of Sleep Medicine*. 2009; 5(2 Suppl):S6–15. Epub 2009/12/17. PMID: 19998869.
90. Brenner S. The genetics of *Caenorhabditis elegans*. *Genetics*. 1974; 77(1):71–94. Epub 1974/05/01. PMID: 4366476.
91. Ahringer A. Reverse genetics. *WormBook*, ed The *C. elegans* Research Community. 2006.
92. Merritt C, Seydoux G. Transgenic solutions for the germline. *WormBook*. 2010:1–21. Epub 2010/02/20. <https://doi.org/10.1895/wormbook.1.148.1> PMID: 20169625.
93. Redemann S, Schloissnig S, Ernst S, Pozniakowsky A, Ayloo S, Hyman AA, et al. Codon adaptation-based control of protein expression in *C. elegans*. *Nat Methods*. 2011; 8(3):250–2. Epub 2011/02/01. <https://doi.org/10.1038/nmeth.1565> PMID: 21278743.
94. Praitis V, Casey E, Collar D, Austin J. Creation of low-copy integrated transgenic lines in *Caenorhabditis elegans*. *Genetics*. 2001; 157(3):1217–26. Epub 2001/03/10. PMID: 11238406.
95. Wilm T, Demel P, Koop HU, Schnabel H, Schnabel R. Ballistic transformation of *Caenorhabditis elegans*. *Gene*. 1999; 229(1–2):31–5. Epub 1999/03/30. [https://doi.org/10.1016/s0378-1119\(99\)00043-8](https://doi.org/10.1016/s0378-1119(99)00043-8) PMID: 10095101.

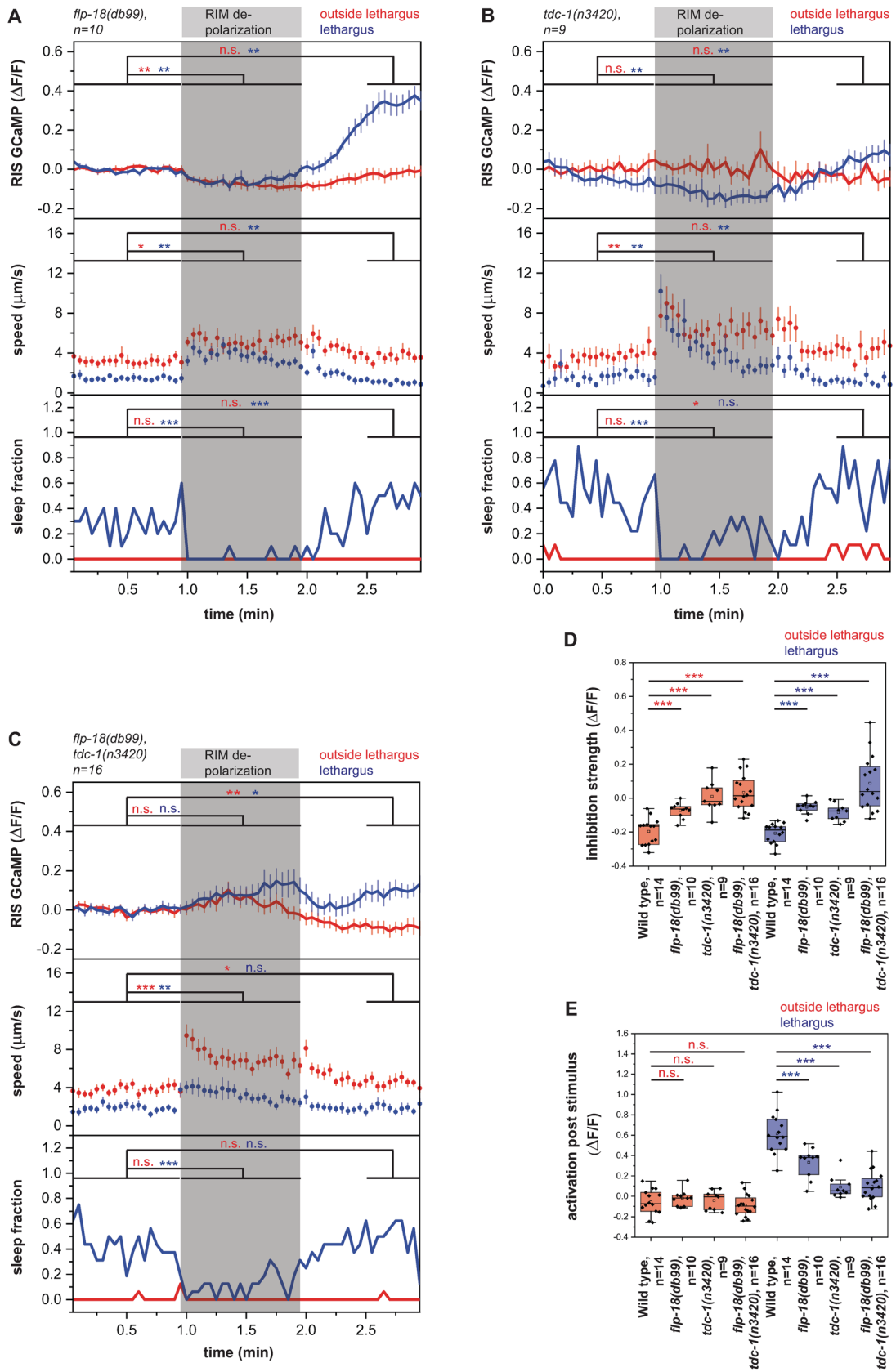
96. Bringmann H. Agarose hydrogel microcompartments for imaging sleep- and wake-like behavior and nervous system development in *Caenorhabditis elegans* larvae. *J Neurosci Methods*. 2011; 201(1):78–88. Epub 2011/08/02. <https://doi.org/10.1016/j.jneumeth.2011.07.013> PMID: 21801751.
97. Turek M, Besseling J, Bringmann H. Agarose Microchambers for Long-term Calcium Imaging of *Caenorhabditis elegans*. *Journal of visualized experiments: JoVE*. 2015;(100):e52742. Epub 2015/07/02. <https://doi.org/10.3791/52742> PMID: 26132740.
98. Stiernagle T. Maintenance of *C. elegans*. *WormBook*. 2006:1–11. Epub 2007/12/01. <https://doi.org/10.1895/wormbook.1.101.1> PMID: 18050451.
99. Kim E, Sun L, Gabel CV, Fang-Yen C. Long-term imaging of *Caenorhabditis elegans* using nanoparticle-mediated immobilization. *PLoS ONE*. 2013; 8(1):e53419. Epub 2013/01/10. <https://doi.org/10.1371/journal.pone.0053419> PMID: 23301069.
100. Hart AC, Sims S, Kaplan JM. Synaptic code for sensory modalities revealed by *C. elegans* GLR-1 glutamate receptor. *Nature*. 1995; 378(6552):82–5. Epub 1995/11/02. <https://doi.org/10.1038/378082a0> PMID: 7477294.
101. Nguyen JP, Linder AN, Plummer GS, Shaevitz JW, Leifer AM. Automatically tracking neurons in a moving and deforming brain. *PLoS Comput Biol*. 2017; 13(5):e1005517. Epub 2017/05/26. <https://doi.org/10.1371/journal.pcbi.1005517> PMID: 28545068.
102. Schwarz J, Lewandrowski I, Bringmann H. Reduced activity of a sensory neuron during a sleep-like state in *Caenorhabditis elegans*. *Curr Biol*. 2011; 21(24):R983–4. Epub 2011/12/24. <https://doi.org/10.1016/j.cub.2011.10.046> PMID: 22192827.
103. Nagy S, Raizen DM, Biron D. Measurements of behavioral quiescence in *Caenorhabditis elegans*. *Methods*. 2014. Epub 2014/03/20. <https://doi.org/10.1016/j.ymeth.2014.03.009> PMID: 24642199.

Supplementary Information

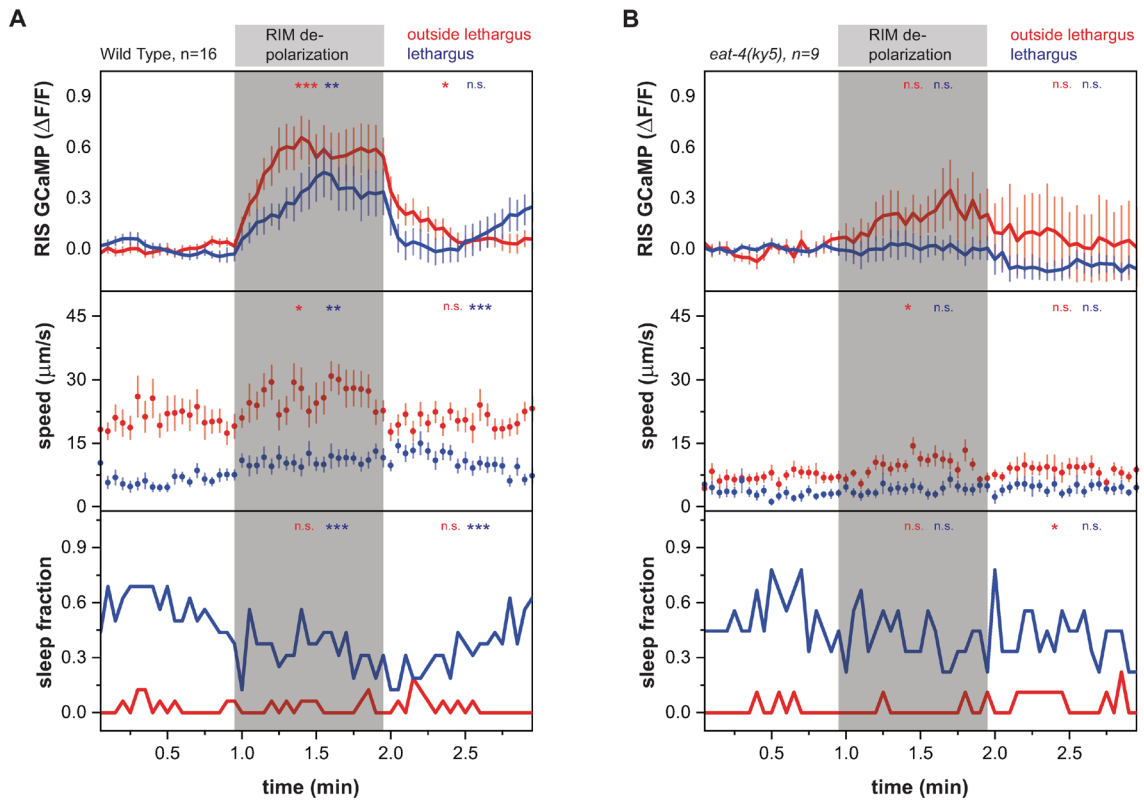
S1 Fig



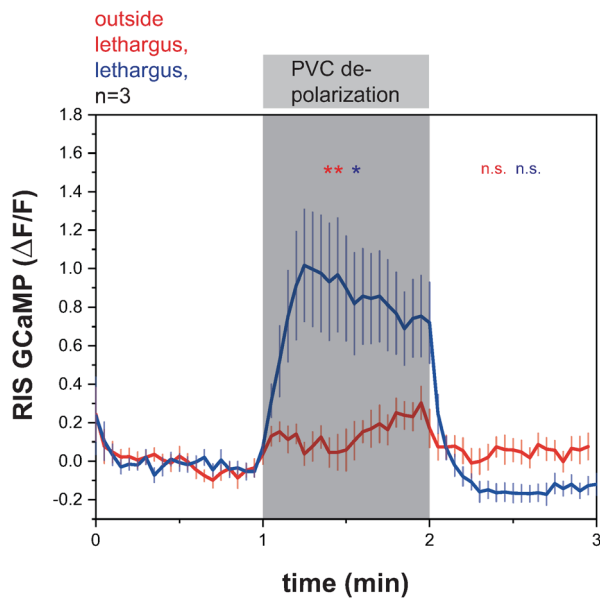
S2 Fig



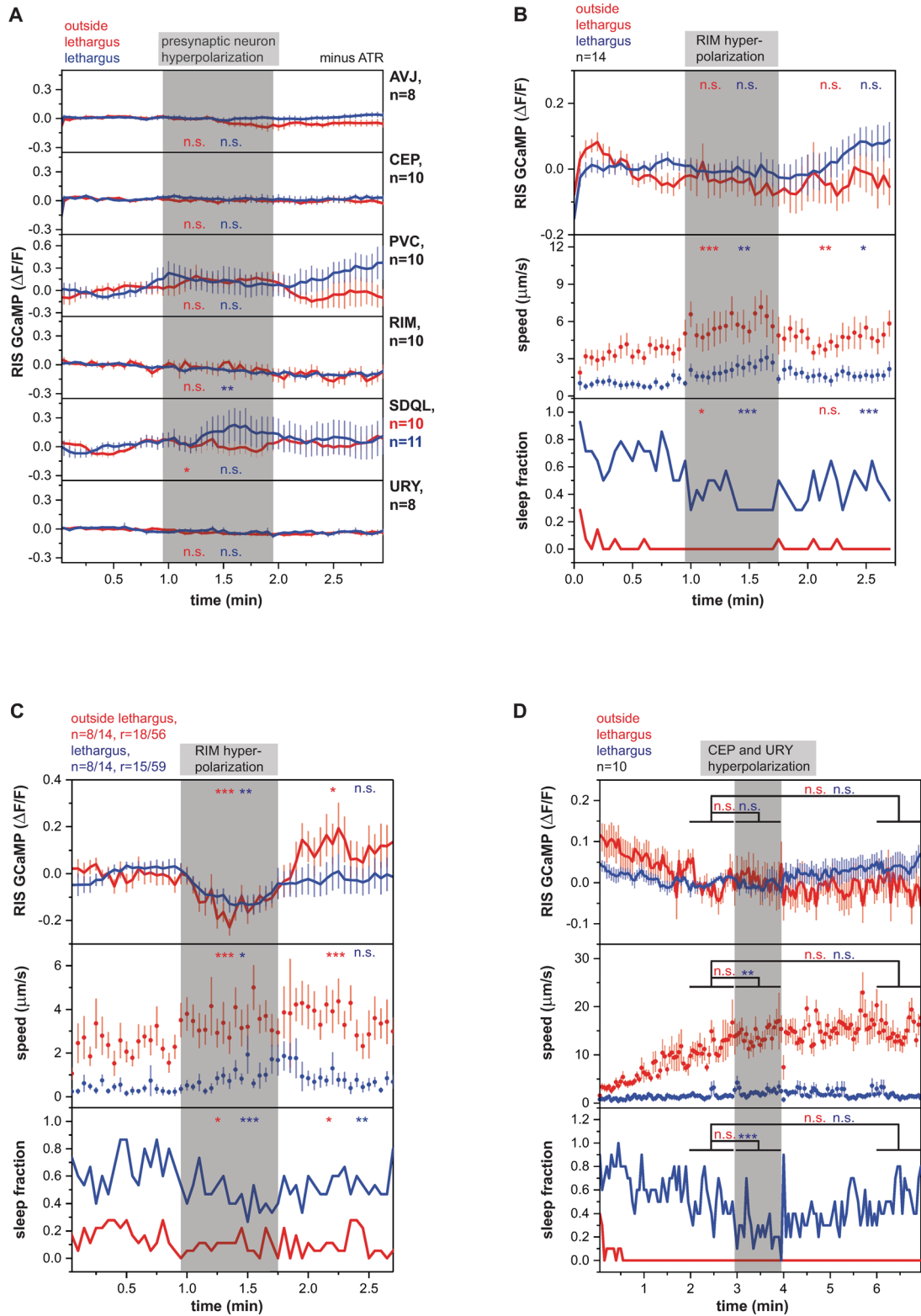
S3 Fig



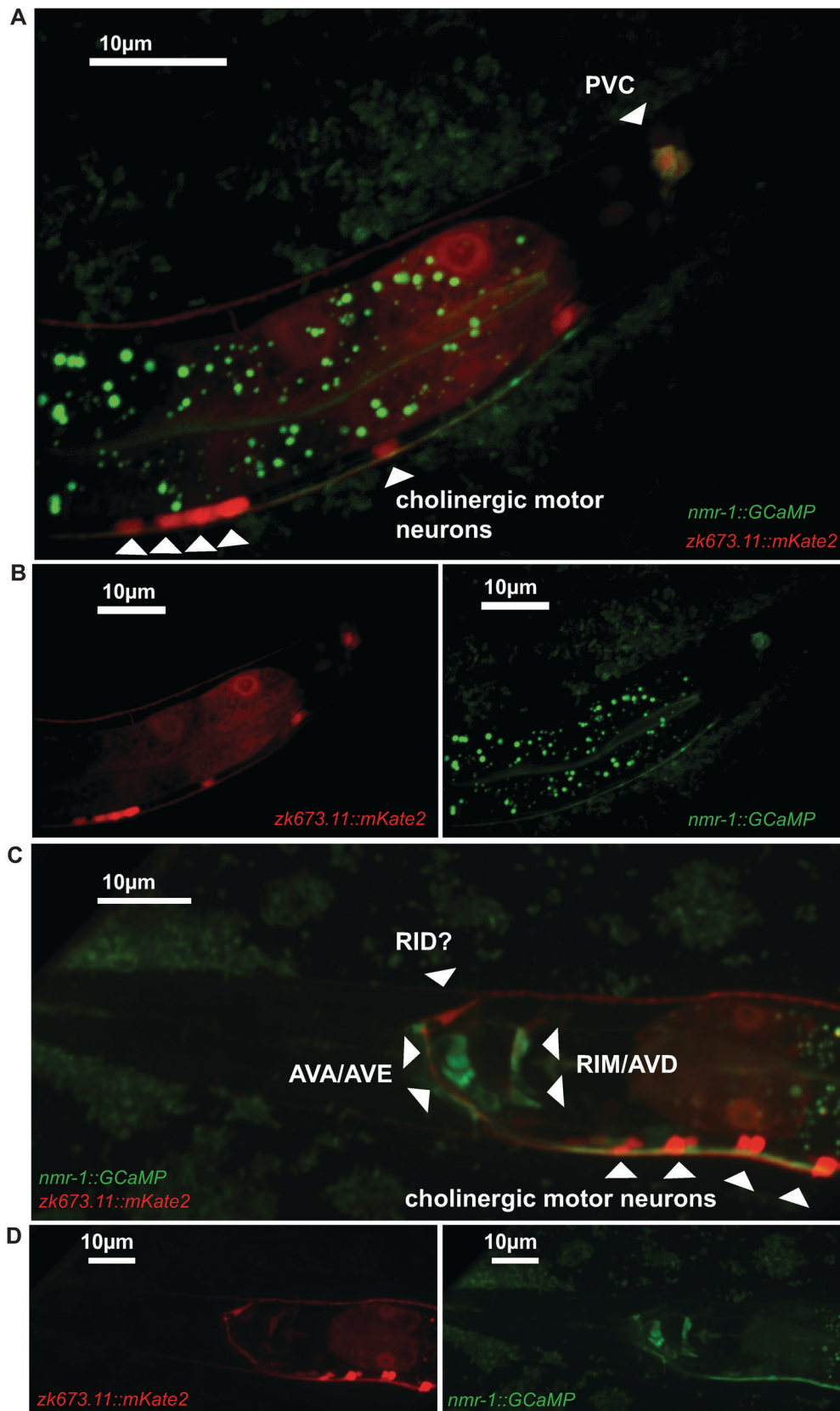
S4 Fig



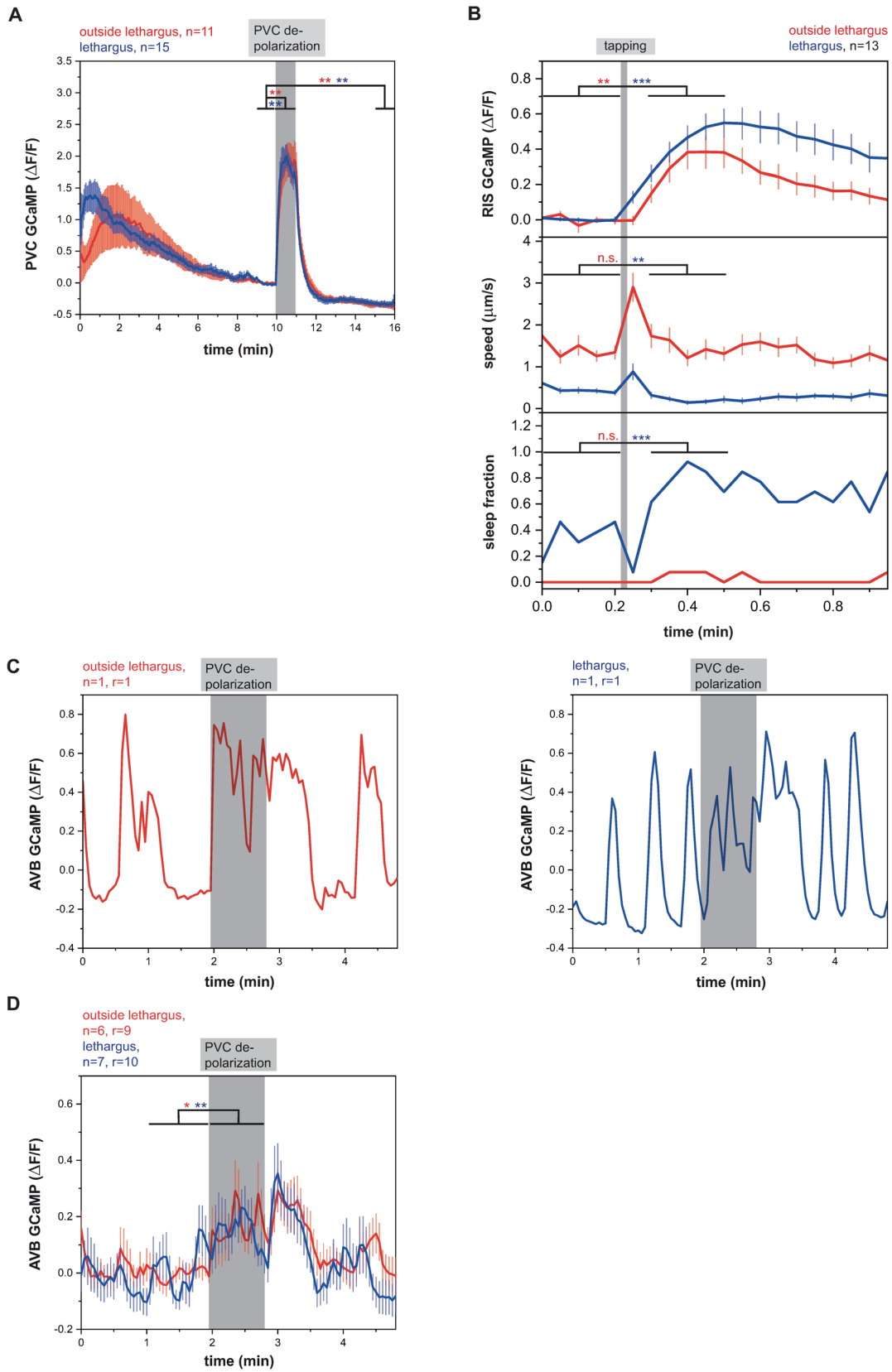
S5 Fig



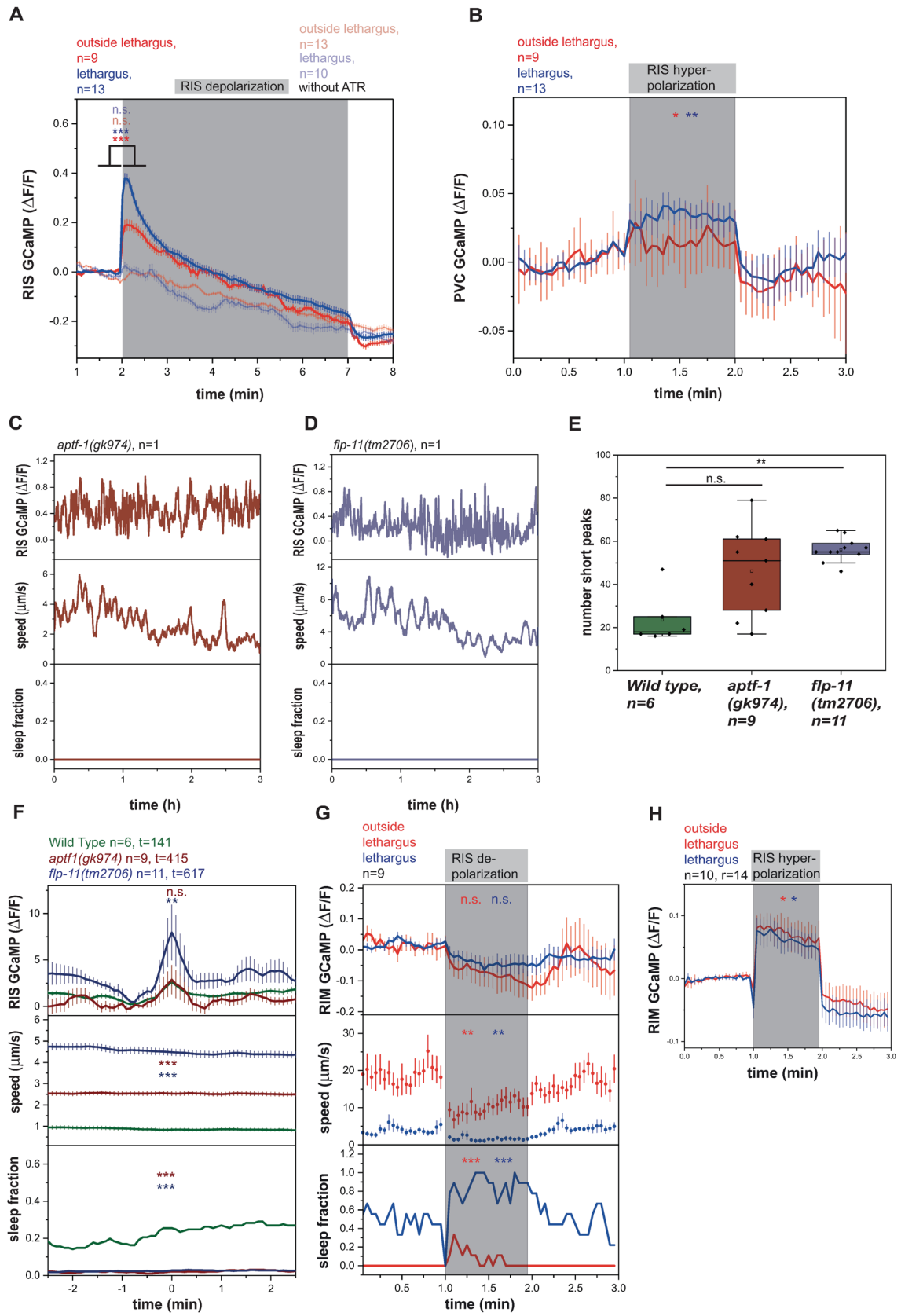
S6 Fig



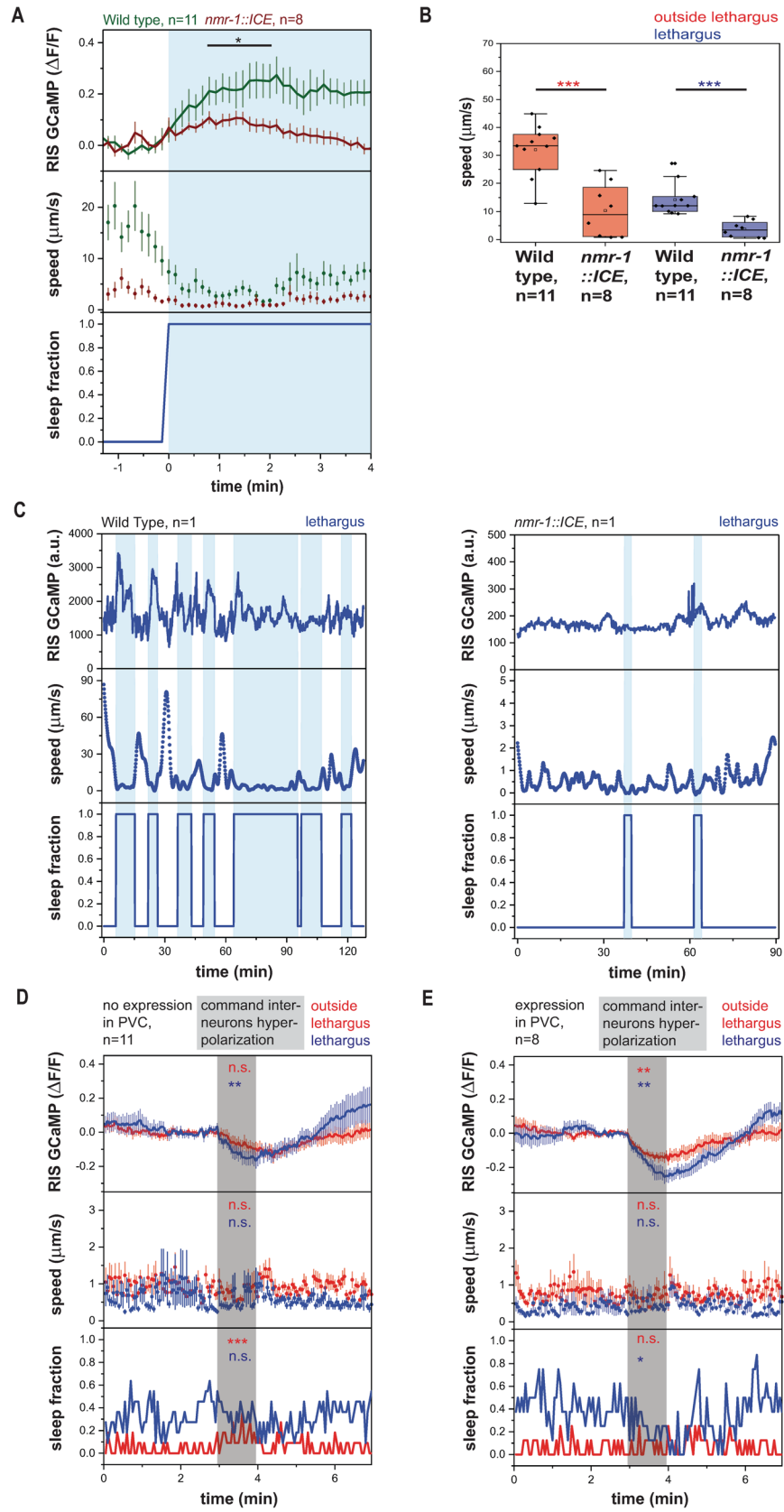
S7 Fig



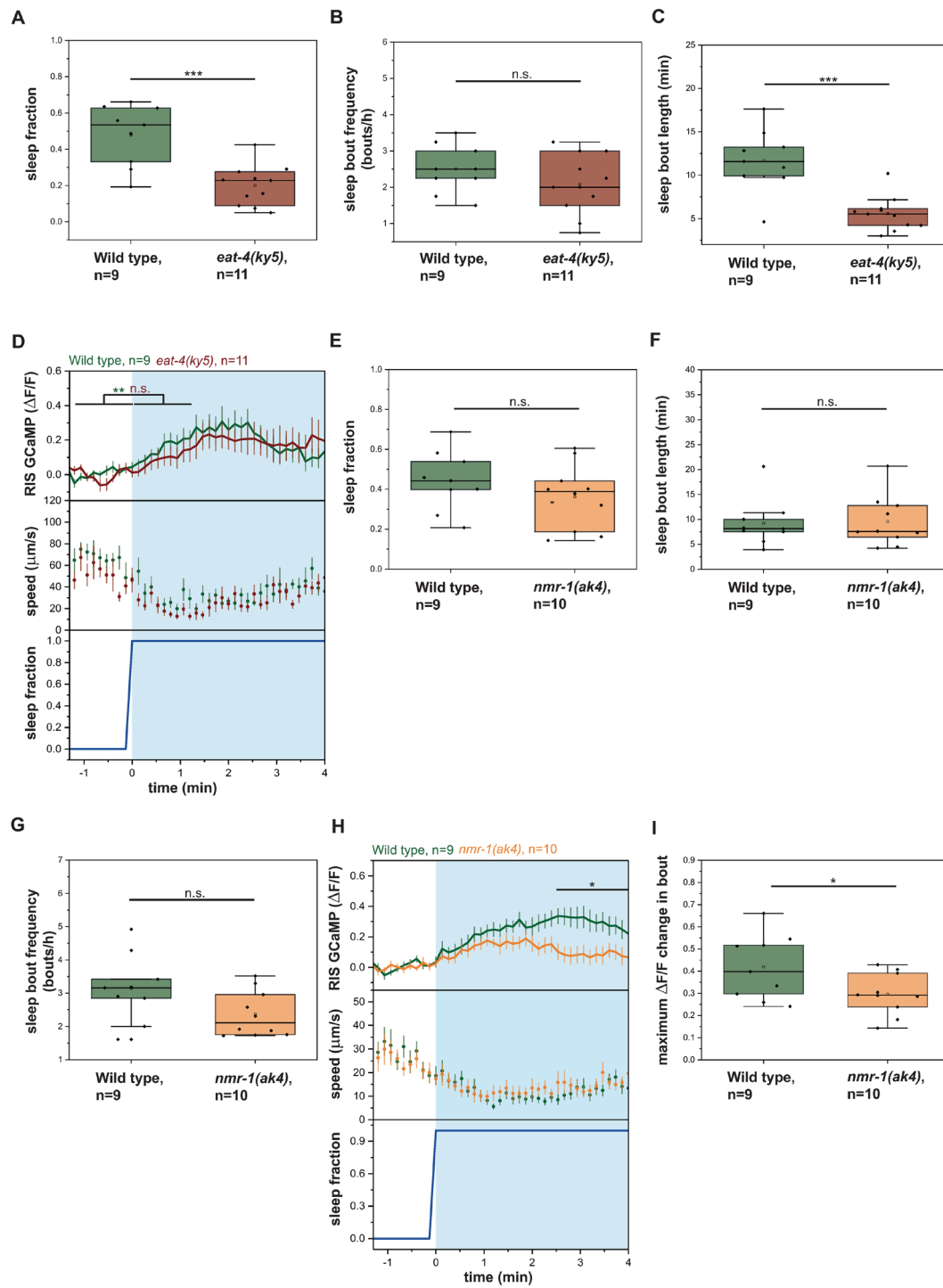
S8 Fig



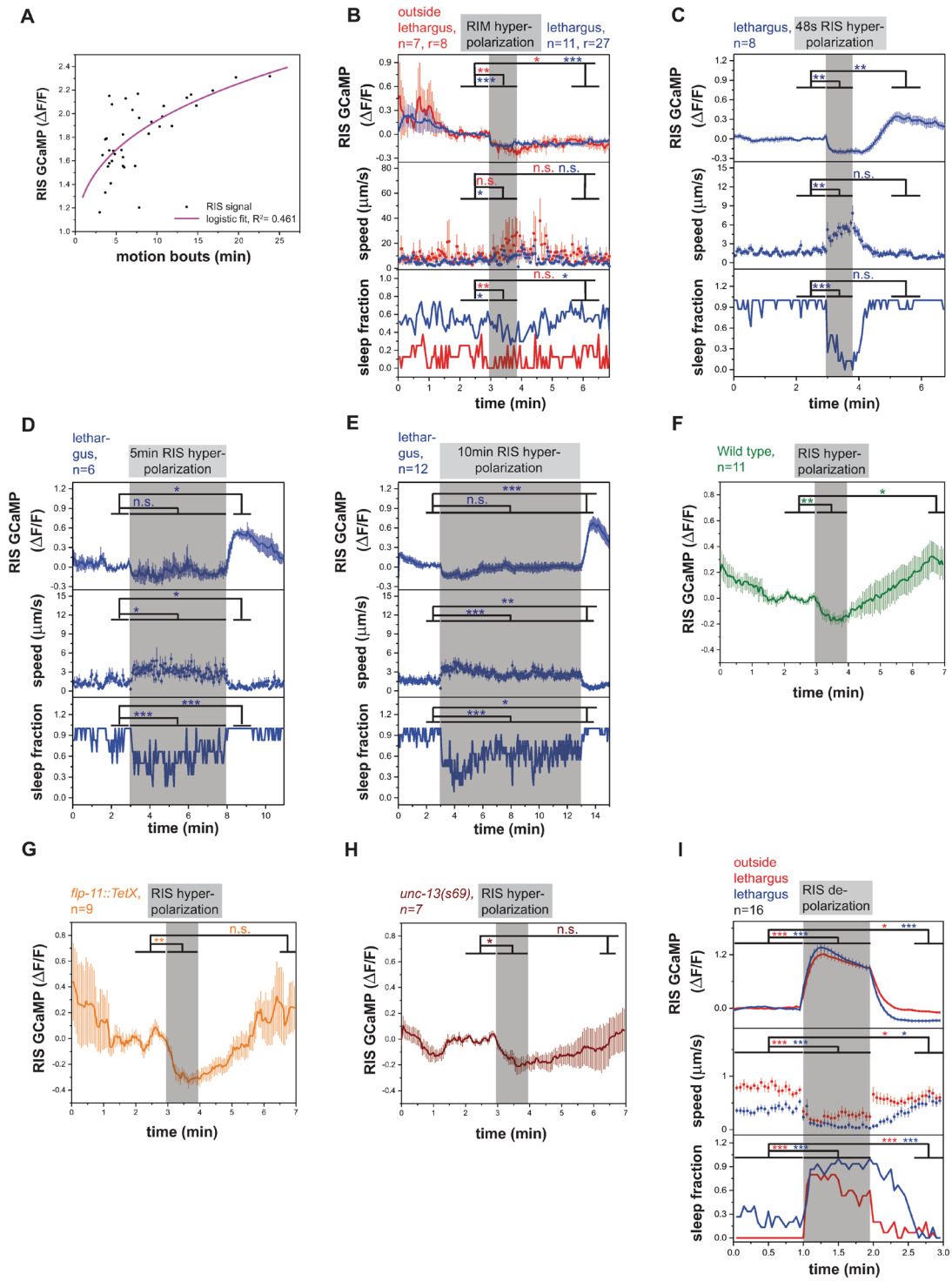
S9 Fig



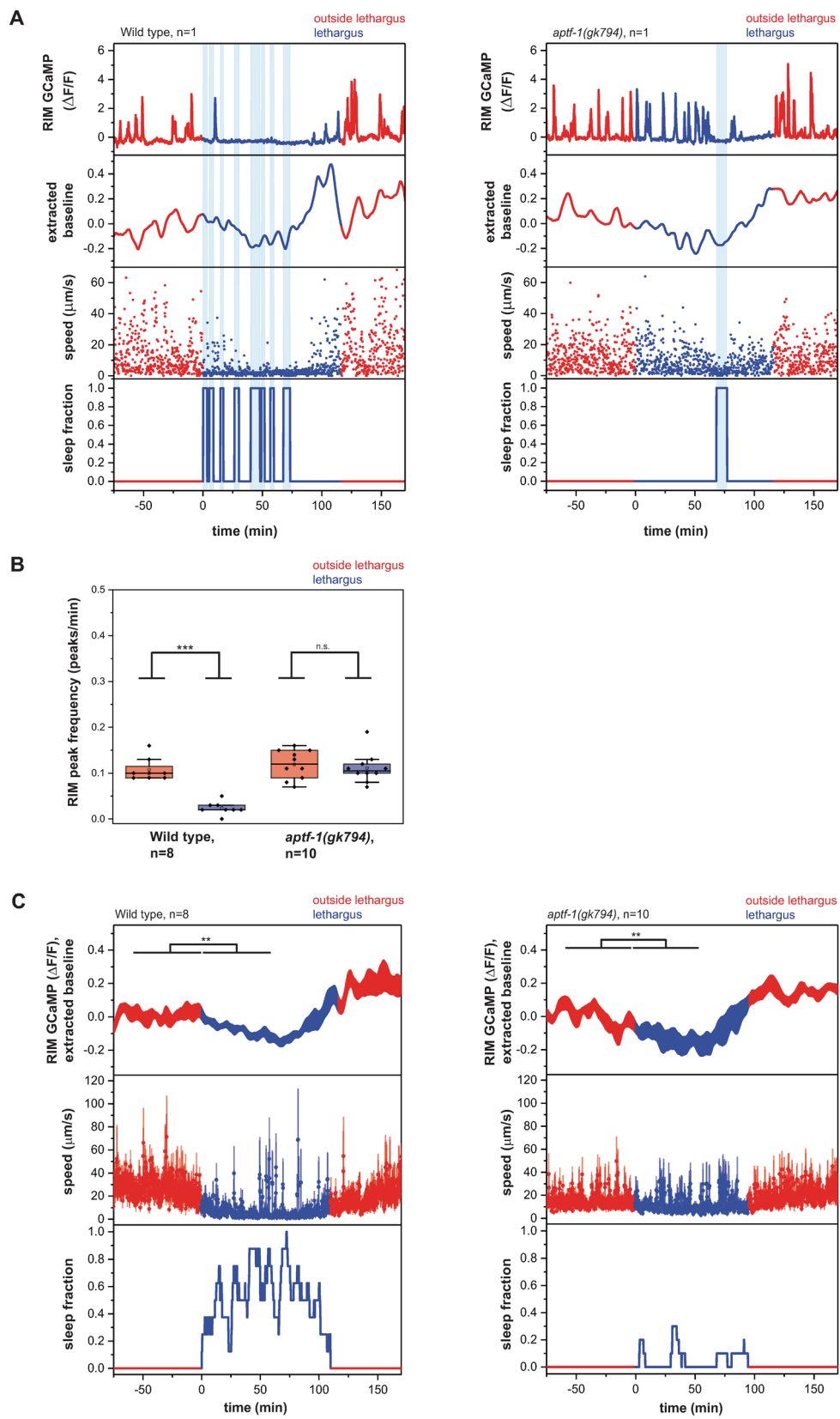
S10 Fig



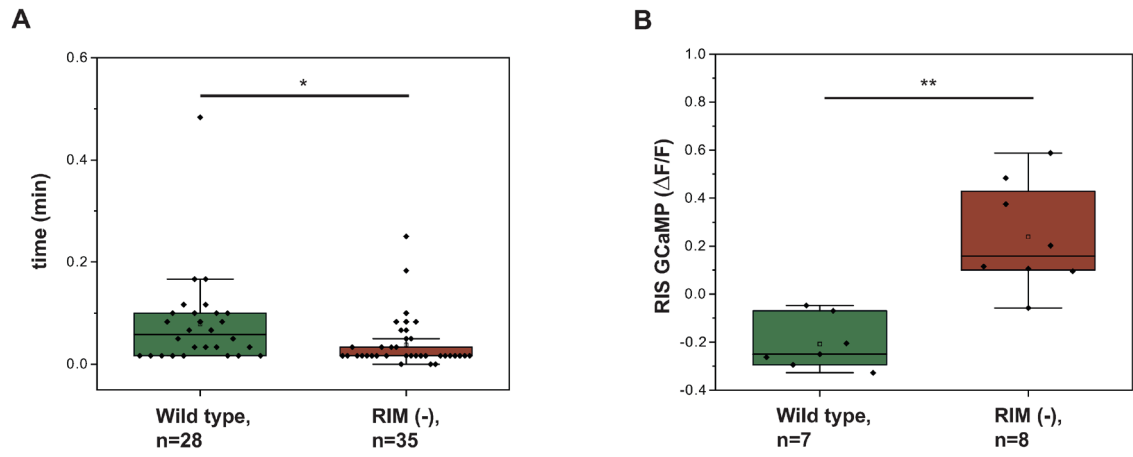
S11 Fig



S12 Fig



S13 Fig



S1 Text. Strain list.

The following *C. elegans* strains were used for this study:

- HBR227 *aptf-1(gk794) II*. [1]
- HBR430 *goeIs64 [aptf-1p::SL1-GCaMP3.35-SL2::mKate2-unc-54-3'utr, unc-119(+)]*. [1]
- HBR448 *aptf-1(gk794) II; goeIs64 [aptf-1p::SL1-GCaMP3.35-SL2::mKate2-unc-54-3'utr, unc-119(+)]*. [1]
- HBR531 *yxIs1 [glr-1p::GCaMP3, unc-122p::gfp]; aptf-1(gk794) II*. [1]
- HBR560 *goeIs120 [tdc-1p::SL1-GCaMP3.35-SL2::mKate2-unc-54-3'utr, unc119(+)]*.
Generated for this study.
- HBR1009 *flp-11(tm2706)X, goeIs118 [aptf-1p::SL1-GCaMP3.35-SL2::mKate2-aptf-1-3'utr, unc-119(+)]*. [2]
- HBR1118 *aptf-1(gk794) II; goeIs120 [tdc-1p::SL1-GCaMP3.35-SL2::mKate2-unc-54-3'utr, unc119(+)]*. Generated for this study.
- HBR1228 *goeIs268 [aptf-1p::SL1-GCaMP3.35-SL2::aptf-1-3'utr, unc-119(+)]*. [1]
- HBR1361 *goeIs304 [flp-11p::SL1-GCaMP3.35-SL2::mKate2-unc-54-3'UTR, unc-119(+)]*. [3]
- HBR1374 *goeIs307 [flp-11p::ArchT::SL2mKate2-unc-54-3'utr,unc-119(+)]*; *goeIs304 [flp-11p::SL1-GCaMP3.35-SL2::mKate2-unc-54-3'UTR, unc-119(+)]*. [3]
- HBR1391 *goeIs268 [aptf-1p::SL1-GCaMP3.35-SL2::aptf-1-3'utr, unc-119(+)]*; *goeIs273 [tdc-1p::ReaChR::mKate2-unc-54-3'utr, unc-119(+)]*. Generated for this study.

- HBR1394 *goeIs268 [aptf-1p::SL1-GCaMP3.35-SL2::aptf-1-3'utr, unc-119(+)]*; *goeIs273 [tdc-1p::ReaChR::mKate2-unc-54-3'utr, unc-119(+)]*; *tdc-1 (n3420) II*. Generated for this study, *tdc-1(n3420)* was crossed from MT10661 [4-6].
- HBR1465 *goeIs120 [tdc-1p::SL1-GCaMP3.35-SL2::mKate2-unc-54-3'utr, unc119(+)]*; *goeIs315 [flp-11p::ReaChR::mKate2-unc-54-3'UTR, unc-119(+)]*. Generated for this study.
- HBR1466 *goeIs268 [aptf-1p::SL1-GCaMP3.35-SL2::aptf-1-3'utr, unc-119(+)]*; *goeIs315 [flp-11p::ReaChR::mKate2-unc-54-3'UTR, unc-119(+)]*. Generated for this study.
- HBR1472 *goeIs268 [aptf-1p::SL1-GCaMP3.35-SL2::aptf-1-3'utr unc-119(+)]*; *goeIs307 [flp-11p::ArchT::SL2mKate-2-unc-54-3'utr, unc-119(+)]*. Generated for this study.
- HBR1478 *goeIs268 [aptf-1p::SL1-GCaMP3.35-SL2::aptf-1-3'utr, unc-119(+)]*; *goeEx557 [gcy-13p::ArchT::mKate-2-unc-54-3'-utr, unc-119(+)]*. Generated for this study.
- HBR1482 *goeIs268 [aptf-1p::SL1-GCaMP3.35-SL2::aptf-1-3'utr, unc-119(+)]*; *goeEx561 [gcy-13p::ReaChR-mKate-2-unc-54-3'-utr, unc-119(+)]*. Generated for this study.
- HBR1533 *goeIs268 [aptf-1p::SL1-GCaMP3.35-SL2::aptf-1-3'utr, unc-119(+)]*; *goeIs273 [tdc-1p::ReaChR::mKate2-unc-54-3'utr, unc-119(+)]*; *flp-18(db99) X*. Generated for this study, *flp-18(db99)* was crossed from AX1410 [4,5,7].
- HBR1537 *goeIs268 [aptf-1p::SL1-GCaMP3.35-SL2::aptf-1-3'utr, unc-119(+)]*; *goeIs308 [dat-1p::ReaChR::mKate2-unc-54-3'UTR, unc-119(+)]*. Generated for this study.

- HBR1572 *goeIs268 [aptf-1p::SL1-GCaMP3.35-SL2::aptf-1-3'utr, unc-119(+)]*; *goeIs273 [tdc-1p::ReaChR::mKate2-unc-54-3'utr, unc-119(+)]*; *flp-18(db99) X*; *tdc-1(n3420) II*. Generated for this study, *flp-18(db99)* was crossed from AX1410 [4,5,7] and *tdc-1(n3420)* was crossed from MT10661 [6].
- HBR1589 *goeIs268 [aptf-1p::SL1-GCaMP3.35-SL2::aptf-1-3'utr, unc-119(+)]*; *goeIs330 [nmr-1p::ArchT::mKate2-unc-54-3'utr, unc-119(+)]*. Generated for this study.
- HBR1597 *goeIs268 [aptf-1p::SL1-GCaMP3.35-SL2::aptf-1-3'utr, unc-119(+)]*, *goeIs332 [nmr-1p::ReaChR::mKate2-unc-54-3'utr, unc-119(+)]*. Generated for this study.
- HBR1659 *unc-119(ed3) III*; *goeIs364 [tdc-1p::egl-1::SL2-mKate2-unc-54-3'utr, unc-119(+)]*. Generated for this study.
- HBR1753 *wfIs5 [rab-3p::NLS::GCaMP6s; rab-3p::NLS::tagRFP]*. Generated for this study, *wfIs5* was backcrossed from AML32 with N2 twice [8].
- HBR1776 *wfIs5 [rab-3p::NLS::GCaMP6s; rab-3p::NLS::tagRFP]*; *goeIs307 [flp-11p::ArchT::SL2mKate2-unc-54-3'utr, unc-119(+)]*. Generated for this study, *wfIs5* was crossed from AML32 [4,5,8].
- HBR1793 *goeIs268 [aptf-1p::SL1-GCaMP3.35-SL2::aptf-1-3'utr, unc-119(+)]*; *goeIs293 [tol-1p::ReaChR::mKate2-unc-54-3'utr, unc-119(+)]*. Generated for this study.
- HBR1807 *goeIs232 [sra-6p::ReaChR::mKate2-unc-54-3'utr, unc-119(+)]*; *goeIs304 [flp-11p::SL1-GCaMP3.35-SL2::mKate2-unc-54-3'UTR, unc-119(+)]*. [3]
- HBR1844 *goeIs268 [paptf-1p::SL1-GCaMP3.35-SL2::aptf-1-3'utr, unc-119(+)]*; *goeIs340 [dat-1 p::ArchT::SL2mKate2-unc-54-3'UTR]*. Generated for this study.
- HBR1845 *goeIs268 [paptf-1p::SL1-GCaMP3.35-SL2::aptf-1-3'utr, unc-119(+)]*; *goeIs370 [lad-2p::ReaChR::mKate2-unc-54-3'UTR, unc-119(+)]*. Generated

for this study.

- HBR1849 *goeIs304* [*flp-11p::SL1-GCaMP3.35-SL2::mKate2-unc-54-3'UTR, unc-119(+)*]; *goeIs364* [*tdc-1p::egl-1::SL2-mKate2-unc-54-3'utr, unc-119(+)*]; *goeIs232* [*sra-6p::ReaChR::mKate2-unc-54-3'utr, unc-119(+)*]. Generated for this study.
- HBR1873 *goeIs268* [*paptf-1p::SL1-GCaMP3.35-SL2::aptf-1-3'utr, unc-119(+)*]; *goeIs373* [*lad-2p::ArchT::SL2-mKate2-unc-54-3'UTR, unc-119(+)*]. Generated for this study.
- HBR1889 *goeIs120* [*tdc-1p::SL1-GCaMP3.35-SL2::mKate2-unc-54-3'utr, unc-119(+)*]; *goeIs232* [*sra-6p::ReaChR::mKate2-unc-54-3'utr, unc-119(+)*]. Generated for this study.
- HBR1951 *ynIs40* [*flp-11p::GFP*] *V*; *goeIs359* [*nmr-1p::egl-1::SL2-mKate2-unc-54-3'utr, unc-119(+)*]. Generated for this study, *ynIs40* [*flp-11p::GFP*] was crossed from NY2040 [9].
- HBR1952 *goeIs304* [*flp-11p::SL1-GCaMP3.35-SL2::mKate2-unc-54-3'UTR, unc-119(+)*]; *goeIs343* [*tdc-1p::ArchT::mKate2-unc-54-3'utr, unc-119(+)*]. Generated for this study.
- HBR1967 *goeIs304* [*flp-11p::SL1-GCaMP3.35-SL2::mKate2-unc-54-3'UTR, unc-119(+)*], *goeEx705* [*nmr-1p::ArchT::mKate2-unc-54-3'utr, unc-119(+)*]. Generated for this study.
- HBR1982 *goeIs402* [*tol-1p::ArchT::SL2-mKate2-unc-54-3'UTR, unc-119(+)*]; *goeIs304* [*flp-11p::SL1-GCaMP3.35-SL2::mKate2-unc-54-3'UTR, unc-119(+)*]. Generated for this study.
- HBR2019 *akIs11* [*nmr-1p::ICE*]; *goeIs307* [*flp-11p::ArchT::SL2mKate2-unc-54-3'utr, unc-119(+)*]; *goeIs304* [*flp-11p::SL1-GCaMP3.35-SL2::mKate2-unc-54-3'UTR, unc-119(+)*]. Generated for this study, *akIs11* was obtained from A. V.

Maricq [10].

- HBR2021 *goeIs307 [flp-11p::ArchT::SL2mKate2-unc-54-3'utr,unc-119(+)]*; *goeIs304 [flp-11p::SL1-GCaMP3.35-SL2::mKate2-unc-54-3'UTR, unc-119(+)]*; *nmr-1(ak4) II*. Generated for this study, *ak4* was crossed from VM487 [11].
- HBR2033 *goeIs195 [nmr-1p::SL1-GCaMP6s::mKate2-unc-54-3'utr, unc-119(+)]*; *goeIs403 [flp-11p::ArchT::mKate2-flp-11-3'utr, unc-119(+)]*. Generated for this study.
- HBR2039 *goeIs307 [flp-11p::ArchT::SL2mKate2-unc-54-3'utr, unc-119(+)]*; *goeIs120 [tdc-1p::SL1-GCaMP3.35-SL2::mKate2-unc-54-3'utr, unc119(+)]*. Generated for this study.
- HBR2058 *goeIs304 [flp-11p::SL1-GCaMP3.35-SL2::mKate2-unc-54-3'UTR, unc-119(+)]*; *goeEx716 [tbh-1p::ReaChR::mKate2unc-54 3'UTR, unc119(+)]*; *unc-122::RFP*. Generated for this study.
- HBR2109 *goeIs195 [nmr-1p::SL1-GCaMP6s::mKate2-unc-54-3'utr, unc-119(+)]*; *goeIs315 [flp-11p::ReaChR::mKate2-unc-54-3'UTR, unc-119(+)]*. Generated for this study.
- HBR2123 *goeIs268 [aptf-1p::SL1-GCaMP3.35-SL2::aptf-1-3'utr, unc-119(+)]*; *goeEx561 [gcy-13p::ReaChR-mkate-2-unc-54-3'-utr, unc-119(+)]*; *eat-4(ky5) III*. Generated for this study, *eat-4(ky5)* was crossed from MT6308 [12].
- HBR2128 *goeIs304 [flp-11p::SL1-GCaMP3.35-SL2::mKate2-unc-54-3'UTR, unc-119(+)]*; *eat-4(ky5) III*. Generated for this study, *eat-4(ky5)* was crossed from MT6308 [12].
- HBR2169 *goeEx718 [hlh-34p::ReaChR::mKate2-unc-54-3'UTR,unc-119(+)]*; *myo-2p::mCherry*; *goeIs304 [flp-11p::SL1-GCaMP3.35-SL2::mKate2-unc-54-3'UTR, unc-119(+)]*. Generated for this study.

- HBR2180 *goeEx725 [hlh-34p::ArchT::SL2mKate2-unc-54-3'UTR, unc-119(+); myo-3p::mCherry]; goeIs304 [flp-11p::SL1-GCaMP3.35-SL2::mKate2-unc-54-3'UTR, unc-119(+)].* Generated for this study.
- HBR2231 *goeIs445 [zk673.11p::ArchT::SL2mKate2-unc-54 3' UTR, unc-119(+)].* Generated for this study.
- HBR2243 *goeIs445 [zk673.11p::ArchT::SL2mKate2-unc-54 3' UTR, unc-119(+)]; goeIs5 [nmr-1p::SL1-GCaMP3.35-SL2::unc-54-3'utr, unc-119(+)].* Generated for this study.
- HBR2271 *flp-11(syb816 [SL2::mKate2::linker(GSGSG)::tetanustoxin_LC])X; goeIs307 [flp-11p::ArchT::SL2mKate2-unc-54-3'utr, unc-119(+)], goeIs304 [flp-11p::SL1-GCaMP3.35-SL2::mKate2-unc-54-3'UTR, unc-119(+)].* Generated for this study.
- HBR2272 *goeIs120 [tdc-1p::SL1-GCaMP3.35-SL2::mKate2-unc-54-3'utr, unc-119(+)]; goeEx557 [gcy-13p::ArchT-mkate-2-unc-54-3'-utr, unc-119(+)].* Generated for this study.
- HBR2274 *goeIs304 [flp-11p::SL1-GCaMP3.35-SL2::mKate2-unc-54-3'UTR, unc-119(+)], goeIs195 [nmr-1p::SL1-GCaMP6s::mKate2-unc-54-3'utr, unc-119(+)].* Generated for this study.
- HBR2275 *goeIs307 [flp-11p::ArchT::SL2mKate2-unc-54-3'utr,unc-119(+)]; goeIs304 [flp-11p::SL1-GCaMP3.35-SL2::mKate2-unc-54-3'UTR, unc-119(+)]; unc-13(s69) I.* Generated for this study, *unc-13(s69)* was crossed from EG9631 [4,5].
- HBR2287 *goeIs195 [nmr-1p::SL1-GCaMP6s::mkate2-unc-54-3'utr, unc-119(+)]; goeIs332 [nmr-1p::ReaChR::mKate2-unc-54-3'utr, unc-119(+)].* Generated for this study.
- HBR2288 *nsEx2846(pept-3p::TeTX, elt-2p::mCherry), goeIs195 [nmr-1p::SL1-GCaMP6s::mKate2-unc-54-3'utr, unc-119(+)]; goeIs315 [flp-*

11p::ReaChR::mKate2-unc-54-3'UTR, unc-119(+). Generated for this study, *pept-3p::TeTX* was crossed from OS4976 [13].

HBR2289 *goeIs195 [nmr-1p::SL1-GCaMP6s::mKate2-unc-54-3'utr, unc-119(+)]*;
goeIs315 [flp-11p::ReaChR::mKate2-unc-54-3'UTR, unc-119(+)], *flp-11(tm2706)X*. Generated for this study.

HBR2316 *goeIs332 [nmr-1p::ReaChR::mKate2-unc-54-3'utr, unc-119(+)]*;
mzmEx324(sra-11p::mCherry, sra-11p::GCaMP5K). Generated for this study, *sra-11p::GCaMP5K* was crossed from ZIM498 [14].

HBR2321 *goeIs332 [nmr-1p::ReaChR::mKate2-unc-54-3'utr, unc-119(+)]*, *lite-1(ce314) X*.
Generated for this study, *lite-1(ce314)* was crossed from ZIM1048 [4,5,15,16].

HBR2323 *goeIs304 [flp-11p::SL1-GCaMP3.35-SL2::mKate2-unc-54-3'UTR, unc-119(+)]*;
goeIs340 [dat-1p::ArchT::SL2mKate2unc-54-3'UTR]; *goeIs402 [tol-1p::ArchT::SL2-mKate2-unc-54-3'UTR, unc-119(+)]*. Generated for this study.

HBR2336 *goeIs120 [ptdc-1p::SL1-GCaMP3.35-SL2::mKate2-unc-54-3'utr, unc-119(+)]*;
goeIs273 [tdc-1p::ReaChR::mKate2-unc-54-3'utr, unc-119(+)]. Generated for this study.

The following strains not created in the lab were used:

AML32 *wfIs5 [Prab-3::NLS::GCaMP6s; Prab-3::NLS::tagRFP]*. [8]

CX14845 *kyEx4863 [rig-3p::HisC11:sl2mCherry]*. [17]

N2 Wild type (Bristol) [18]

OS4976 *nsEx2846 (pept-3p::TeTX, elt-2p::mCherry)*. [13]

PHX816 *flp-11(syb816 [SL2::mKate2::linker(GSGSG)::tetamustoxin_LC])*. X.

Generated by SunyBiotech according to our design for this study.

ZC1148 *yxIs1 [glr-1p::GCaMP3.35, unc-122p::gfp]*. [19]

ZIM498 *mzmEx324(sra-11p::mCherry, sra-11p::GCaMP5K)*. [14]

References

1. Turek M, Lewandrowski I, Bringmann H. An AP2 transcription factor is required for a sleep-active neuron to induce sleep-like quiescence in *C. elegans*. *Curr Biol*. 2013;23(22):2215-23. Epub 2013/11/05. doi: 10.1016/j.cub.2013.09.028. PubMed PMID: 24184105.
2. Turek M, Besseling J, Spies JP, Konig S, Bringmann H. Sleep-active neuron specification and sleep induction require FLP-11 neuropeptides to systemically induce sleep. *eLife*. 2016;5. Epub 2016/03/08. doi: 10.7554/eLife.12499. PubMed PMID: 26949257; PubMed Central PMCID: PMC4805538.
3. Wu Y, Masurat F, Preis J, Bringmann H. Sleep Counteracts Aging Phenotypes to Survive Starvation-Induced Developmental Arrest in *C. elegans*. *Curr Biol*. 2018;28(22):3610-24 e8. Epub 2018/11/13. doi: 10.1016/j.cub.2018.10.009. PubMed PMID: 30416057; PubMed Central PMCID: PMC6264389.
4. Rose AM, Baillie DL. Genetic organization of the region around UNC-15 (I), a gene affecting paramyosin in *Caenorhabditis elegans*. *Genetics*. 1980;96(3):639-48. Epub 1980/11/01. PubMed PMID: 7262541; PubMed Central PMCID: PMC1214366.
5. Richmond JE, Davis WS, Jorgensen EM. UNC-13 is required for synaptic vesicle fusion in *C. elegans*. *Nat Neurosci*. 1999;2(11):959-64. Epub 1999/10/20. doi: 10.1038/14755. PubMed PMID: 10526333; PubMed Central PMCID: PMC2585767.
6. Alkema MJ, Hunter-Ensor M, Ringstad N, Horvitz HR. Tyramine Functions independently of octopamine in the *Caenorhabditis elegans* nervous system. *Neuron*. 2005;46(2):247-60. Epub 2005/04/26. doi: S0896-6273(05)00167-4 [pii] 10.1016/j.neuron.2005.02.024. PubMed PMID: 15848803.
7. Cohen M, Reale V, Olofsson B, Knights A, Evans P, de Bono M. Coordinated regulation of foraging and metabolism in *C. elegans* by RFamide neuropeptide signaling. *Cell Metab*. 2009;9(4):375-85. Epub 2009/04/10. doi: 10.1016/j.cmet.2009.02.003. PubMed PMID: 19356718.
8. Nguyen JP, Linder AN, Plummer GS, Shaevitz JW, Leifer AM. Automatically tracking neurons in a moving and deforming brain. *PLoS computational biology*. 2017;13(5):e1005517. Epub 2017/05/26. doi: 10.1371/journal.pcbi.1005517. PubMed PMID: 28545068; PubMed Central PMCID: PMC5436637.
9. Kim K, Li C. Expression and regulation of an FMRFamide-related neuropeptide gene family in *Caenorhabditis elegans*. *The Journal of comparative neurology*. 2004;475(4):540-50. Epub 2004/07/06. doi: 10.1002/cne.20189. PubMed PMID: 15236235.
10. Zheng Y, Brockie PJ, Mellem JE, Madsen DM, Maricq AV. Neuronal control of locomotion in *C. elegans* is modified by a dominant mutation in the GLR-1 ionotropic glutamate receptor. *Neuron*. 1999;24(2):347-61. Epub 1999/11/26. PubMed PMID: 10571229.
11. Brockie PJ, Mellem JE, Hills T, Madsen DM, Maricq AV. The *C. elegans* glutamate receptor subunit NMR-1 is required for slow NMDA-activated currents that regulate reversal frequency during locomotion. *Neuron*. 2001;31(4):617-30. Epub 2001/09/08. PubMed PMID: 11545720.

12. Lee RY, Sawin ER, Chalfie M, Horvitz HR, Avery L. EAT-4, a homolog of a mammalian sodium-dependent inorganic phosphate cotransporter, is necessary for glutamatergic neurotransmission in *Caenorhabditis elegans*. *J Neurosci*. 1999;19(1):159-67. Epub 1998/12/31. PubMed PMID: 9870947; PubMed Central PMCID: PMCPMC3759158.
13. Katz M, Corson F, Iwanir S, Biron D, Shaham S. Glia Modulate a Neuronal Circuit for Locomotion Suppression during Sleep in *C. elegans*. *Cell reports*. 2018;22(10):2575-83. Epub 2018/03/08. doi: 10.1016/j.celrep.2018.02.036. PubMed PMID: 29514087; PubMed Central PMCID: PMCPMC5870883.
14. Kato S, Kaplan HS, Schrodell T, Skora S, Lindsay TH, Yemini E, et al. Global brain dynamics embed the motor command sequence of *Caenorhabditis elegans*. *Cell*. 2015;163(3):656-69. Epub 2015/10/20. doi: 10.1016/j.cell.2015.09.034. PubMed PMID: 26478179.
15. Edwards SL, Charlie NK, Milfort MC, Brown BS, Gravlin CN, Knecht JE, et al. A novel molecular solution for ultraviolet light detection in *Caenorhabditis elegans*. *PLoS biology*. 2008;6(8):e198. Epub 2008/08/09. doi: 10.1371/journal.pbio.0060198. PubMed PMID: 18687026; PubMed Central PMCID: PMC2494560.
16. Nichols ALA, Eichler T, Latham R, Zimmer M. A global brain state underlies *C. elegans* sleep behavior. *Science*. 2017;356(6344). Epub 2017/06/24. doi: 10.1126/science.aam6851. PubMed PMID: 28642382.
17. Pokala N, Liu Q, Gordus A, Bargmann CI. Inducible and titratable silencing of *Caenorhabditis elegans* neurons in vivo with histamine-gated chloride channels. *Proc Natl Acad Sci U S A*. 2014;111(7):2770-5. Epub 2014/02/20. doi: 10.1073/pnas.1400615111. PubMed PMID: 24550306; PubMed Central PMCID: PMC3932931.
18. Brenner S. The genetics of *Caenorhabditis elegans*. *Genetics*. 1974;77(1):71-94. Epub 1974/05/01. PubMed PMID: 4366476.
19. Hendricks M, Ha H, Maffey N, Zhang Y. Compartmentalized calcium dynamics in a *C. elegans* interneuron encode head movement. *Nature*. 2012;487(7405):99-103. Epub 2012/06/23. doi: 10.1038/nature11081. PubMed PMID: 22722842; PubMed Central PMCID: PMC3393794.

S2 Text. List of constructs generated during this study.

- K31 *nmr-1p::SL1-GCaMP3.35-SL2::mKate2-unc-54-3UTR, unc-119(+)*
- K78 *tdc-1p::SL1-GCaMP3.35-SL2::mKate2-unc-54-3UTR, unc-119(+)*
- K133 *nmr-1p::SL1-GCaMP6s-SL2::mKate2-unc-54-3UTR, unc-119(+)*
- K183 *nmr-1p::ReaChR::mKate2-unc-54-3UTR, unc-119(+)*
- K189 *tdc-1p::ReaChR::mKate2-unc-54-3UTR, unc-119(+)*
- K190 *tdc-1p::ArchT::mKate2 unc-54 3'UTR, unc-119(+)*
- K196 *gcy-13p::ArchT::SL2 mKate2 unc-54 3'UTR, unc-119(+)*
- K197 *gcy-13p::ReaChR::mKate2-unc-54-3UTR, unc-119(+)*
- K200 *nmr-1p::ArchT::SL2 mKate2 unc-54 3'UTR, unc-119(+)*
- K204 *tol-1p::ReaChR::mKate2-unc-54-3UTR, unc-119(+)*
- K215 *flp11p::ReaChR::SL2mKate2-unc-54-3UTR, unc-119(+)*
- K249 *dat-1p::ReaChR::mKate2-unc-54-3UTR, unc-119(+)*
- K257 *lad-2p::ReaChR::mKate2-unc-54-3UTR, unc-119(+)*
- K259 *dat-1p::ArchT::SL2 mKate2 unc-54 3'UTR, unc-119(+)*
- K260 *tol-1p::ArchT::SL2 mKate2 unc-54 3'UTR, unc-119(+)*
- K300 *lad-2p::ArchT::SL2 mKate2 unc-54 3'UTR, unc-119(+)*
- K308 *tdc-1p::egl-1::SL2mKate2-unc-54-3UTR, unc-119(+)*
- K309 *nmr-1p::egl-1::SL2mKate2-unc-54-3UTR, unc-119(+)*
- K345 *tbh-1p::ReaChR::mKate2-unc-54-3UTR, unc-119(+)*
- K355 *hlh-34p::ReaChR::mKate2-unc-54-3UTR, unc-119(+)*
- K356 *hlh-34p::ArchT::SL2 mKate2 unc-54 3'UTR, unc-119(+)*
- K364 *zk673.11p::ArchT::SL2 mKate2 unc-54 3'UTR, unc-119(+)*

S3 Text. Sequence of the strain PHX816.

PHX816: *flp-11(syb816 [SL2::mKate2::linker(GSGSG)::tetanustoxin_LC]) X*.

```
>flp-11b-SL2(gpd-2)-mKate2 linker (GSGSG) tetanustoxin LC
TGGCACTTCTCCTTATTGTCTTCGTTGCCGCTTCTTTTGGCTCAATCTTATGATGACGTCAGgt
atagtttttcttaaaacaattttatcaattacccatataaaatctattgtagTGCGGAGAAACGTGCCATGCGGAACGCC
TTGGTTTCGATTTGGAAGAGCTAGTGGTGGAAATGAGAAATGCTCTCGTTAGATTCGGAAAGA
GGTCTCCATTGGACGAGGAAGACTTTGCTCCAGAGAGCCACTCCAGGGAAAACGGAACG
GTGCCCCACAACCATTGgtaagttgtcttaaaattttctccgcttttgcccttgctcatgtgctgtttatttgccttgcagttgc
ttggccgatccggtcaactcgaccacatgcacgacctttgtcgactctcagAAGCTCAAGTTCGCCAACAAACAAGT
AATGACCGAGGACGACCGTCTTCTGCTCGAACAACCTCCTGCGACGAATTCATCATTAAgctgt
ctcatcctacttccacagtaactgctgtcttaaaatctatgcttctttagtatctaaaatttctagaagcttacaagtatataatggc
tcttctcaataaaggtgtatatttattcatcttattgaatcgccatttctcgttttgcgagttatataacctccaattttcttattgtatttcaa
cttctaatttaattcagggaaactgctcaacgcatcATGTCCGAGCTCATCAAGGAGAACATGCACATGAAG
CTCTACATGGAGGGAACCGTCAACAACCACCACTTCAAGTGCACCTCCGAGGGAGAGGGA
AAGCCATACGAGGGAACCCAAACCATGCGTATCAAGgtaagtttaacatataataactaactaacctgatta
tttaattttcagGCCGTCGAGGGAGGACCACTCCCATTCGCCTTCGACATCCTCGCCACCTCCTT
CATGTACGGATCCAAGACCTTCATCAACCACACCCAAGGAATCCCAGACTTCTTCAAGCAA
TCCTTCCCAGAGGGATTCACTGGGAGCGTGTCAACCACCTACGAGGACGGAGGAGTCCCT
ACCGCCACCCAAGACACCTCCCTCCAAGACGGATGCCTCATCTACAACGTCAAGATCCGT
GGAGTCAACTTCCCATCCAACGGACCAGTCATGCAAAAAGAAGACCCTCGGATGGGAGGCC
TCCACCGAGACCTTACCCAGCCGAGGACTCGAGGGACGTGCCGACATGGCCCT
CAAGCTCGTCGGAGGACACTCATCTGCAACCTCAAGgtaagtttaaacatgatttactaactaacta
atctgatttaattttcagACCACCTACCGTTCCAAGAAGCCAGCCCAAGAACCTCAAGATGCCGAGG
TCTACTACGTCCGACCGTCTCGAGCGTATCAAGGAGGCCGACAAGGAGACCTACGTCCG
AGCAACACGAGGTCGCCGTCGCCGTTACTGCGACCTCCCATCCAAGCTCGGACACCGT
GGATCCGGATCCGGAATGCCAATCACCATCAACAACCTCCGTTACTCCGACCCAGTCAACA
ACGACACCATCATCATGATGGAGCCACCATACTGCAAGGGACTCGACATCTACTACAAGG
CCTTCAAGATCACCGACCGTATCTGGATCGTCCCAGAGCGTTACGAGTTCGGAACCAAGC
CAGAGGACTTCAACCCACCATCCTCCCTCATCGAGGGAGCCTCCGAGTACTACGACCCAA
ACTACCTCCGTACCGACTCCGACAAGGACCGTTTTCTCCAAACCATGGTCAAGCTCTTCAA
CCGTATCAAGAACAACGTCCGCCGAGAGGCCCTCCTCGACAAGATCATCAACGCCATCCC
ATACCTCGGAAACTCCTACTCCCTCCTCGACAAGTTCGACACCAACTCCAACCTCCGTCTCC
TTCAACCTCCTCGAGCAAGACCCATCCGGAGCCACCACCAAGTCCGCCATGCTCACCAAC
CTCATCATCTTCGGACCAGGACCAGTCTCAACAAGAACGAGGTCCGTGGAATCGTCTCTC
CGTGTGACAACAAGgtaagtttaaacagttcggtaactaactaaccatacatatttaattttcagAACTACTTCCCAT
GCCGTGACGGATTCGGATCCATCATGCAAATGGCCTTCTGCCAGAGTACGTCCCAACCT
TCGACAACGTTCATCGAGAACATCACCTCCCTCACCATCGGAAAGTCCAAGTACTTCCAAGA
CCCAGCCCTCCTCCTCATGCACGAGCTCATCCACGTCTCCACGGACTCTACGGAATGCA
AGTCTCCTCCCACGAGATCATCCCATCCAAGCAAGAGATCTACATGCAACACACCTACCCA
ATCTCCGCCGAGGAGCTCTTACCTTCGGAGGACAAGACGCCAACCTCATCTCCATCGAC
ATCAAGAACGACCTTACGAGAAGACCCTCAACGACTACAAGGCCATCGCCAACAAGCTC
TCCCAAGTACCTCCTGCAACGACCCAAACATCGACATCGACTCCTACAAGCAAATCTACC
AACAAAAGTACCAATTCGACAAGGACTCCAACGGACAATACATCGTCAACGAGGACAAGTT
CCAAATCCTCTACAACCTCATGTACGGATTACCCGAGATCGAGCTCGGAAAGAAGTTC
AACATCAAGACCCGTCTCTCTACTTCTCCTTGAACCACGACCCAGTCAAGTCCCAACCC
TCTCGACGACACCATCTACAACGACACCCGAGGATTCAACATCGAGTCCAAGGACCTCA
AGTCCGAGTACAAGGGACAAAACATGCGTGTCAACACCAACGCCTTCCGTAACGTTCGACG
GATCCGACTCGTCTCAAGCTCATCGGACTCTGCAAGAAGATCATCCACCAACCAACAT
CCGTGAGAACCTCTACAACCGTACCGCCTAAaatcatatgttttct
```

S1 Table. Primers used in this study.

	Primer sequence 5'-3'
<i>aptf-1(gk794)</i>	
	CGACAATCTTCCCAAAGACC
	CGGATCGATTGCTAGAGAGG
	GCTTGGACGGCTTTAGTTGA
ArchT	
	ACTTCATCGTCAAGGGATGG
	CATGCAGATGGTGGAGAAGA
<i>eat-4(ky5)</i>	
	GGGGCGTTTCCTTTTCTTTA
	AAAATGCTCCGACTCCGATT
	ACAGATCCATACGGAAAAGTTC
<i>flp-11(tm2706)</i>	
	CAGGAGTTGTTGAGCAGAA
	TCGTCCAATGGAGACCTCTT
	TAGCCGCTCGTCTCACTTTT
<i>flp-18(db99)</i>	
	CGAACGAATCAGCCATGTAA
	GAGATTCGACGATGACACGA
	GGCTTGGGAGGAAGATTTTT
ICE	
	CCGAGCTTTGATTGACTCCG
	AGTCATGTCCGAAGCAGTGA
<i>nmr-1(ak4)</i>	
	TGCTGGTGACTTATGAGCCT
	TGCTGGCGATCTTACTGGAA
	CAACACCGATGCAGAGCTC
<i>tdc-1(n3420)</i>	
	GAGGATCCACGCCAGAATGA
	CATGTGAATCCGCCCAGAAG

S2 Table. Plasmids used for this study.

plasmid name	transgene	length of transgene (kb)	source / reference
pMK-RQ-aptf-1p	<i>aptf-1p</i>	1,500	[1]
pTNZ001_pENTR_4-1_dat1p	<i>dat-1p</i>	784	[2]
pMK-RQ-flp-11p	<i>flp-11p</i>	2,746	[3]
pPUC57-gcy-13p	<i>gcy-13p</i>	2,192	[4]
pPUC57-kan-tbh-1p	<i>tbh-1p</i>	1,407	[5]
pKA1261 hlh-34 prom	<i>hlh-34p</i>	2,500	[6]
pEntr P4-P1R plad-2	<i>lad-2p</i>	4,038	[7]
pEntrL4-R1 pnmr-1 (pIR11)	<i>nmr-1p</i>	2,244	[8]
pEntrL4-R1 psra-6	<i>sra-6p</i>	4,090	[9]
pTNZ024-5_pENTR_4-1_tdc-1p	<i>tdc-1p</i>	3,452	[5, 10]
pMK-tol-1p	<i>tol-1p</i>	3,988	[11]
pBSK(+)-Kan-zk673.11p	<i>zk673.11p</i>	2,000	[12]
pMK-SL1GCaMP3.35-SL2	<i>GCaMP3.35</i>	1,865	[13]
pMK-RQ-ArchT	<i>ArchT</i>	955	[14]
pMK-ReaChR-STOP	<i>ReaChR-STOP</i>	1,412	[15]
pMK-egl-1	<i>egl-1</i>	376	[14]
pMK-RQ-SL2mKate2unc-54-3UTR	<i>mKate2::unc-54 3' UTR</i>	1,995	[13]

References

1. Turek M, Lewandrowski I, Bringmann H. An AP2 transcription factor is required for a sleep-active neuron to induce sleep-like quiescence in *C. elegans*. *Curr Biol*. 2013;23(22):2215-23. Epub 2013/11/05. doi: 10.1016/j.cub.2013.09.028. PubMed PMID: 24184105.
2. Ezcurra M, Tanizawa Y, Swoboda P, Schafer WR. Food sensitizes *C. elegans* avoidance behaviours through acute dopamine signalling. *EMBO J*. 2011;30(6):1110-22. Epub 2011/02/10. doi: [emboj201122](https://doi.org/10.1038/emboj.2011.22) [pii] 10.1038/emboj.2011.22. PubMed PMID: 21304491.
3. Turek M, Besseling J, Spies JP, König S, Bringmann H. Sleep-active neuron specification and sleep induction require FLP-11 neuropeptides to systemically induce sleep. *eLife*. 2016;5. Epub 2016/03/08. doi: 10.7554/eLife.12499. PubMed PMID: 26949257; PubMed Central PMCID: PMC4805538.
4. Ortiz CO, Etchberger JF, Posy SL, Frokjaer-Jensen C, Lockery S, Honig B, et al. Searching for neuronal left/right asymmetry: genomewide analysis of nematode receptor-type

- guanylyl cyclases. *Genetics*. 2006;173(1):131-49. Epub 2006/03/21. doi: 10.1534/genetics.106.055749. PubMed PMID: 16547101; PubMed Central PMCID: PMCPMC1461427.
5. Alkema MJ, Hunter-Ensor M, Ringstad N, Horvitz HR. Tyramine Functions independently of octopamine in the *Caenorhabditis elegans* nervous system. *Neuron*. 2005;46(2):247-60. Epub 2005/04/26. doi: S0896-6273(05)00167-4 [pii] 10.1016/j.neuron.2005.02.024. PubMed PMID: 15848803.
 6. Cunningham KA, Hua Z, Srinivasan S, Liu J, Lee BH, Edwards RH, et al. AMP-activated kinase links serotonergic signaling to glutamate release for regulation of feeding behavior in *C. elegans*. *Cell Metab*. 2012;16(1):113-21. Epub 2012/07/10. doi: 10.1016/j.cmet.2012.05.014. PubMed PMID: 22768843; PubMed Central PMCID: PMCPMC3413480.
 7. Wang X, Zhang W, Cheever T, Schwarz V, Opperman K, Hutter H, et al. The *C. elegans* L1CAM homologue LAD-2 functions as a coreceptor in MAB-20/Sema2 mediated axon guidance. *J Cell Biol*. 2008;180(1):233-46. Epub 2008/01/16. doi: 10.1083/jcb.200704178. PubMed PMID: 18195110; PubMed Central PMCID: PMCPMC2213605.
 8. Ben Arous J, Tanizawa Y, Rabinowitch I, Chatenay D, Schafer WR. Automated imaging of neuronal activity in freely behaving *Caenorhabditis elegans*. *J Neurosci Methods*. 2010;187(2):229-34. Epub 2010/01/26. doi: 10.1016/j.jneumeth.2010.01.011. PubMed PMID: 20096306.
 9. Hilliard MA, Apicella AJ, Kerr R, Suzuki H, Bazzicalupo P, Schafer WR. In vivo imaging of *C. elegans* ASH neurons: cellular response and adaptation to chemical repellents. *EMBO J*. 2005;24(1):63-72. Epub 2004/12/04. doi: 7600493 [pii] 10.1038/sj.emboj.7600493. PubMed PMID: 15577941.
 10. Guo ZV, Hart AC, Ramanathan S. Optical interrogation of neural circuits in *Caenorhabditis elegans*. *Nat Methods*. 2009;6(12):891-6. Epub 2009/11/10. doi: nmeth.1397 [pii] 10.1038/nmeth.1397. PubMed PMID: 19898486.
 11. Brandt JP, Ringstad N. Toll-like Receptor Signaling Promotes Development and Function of Sensory Neurons Required for a *C. elegans* Pathogen-Avoidance Behavior. *Curr Biol*. 2015;25(17):2228-37. Epub 2015/08/19. doi: 10.1016/j.cub.2015.07.037. PubMed PMID: 26279230; PubMed Central PMCID: PMCPMC4642686.
 12. Gonzales DL, Zhou J, Fan B, Robinson JT. Microfluidic-Induced Sleep: A Spontaneous *C. elegans* Sleep State Regulated by Satiety, Thermosensation and Mechanosensation. *BioArXiv*. 2019. doi: <https://doi.org/10.1101/547075>
 13. Schwarz J, Lewandrowski I, Bringmann H. Reduced activity of a sensory neuron during a sleep-like state in *Caenorhabditis elegans*. *Curr Biol*. 2011;21(24):R983-4. Epub 2011/12/24. doi: S0960-9822(11)01207-3 [pii] 10.1016/j.cub.2011.10.046. PubMed PMID: 22192827.
 14. Wu Y, Masurat F, Preis J, Bringmann H. Sleep Counteracts Aging Phenotypes to Survive Starvation-Induced Developmental Arrest in *C. elegans*. *Curr Biol*. 2018;28(22):3610-24 e8. Epub 2018/11/13. doi: 10.1016/j.cub.2018.10.009. PubMed PMID: 30416057; PubMed Central PMCID: PMCPMC6264389.
 15. Urmersbach B, Besseling J, Spies JP, Bringmann H. Automated analysis of sleep control via a single neuron active at sleep onset in *C. elegans*. *Genesis*. 2016;54(4):212-9. Epub 2016/02/03. doi: 10.1002/dvg.22924. PubMed PMID: 26833569.

S3 Table. Optogenetic experimental details.

Figure	Optogenetic Manipulation		Age	Mobile (m)/ Immobile (i)	AT R mM	Light Intensity mW/mm ²		Protocol				
	Genetic Tool	Neuron				490n m	585n m	Cycles	Delay	base- line	stimu- lation	recov- ery
1B	tol-1::ReaChR	URY	L1	m	50	0.33	0.37	15min	-	1min	1min	1min
	lad-2::ReaChR	SDGL	L4	i	0.5	0.05	0.04	4	2min	1min	1min	1min
	tdc-1::ReaChR	RIM	L1	m	50	0.15	0.09	15min	-	1min	1min	1min
	nmr-1:: ReaChR	PVC	L1	i	50	0.05	0.26	1	5min	2min	1min	2min
	daf-1::ReaChR	CEP	L4	m	0.5	0.14	0.09	30min	-	1min	1min	1min
	hh-34:: ReaChR	AVJ	L1	m	50	0.33	0.37	15min	-	1min	1min	1min
1C	tol-1::ArchT	URY	L4	m	0.5	0.11	0.39	30min	-	3min	3min	8min
	lad-2::ArchT	SDGL	L4	i	0.5	0.05	0.09	4	5min	1min	1min	1min
	tdc-1::ArchT	RIM	L1	m	0.5	0.15	0.24	15min	-	1min	1min	1min
	nmr-1::ArchT	PVC	L1	i	50	0.12	0.26	1	5min	2min	1min	2min
	daf-1::ArchT	CEP	L1	m	50	0.33	0.17	15min	-	1min	1min	1min
	hh-34::ArchT	AVJ	L1	m	50	0.33	0.37	15min	-	1min	1min	1min
2B	zk673.11::ArchT	PVC	L1	m	10	0.07	0.17	20min	-	2min	1min	3min
2C	zk637.11::ArchT	PVC	L1	i	50	0.05	0.06	1	5min	3min	1min	3min
2D	nmr-1::ReaChR	PVC	L1	m	10	-	0.7	-	-	1	3min	3min
3C-E	flp-11:: ReaChR	RIS	L1	i	10	0.28	3.39	2	1min	2min	5min	1min
4E	tdc-1::ReaChR	RIM	L1	m	50	0.15	0.09	1	-	1min	1min	1min
4F,G	tdc-1::ReaChR	RIM	L1	i	50	0.05	0.09	1	5min	3min	1min	3min
5B	nmr-1::ArchT	command interneurons	L1	m	50	0.15	0.17	15min	-	1min	3min	1min
6C (RIS)	flp-11::ArchT	RIS	L1	m	50	0.07	0.17	30min	-	3min	3min	8min
6C (pan-neuronal)	flp-11::ArchT	RIS	L1	m	50	0.07	0.17	30min	-	3min	3min	3min
8A-C	sra-6::ReaChR	ASH	L4	m	0.2	0.6	0.14	15min	-	1.5min	3s	8s
S1A	tol-1::ReaChR	URY	L1	m	0	0.33	0.37	15min	-	1min	1min	1min
	lad-2::ReaChR	SDGL	L4	i	0	0.05	0.04	4	2min	1min	1min	1min
	tdc-1::ReaChR	RIM	L1	m	0	0.15	0.09	15min	-	1min	1min	1min
	nmr-1:: ReaChR	PVC	L1	i	0	0.05	0.26	1	5min	2min	1min	2min
	daf-1::ReaChR	CEP	L4	m	0	0.14	0.09	30min	-	1min	1min	1min
	hh-34:: ReaChR	AVJ	L1	m	0	0.33	0.37	15min	-	1min	1min	1min
S1B	lth-1::ReaChR	RIC	L1	m	50	0.15	0.37	15min	-	1min	1min	1min
S1C-E	gcy-13:: ReaChR	RIM	L1	m	50	0.33	0.37	30min	-	1min	1min	1min
S2A	tdc-1::ReaChR	RIM	L1	m	50	0.15	0.09	15min	-	1min	1min	1min
S2B	tdc-1::ReaChR	RIM	L1	m	50	0.15	0.09	15min	-	2min	1min	5min
S2C	tdc-1::ReaChR	RIM	L1	m	50	0.15	0.09	15min	-	1min	1min	1min
S3A	gcy13::ReaChR	RIM	L4	m	0.5	0.15	0.09	35min	-	1min	1min	1min
S3B	gcy13::ReaChR	RIM	L4	m	50	0.33	0.09	35min	-	1min	1min	1min
S4	nmr-1:: ReaChR	PVC	L2	i	50	0.05	0.01	2-3	-	1min	1min	1min
S5A	tol-1::ArchT	URY	L4	m	0	0.11	0.39	30min	-	3min	3min	8min
	lad-2::ArchT	SDGL	L4	i	0	0.05	0.09	4	5min	1min	1min	1min
	tdc-1::ArchT	RIM	L1	m	0	0.15	0.24	15min	-	1min	1min	1min
	nmr-1::ArchT	PVC	L1	i	0	0.12	0.26	1	5min	2min	1min	2min
	daf-1::ArchT	CEP	L1	m	0	0.33	0.17	15min	-	1min	1min	1min
	hh-34::ArchT	AVJ	L1	m	0	0.33	0.37	15min	-	1min	1min	1min
S5B-C	gcy-13::ArchT	RIM	L1	m	50	0.33	0.37	30min	-	1min	1min	1min
S5D	daf-1::ArchT, tol-1::ArchT	CEP, URY	L1	m	50	0.33	0.37	30min	-	3min	1min	3min
S7A	nmr-1::ReaChR	PVC	L1	i	50	0.12	0.27	1	5min	10min	1min	5min
S7C-D	nmr-1::ReaChR	PVC	L1	i	50	0.12	0.26	1-2	5min	2min	1min	2min
S8A	flp-11:: ReaChR	RIS	L1	i	10	0.28	3.39	2	1min	2min	5min	1min
S8B	flp-11:: ArchT	RIS	L1	i	10	0.05	0.09	2	1min	1min	1min	1min
S8C	flp-11::ReaChR	RIS	L1	m	50	0.15	0.09	15min	-	1min	1min	1min
S8H	flp-11::ArchT	RIS	L1	i	50	0.93	0.76	2	5min	1min	1min	1min
S9D-E	nmr-1::ArchT	command interneurons	L1	m	50	0.07	0.70	15min	-	3min	1min	3min
S11B	gcy13::ArchT	RIM	L1	m	50	0.07	0.37	30min	-	3min	1min	3min
S11C	flp-11::ArchT	RIS	L1	m	50	0.15	0.17	15min	-	1min	48s	1min
S11D	flp-11::ArchT	RIS	L1	m	50	0.15	0.17	15min	-	3min	5min	3min
S11E	flp-11::ArchT	RIS	L1	m	50	0.1	0.17	15min	-	3min	10min	3min
S11F-H	flp-11::ArchT	RIS	L1	m	50	0.07	0.17	30min	-	3min	1min	3min
S11I	flp-11:: ReaChR	RIS	L1	m	50	0.15	0.09	15min	-	1min	1min	1min

4.1.2. Command interneurons regulate the sleep neuron RIS

4.1.2.1. Locomotion regulating command interneurons additionally regulate starvation induced sleep

A very important and interesting finding of our previous publication was that the NMR-1 expressing interneurons (most importantly PVC and RIM), which had already been known to regulate locomotion in *C. elegans*, are also important regulators of the sleep neuron RIS during lethargus (114). For the experiments, command interneurons were ablated by expression of a human interleukin-1 β -converting enzyme (ICE), which is a pro-apoptosis regulator, with the *nmr-1* promoter. However, while the amount of sleep is highly reduced in command interneuron ablated worms (24% of wild type) in lethargus, there is still a small amount of sleep remaining (Publication I, Figure 5A). To investigate whether this remaining amount of sleep is RIS dependent, I tested worms, in which command interneurons were ablated in the *aptf-1(gk794)* background. In this background, RIS is non-functional. Indeed, these double mutant worms did not show any sleep bouts, comparable to single *aptf-1(gk794)* mutants (Figure 7A and B). This result points to a minor missing component in the neuronal circuit for RIS regulation since a small amount of RIS dependent sleep is still induced in command interneuron ablated worms.

The discovered neuronal circuit for RIS regulation and sleep homeostasis was so far only investigated in lethargus. Sleep can be induced in many different ways in *C. elegans* and I wondered if RIS regulation in other sleep states is also dependent on command interneurons. I therefore imaged command interneuron ablated worms and wild-type worms for starvation-induced L1 arrest sleep. Similarly to the results in lethargus, *C. elegans* without functional command interneurons show a significantly reduced amount of starvation-induced sleep in L1 arrest of 25% of wild-type sleep (Figure 7C-E). The neuronal circuit for RIS activation therefore seems to be a more general circuit for sleep induction that acts downstream of different molecular sleep-inducing pathways.

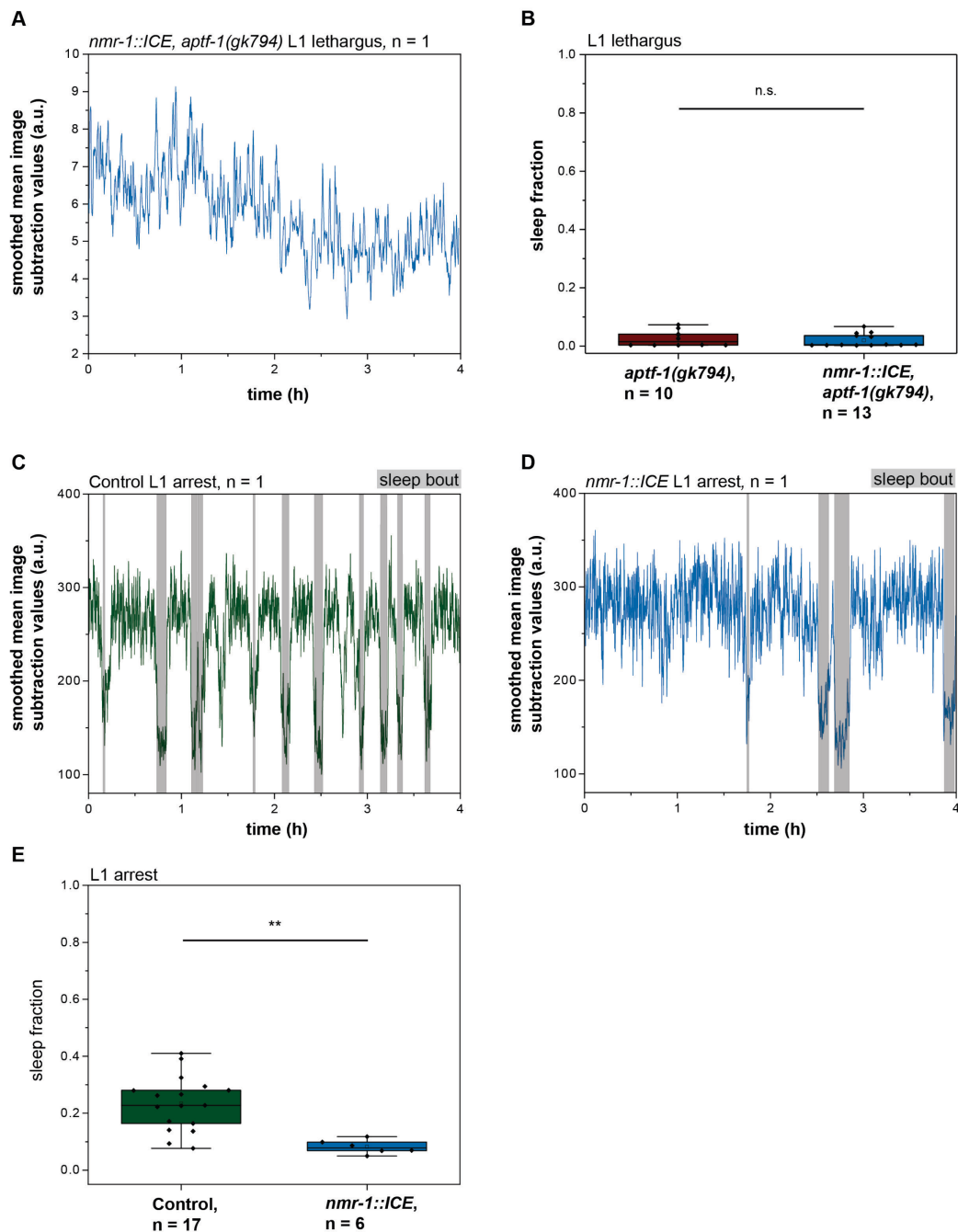


Figure 7. Command interneuron ablation in L1 lethargus and L1 arrest.

(A) Smoothed mean image subtraction sample trace of a command interneuron ablated worm in an *aptf-1(gk794)* background. (B) There is no detectable sleep in neither *aptf-1(gk794)* nor *nmr-1::ICE, aptf-1(gk794)* mutants. n.s. $p > 0.05$, Welch test. (C-D) Smoothed mean image subtraction sample traces of control and command interneuron ablated worms after 24h in L1 arrest. (E) Command interneuron ablation leads to a strong reduction of starvation induced sleep after 24h in L1 arrest. ** $p < 0.01$, Welch test.

4.1.2.2. Loss of function of AMPA and NMDA type glutamate receptors does not cause a sleep phenotype

Glutamatergic signaling controls command interneurons (133, 144) and we could show that the activation of RIS by RIM is glutamate-dependent (114). Additionally, glutamate plays an important role in sleep induction as we could show in Publication I that *eat-4(ky5)* mutants lacking glutamatergic signaling have a reduced amount of sleep and a reduced RIS activation in lethargus (114). To test whether this phenotype is dependent on glutamate ionotropic AMPA type receptors, which are expressed in command interneurons, I imaged for sleep behavior of *glr-1(n2461)* mutants. These mutants did not show a sleep phenotype (Figure 8A-C). There are several glutamate receptors in *C. elegans* so that redundancies are possible. Next, I tested if glutamatergic signaling via the AMPA as well as the NMDA type receptor is required by imaging *glr-1(n2461); nmr-1(ak4)* double mutants. The double mutants also do not have a sleep phenotype compared to wild type (Figure 8D and E). However, other untested glutamate receptors might act redundantly.

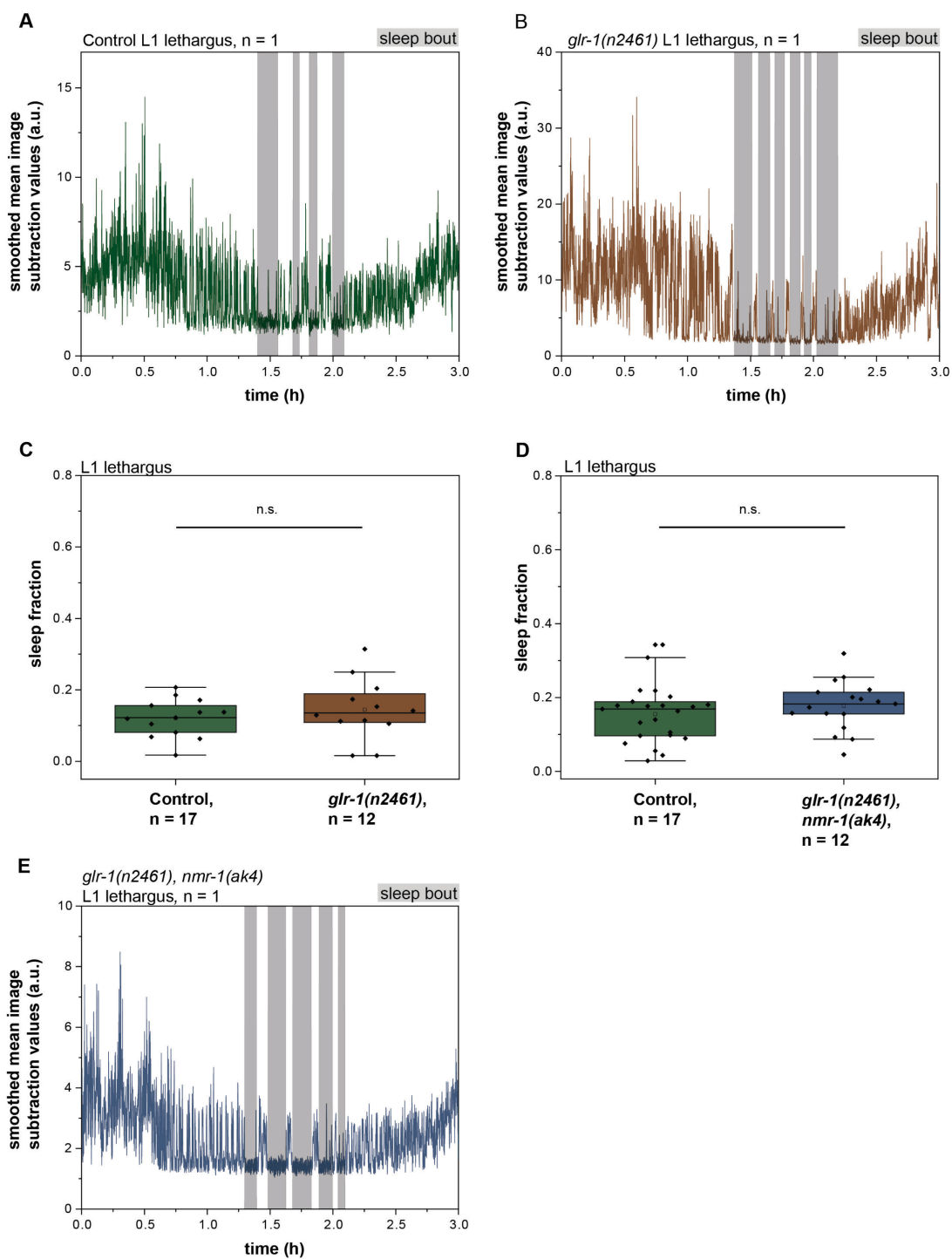


Figure 8. AMPA and NMDA type receptors are not necessary for sleep induction.

(A-C) *glr-1(n2461)* mutants do not have a sleep phenotype. n.s. $p > 0.05$, Welch test. (D-E) *glr-1(n2461); nmr-1(ak4)* double mutants do not have a sleep phenotype. n.s. $p > 0.05$, Welch test.

4.1.2.3. Sleep affects forward and reverse locomotion equally

The interneurons PVC and RIM are the major RIS regulators and they are also involved in regulating forward and reverse locomotion. In our model, sleep is induced right at the transition from forward to reverse locomotion (114). The question arose if as a consequence, reverse locomotion is reduced during lethargus since the worms fall asleep rather than stop and move backwards. To investigate this further, I imaged wild-type worms and characterized the type of locomotion as of 4 hours pre molting until molting. This period included the lethargus phase. Additionally, I imaged non-sleeping *aptf-1(gk794)* mutants. Both, the fraction of forward as well as reverse locomotion were equally reduced during lethargus in the wild type (2-0.5h prior to molting) (Figure 9A). In the *aptf-1(gk794)* mutants, the fraction of forward and reverse locomotion was not changed much prior to molting (Figure 9B). This suggests that reverse and forward locomotion are equally affected by sleep.

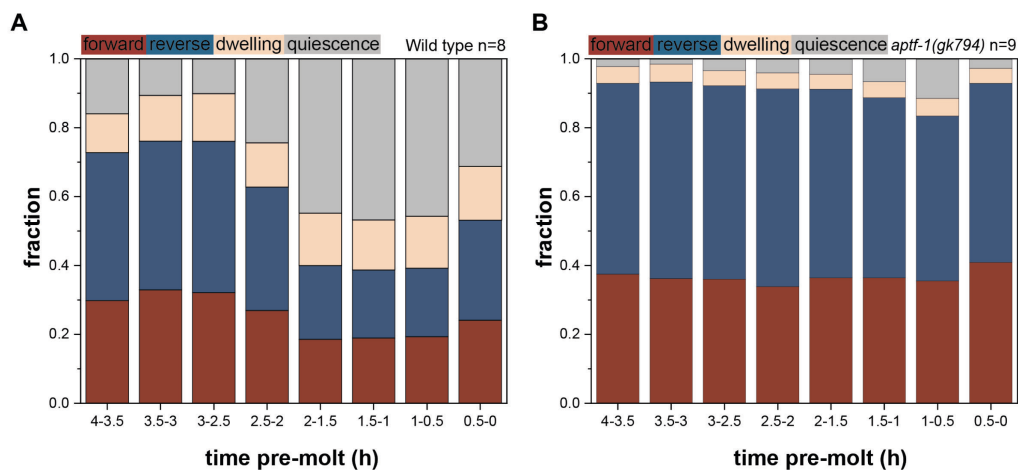


Figure 9. Sleep affects forward and reverse locomotion.

(A) The fraction of both, forward and reverse, locomotion changes in wild-type worms during lethargus. (B) There is no change of the distribution of direction of locomotion in *aptf-1(gk794)* worms prior to molting.

4.1.2.4. Disturbance of the command interneuron circuit can cause ectopic sleep bouts outside of lethargus

The command interneuron circuit plays a key role in regulating RIS and sleep in *C. elegans* in lethargus. I was wondering how a disturbance of this circuit impacts locomotion and sleep behavior outside of lethargus when wild-type worms usually do

not show sleep bouts. PVC can be inhibited stronger outside of lethargus, which might be responsible for RIS not getting depolarized and therefore not allowing for sleep bouts outside of lethargus (114). AVE and AVA are command interneurons involved in reverse locomotion and known inhibitors of PVC (92, 143). To see if interferences in this circuit affect sleep behavior outside of lethargus, I imaged AVE and AVA ablated worms. Since AVE and AVA are inhibitors of PVC I hypothesized that ablation of each neuron might lead to an increased activation of PVC, which might make the worm more prone to RIS activation and sleep induction. AVE was specifically ablated through the expression of tetanus toxin from the *pept-3* promoter and AVA inhibited by activating genetically expressed histamine gated chloride channels in AVA with histamine (127). Concluding, 2h prior to the onset of lethargus there were no detectable sleep bouts in worms with inhibited AVA. However, one could see significant ectopic sleep in AVE ablated worms (Figure 10). AVE thus seems to be a stronger PVC inhibitor and a disturbance of the command interneuron circuit sometimes but not always leads to ectopic sleep bouts when worms are normally awake outside of lethargus.

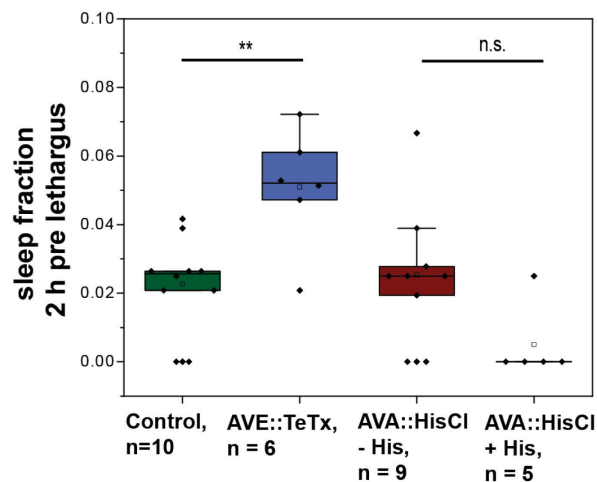


Figure 10. Reverse command interneuron ablation can cause ectopic sleep bouts before lethargus.

AVE ablated worms show ectopic sleep 2h prior to L1 lethargus whereas AVA inhibited worms have no significant sleep phenotype compared to worms without the addition of histamine. n.s. $p > 0.05$, $**p < 0.01$, Welch test.

4.1.2.5. AVB activates in lethargus during motion bouts, prior to sleep bouts

RIS is not the only neuron that can get activated by PVC. Another neuron that is known to get activated by PVC, for example as part of the tail touch response, is the forward locomotion inducing interneuron AVB (133, 145). The activation of RIS by PVC is state-dependent on lethargus and I was interested to see how AVB activates throughout lethargus as this had not been measured before and could further characterize the locomotion circuit. As AVB is forward locomotion inducing (133, 145), it might get less activated by PVC during lethargus. Interestingly, AVB seemed to have stronger activation peaks before sleep bouts compared to the activation peaks throughout longer motion bouts in lethargus (Figure 11A). This is interesting since it's known that PVC is less inhibited throughout lethargus (114). However, the calcium imaging was conducted every 10s and an AVB activation transient only lasts around 10s so that the maximum amplitude was very likely not detected for each peak. AVB activated before sleep bouts (Figure 11B and C). AVB activation is still possible throughout lethargus during motion and before sleep bouts.

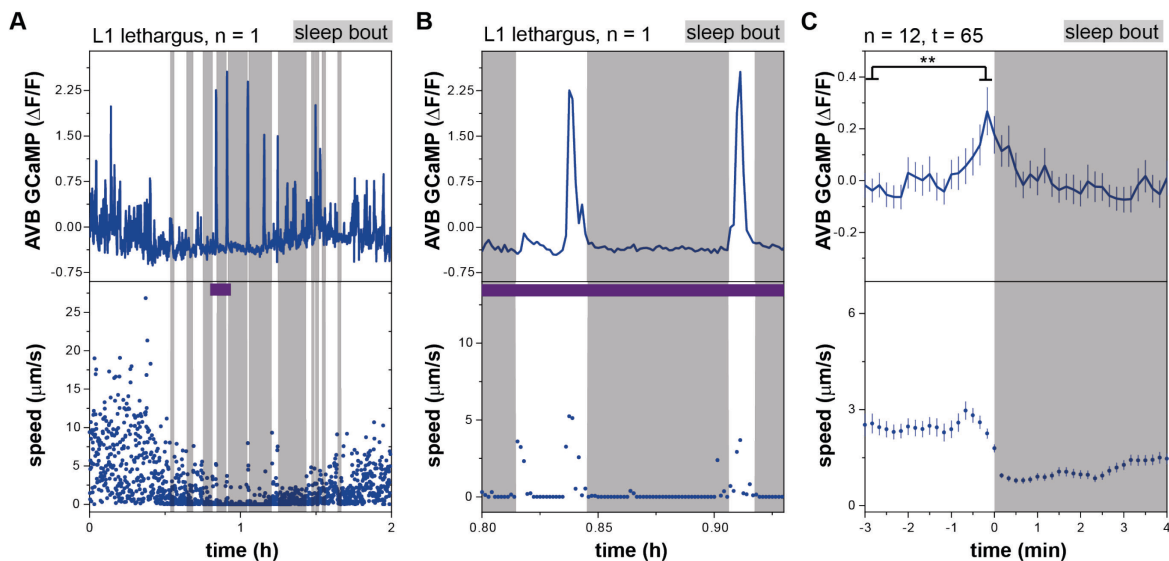


Figure 11. AVB activity measurements during lethargus.

(A) A sample trace for AVB GCaMP intensities and corresponding speeds in lethargus. (B) The previous same sample trace was zoomed in. One can see that AVB activates correlating to speed increases during motion bouts in lethargus. (C) AVB intensities were aligned to sleep bout onset. AVB activates before sleep bouts. ** $p < 0.01$, Wilcoxon signed rank test.

4.1.3. How sleep dampens the nervous system in *C. elegans*

The previous results demonstrate how the nervous system, or to be more precise, the command interneurons, regulate RIS and therefore sleep. Next, I was interested to see how sleep in turn regulates the nervous system. Previous studies have shown that hypoxia-induced sleep of *npr-1* mutants leads to down-regulation of the nervous system (146). The same study suggests that there are phases of overall neuronal inactivity throughout lethargus. However, the study imaged fixed animals so that it was not possible to correlate the worm's behavior to neuronal intensities. I was interested in how neuronal intensities change in correlation to sleep and wake bouts in lethargus and hence imaged free-moving animals. During lethargus, the worm cycles between sleep and wake bouts. As expected, the nervous system shuts down during sleep bouts (Figure 12A and B).

Homeostatic regulation is an important characteristic of sleep and we could show in Publication I that RIS is homeostatically regulated and activates stronger the longer the preceding motion bout (114). I was now interested to see if this stronger RIS activation also leads to varying levels of overall nervous system inhibition. However, the nervous system activity during sleep bouts is independent of the length of the preceding motion bout (Figure 12C). It is additionally independent of the mean overall nervous system activity during the preceding motion bout (Figure 12D). It seems that there is just one absolute off state of the nervous system, which is activated during a sleep bout. To control for the changes of the utilized pan-neuronal *rab-3* promoter I also imaged worms only expressing GFP with this promoter from 6 hours prior to molting until 2 hours after molting. One can see that the promoter activity is independent of lethargus (Figure 12E). Instead, the GFP intensity increases over time, which is probably caused by growth of the animal.

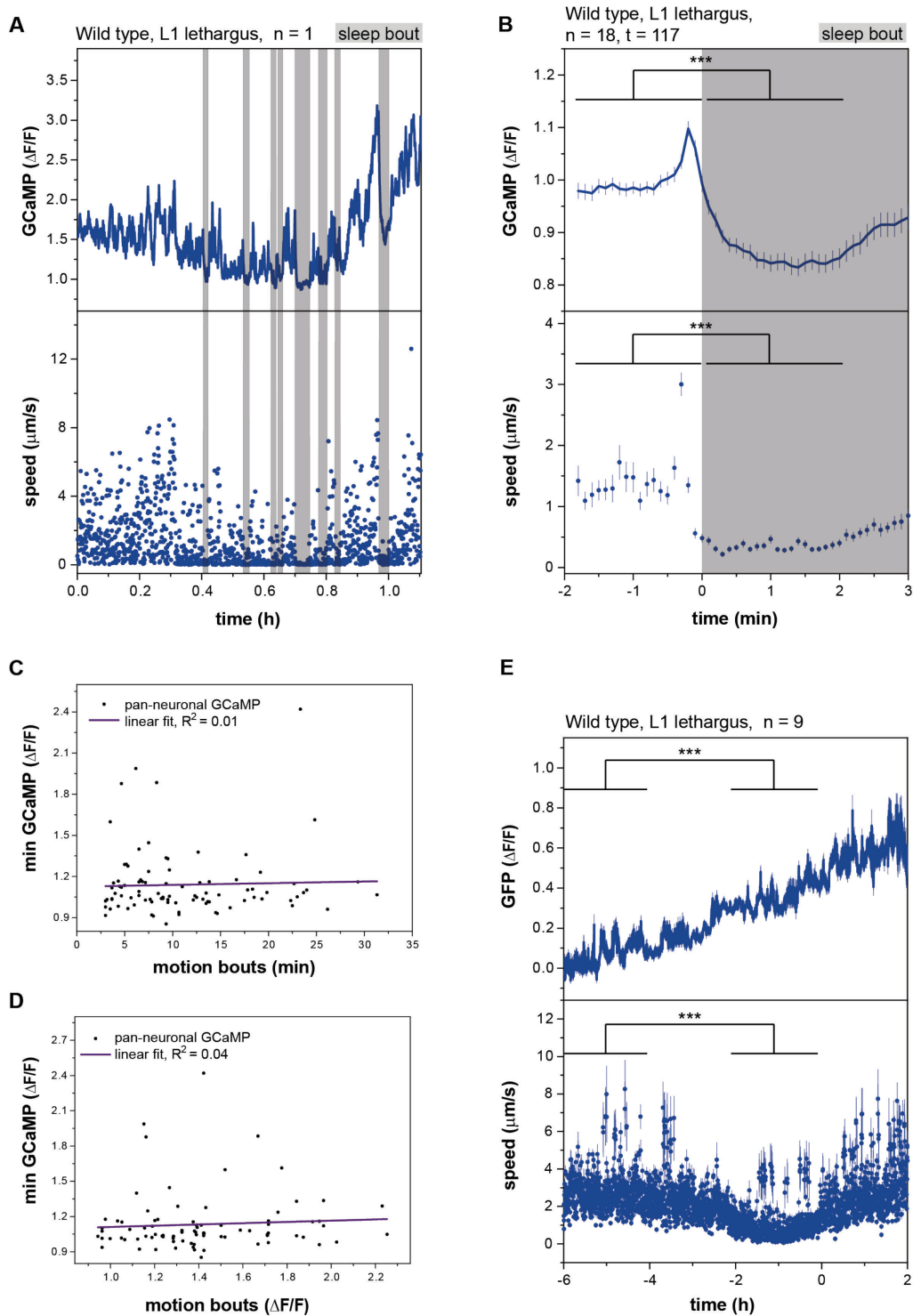


Figure 12. Sleep dampens the nervous system.

(A) Sample trace of a wild-type worm. The nervous system is mostly inactive during sleep bouts. (B) Sleep bout alignment of the pan-neuronal activity and speeds. During sleep bouts, the nervous system gets turned off. *** $p < 0.001$, Wilcoxon signed rank test. (C-D) The inhibition of the nervous system is independent of the length of the previous motion bout or the mean activity of the preceding motion bout. (E) *rab-3* promoter activity increases over time from 6 hours prior to molting until 2 hours after molting, independent of lethargus (approximately hours -2 to 0).

4.1.4. Optogenetic manipulation of the sleep neuron RIS directly influences the overall nervous system activity

RIS is the single neuron that depolarizes at the beginning of a sleep bout. If furthermore induces sleep. In our Publication I, we could show that RIS is homeostatically regulated and that worms increase their speed when RIS is inhibited during sleep bouts (114). Furthermore, we demonstrated how the nervous system responds to RIS inhibition. For this we specifically expressed the outward proton pump ArchT in RIS with the *flp-11* promoter and calcium imaged pan-neuronal GCaMP. RIS inhibition led to a strong increase of neuronal activity and an awakening during lethargus and a small nervous system activity increase when the worms were awake outside of lethargus (Publication I, Figure 6).

RIS inhibition seems to impact the nervous system stronger during lethargus, or more specifically sleep. However, how does RIS depolarization impact the overall nervous system activity? To answer this question, I calcium imaged worms expressing pan-neuronal GCaMP, before and during L1 lethargus. ReaChR for optogenetic activation upon green light stimulation was expressed in RIS utilizing a single-copy knock-in loci for defined gene expression (SKI LODGE) system (147) (see details Appendix). Trials were executed all 20min. One trial consisted of a baseline period (3min), an activation period (1min) and a recovery period (3min). Optogenetic RIS activation led to a significant reduction of nervous system activity at any time during the first larval stage (Figure 13A). Additionally, RIS activation caused a reduction of speed outside of and in lethargus. Control animals that were not supplemented with all-trans-retinal (ATR) and hence not RIS depolarized by green light did not have a significant response to the green light (Figure 13B). This shows that sleep and more specifically activation of the sleep neuron RIS directly regulate the nervous system.

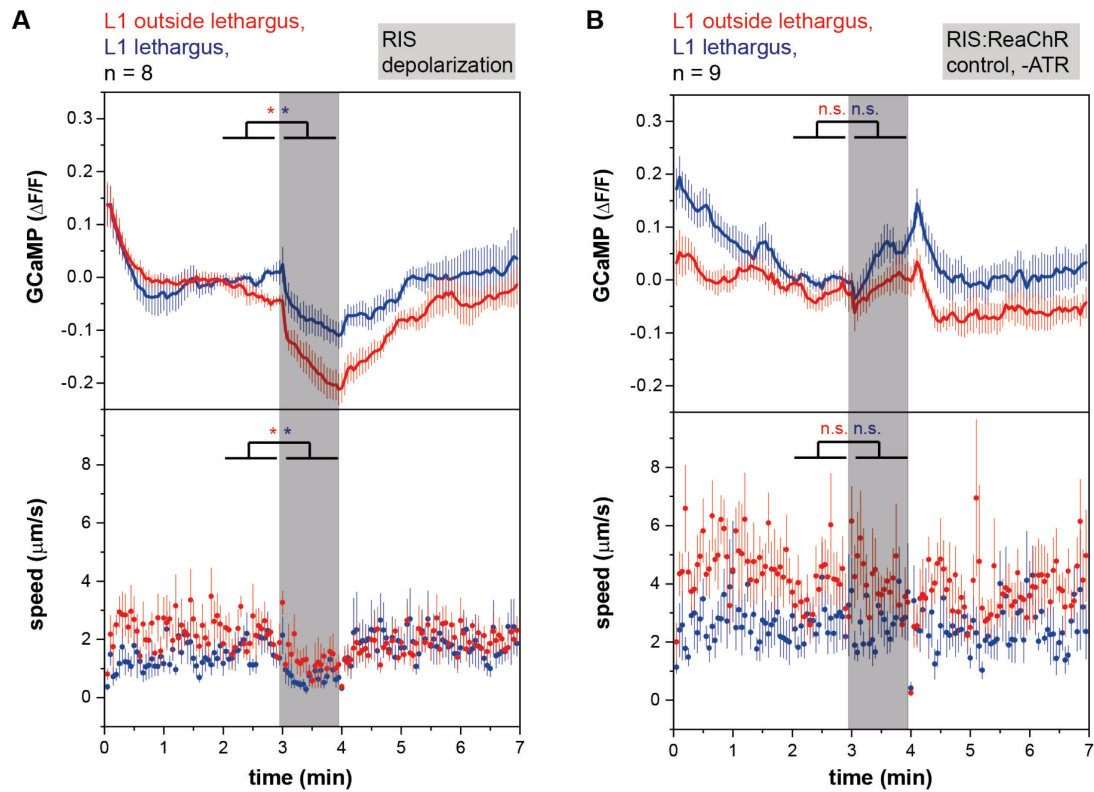


Figure 13. Optogenetic depolarization of RIS inhibits nervous system activity.

(A) Optogenetic RIS depolarization shuts down the nervous system and leads to a reduction of speed. $*p < 0.05$, Wilcoxon signed rank test. (B) Control worms that expressed RIS:ReaChR without ATR treatment did not show a significant response to the green light stimulus. n.s. $p > 0.05$, Wilcoxon signed rank test.

4.2. Aim 2 - Implementation of the OptoGenBox: a device to conduct optogenetic long-term experiments in *C. elegans*

4.2.1. Publication II

Busack I, Jordan F, Sapir P & Henrik Bringmann (2020) The OptoGenBox – a device for long-term optogenetics in *C. elegans*, Journal of Neurogenetics, DOI: 10.1080/01677063.2020.1776709

This project was done in collaboration with Florian Jordan, Peleg Sapir and Henrik Bringmann. It was published on June 20 2020 in the Journal of Neurogenetics.

I had the idea for the OptoGenBox and instructed its set-up. Together with Florian Jordan, I designed the OptoGenBox. Additionally, I designed, performed and analyzed the experiments in Figures 5 and 6. I illustrated the panels from the previously mentioned figures and additionally Figure 2. Furthermore, I contributed to the illustration of Figures 1, 4, S3, S4, S5 and S6. Finally, I wrote the manuscript.

Due to copyright rules by the Journal of Neurogenetics, this PhD thesis includes the accepted manuscript. The final version is available online:

<https://www.tandfonline.com/doi/full/10.1080/01677063.2020.1776709>

The OptoGenBox - a device for long-term optogenetics in *C. elegans*

Inka Busack^{1,2}, Florian Jordan¹, Peleg Sapir¹, Henrik Bringmann^{*1,2}

¹ *Max Planck Institute for Biophysical Chemistry, Am Fassberg 11, 37077 Göttingen, Germany*

² *Department of Biology, University of Marburg, Karl-von-Frisch-Str. 8, 35043 Marburg, Germany*

* correspondence to: henrik.bringmann@biologie.uni-marburg.de

Inka Busack is currently a PhD student of Systems Neuroscience at the University of Göttingen, Germany. She works in the group of Prof. Bringmann with a focus on sleep in *C. elegans*. She received a Bachelor degree in physics from Princeton University, USA, in 2016. After that she started her PhD work in Prof. Bringmann's lab at the Max Planck Institute for Biophysical Chemistry in Göttingen, Germany. The lab moved to Marburg, Germany, in May 2019, where she since then conducts her research and finishes her PhD projects.

Florian Jordan works as an electronics technician for the electronics service at the Max Planck Institute for Biophysical Chemistry in Göttingen, Germany. He finished his occasional training there in 2014 and since then he develops and repairs electrical equipment for research groups. In 2016 he received the CID certification, following this he started to study to become a state-certified technician.

Peleg Sapir was employed by the IT Service at the Max Planck for Biophysical Chemistry in Göttingen, Germany, during 2018. He is currently a PhD at the Max Planck Institute for Dynamics and Self-Organisation in Göttingen, Germany, focusing on control of spatiotemporal organization of cardiac fibrillation, in the Biomedical Physics Research Group of Prof. Stefan Luther. He received his bachelor degree in chemistry from Tel-Aviv University, Israel, in 2012 and his master's degree in chemistry from the Free University of Berlin, Germany, in 2020, with the master's thesis done under the supervision of Prof. Helmut Grubmüller in the department of Theoretical and Computational Biophysics at the Max Planck Institute for Biophysical Chemistry in Göttingen, Germany.

Henrik Bringmann is a Professor at the University of Marburg, Germany, where he teaches Animal Physiology and investigates sleep in *C. elegans*. In 2007, he received his PhD in Cell Biology at the Max Planck Institute for Cell Biology and Genetics in Dresden, Germany. After a postdoc at the MRC Laboratory of Molecular Biology in Cambridge, UK, in 2009 he became a Max Planck Research Group Leader at the Max Planck Institute for Biophysical Chemistry in Göttingen. Since 2018 he is a full Professor at the University of Marburg.

The OptoGenBox - a device for long-term optogenetics in *C. elegans*

Optogenetics controls neural activity and behavior in living organisms through genetically targetable actuators and light. This method has revolutionized biology and medicine as it allows controlling cells with high temporal and spatial precision. Optogenetics is typically applied only at short time scales, for instance to study specific behaviors. Optogenetically manipulating behavior also gives insights into physiology, as behavior controls systemic physiological processes. For example, arousal and sleep affect aging and health span. To study how behavior controls key physiological processes, behavioral manipulations need to occur at extended time scales. However, methods for long-term optogenetics are scarce and typically require expensive compound microscope setups. Optogenetic experiments can be conducted in many species. Small model animals such as the nematode *C. elegans*, have been instrumental in solving the mechanistic basis of medically important biological processes. We developed the OptoGenBox, an affordable stand-alone and simple-to-use device for long-term optogenetic manipulation of *C. elegans*. The OptoGenBox provides a controlled environment and is programmable to allow the execution of complex optogenetic manipulations over long experimental times of many days to weeks. To test our device, we investigated how optogenetically increased arousal and optogenetic sleep deprivation affect survival of arrested first larval stage *C. elegans*. We optogenetically activated the nociceptive ASH sensory neurons using ReaChR, thus triggering an escape response and increase in arousal. In addition, we optogenetically inhibited the sleep neuron RIS using ArchT, a condition known to impair sleep. Both optogenetic manipulations reduced survival. Thus, the OptoGenBox presents an affordable system to study the long-term consequences of optogenetic manipulations of key biological processes in *C. elegans* and perhaps other small animals.

Keywords: *Caenorhabditis elegans*, *C. elegans*, optogenetics, arousal, sleep, lifespan

Introduction

Optogenetics can control many physiological processes by actively influencing biochemical reactions and manipulating neuronal activity (Fenno, Yizhar, & Deisseroth, 2011). A light-sensitive actuator can be genetically expressed in specific cells of organisms and activated by light. Different tools exist for either activation or inhibition of excitable cells. Some of the most-used tools are channelrhodopsins, which have first been discovered in algae (Nagel et al., 2002, 2003), and ion pumps, which were found in halobacteria (Han et al., 2011). Both can now be genetically expressed in other organisms to depolarize or hyperpolarize cells upon light stimulation. Optogenetics has become widely established in different model organisms, e.g. small nematodes and flies but also mammals such as mice and monkeys (Fenno et al., 2011). *C. elegans* is well suited and established for optogenetic studies (Husson, Gottschalk, & Leifer, 2013; Schmitt, Schultheis, Husson, Liewald, & Gottschalk, 2012). Many physiological processes are conserved across species and can be studied in less complex organisms such as the 1mm long nematode *C. elegans*. 83% of its genes have human homologs, allowing molecular studies that are of relevance also to human biology (Lai, Chou, Ch'ang, Liu, & Lin, 2000). With 302 neurons, its nervous system is more manageable than that of other animals. Additionally, a single neuron in *C. elegans* can act similarly to brain regions in mammals (Altun, Z.F. and Hall, 2011). Due to the nematode's transparency, optogenetic experiments can be conducted in a non-invasive manner (Husson et al., 2013). *C. elegans* was the first animal in which optogenetics was established (Husson et al., 2013; Nagel et al., 2003).

However, there are still limitations that hinder the complete realization of the potential of optogenetics. In particular, long-term optogenetic experiments have rarely been conducted (Schultheis, Liewald, Bamberg, Nagel, & Gottschalk, 2011). In a standard experiment the neuronal manipulation only lasts for seconds or minutes. While it is true that some reactions and neuronal signals are fast acting, to manipulate physiology in the long term, one typically has to manipulate biological processes for days or even longer. Optogenetic long-term experiments are challenging for several reasons:

- (1) It is necessary to control the environment of the tested organisms.

- (2) For high-throughput experiments, many different conditions should be processed in parallel.
- (3) There is currently no inexpensive device available to account for 1 and 2.

Through optogenetic long-term manipulations, it is possible to investigate how a specific behavior affects organisms systemically (Altun, Z.F. and Hall, 2011; Husson et al., 2013; Lai et al., 2000; Schmitt et al., 2012). Even in *C. elegans* research the above-mentioned challenges in long-term optogenetic studies persist. Due to the development of new rhodopsins, first steps towards long-term optogenetics have been made. These newer genetic tools can continually be activated for minutes (Gengyo-Ando et al., 2017) or even for up to 2 days (Schultheis et al., 2011) after a shorter light pulse. The longest optogenetic lifespan experiment to date lasted 2.5 hours (De Rosa et al., 2019). Optogenetic survival assays lasting several days or weeks have not yet been conducted in *C. elegans*.

One additional reason that explains why long-term experiments have rarely been conducted in *C. elegans* is, that blue light, which is often used in optogenetic experiments, is harmful to the worms. Blue light causes a negative phototaxis and prolonged exposure leads to paralysis and death of *C. elegans* (Edwards et al., 2008; Ward, Liu, Feng, & Xu, 2008). Alternative optogenetic actuators have been developed that can be excited with a higher wavelength, thus causing less stress to *C. elegans*. For example, the red-shifted channelrhodopsin (ReaChR) can be used for neuronal activation (Lin, Knutsen, Muller, Kleinfeld, & Tsien, 2013) or ArchT, which hyperpolarizes neurons by pumping out protons, can be used for inhibition (Okazaki, Sudo, & Takagi, 2012). These genetic tools allow the use of yellow to orange light (585-605nm) for excitation.

Increased arousal and decreased sleep affect the survival of *C. elegans* (De Rosa et al., 2019; Wu, Masurat, Preis, & Bringmann, 2018). Many assays that control arousal and sleep deprivation in *C. elegans* build on external stimuli such as tapping mechanisms, the ablation of neurons or mutation (Bringmann, 2019; Driver, Lamb, Wyner, & Raizen, 2013; Hill, Mansfield, Lopez, Raizen, & Van Buskirk, 2014; Schwarz & Bringmann, 2013; Singh, Ju, Walsh, DiIorio, & Hart, 2014; Spies & Bringmann, 2018; Van Buskirk

& Sternberg, 2007). Optogenetics activates or inhibits specific neurons and therefore allows the dissection of neuronal mechanisms. ASH is a nociceptor and its activation causes a reverse escape response by activating the second layer RIM interneurons and by inhibiting the sleep neuron RIS (Kaplan & Horvitz, 1993; Maluck et al., 2020). Mechanical tapping or optogenetic RIM activation, which causes a flight response and increase in arousal, shortens the lifespan of adult *C. elegans* (De Rosa et al., 2019). Depolarization of ASH causes a complex response. It activates RIM, therefore triggering release of tyramine and promoting the flight response (De Rosa et al., 2019; Maluck et al., 2020). Additionally, strong RIM activation inhibits the sleep neuron RIS which leads to sleep deprivation (Maluck et al., 2020). RIS is a single neuron that acts as the motor of sleep in *C. elegans*. RIS is active during sleep, its activation induces sleep and its depolarization is homeostatically regulated (Bringmann, 2018; Maluck et al., 2020; Michal Turek, Lewandrowski, & Bringmann, 2013). A more specific experiment for sleep deprivation, in which arousal also gets increased, is hence the inhibition of the sleep neuron RIS through optogenetics (Maluck et al., 2020; Wu et al., 2018).

To solve the problem of long-term optogenetic manipulation, we have developed the OptoGenBox, a simple-to-use stand-alone device, which provides a controllable environment and allows for the execution of complex optogenetic protocols. The total material costs of less than 3500 USD (Table S1) makes it substantially more inexpensive than the use of standard microscope set-ups. The OptoGenBox therefore presents the currently best solution for long-term optogenetic experiments in *C. elegans*. We successfully tested the OptoGenBox by optogenetically activating the sensory neuron ASH and inhibiting the sleep neuron RIS. Optogenetic activation of ASH or inhibition of RIS in L1 arrested animals both reduced lifespan. Our results show that the OptoGenBox is a valuable tool for long-term optogenetic experiments in *C. elegans*, and potentially also for other small animals.

Results

A device for optogenetic long-term imaging

We developed the OptoGenBox to enable long-term optogenetic experiments in *C. elegans* (Figure 1). Worms were kept in a temperature-controlled environment and illuminated with orange light from the bottom (Figure 2A). For this, the OptoGenBox was built as a 70x70x90cm large device that is programmable via a touch display (Figure 2B). The inside consists of a 22x22cm sized experimentation area partitioned into 13 cells (Figure 2C). Each cell can hold small plates with nematode growth medium or microfluidic chambers (Bringmann, 2011; M Turek, Besseling, & Bringmann, 2015) with a diameter of 3.5cm, and can thus fit up to 100 worms. Worm plates are placed on 4mm thick glass (B270), which was polished on the bottom (400 polish) to homogeneously distribute the LED light throughout the worm plate (Figure 3). 6 LEDs are distributed throughout an LED module (Figure 4) 7.4mm below the glass to illuminate the worms from the bottom. An aluminum casing keeps external light out and creates optically isolated cells. Furthermore, the box is temperature controlled through Peltier devices and protected from external disturbances via foam and an acrylic case (Figure S1). The LED intensities of all 13 cells were measured with a light voltmeter (ThorLabs PM100A) and calibrated through the software while setting up the system to assure equal light intensities between the cells. The temperature for all cells is uniform and can only be determined when no experiments are running. Each cell contains environmental sensors for light intensity and air quality, and temperature recordings are carried out for each cell. Humidity stays constant in the closed plastic dishes that contain the microfluidic devices (M Turek et al., 2015) and thus humidity measurements are not necessary when the microfluidic devices are used. Nevertheless, sensors are included to monitor humidity inside the device in case other types of samples need to be used.

The researcher can easily program the optogenetic protocol through the touch screen. The system is written in Python and implemented on a Raspberry Pi (Figure S2). To start an experiment the exact cells can be selected individually for each experiment and then the optogenetic protocol can be defined (Figure S3). The experimenter can choose how many cycles should run with how much time (hours or minutes) in light and how

much time in darkness and can define the light intensity for the experimentation area (between 2-40mW) during the light times. LEDs can be programmed to be either on or off for minutes or hours. The minimum continuous amount of time for a light cycle is hence 1min and the maximum is 25h. The same holds for dark phases. The maximum number of cycles is 5000. Theoretically, worms could get illuminated for up to 2083 days. The temperature can only be chosen for the entire OptoGenBox and not individual cells between 15-25°C (Figure S4).

While one experiment can include up to 13 cells, light intensities and optogenetic protocols of individual or groups of cells can also be programmed separately to allow for parallel experiments (Figure S5). The total material costs of less than 3500 USD (Table S1) make it much less expensive than microscopic set-ups, which one could also use for optogenetic long-term experiments. All code is freely available (<https://gitlab.gwdg.de/psapir/inkubator>). The OptoGenbox presents an inexpensive and user-friendly tool to conduct optogenetic long-term experiments.

Optogenetic ASH activation in the OptoGenBox triggers an escape response

The sensory neuron ASH is known to promote reverse escape locomotion upon different harmful stimuli (Kaplan & Horvitz, 1993; Zheng, Brockie, Mellem, Madsen, & Maricq, 1999). To test for the functionality of the box, we developed an escape assay in which we optogenetically activated ASH and tested for its effects on behavior. ReaChR was genetically expressed in worms under the *sra-6* promoter to cause ASH activation upon addition of ATR (Wu et al., 2018). For the experiment, a small plate was prepared with a small lawn of bacteria of the *E. coli* strain OP50 as a food source on one half of the plate and an opaque sticky tape, which caused an area of shade in the OptoGenBox, on the other half (Figure 5A). Worms without any optogenetic activation were expected to mostly assemble by the food. On the contrary, after ASH activation worms were expected to not gather at the food but to either distribute throughout the plate or gather in the shade, where the activation is interrupted. An optogenetic protocol was run for one hour and the distribution of worms was counted. Indeed, an average of 80% of the control worms gathered by the food. Only around 20% of the ASH-activated *C. elegans* could be counted at the food drop. This significant decrease in worms at the food drop confirms that the worms show an escape response upon ASH activation.

Worms did not aggregate in the shade caused by the sticky tape but mostly distributed across the plate. This could potentially be explained by a remaining low light intensity of 0.02mW in the shade (outside the shade there was an intensity of 10mW, so 0.2% of the light intensity could be measured above the sticky tape), which may have still been sufficient for ASH activation and hence an escape response of the worm. The low light intensity in the shade could perhaps be caused by light reflections. Neither the worms in which ASH was activated nor control worms were able to flee from the plate (Figure 5B). These results demonstrate the functionality of the OptoGenBox.

Increased arousal and decreased sleep by optogenetic manipulations shortens the lifespan of arrested L1 larvae

Increased arousal and sleep deprivation has been shown to shorten the lifespan in *C. elegans* (De Rosa et al., 2019; Wu et al., 2018). We wanted to test if an increase in arousal or inhibition of sleep can affect the survival of arrested L1 larvae. We therefore conducted experiments in which arousal gets increased or sleep is reduced through different optogenetic manipulations.

The optogenetic manipulations were achieved by treating transgenic worms carrying the optogenetic tool with ATR. Since a toxicity of ATR could not be excluded we first investigated the effects of ATR on the wild type. Two rounds of experiments confirmed that the addition of ATR without optogenetic manipulation did not lead to a significant reduction of survival (Figure 6A). Hence, any lifespan phenotypes in our optogenetic experiments can be attributed to the optogenetic manipulations and not the treatment with ATR.

To test for survival phenotypes upon increased arousal, we conducted two experiments, a first experiment in which optogenetic activation of a nociceptive neuron causes an escape response and increases arousal and a second experiment in which optogenetic inhibition of a sleep neuron causes sleep deprivation.

For the optogenetic activation experiment, we used the ASH::ReaChR strain as described before (Wu et al., 2018). All-trans retinal (ATR) was present throughout the L1 arrest lifespan to ensure functionality of the optogenetic tool. Control worms were

used that carried the ReaChR transgene but did not receive ATR. In both rounds of the experiment, animals in which ASH was activated died significantly earlier than control worms (Figure 6B).

Next, we tested how sleep deprivation caused by the inhibition of the sleep neuron RIS affects survival in L1 arrest. We expressed ArchT under the *flp-11* promoter so that it was specifically expressed in RIS and all-trans retinal was supplemented (Wu et al., 2018). Again, control worms for comparison did not receive ATR treatment. Optogenetic sleep deprivation led to a small but significant reduction of survival in arrested L1 animals by 8.3 % (Figure 6C).

Discussion

Here we developed the OptoGenBox as a device for optogenetic long-term experiments. The OptoGenBox combines a controlled environment and allows for parallel processing of many experiments for *C. elegans* and perhaps other small animal models. With material costs of less than 3500 USD it is rather inexpensive. While there exist lower cost alternatives such as the DART system for *Drosophila* (Faville, Kottler, Goodhill, Shaw, & Van Swinderen, 2015), the DART system does not allow for parallel processing and temperature control. Hence, the OptoGenBox currently presents the best solution to allow for parallel optogenetic long-term experiments. Experiments in the OptoGenBox can last up to several weeks. The device allows for optogenetic long-term experiments in a highly controlled environment. The OptoGenBox is not equipped with an imaging system. For performing measurements on the worms, the samples containing the worms thus need to be taken out of the system, which could perturb the measurements. However, an imaging system could be added to the device in the future. We could demonstrate that different optogenetic manipulations that increase arousal or inhibit sleep have a detrimental effect on *C. elegans*. The activation of the nociceptor ASH led to a reduced survival in L1 arrest. While ASH activation also leads to an inhibition of the sleep neuron RIS (Maluck et al., 2020), the lifespan shortage of ASH activated animals cannot solely be accounted for by sleep inhibition (Maluck et al., 2020). More likely, the reduced survival upon ASH activation is caused by the inhibition of cytoprotective mechanisms through the activation of RIM and release of tyramine as has been previously described (De Rosa et al., 2019).

The optogenetic inhibition of RIS presents a very specific and therefore suitable experiment to investigate the effects of sleep deprivation on *C. elegans*. The shortened survival upon RIS inhibition confirms that sleep plays an essential role in arrested L1 worms as has been previously demonstrated with *aptf-1(gk794)* mutants in which RIS is not functional and with worms in which RIS was genetically ablated (Wu et al., 2018). However, the previously reported phenotypes with *aptf-1(gk794)* mutants were stronger, having a reduction of lifespan of approximately 40% compared to the wild type. In comparison, in the lifespans in which RIS was optogenetically inhibited, the reduction of lifespan was rather small (around 8.3%). There might be several reasons for these differences. The previously reported stronger lifespan effects were obtained in liquid cultures whereas during the optogenetic experiments, worms were kept isolated in microfluidic devices, making a direct comparison impossible. Furthermore, genetic sleep deprivation by a loss of functional APTF-1 can be presumed to lead to more severe effects than temporally-restricted optogenetic sleep deprivation. The advantages of optogenetics are that behavior can be controlled with temporal precision. Instead of completely depriving the worms of sleep it is possible to study the effects of periodic sleep deprivation. For the results presented here, a long light phase (11h) was followed by only a short dark phase (1h) in each cycle throughout the lifespan. This is a rather long optogenetic stimulation phase, in which neurons could perhaps get desensitized as desensitization has been shown before in optogenetic experiments in *C. elegans* (Bergs et al., 2018; Berndt, Yizhar, Gunaydin, Hegemann, & Deisseroth, 2009). It is possible that shorter intervals of light/dark phases might be even more effective for optogenetic sleep deprivation in future experiments.

In experiments with worms in which RIS function was impaired, it was shown that sleep counteracts aging phenotypes (Wu et al., 2018). It would be interesting to see how aging phenotypes progress when RIS is inhibited optogenetically. Additionally, how exactly sleep counteracts aging and causes premature death needs further investigation.

Conclusions

With the newly developed OptoGenBox, we have mostly investigated how an increase in arousal and a loss of sleep affects survival in L1 arrest. However, many other questions could be answered with our device. Optogenetics is a method that cannot only

be utilized for depolarizing or hyperpolarizing neurons but also any other type of cell such as epidermal or muscle cells. Silencing of body wall muscles for example leads to an inhibition of feeding (Takahashi & Takagi, 2017) and photoablation of epidermal cells causes paralysis in *C. elegans* (Xu & Chisholm, 2016). The OptoGenBox should allow for many optogenetic long-term experiments in *C. elegans* and potentially also other small animals. Long-term optogenetics should thus help understand how behavior affects systemic physiology in the long term.

Methods

Development of the OptoGenBox

The OptoGenBox consists of several parts to allow for orange light illumination and temperature control (Figure 1-3). The user can select the cells and set the exact light level through the touch display of the raspberry pi computer. Signals from and to the raspberry pi are transferred by an inter-integrated circuit bus (I²C bus). There are four LED controllers that address the LEDs of cells, which the researcher previously chose. The LED controllers convert the set illumination level into a pulse width modulated (PWM) signal. This signal allows a constant current through the LEDs and their current source so that the selected cell gets illuminated. The PWM current finally supplies 6 single high brightness LEDs on one single LED-PCB. A light sensor for each cell gives feedback to the raspberry pi about the activation and wavelengths of the LEDs.

A digital to analogue converter (DAC) connects the digital temperature signal, set by the user, with the analogue temperature control unit. This unit gets the actual value from a PT 100 temperature sensor located at the bottom of the chamber and regulates the power output for six 100W Peltier devices. With this closed control loop the OptoGenBox can operate at a constant temperature between 15°C-25°C

An additional temperature measuring takes part by several evenly placed environmental sensors located in the lid. These sensors measure temperature, air quality (based on gas measurements, 0-50 is excellent air) and humidity. The obtained temperature is displayed on the screen.

The system is built on several printed circuit boards (PCBs), which are separated by function. These different PCBs are: the LED-controlling PCB, the environment

measuring PCB, the analogue temperature-control PCB, an analogue power module PCB and an overall supplying PCB.

Assembly of the OptoGenBox

The OptoGenBox consists of a few electronic units (Figure 1), which are: 1) the raspberry pi inclusive the touch display, 2) LED-control-units, 3) LED modules, 4) a sensor-unit, 5) a main-control-unit and 6) a DC/DC-power-supply-unit, These units were specifically produced for the OptoGenBox (except the raspberry pi with its display). Furthermore, all PCBs were assembled manually at the Max Planck Institute for Biophysical Chemistry (MPI-bpC). The bare PCBs were produced by different distributors available in Germany (market compliant).

To assemble a PCB, a soldering iron was sufficient for most PCBs. However, for some PCBs, a reflow-oven was used either because it was required or for a more reliable and time efficient soldering procedure.

Reflow Soldering

Reflow soldering requires a special set of tools, which consists of a disposing tool for the soldering paste, a placing machine (not necessary, but facilitates the procedure), and an oven that heats up to at least 270°C.

Hand soldering

Hand soldering doesn't require as specific tools as reflow soldering but requires more skills from the executing person. To produce reliable PCBs, different types of soldering tips are recommended and a set of tweezers should be available.

After PCB assembly, the PCBs were connected. For different types of signals, different connectors and cables were selected. Every connector has its special crimping tool so that in total four crimping pliers were used. Additionally, a set of screwdrivers and pliers should be available. A digital multi-meter was utilized to adjust the LED voltage and to tune the analogue temperature control circuit.

Mechanical assembly

The components of the OptoGenBox were placed in a modified case originally built for a water-cooled PC system (Figure S7). In the lower tier, all of the AC/DC power supplies and the temperature-control-unit are placed. The incubator sits in the upper tier of the case. The main-control-unit and the raspberry-pi are placed around the incubator (Figure 2).

The incubator itself is assembled in the following manner:

The outside of the incubator is a plastic cover (Figure 3, number 1) around an insulating foam material (Figure 3, number 2). These two materials provide for a stable temperature environment in the incubator inlet (Figure 3, number 3). The worm plates or microfluidic devices (Figure 3, number 4) can be placed on a one-side sanded glass (Figure 3, number 5) in the inlet. The lid of the incubator contains the sensor-unit (Figure 3, number 6). The LED modules (Figure 3, number 7) and the Peltier devices (Figure 3, number 8) are placed in cut-outs beneath the inlet and each mounted with two screws. This construction makes it possible to change the pre-assembled LED modules. While exchanging the LEDs, one has to pay attention to match the current and voltage to the new LED type for ideal light results. Matching the electrical parameters can be done via already implemented options on the LED-control-unit and DC/DC-power-supply-units.

For an optimized thermal solution, the Peltier devices are clamped with thermal pads between two brackets. One bracket (Figure 3, number 9) is directly attached to the inlet. The other is a two-piece bracket (Figure 3, number 10) clamping the Peltier devices and holding the heat pipes (Figure 3, number 11). The heat pipes transport the emerging heat when the device is cooling the incubator. The elements holding the heat pipes can be assembled separately. The heat pipes were manually bend from a straight pipe to fit in the shape that was needed. All bracket parts were specifically designed for the OptoGenBox. The LED control units were attached to the plastic cover (with standard bolts and screws) and then wired with the 13 LED modules.

With the LED modules and the Peltier devices attached to the insulated, covered aluminium inlet, it was installed on fitting brackets in the upper tier of the modified PC

case. The LED-control-unit was wired to the main control unit and to the power supply for the LEDs at the DC/DC power supply unit

Fans were installed on both sides of the case to avoid a cushion of heat beneath the incubator and to create a constant airflow so the LED modules, heatsinks for Peltier devices and the electronics would not get damaged by elevated temperature.

The LED module

One LED module consists of six high-power LEDs (Osram Opto Semiconductors LCY-CLBP Series) with a peak wavelength at approximately 590nm with 80lm each (Figure 4). In order to reach a maximum light power of 40mW we placed 6 LEDs in a circle with a diameter of 8.4mm. The individual LED modules were calibrated after the installation to have the same light intensities. At 10mW, the light intensity difference between the center and the periphery of the experimentation area was measured to be 0.04mW (0.4% difference). The PCB of the LED module is an IMS-Core PCB, (insulated metal substrate) to absorb most of the thermal energy and conduct it through a thermal pad to the attached round heat sink away from the temperature-controlled area.

The Lid

The lid is made of insulating foam material covered with plastic. To locate the necessary sensors at the designated position, the lid got a fitting cut-out. In this cut-out, an overall covering PCB with a pair of sensors (light & environment) for each individual chamber was placed. It is directly attached to the plastic that covers the aluminium inlet from above, aligned to small holes so that the light can be detected and measured. Through a separated hole the air-quality is measured. This PCB and the plastic, on which it is mounted, could be modified to add several other functions as for example an IR-camera with an integrated light source.

C. elegans maintenance

Worms were grown at 20°C on Nematode Growth Medium (NGM) plates. The plates were seeded with *E. coli* OP50, which served as food for the worms (Brenner, 1974). The following strains were used for this study:

HBR974	<i>goeIs232(psra-6::ReaChr::mKate2-unc-54-3'utr, unc-119(+))</i>
HBR1463	<i>goeIs307(pflp-11::ArchT::SL2mKate2-unc-54-3'utr, unc-119(+))</i>
N2	wild type (Bristol) (Brenner, 1974)

Escape Assay

Late L4 stage worms were picked onto NGM plates with 0.2 mM all-*trans* retinal (ATR, Sigma Aldrich). Control late L4 stage worms were picked onto NGM plates without ATR. 9.6 cm² large NGM plates were prepared for the experiment by placing a 1 cm² opaque tape on the bottom of one side of the plate and a drop of *E. coli* OP50 on the other side (Figure 5A). After 4 hours, 10 young adult worms were picked into the food drop of the experimental plate for each trial.

The experimental plates were then placed in the OptoGenBox and stimulated with 10mW orange light for 1 hour at 20°C. After one hour the plates were removed from the OptoGenBox and the distribution of worms on the plates was counted.

Lifespan assay

It was shown before that sleep is important for the survival of *C. elegans* by counteracting aging phenotypes. However, non-sleeping *aptf-1(gk794)* mutants only have a reduced lifespan when worms starve upon hatching and arrest in the first larval stage (L1 arrest) and not when they are adults (Wu et al., 2018). For this reason, we conducted our experiments with L1 arrested animals.

Worms were kept in microfluidic devices as previously described (Bringmann, 2011; M Turek et al., 2015). A PDMS mold was used as a stamp to cast 110x110x10µm cuboids into a hydrogel. The hydrogel consisted of 3% agarose dissolved in S-Basal (Stiernagle, 2006). Eggs were transferred from a growing plate to a plate without food and then picked into chambers without transferring food. Between 29 and 45 worms were in one microfluidic device housed in individual chambers.

For optogenetic activation or inhibition, chambers were replenished with 10µl of 10mM all-*trans*-retinal (ATR, Sigma Aldrich) every 3-4 days. Control chambers did not receive

ATR. To avoid fungal contamination, 20 μ l of 10 μ g/ml nystatin was pipetted to each chamber 2-4 times throughout the lifespan. Additionally, 20 μ l of sterile water was added every 2 days until day 15 of the lifespan and then each day to counteract the agarose drying out over time. In the beginning of the lifespan experiment, worms were counted every second day, in the later stages of the survival assay they were counted every day. A worm was counted as dead if it didn't move for 2 min under stimulation with a blue light LED. This was necessary to distinguish dead from sleeping worms.

The worms were placed in the OptoGenBox and illuminated with 10mW for 11h to attain a long continuous neuronal manipulation. This was followed by 1h of darkness to allow the optogenetic tools to recover without giving too much time to sleep homeostasis processes, which initiate a deeper and prolonged sleep upon sleep deprivation. This protocol was repeated until all worms were dead. The temperature of the incubator was set to 20°C.

Statistics

Sample sizes were determined empirically based on previous studies. The researcher was not blinded since the addition of ATR is easily detectable. Conditions in the escape assay were compared with the Kolmogorov Smirnov Test. The lifespans were compared with the Logrank test.

Acknowledgements

We thank the CGC, which is funded by NIH Office of Research Infrastructure Programs (P40 OD010440), for the N2 strain. The mechanics workshop at the MPI BPC provided us with valuable advice for the design and parts of the OptoGenBox. We would also like to thank Juliane Haase for assisting with laboratory work. This work was funded by the Max Planck Society (Max Planck Research Group), a European Research Council Starting Grant (ID: 637860, SLEEPCONTROL), and the University of Marburg.

Author Contributions

IB and FJ designed the OptoGenBox. IB designed, performed and analyzed the experiments and wrote the manuscript. FJ built the hardware of the OptoGenBox and contributed to the manuscript. PS programmed the software of the OptoGenBox. HB

acquired funding, conceived the project, supervised the work, and edited the manuscript.

Disclosure of Interest

The authors declare that they have no competing interest.

Supplementary Material

There are 7 supplementary figures and 1 supplementary table. The code for the OptoGenbox can be found on github (<https://gitlab.gwdg.de/psapir/inkubator>). Data for the experiments is published on Mendeley Data (<http://dx.doi.org/10.17632/d7wfc9fdbb.2>).

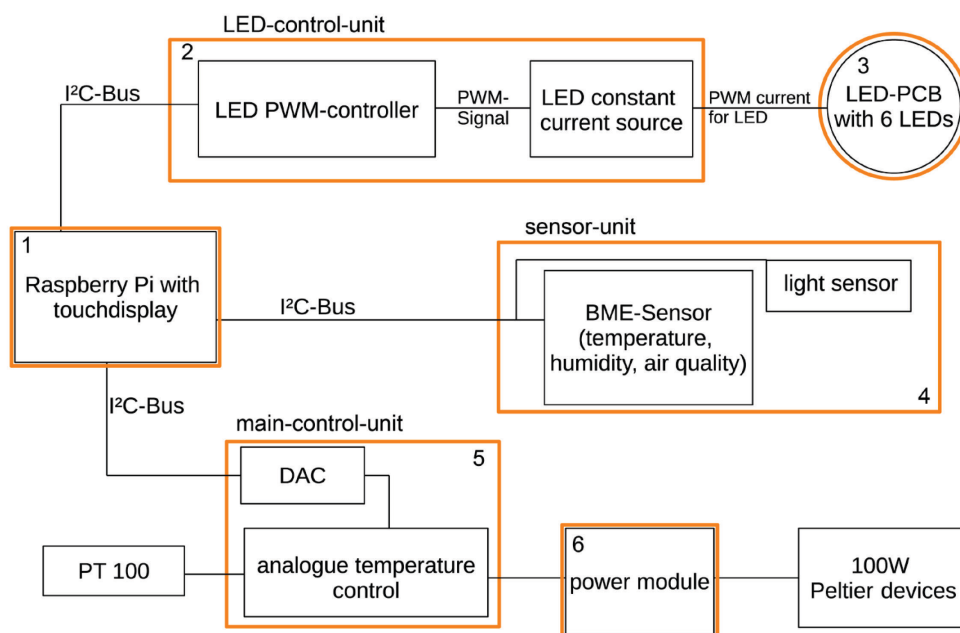


Figure 1. Functional scheme of the OptoGenBox. The box consists of several printed circuit boards (PCBs in coloured outlines), that are connected and controlled by a Raspberry Pi computer.

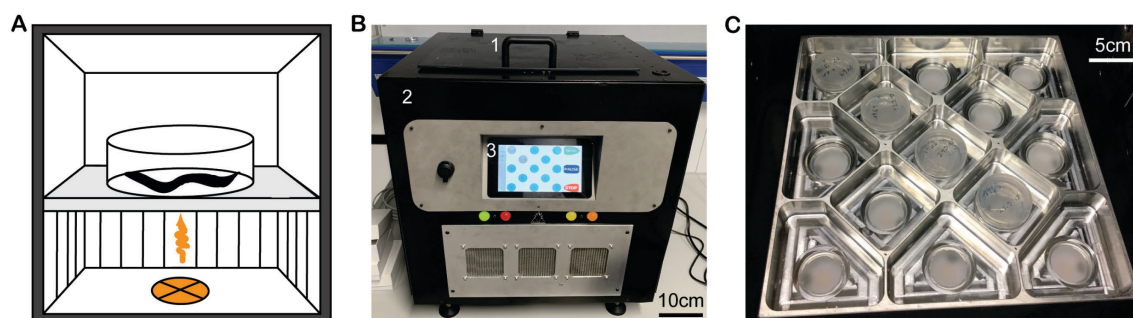


Figure 2. The OptoGenBox is a device for long-term optogenetic experiments in *C. elegans*.

A) Worms are kept in a controlled environment and illuminated with orange light.

B) The outside of the OptoGenBox. (1) opening handle, (2) exterior case and (3) touch screen.

C) The inside of the OptoGenBox is comprised of 13 groupable or separately programmable cells.

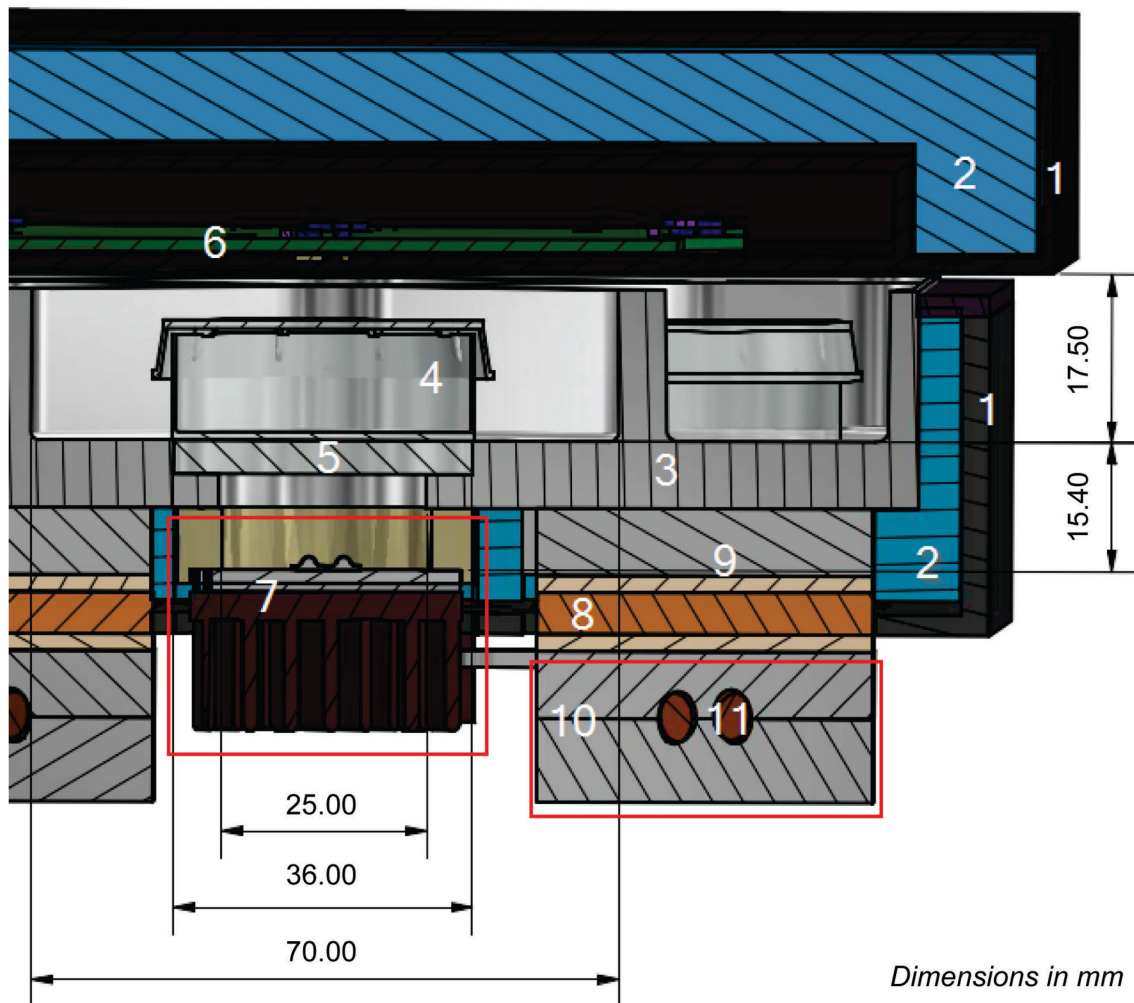


Figure 3. Cross-section of the OptoGenBox incubator.

(1) plastic cover, (2) insulating foam, (3) incubator inlet (4) worm plates or microfluidic devices, (5) sanded glass, (6) sensor PCB (in the lid), (7) LED module, (8) mounting bracket Peltier device, (9) Peltier device covered with thermal pads, (10) heat pipe brackets and (11) heat pipe.

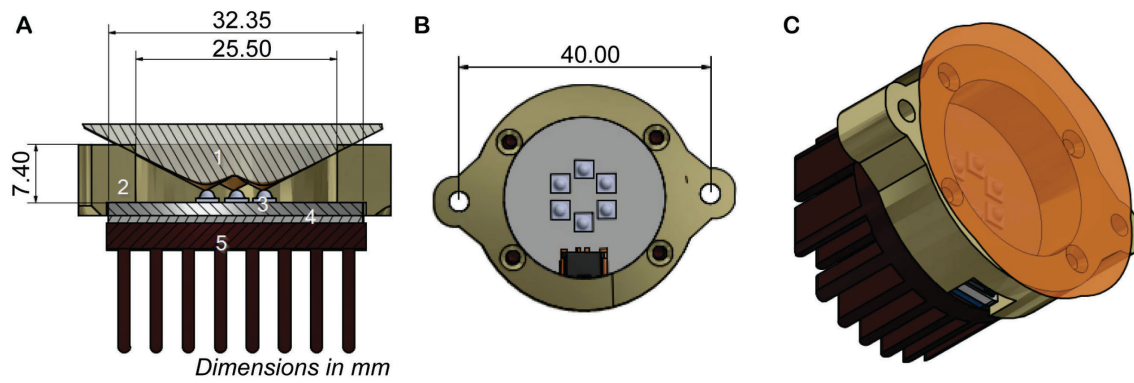


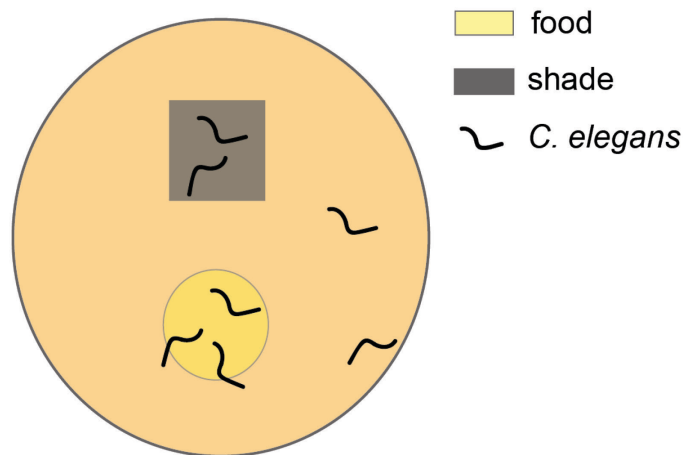
Figure 4. LED module.

A) Cross section of an LED module. (1) calculated light beam (LED current at 50%), (2) distance ring to mount the module, (3) the IMS-PCB with single LEDs on it, (4) the thermal pad and (5) the heat sink.

B) Top view of the LED module.

C) Side view of the LED module with the light distribution.

A



B

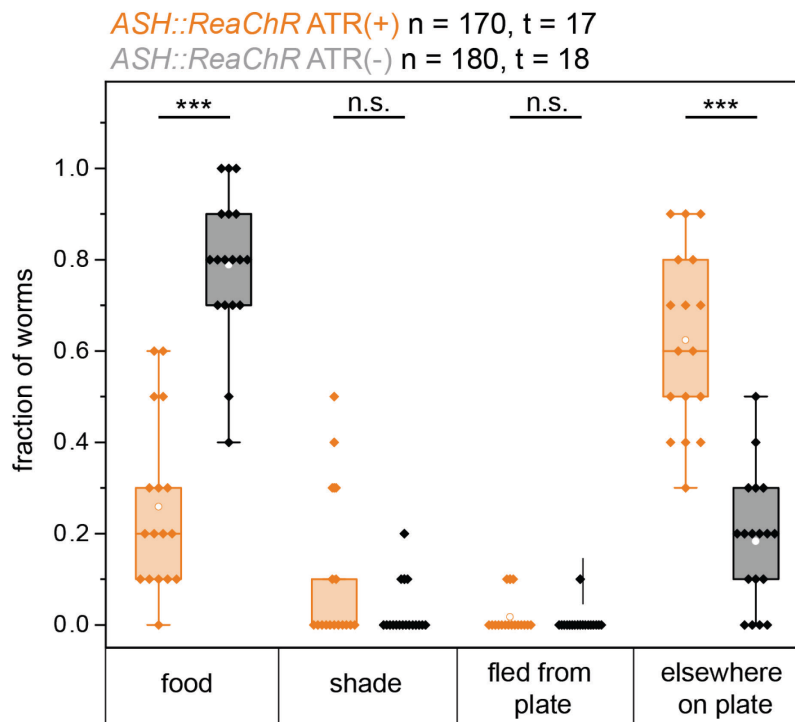


Figure 5. ASH activation in the OptoGenBox caused an escape response.

A) Preparation of the experimental plate. A small NGM plate is prepared with a drop of food (*E. coli* OP50). An opaque sticky tape is used to block the stimulating light.

B) After ASH activation through ReaChR and ATR, worms did not stay on the food drop but distributed throughout the plate. Neither ASH-activated nor control animals fled from the plate. *** $p < 0.001$, Kolmogorov Smirnov Test.

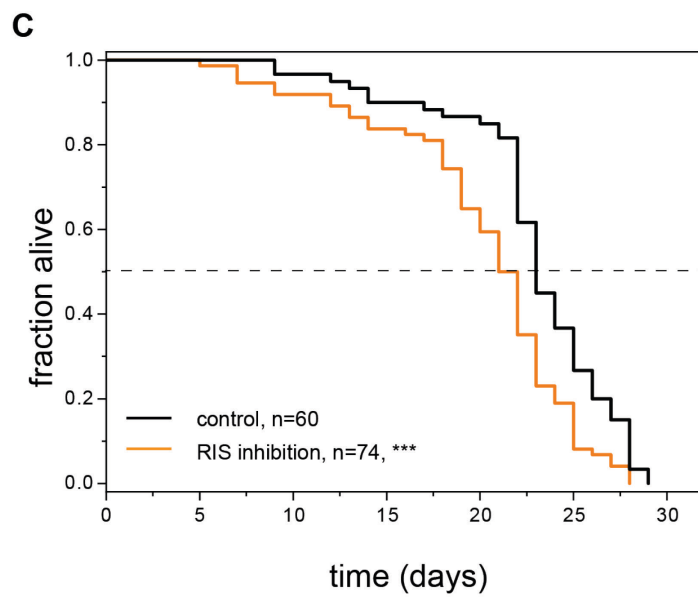
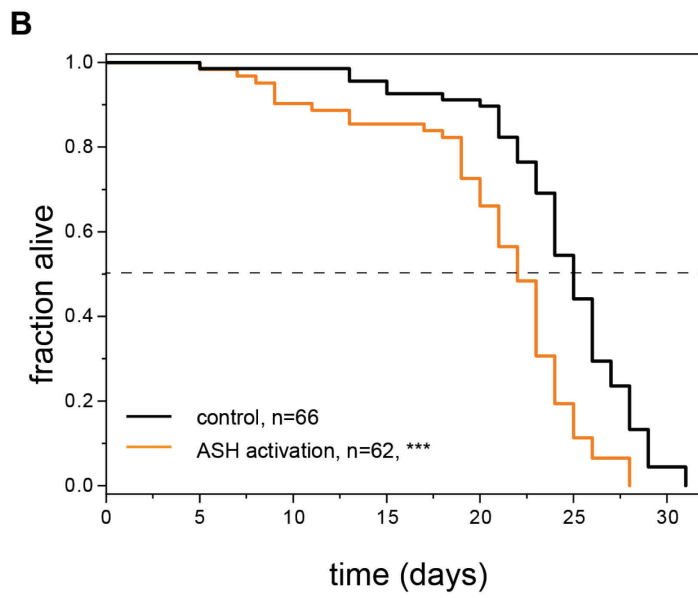
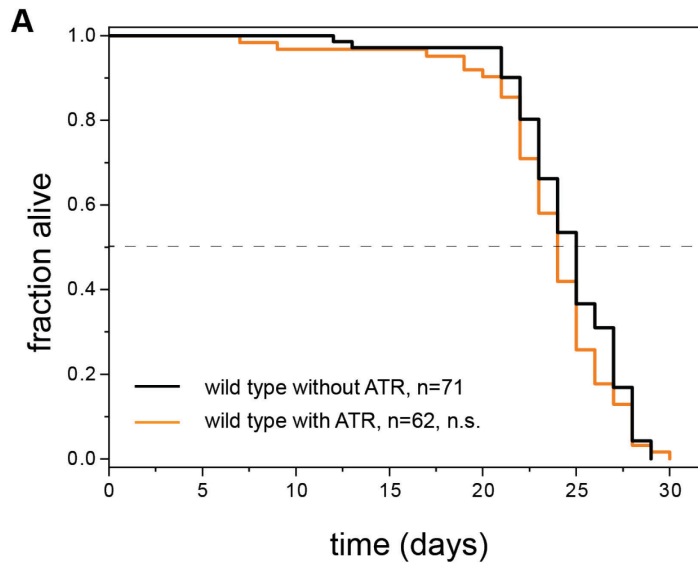


Figure 6. An increase in arousal and sleep deprivation reduces the lifespan of arrested L1 *C. elegans*.

A) All-trans retinal (ATR) did not affect survival of wild-type arrested L1 larvae. The graph includes data from 2 replicates. n.s. $p=0.2$, Logrank test.

B) ASH activation causes a reduction in lifespan compared to control animals without the addition of ATR. The graph includes data from 2 replicates. $***p=9.996*10^{-7}$, Logrank test.

C) RIS inhibition causes a reduction in lifespan compared to control animals without the addition of ATR. The graph includes data from 2 replicates. $***p=3.4*10^{-4}$, Logrank test.

References

- Altun, Z.F. and Hall, D. H. 2011. (2011). Nervous system, general description. <https://doi.org/doi:10.3908/wormatlas.1.18>
- Bergs, A., Schultheis, C., Fischer, E., Tsunoda, S. P., Erbguth, K., Husson, S. J., ... Liewald, J. F. (2018). Rhodopsin optogenetic toolbox v2.0 for light-sensitive excitation and inhibition in *Caenorhabditis elegans*. *PLoS ONE*. <https://doi.org/10.1371/journal.pone.0191802>
- Berndt, A., Yizhar, O., Gunaydin, L. A., Hegemann, P., & Deisseroth, K. (2009). Bistable neural state switches. *Nature Neuroscience*. <https://doi.org/10.1038/nn.2247>
- Brenner, S. (1974). The genetics of *Caenorhabditis elegans*. *Genetics*, 77(1), 71–94. <https://doi.org/10.1002/cbic.200300625>
- Bringmann, H. (2011). Agarose hydrogel microcompartments for imaging sleep- and wake-like behavior and nervous system development in *Caenorhabditis elegans* larvae. *Journal of Neuroscience Methods*, 201(1), 78–88. <https://doi.org/10.1016/j.jneumeth.2011.07.013>
- Bringmann, H. (2018). Sleep-active neurons: Conserved motors of sleep. *Genetics*. <https://doi.org/10.1534/genetics.117.300521>
- Bringmann, H. (2019). Genetic sleep deprivation: using sleep mutants to study sleep functions. *EMBO Reports*. <https://doi.org/10.15252/embr.201846807>
- De Rosa, M. J., Veuthey, T., Florman, J., Grant, J., Blanco, M. G., Andersen, N., ... Alkema, M. J. (2019). The flight response impairs cytoprotective mechanisms by activating the insulin pathway. *Nature*. <https://doi.org/10.1038/s41586-019-1524-5>
- Driver, R. J., Lamb, A. L., Wyner, A. J., & Raizen, D. M. (2013). DAF-16/FOXO regulates homeostasis of essential sleep-like behavior during larval transitions in *C. elegans*. *Current Biology*. <https://doi.org/10.1016/j.cub.2013.02.009>
- Edwards, S. L., Charlie, N. K., Milfort, M. C., Brown, B. S., Gravlin, C. N., Knecht, J. E., & Miller, K. G. (2008). A novel molecular solution for ultraviolet light detection in *Caenorhabditis elegans*. *PLoS Biology*. <https://doi.org/10.1371/journal.pbio.0060198>

- Faville, R., Kottler, B., Goodhill, G. J., Shaw, P. J., & Van Swinderen, B. (2015). How deeply does your mutant sleep? Probing arousal to better understand sleep defects in *Drosophila*. *Scientific Reports*. <https://doi.org/10.1038/srep08454>
- Fenko, L., Yizhar, O., & Deisseroth, K. (2011). The Development and Application of Optogenetics. *Annual Review of Neuroscience*. <https://doi.org/10.1146/annurev-neuro-061010-113817>
- Gengyo-Ando, K., Kagawa-Nagamura, Y., Ohkura, M., Fei, X., Chen, M., Hashimoto, K., & Nakai, J. (2017). A new platform for long-term tracking and recording of neural activity and simultaneous optogenetic control in freely behaving *Caenorhabditis elegans*. *Journal of Neuroscience Methods*. <https://doi.org/10.1016/j.jneumeth.2017.05.017>
- Han, X., Chow, B. Y., Zhou, H., Klapoetke, N. C., Chuong, A., Rajimehr, R., ... Boyden, E. S. (2011). A High-Light Sensitivity Optical Neural Silencer: Development and Application to Optogenetic Control of Non-Human Primate Cortex. *Frontiers in Systems Neuroscience*. <https://doi.org/10.3389/fnsys.2011.00018>
- Hill, A. J., Mansfield, R., Lopez, J. M. N. G., Raizen, D. M., & Van Buskirk, C. (2014). Cellular stress induces a protective sleep-like state in *C. elegans*. *Current Biology*. <https://doi.org/10.1016/j.cub.2014.08.040>
- Husson, S. J., Gottschalk, A., & Leifer, A. M. (2013). Optogenetic manipulation of neural activity in *C. elegans*: From synapse to circuits and behaviour. *Biology of the Cell*. <https://doi.org/10.1111/boc.201200069>
- Kaplan, J. M., & Horvitz, H. R. (1993). A dual mechanosensory and chemosensory neuron in *Caenorhabditis elegans*. *Proceedings of the National Academy of Sciences of the United States of America*. <https://doi.org/10.1073/pnas.90.6.2227>
- Lai, C. H., Chou, C. Y., Ch'ang, L. Y., Liu, C. S., & Lin, W. C. (2000). Identification of novel human genes evolutionarily conserved in *Caenorhabditis elegans* by comparative proteomics. *Genome Research*. <https://doi.org/10.1101/gr.10.5.703>
- Lin, J. Y., Knutsen, P. M., Muller, A., Kleinfeld, D., & Tsien, R. Y. (2013). ReaChR: A red-shifted variant of channelrhodopsin enables deep transcranial optogenetic excitation. *Nature Neuroscience*. <https://doi.org/10.1038/nn.3502>
- Maluck, E., Busack, I., Besseling, J., Masurat, F., Turek, M., Busch, K. E., & Bringmann, H. (2020). A wake-active locomotion circuit depolarizes a sleep-active neuron to switch on sleep. *PLOS Biology*, *18*(2), e3000361. Retrieved from <https://doi.org/10.1371/journal.pbio.3000361>
- Nagel, G., Ollig, D., Fuhrmann, M., Kateriya, S., Musti, A. M., Bamberg, E., & Hegemann, P. (2002). Channelrhodopsin-1: A light-gated proton channel in green algae. *Science*. <https://doi.org/10.1126/science.1072068>
- Nagel, G., Szellas, T., Huhn, W., Kateriya, S., Adeishvili, N., Berthold, P., ... Bamberg, E. (2003). Channelrhodopsin-2, a directly light-gated cation-selective membrane channel. *Proceedings of the National Academy of Sciences of the United States of America*. <https://doi.org/10.1073/pnas.1936192100>
- Okazaki, A., Sudo, Y., & Takagi, S. (2012). Optical silencing of *c. elegans* cells with arch proton pump. *PLoS ONE*. <https://doi.org/10.1371/journal.pone.0035370>
- Schmitt, C., Schultheis, C., Husson, S. J., Liewald, J. F., & Gottschalk, A. (2012). Specific Expression of Channelrhodopsin-2 in Single Neurons of *Caenorhabditis elegans*. *PLoS ONE*. <https://doi.org/10.1371/journal.pone.0043164>
- Schultheis, C., Liewald, J. F., Bamberg, E., Nagel, G., & Gottschalk, A. (2011). Optogenetic long-term manipulation of behavior and animal development. *PLoS ONE*. <https://doi.org/10.1371/journal.pone.0018766>

- Schwarz, J., & Bringmann, H. (2013). Reduced Sleep-Like Quiescence in Both Hyperactive and Hypoactive Mutants of the Galphaq Gene *egl-30* during lethargus in *Caenorhabditis elegans*. *PLoS ONE*. <https://doi.org/10.1371/journal.pone.0075853>
- Singh, K., Ju, J. Y., Walsh, M. B., DiIorio, M. A., & Hart, A. C. (2014). Deep Conservation of Genes Required for Both *Drosophila melanogaster* and *Caenorhabditis elegans* Sleep Includes a Role for Dopaminergic Signaling. *Sleep*. <https://doi.org/10.5665/sleep.3990>
- Spies, J., & Bringmann, H. (2018). Automated detection and manipulation of sleep in *C. Elegans* reveals depolarization of a sleep-active neuron during mechanical stimulation-induced sleep deprivation. *Scientific Reports*. <https://doi.org/10.1038/s41598-018-28095-5>
- Stiernagle, T. (2006). Maintenance of *C. elegans*. *WormBook: The Online Review of C. Elegans Biology*. <https://doi.org/10.1895/wormbook.1.101.1>
- Takahashi, M., & Takagi, S. (2017). Optical silencing of body wall muscles induces pumping inhibition in *Caenorhabditis elegans*. *PLoS Genetics*. <https://doi.org/10.1371/journal.pgen.1007134>
- Turek, M., Besseling, J., & Bringmann, H. (2015). Agarose Microchambers for Long-term Calcium Imaging of *Caenorhabditis elegans*. *J Vis Exp*, (100), e52742. <https://doi.org/10.3791/52742>
- Turek, Michal, Lewandrowski, I., & Bringmann, H. (2013). An AP2 transcription factor is required for a sleep-active neuron to induce sleep-like quiescence in *C. elegans*. *Current Biology*, 23(22), 2215–2223. <https://doi.org/10.1016/j.cub.2013.09.028>
- Van Buskirk, C., & Sternberg, P. W. (2007). Epidermal growth factor signaling induces behavioral quiescence in *Caenorhabditis elegans*. *Nature Neuroscience*. <https://doi.org/10.1038/nn1981>
- Ward, A., Liu, J., Feng, Z., & Xu, X. Z. S. (2008). Light-sensitive neurons and channels mediate phototaxis in *C. elegans*. *Nature Neuroscience*, 11(8), 916–922. <https://doi.org/10.1038/nn.2155>
- Wu, Y., Masurat, F., Preis, J., & Bringmann, H. (2018). Sleep Counteracts Aging Phenotypes to Survive Starvation-Induced Developmental Arrest in *C. elegans*. *Current Biology*. <https://doi.org/10.1016/j.cub.2018.10.009>
- Xu, S., & Chisholm, A. D. (2016). Highly efficient optogenetic cell ablation in *C. Elegans* using membrane-targeted miniSOG. *Scientific Reports*. <https://doi.org/10.1038/srep21271>
- Zheng, Y., Brockie, P. J., Mellem, J. E., Madsen, D. M., & Maricq, A. V. (1999). Neuronal control of locomotion in *C. elegans* is modified by a dominant mutation in the GLR-1 ionotropic glutamate receptor. *Neuron*. [https://doi.org/10.1016/S0896-6273\(00\)80849-1](https://doi.org/10.1016/S0896-6273(00)80849-1)

Supplementary Information for

The OptoGenBox - a device for long-term optogenetics in *C. elegans*

Inka Busack, Florian Jordan, Peleg Sapir, Henrik Bringmann*

The set-up of the OptoGenBox

Thermal control of cells

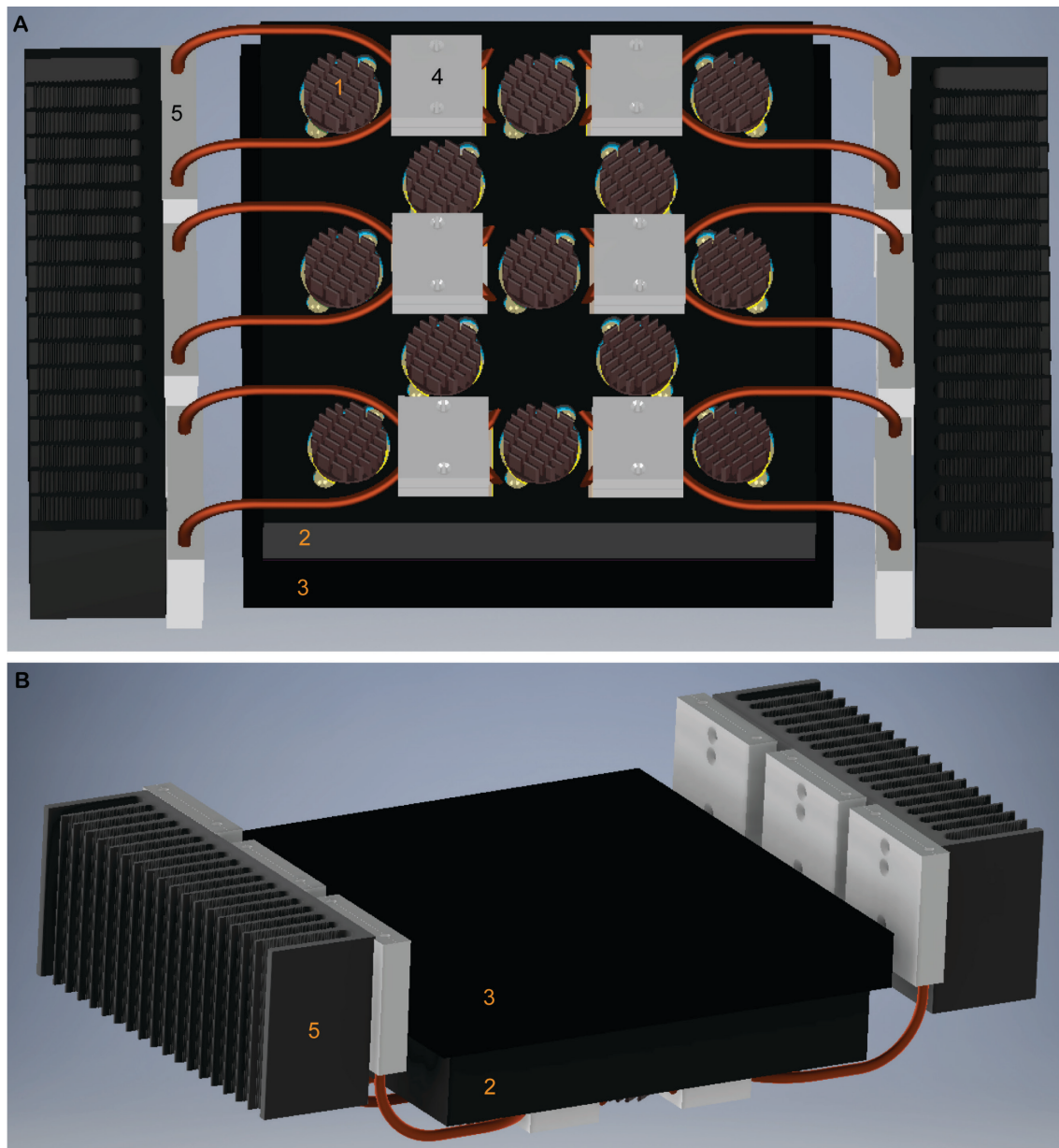


Figure S1. The incubator.

Bottom (A) and top side (B) view of the incubator. The (1) 13 LED modules are spread throughout (2) an incubator chamber and covered by (3) a lid. Six Peltier devices are covered with (4) heat spreaders. On the site are (5) heat sinks.

Software of the OptoGenBox

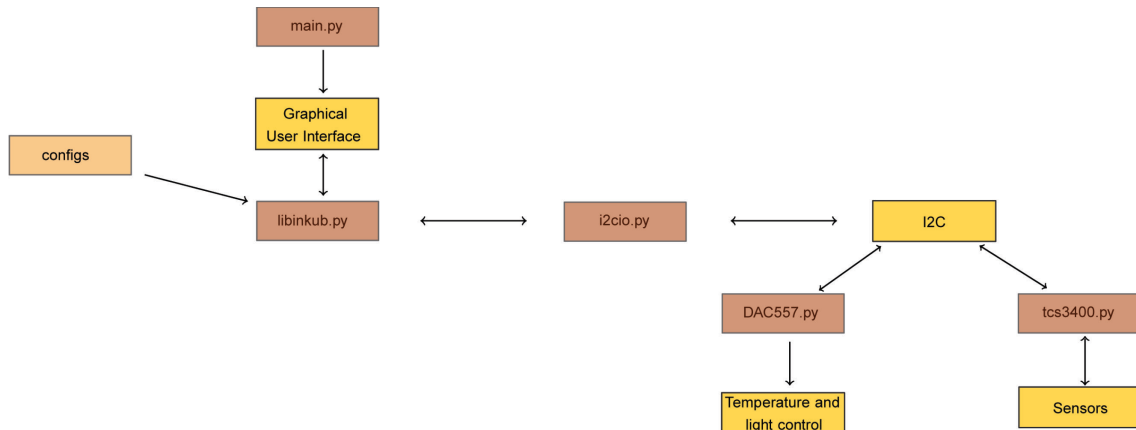


Figure S2. Scheme for the code of the OptoGenBox.

The software was written in python. The python library `i2cio` reads and writes commands via the device I²C bus. The python library `tcs3400` controls the lightsensor TCS3400. The digital-to-analogue converter DAC5571 is needed for the temperature control and controlled by the `DAC5571` python library. The main library starts the graphical user interface. The `libinkub` library manages the abstraction of cells and group of cells, light cycles and sensor readings. The `configs` file hosts all configurations for the OptoGenBox such as the users, the temperature and light intensity steps and how thoroughly the sensors get calibrated (how many calibration points get initiated). The code is published on github (<https://gitlab.gwdg.de/psapir/inkubator>).

Graphical User Interface

The OptoGenBox program starts by running the main script in the inkub directory in the terminal with the command lines:

```
cd inkub
```

```
./main.py
```

The program initiates by calibrating the environmental sensors. This might take a few minutes.

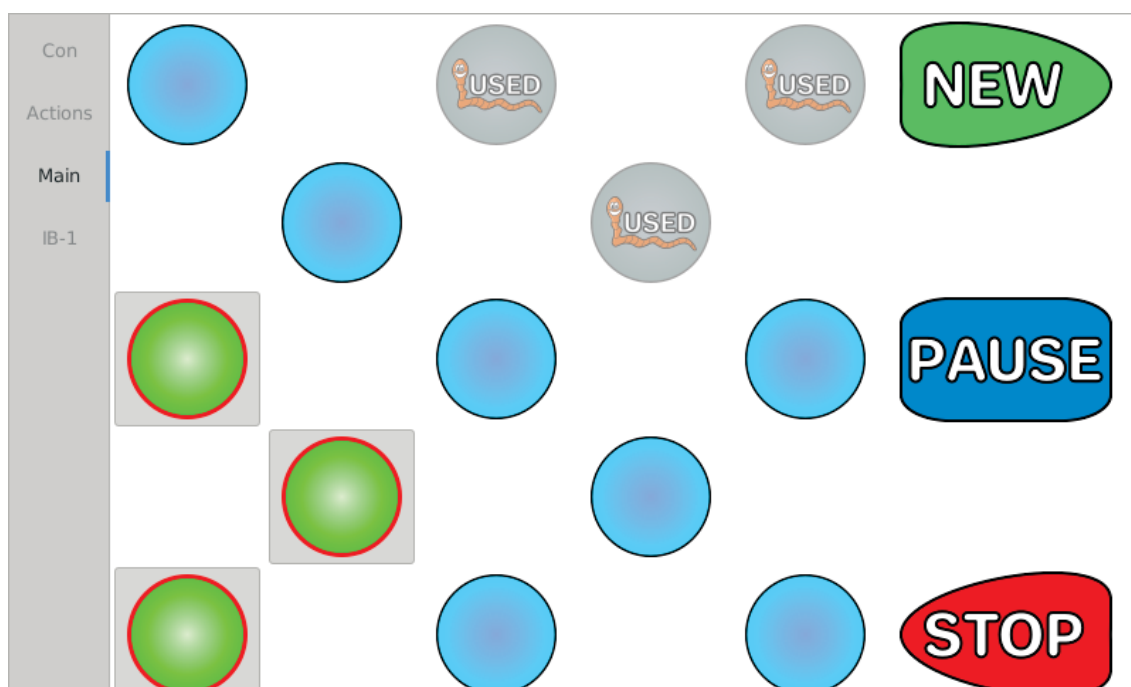
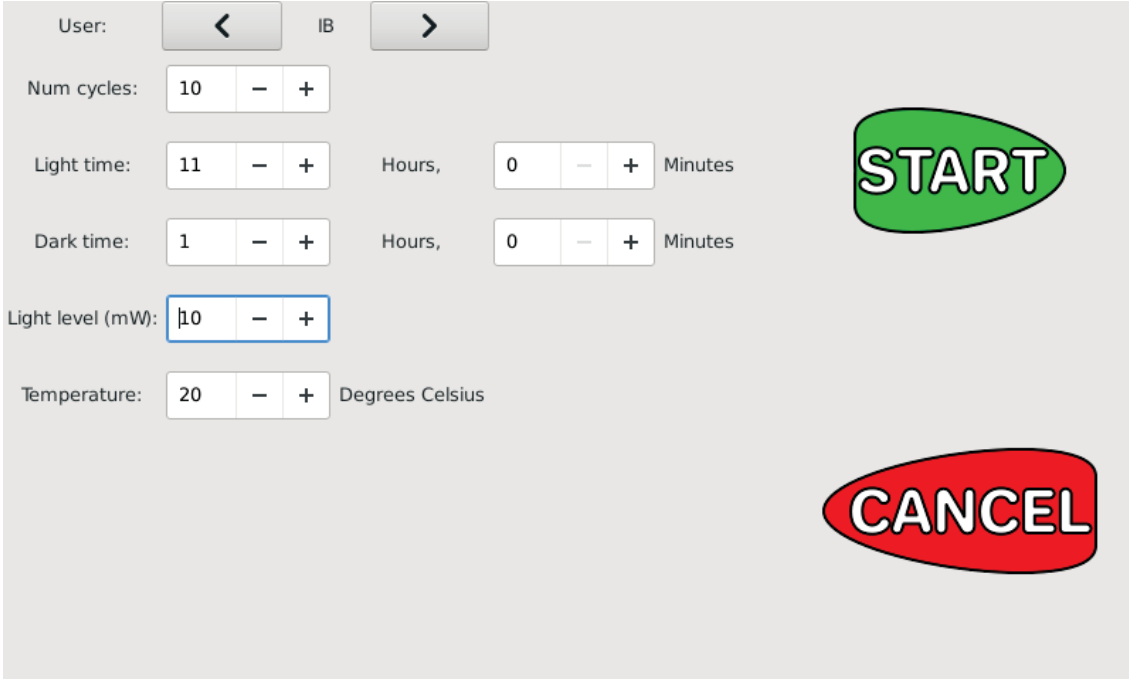


Figure S3. Main menu.

The graphical user interface allows for an intuitive usage of the OptoGenBox. The researcher first selects the cells for one experiment via the touch screen in the main menu and presses *NEW*. Once an optogenetic protocol (light and dark cycles) is defined for selected cells, these cells are displayed as used in the main menu.



The screenshot shows a configuration interface for an optogenetic protocol. It features several control elements:

- User:** A selection menu with left and right arrow buttons and the text "IB".
- Num cycles:** A numeric input field set to "10" with minus and plus buttons.
- Light time:** A numeric input field set to "11" with minus and plus buttons, followed by "Hours," and another numeric input field set to "0" with minus and plus buttons, followed by "Minutes".
- Dark time:** A numeric input field set to "1" with minus and plus buttons, followed by "Hours," and another numeric input field set to "0" with minus and plus buttons, followed by "Minutes".
- Light level (mW):** A numeric input field set to "10" with minus and plus buttons.
- Temperature:** A numeric input field set to "20" with minus and plus buttons, followed by "Degrees Celsius".

On the right side of the interface, there are two large, stylized buttons: a green "START" button and a red "CANCEL" button.

Figure S4. Optogenetic Protocol.

A new window opens and the researcher can select the user and the number of cycles. Furthermore, the researcher can define the time of light and darkness and the level of light. The temperature of the entire incubator can be chosen whenever no other experiments are running. Once all parameters are defined, the protocol gets started by pressing *START* on the touch screen.

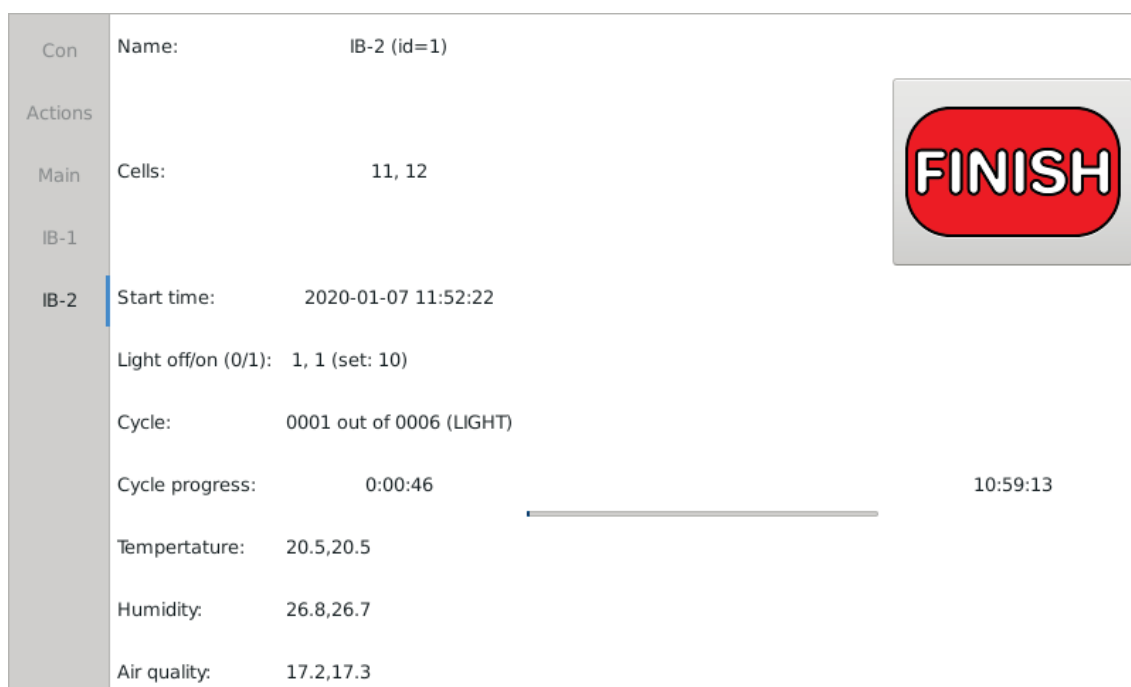


Figure S5. Status of the running protocol.

Running protocols are listed in the left panel below *Main*. To check for the current status of the protocol, one can select it via the touch screen. Information about the name of the experiment, the selected cells and the start time is portrayed. Furthermore, one can see if the light is on or off for each cell and what intensity is set. The next line gives the number of the current cycle. Below that one can see the exact timing in the current cycle. The measured temperature, humidity and air quality is additionally given for each cell. To prematurely quit the experiment one can click the *FINISH* button.



Figure S6. Finishing a running experiment.

Clicking the *FINISH* button on the running protocol screen does not automatically end the experiment. The user has to confirm again that the protocol should be stopped.



Figure S7. Phobya WaCoolT Cube 2 Watercase was modified to serve as external case for the OptoGenBox. This figure was reproduced with permission from Performance PCs.

description	manufacturer	manufacturer number	#	price, total \$
<i>mechanical parts</i>				
case	Phobya	WaCool IT 2	1	\$146
heat pipes	QuickCool Fischer	QY-SHP-D6-250SA	12	\$127
heat sink	elektronics	SK580 200 SA	2	\$78
dust filter	InLine	33378A	3	\$7
LED-mounting Ring	MPI-bpc ES	inhouse design	13	\$130
mounting material		miscellaneous		\$336
material: percision mechanics & optics		inhouse design		\$538
<i>computer elements and accessories</i>				
		Raspberry Pi	2	
raspberry pi	Raspberry Pi	Model B	1	\$22
touchscreen	Raspberry Pi	7", 800x400Pixel	1	\$78
usb connectors		miscellaneous	2	\$34
		Harting:		
RJ-45 connector	Harting	09454521561	1	\$17
fan 80mm	Be quiet	BQT BL044	5	\$34
fan 120mm	Be quiet	BQT BL046	4	\$32
<i>power sources</i>				
Power Adapter AC/DC 330W	Mean Well	HRPG-300-15	2	\$203
Power Adapter AC/DC 200W	Mean Well	SP-240-24	1	\$63
Power Adapter DC/DC	Traco Power	TEL3-2022	1	\$29
Power Apdater DC/DC	Traco Power	TSR3-24150	1	\$38
Power Adapter DC/DC	TDK Lambda	I6A-240-14A-033V/001	2	\$105
PCB (supply) & small parts	MPI-bpc ES	inhouse design	1	\$61
<i>LED module</i>				
PCB	MPI-bpc ES	inhouse design	13	\$131
LED: LCY-CLBP	Osram opto Semiconductors	LCY-CLBP KXKZ-5F5G	78	\$131
connectors	ERNI	Erni MiniBridge,2-pin	13	\$22
heatsink	Fischer elektronics	ICK_LED R33x16,5G	13	\$121
<i>LED-Control-Unit</i>				
PCB	MPI-bpc ES NXP	inhouse design	2	\$157
Controller IC [I ² C]	Semiconductors	PCA9685	4	\$9
constant current	ON	CAT4101	14	\$39

source	Semiconductors			
other	electronical			
parts		miscellaneous	158	\$49
<i>Heating & cooling</i>				
Peltier devices 100W	True Components	HP-127120-40x40	6	\$134
	Texas			
Power Amplifiers	Instruments	OPA541AP	3	\$61
PCB	MPI-bpc ES	inhouse design	1	\$67
temperature sensor	RS Pro	PT100, 8x2mm	1	\$11
other	electronical			
parts		miscellaneous	38	\$56
<i>Main control-unit</i>				
PCB control	MPI-bpc ES	inhouse design	1	\$78
other	electronical			
parts		miscellaneous	85	\$45
<i>Lid-&Sensor Unit</i>				
PCB	MPI-bpc ES	inhouse design	1	\$146
Light-Sensors	AMS	TCS3400	13	\$36
Environment Sensors	Bosch Sensortec	BME680	13	\$110
	NXP			
Multiplexer [I ² C]	Semiconductors	PCA9548A	2	\$3
other	electronical			
parts		miscellaneous	40	\$11
				\$3,496

Table S1. Material list for the OptoGenBox.

Abbreviations

ATR - all-trans retinal

DAC - digital-to-analogue converter

I²C – inter-integrated circuit

IMS – insulated metal substrate

LED – light-emitting diode

NGM- nematode growths medium

PCB – printed circuit board

PWM – pulse width modulation

4.3. Aim 3 - Functions of sleep in *Caenorhabditis elegans*

While many functions of sleep are already known, for example energy conservation (9), sleep counteracting aging (106) and benefiting memory and cognition (19, 21), the underlying main function has yet to be discovered. Additionally, it is not obvious if certain sleep benefits such as improved cognition upon sleeping are evolutionary conserved across all sleeping species or just found in higher organisms with more complex brains such as mammals (8). The non-sleeping *aptf-1(gk794)* mutant presents a very potent tool to investigate sleep benefit phenotypes in *C. elegans*. Here, I conducted different experiments in which I compared wild-type worms to *aptf-1(gk794)* mutants or other non-sleeping mutants in order to investigate sleep functions, which is the third aim of this thesis.

4.3.1. No found evidence for synaptic homeostasis to be a function of sleep in *C. elegans*

The synaptic homeostasis hypothesis declares sleep to be the cost for memory consolidation (148, 149). Sleep in mice is associated with synaptic downscaling and learning with synaptic potentiation (150). Sleep-deprived mice have stronger synapses and impaired cognition (20).

Sleep was found to play a life-prolonging role in L1 arrested animals. In this state, sleep counteracts aging and is therefore essential (106, 151). However, when this project was started, synaptic homeostasis, another function of sleep, had not been investigated before in *C. elegans*. I was hence interested if I could validate the synaptic homeostasis hypothesis in *C. elegans* in this L1 arrested larval state. For this, I designed two experiments that were conducted under my supervision by Chantal Schmidt and Moataz Nouredine, two former students of mine. Pre- as well as postsynaptic markers were imaged throughout L1 arrest and a comparison of non-sleeping *aptf-1(gk794)* mutants and wild-type worms was made.

As a presynaptic marker I selected a fused GFP to RAB-3. RAB-3 is an ortholog of human RAB3A and localizes to the presynaptic active zone (130). In the experiment, *GFP::RAB-3* was expressed with the *mec-7* promoter so that it localized to presynaptic

zones of mechanosensory neurons. Throughout 18 days of L1 arrest, the presynaptic sites in the nerve ring were measured and compared. A comparison of GFP intensities, number of synapses and area of synapses was made to see if presynaptic zones change. During the first 11 days, there was no visible difference between wild type and mutant worms (Figure 14). At day 14 and 18 there was a significant difference only for the intensity of the presynaptic marker. Interestingly, the presynaptic marker intensity was less in *aptf-1(gk794)* mutants than that of wild-type worms (60.7% of wild-type levels on day 14, 38.9% on day 18) (Figure 14A and D).

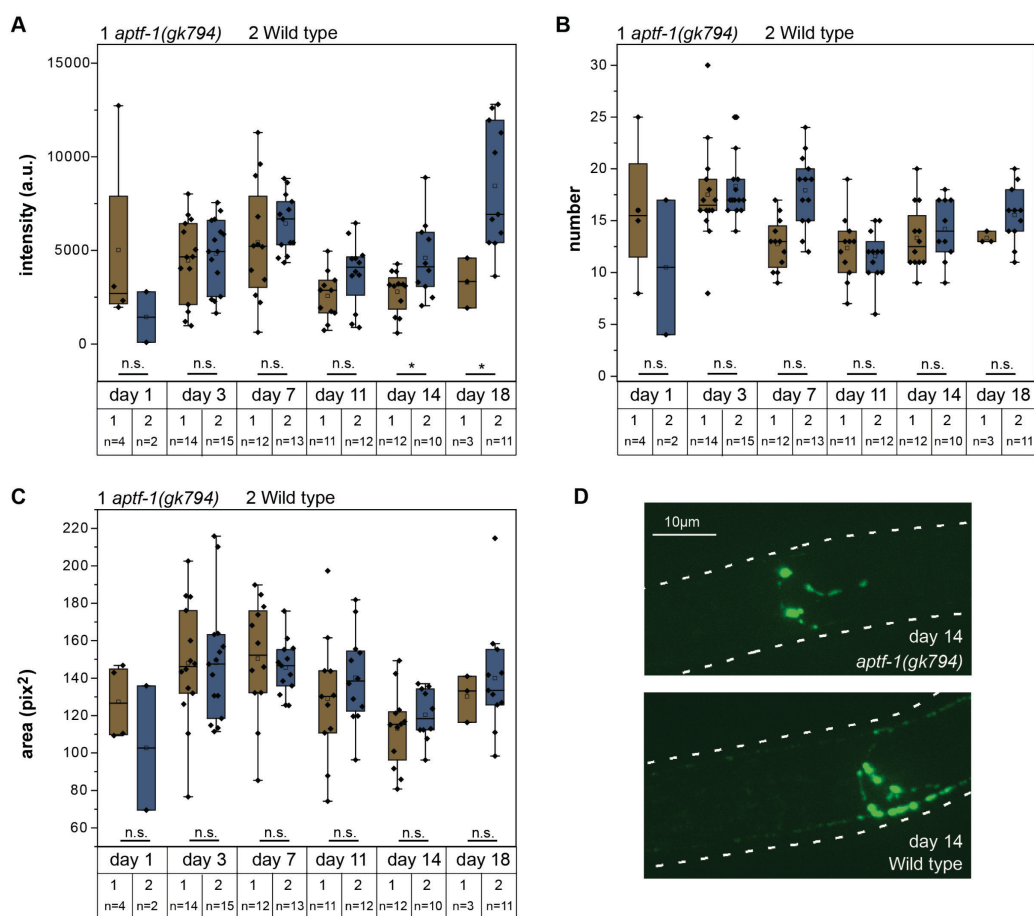


Figure 14. A comparison of presynaptic active zones reveals only a small influence of sleep on synaptic homeostasis.

(A) A comparison of presynaptic marker intensities between *aptf-1(gk794)* mutants and wild-type worms throughout their life in L1 arrest. A small difference can only be observed for day 14 and 18. * $p < 0.05$, Welch test. (B) The number of detected presynaptic zones in the nerve ring did not vary between genotypes and over time. n.s. $p > 0.05$, Welch test. (C) The area of detected presynaptic zones in the nerve ring showed no significant difference between wild-type worms and *aptf-1(gk794)* mutants. n.s. $p > 0.05$, Welch test. (D) Sample maximum intensity z-projections for an *aptf-1(gk794)*

mutant and a wild-type worm on day 14. Data acquired and analyzed under my supervision by my former student Chantal Schmidt.

Since the results for the presynaptic marker were not supportive of the synaptic homeostasis hypothesis, I wondered if the hypothesis really does not hold in *C. elegans* or if I just implemented the wrong assay. I therefore decided to investigate a post-synaptic marker. GLR-1 is a glutamate AMPA type receptor subunit and localizes to the glutamate receptor complex. It is furthermore known to be important for long-term memory formation (152). For the experimental assay, worms were hence chosen that expressed *glr-1::GFP* from the *glr-1* promoter. My former student Moataz Nouredine imaged worms, expressing this marker, over time in the arrested first larval stage. He then compared the mean intensity per area of the five brightest post-synaptic sites of wild-type worms to non-sleeping mutants. Two days, day 8 and day 11, showed a significant difference between wild-type worms and *aptf-1(gk794)* mutants (Figure 15). Surprisingly, the direction of the phenotype was the opposite on these days. While on day 8, *aptf-1(gk794)* worms had brighter post-synaptic sites, the wild type's synapses were brighter on day 11 (Figure 15). It seems that both genotypes have a peak of post-synaptic strength, which comes 3 days earlier in the *aptf-1(gk794)* mutant. While this is a very interesting result and may present another aging phenotype, it does not confirm the synaptic homeostasis hypothesis in *C. elegans*.

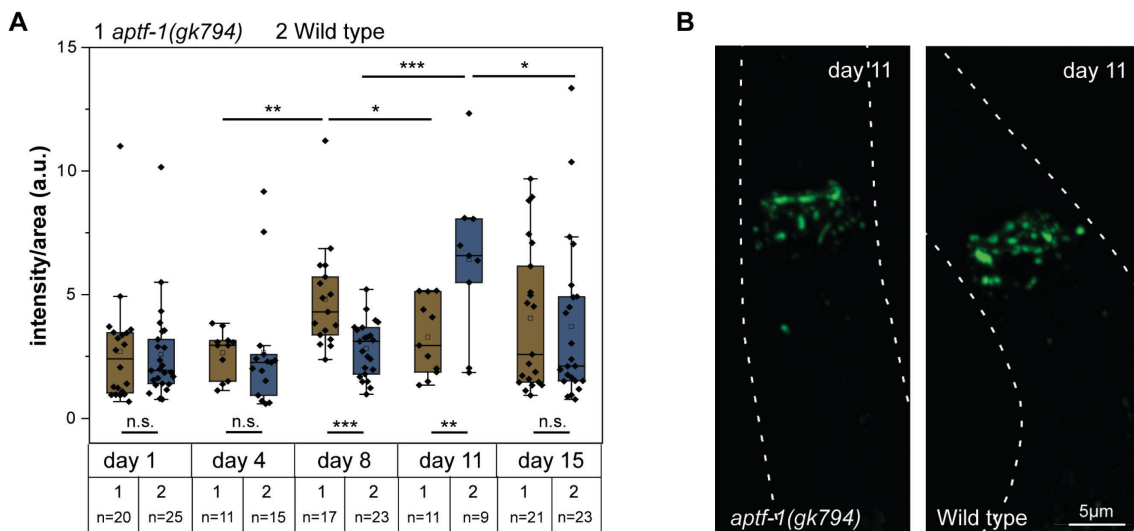


Figure 15. A post-synaptic marker shows a differently timed peaking post-synaptic strength between *aptf-1(gk794)* and wild-type worms.

(A) Quantification of the brightness over the area of a post-synaptic marker expressed from the *glr-1* promoter in *aptf-1(gk794)* and wild-type worms. Both genotypes show a peak. The peak of *aptf-1(gk794)* mutants is 3 days earlier than that of the wild type. * $p < 0.05$, ** $p < 0.01$, *** $p < 0.001$, Welch test. (B) Sample maximum intensity z-projections for an *aptf-1(gk794)* mutant and a wild-type worm on day 11. Data acquired and analyzed under my supervision by my former student Moataz Nouredine.

4.3.2. Early adult stage worms can form a memory during a habituation assay for at least 15min, which is independent of sleep

Sleep is the price for memory according to the synaptic homeostasis hypothesis (148). I could find a difference in synaptic strengths over time between non-sleeping *aptf-1(gk794)* mutants and wild-type worms, which however does not support the synaptic homeostasis hypothesis in *C. elegans*. Regardless, I now wanted to investigate the behavioral component of the theory. I chose a habituation assay as experimental paradigm. How does sleep affect habituation and dishabituation in *C. elegans*? For this I designed an experiment in which adult *C. elegans* of different ages get tapped in one trial every 5s for 20 times in a row. During this trial they are expected to habituate to the tap, which means that they should respond less with backwards locomotion during the later taps. After the initial trial, a second trial was conducted with a 2min pause in between both trials. A third trial with the same worm was conducted after a 15min recovery time. Upon successful memory formation, worms are expected to respond less to the later two trials compared to the first. If memory is not successfully formed, worms dishabituate, which means that they respond similarly as to the first trial. My former student Jasmina Bier conducted the experiment under my supervision.

The results from the initial trial give more insights into a potential difference in habituation between *aptf-1(gk794)* and wild-type worms, whereas the second and third trials in comparison to the first give more information on the necessity of sleep for memory formation in this habituation assay. Early as well as late stage adult non-sleeping *aptf-1(gk794)* worms habituated similarly to wild-type worms of comparable age (Figure 16). Generally, late adult stage worms responded less to taps, which is consistent with previous studies (153). There was no observable difference for late adult stage *aptf-1(gk794)* and wild-type worms in regard to dishabituation and therefore memory formation. Late adult stage worms could only form a lasting memory for 2 minutes but not for 15 minutes. In early stage adult *C. elegans*, non-sleeping mutants responded significantly less to taps after a 15min recovery period compared to the initial

trial. Hence, they seemed to be able to generate a memory that lasts for at least 15min. Wild-type worms could also keep that memory for 15min. Sleep did not seem to have an impact on memory formation in this here chosen habituation assay as wild-type as well as non-sleeping *ap1f-1(gk794)* mutants could form a similar memory. Previous studies have shown that sleep is important for memory formation in mammals (154). With this experiments I could not show this to be true for *C. elegans*. However, there are different types of memory involving different neurons in *C. elegans* and sleep might be needed for others such as olfactory learning.

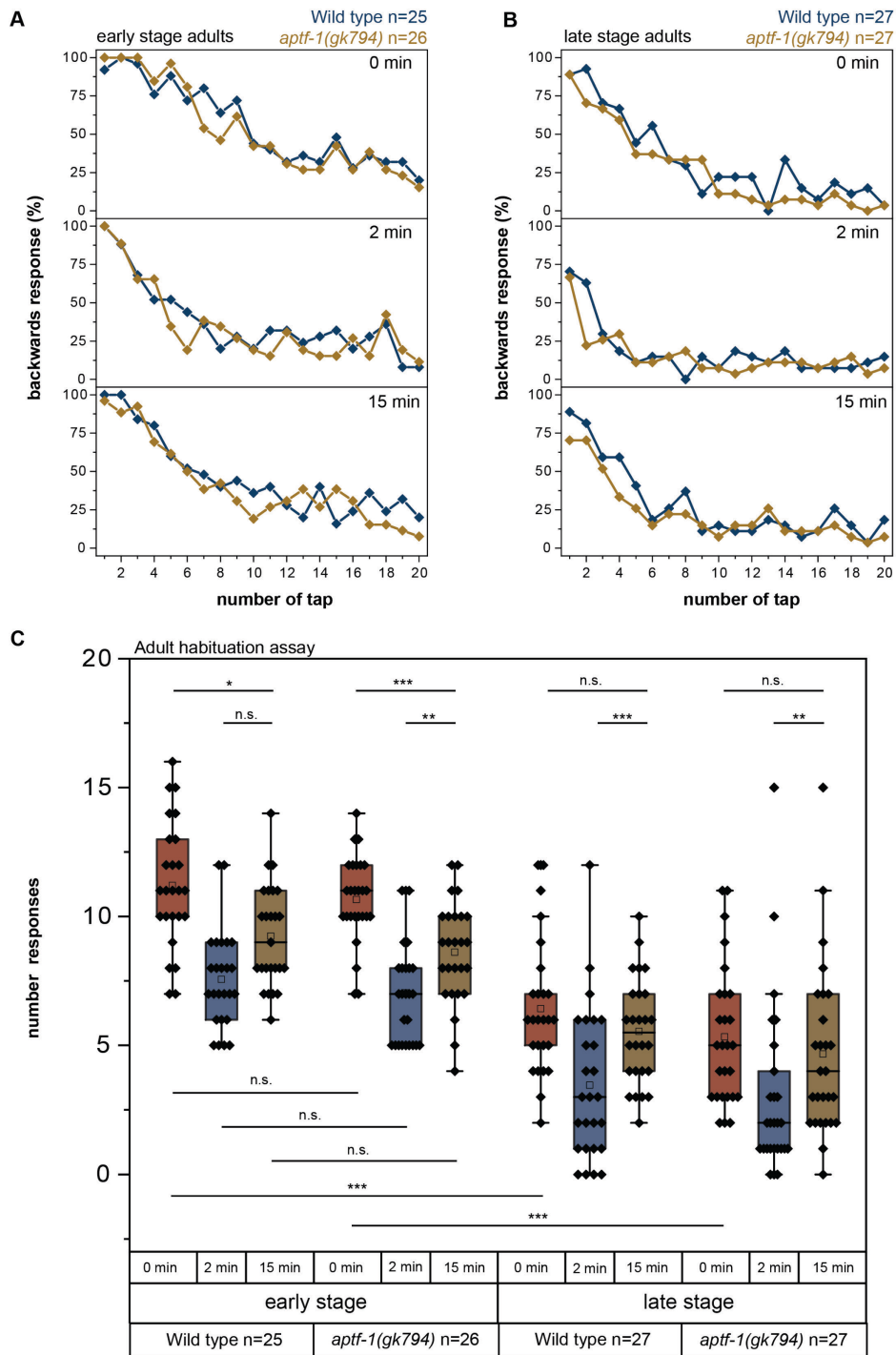


Figure 16. Sleeplessness does not affect habituation and memory in adult *C. elegans*.

(A) Average responses to taps of early stage adult wild-type and *aptf-1(gk794)* worms. The top graph shows the average for the initial trial of 20 taps, the second shows the results for the second trial, which was conducted after a 2min pause and the third trial was conducted after a 15min pause. The taps within one trial were given every 5s. (B) Similar graph as in A but this time the averages for late adult stage worms are plotted. (C) Responses within each trial plotted against each other for early and late adult stage worms as well as different genotypes. * $p < 0.05$, ** $p < 0.01$, *** $p < 0.001$, Wilcoxon

signed rank test to compare between different trials for the same animals and Kolmogorov-Smirnov test to compare early and late adult stage worms and different genotypes. Data acquired and analyzed under my supervision by my former student Jasmina Bier.

4.3.3 Feeding behavior and recovery from coldness as read outs for health span are not affected by sleeplessness

It is known that survival of arrested first larval stage *C. elegans* is dependent on sleep. This is not the case for fed adult worms (106). Survival assays are extremely potent. However, some negative effects of sleeplessness might be less severe and not ultimately lead to premature death of the worm. I hence decided to test for health span in non-sleeping *aptf-1(gk794)* mutants. Many different experiments belong to a rigorous health span analysis such as testing for egg-laying phenotypes, feeding phenotypes or recovery from stresses (155, 156). To get a first overview, one pilot experiment was done in each category.

An impact of sleep on egg-laying behavior has not been observed yet for fed adult *C. elegans* (personal communication with Anastasios Koutsoumparis). An established and easily conductible assay to test for a response to stress is the recovery from coldness. L4 worms were placed in a 4°C refrigerator for 6h. *C. elegans* paralyze upon exposure to such temperatures (157). After retransferring the worms to 20°C, I measured how long it took them to recover from this paralysis. The recovery took similar amounts of time for wild-type worms and non-sleeping mutants (Figure 17A). Therefore, sleep does not seem to be necessary for cold stress recovery. As a next health span assay, I imaged L1 arrested worms in microfluidic chambers for 1min and counted the number of pharyngeal pumps. I compared wild-type worms to *aptf-1(gk794)* mutants and worms with an ablated RIS. The ablation was reached by expressing the apoptosis inducer EGL-1 from the *flp-11* promoter. Sleep did not seem to have an impact on feeding behavior (Figure 17B).

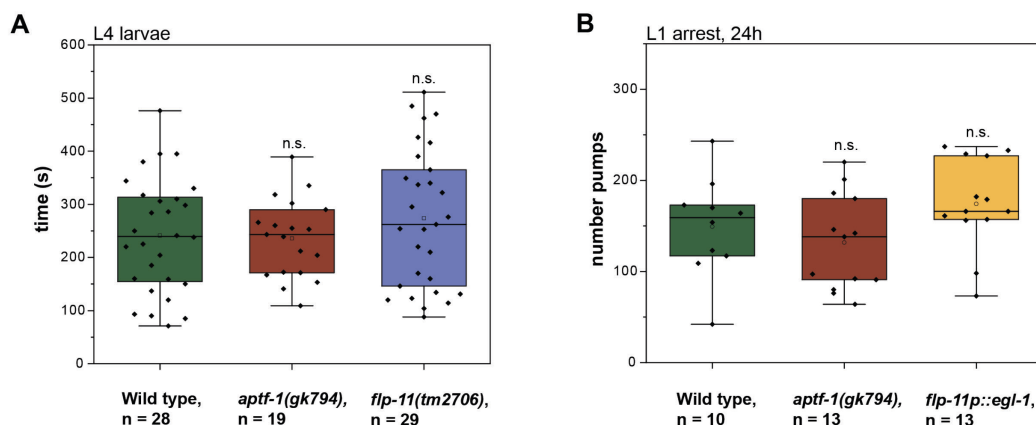


Figure 17. Sleep is not required for recovery from coldness or feeding behavior.

(A) The non-sleeping *aptf-1(gk794)* and *flp-11(tm2706)* mutants need the same amount of time as the wild type to recover upon cold stress. n.s $p > 0.05$, Welch test. (B) There is no significant difference of pumps per minute in L1 arrested larvae after 24h of arrest between wild-type and non-sleeping *C. elegans*. n.s $p > 0.05$, Welch test.

4.3.4. Genetic manipulations of RIS

4.3.4.1. Expression of ion channels in RIS and their consequences on the neuronal potential

Detailed molecular pathways for how sleep active neurons regulate not only the behavior of organisms but furthermore benefits of sleep have yet to be discovered. The existence of sleep-active and sleep-inducing neurons opens up the possibility to actively manipulate behavior and test for consequences of a certain behavior. The single ring interneuron RIS is the major sleep neuron in *C. elegans* and its activation leads to sleep induction (8, 113, 114). Manipulation of RIS's membrane potential can hence be utilized to actively determine behavior as well as to investigate molecular pathways downstream of RIS. New strains were generated via CRISPR genome editing in which ion channels are expressed in RIS. The sequences of the ion channels were inserted into the endogenous locus of the *flp-11* promoter (see Appendix). For an aspired constant depolarization, an UNC-58 gain of function variant (*unc-58(e665)*) was expressed in RIS (Figure 18A). The utilized UNC-58gf is an inward sodium channel that should lead to a constant activation of the expressing neuron (personal communication with Thomas Boulin). The expression in RIS with the *flp-11* promoter is APTF-1 dependent, as worms without functional APTF-1 do not express the channel in RIS (Figure 18B). For

a desired hyperpolarization of RIS, different approaches were tested. TWK-18 and EGL-23 are both outward potassium channels (158) that were expressed in RIS (17C-D). For RIS hyperpolarization by expression of TWK-18, the variant *twk-18(e1913)* was genetically knocked-in. To receive strains in which the inhibition of RIS is of different magnitude, EGL-23 variants of different strengths were knocked-in. For a weaker RIS inhibition *egl-23(L229)* was genetically knocked-in and for a stronger RIS inhibition *egl-23(A383)* was utilized (159). In order to eventually receive an even stronger RIS inhibition, in a third strain the stronger variant was codon optimized (160). If the inhibition levels of RIS differed in these EGL-23 expressing strains as anticipated, the tools would be very valuable for the analysis of a dose response of sleep inhibition.

The expression of these tools was verified via imaging of a tagged mKate. RIS was the neuron most strongly expressing each tool in the different strains (Figure 18A-D). However, a few other neurons, most likely GABAergic motor neurons, showed a weak mKate signal (Figure 18E). This fact should be taken into consideration as it explains for example the uncoordinated phenotype of *RIS:unc-58gf* worms, which is independent of RIS as it is still present in worms in the *aptf-1(gk794)* background. Experiments with *RIS:unc-58gf* worms hence also include worms expressing *RIS:unc-58gf* in the *aptf-1(gk794)* background as a control.

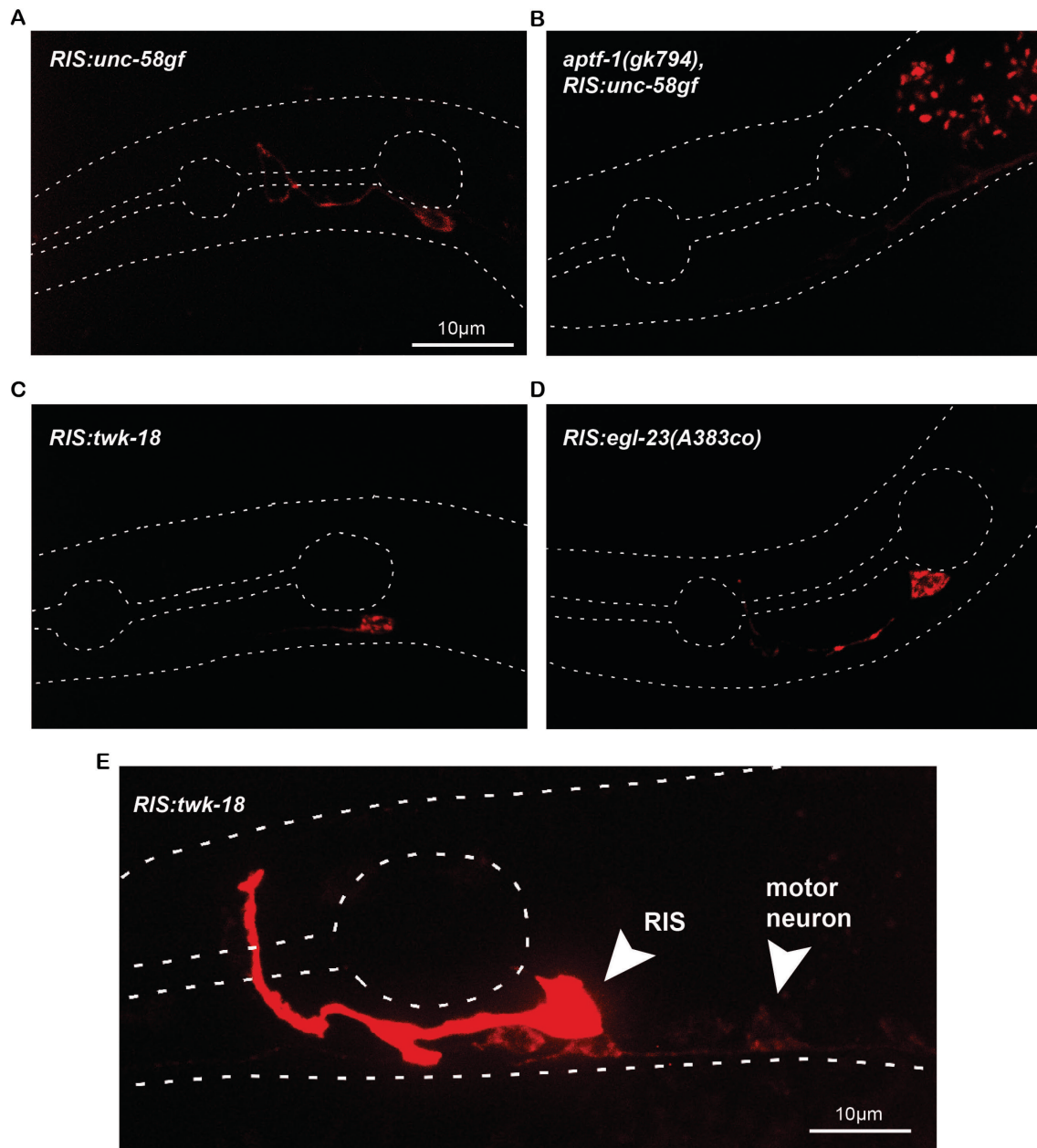


Figure 18. Maximum intensity z-projection of mKate expression of different genetic tools in RIS.

(A) The UNC-58gf channel that leads to neuronal depolarization expresses in RIS in the wild-type L1 larvae. (B) The expression is almost absent in an *aptf-1(gk794)* background in the L1 larvae. (C-D) Hyperpolarization channels express in RIS in the L1 larvae. (E) While the TWK-18 channel expresses most strongly in RIS in the adult worm, it is furthermore weakly expressed in other neurons such as motor neurons.

To verify that these tools actually cause the anticipated changes of RIS's potential, GCaMP expressed in RIS with the *flp-11* promoter was imaged for three hours in the arrested first larval stage (L1a). To account for a potential autoregulation of FLP-11, the measured GCaMP intensities were normalized over additionally imaged *flp-11p::mKate* intensities. As previously reported (106), wild-type worms had very prominent RIS activity peaks during sleep bouts whereas there was little RIS activity during motion bouts (Figure 19A). Worms that expressed the UNC-58gf channel in RIS showed little RIS transients throughout the imaging period but an overall increase of 191% of RIS activity compared to wild type (Figure 19B,D). Hence, these worms have a constantly depolarized sleep neuron as was anticipated. Interestingly, the constantly RIS activated worms behave a bit uncoordinated on the plate and a quantification of speed confirms that they are overall slower than wild type (Figure 19E). This uncoordinated phenotype is still present in an *aptf-1(gk794)* background, in which RIS is non-functional. It must therefore come from other neurons such as motor neurons, which weakly express the UNC-58gf channel.

Expression of TWK-18 in RIS was supposed to lead to RIS hyperpolarization. Indeed, these worms do not have any RIS peaks but instead an overall small activity in RIS comparable to motion bouts in wild type (Figure 19C,D). The overall speed of these worms is similar to wild-type speed (Figure 19E).

Next, worms with the codon optimized EGL-23 expressed in RIS were calcium imaged. GCaMP as well as mKate were expressed very faintly in these worms (Figure 20A-C). For this reason, imaging and analysis had to be changed a bit in comparison to the previous calcium imaging experiments (for details see methods). Regardless, the worms show less RIS transients compared to wild-type worms (Figure 20D) and an overall reduced RIS activity (Figure 20E). The mean speed does not differ between the RIS hyperpolarized worms and wild type (Figure 20F).

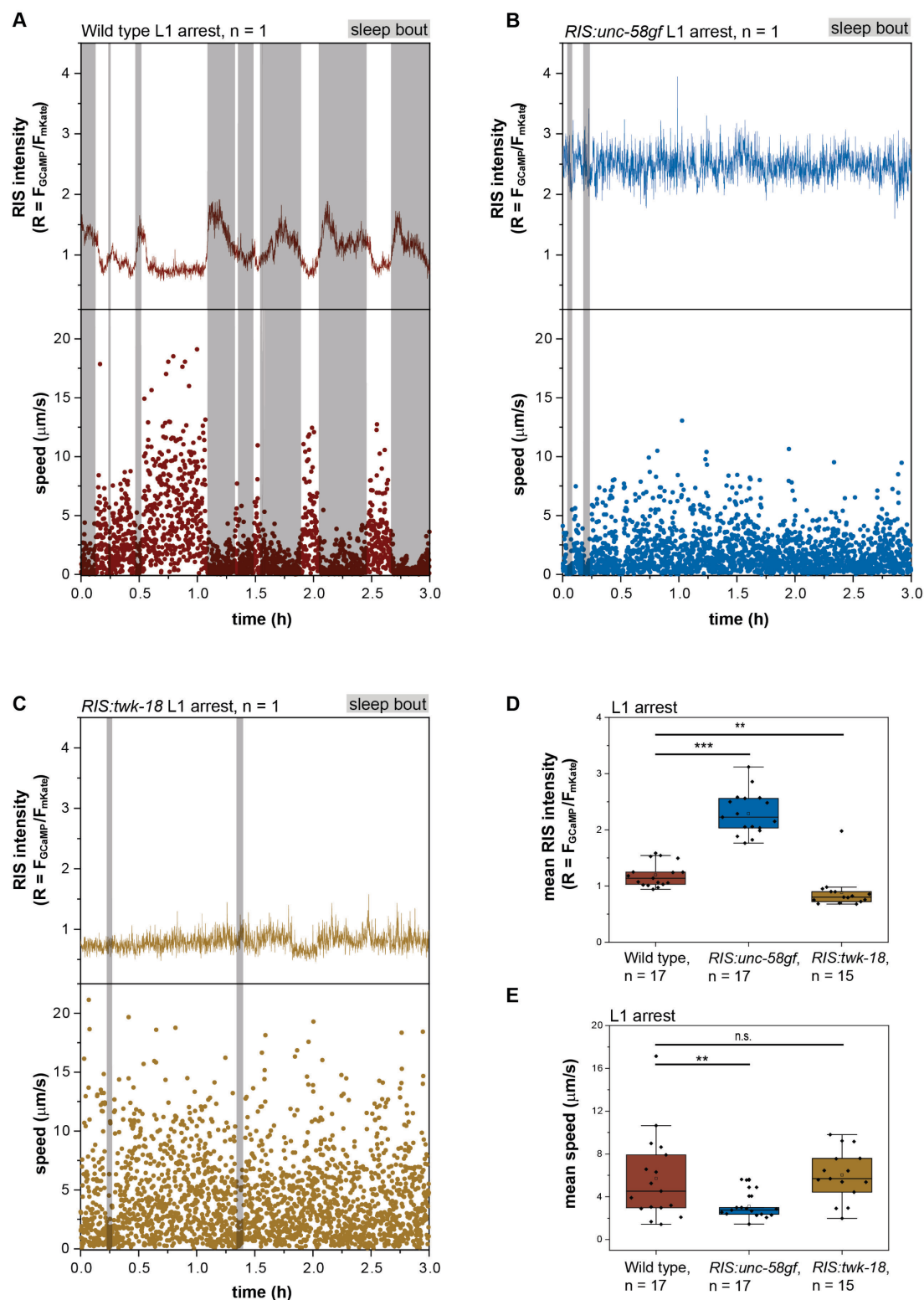


Figure 19. Ion channels expressed in RIS can cause constant de- or hyperpolarization of RIS.

(A) Sample trace of the RIS signal and speed of a wild-type worm in L1 arrest. The worm cycles between wake and sleep bouts. RIS activates during sleep bouts. (B) Sample trace of an *RIS:unc-58gf* worm in L1 arrest. The worm is mostly in wake bouts and has a very high RIS activity. (C) Sample trace of an *RIS:twk-18* worm in L1 arrest.

The worm is mostly mobile and in wake bouts with a low activity of RIS. (D) Quantification of the mean RIS activity and a direct comparison to wild type. RIS is significantly more activated in *RIS:unc-58gf* worms compared to wild-type worms. *RIS:twk-18* worms show a reduced RIS activity. $**p<0.01$, $***p<0.001$, Welch test. (E) Worms expressing *RIS:unc-58gf* are slower than wild-type worms. There is no difference in speeds between *RIS:twk-18* and wild-type worms. $**p<0.01$, Welch test.

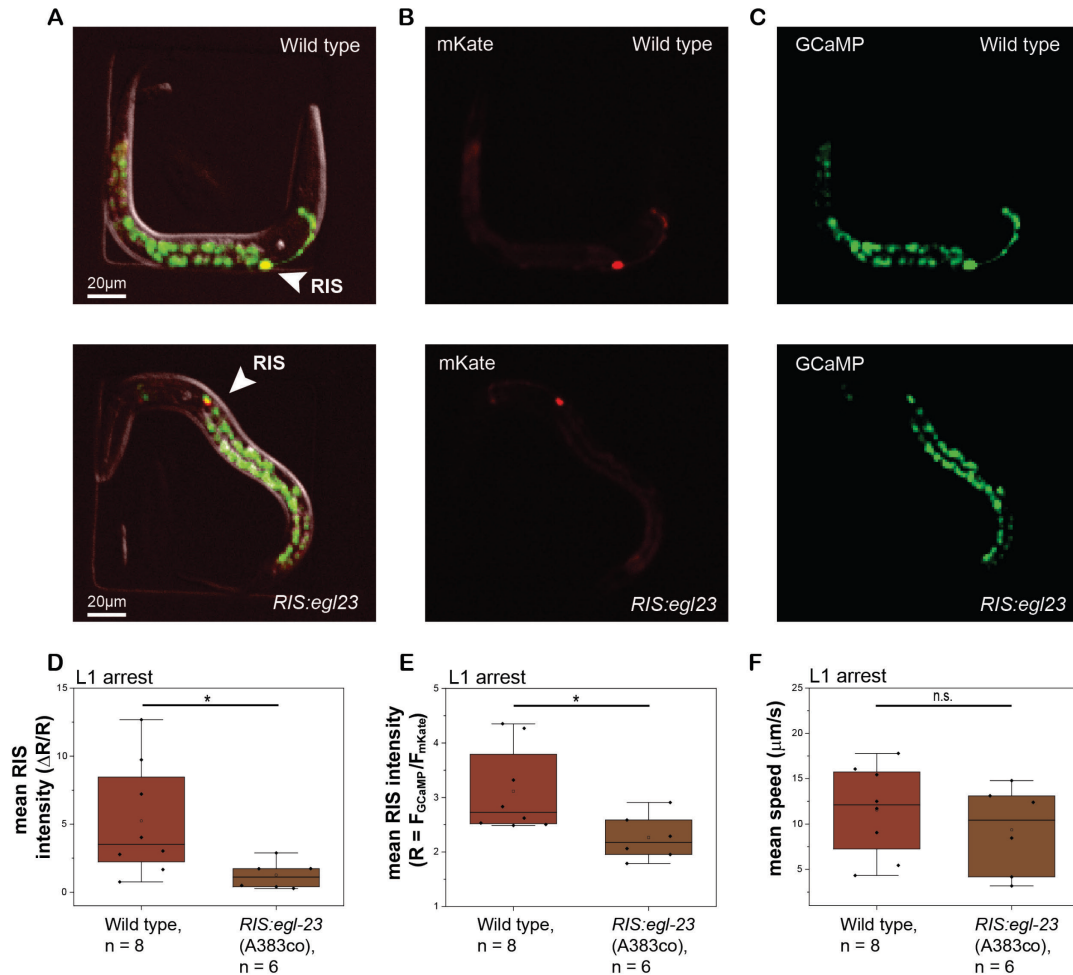


Figure 20. RIS shows little transients and is hyperpolarized in worms expressing EGL-23 in RIS.

(A-C) GCaMP as well as mKate intensities in RIS were imaged. (D) The mean normalized $\Delta R/R$ values represent the average neuronal changes. The RIS hyperpolarization strain shows very little transients in RIS. $*p<0.05$, Welch test. (E) The mean RIS intensity is significantly smaller than that of wild type. $*p<0.05$, Welch test. (F) There is no significant difference in speed of wild-type versus *RIS:egl-23*(A383co) worms. n.s. $p>0.05$, Welch test.

4.3.4.2. Constant de- and hyperpolarization of a sleep neuron both lead to a reduced amount of sleep

Since the new genetic knock-in strains led to the expected changes of potential in RIS, the question arose, how constant de- or hyperpolarization of the sleep neuron RIS changes behavior. One might expect a constant depolarization to cause an increased amount of sleep in the worms whereas a constant hyperpolarization could be followed by reduced amounts of sleep. To actually test for the behavior, I first imaged the worms for 12h in the arrested first larval stage beginning at 48h of starvation. The RIS hyperpolarization strain (*RIS:twk-18*) and surprisingly also the depolarization strain (*RIS:unc-58gf*) both have reduced amounts of sleep (Figure 21A-D). The RIS hyperpolarization strain sleeps on average 10.6% of wild-type sleep and the RIS depolarization strain 23.9% of wild-type sleep.

The *RIS:egl-23* variants were designed to achieve varying levels of sleep inhibition through hyperpolarization of different strengths of RIS. Indeed, imaging after 48h of starvation in L1 arrest revealed that the weaker *egl-23(L229)* allele leads to an only mildly decreased sleep fraction compared to the wild type (75.5% of total wild-type sleep), whereas worms expressing the stronger variant *egl-23(A383)* sleep 23.9% of the wild type. Worms with the strong and codon optimized *RIS:egl-23(A383co)* sleep on average 10.6% of the wild-type fraction (Figure 21E-H). Concluding, these strains are well suited for future dose-response experiments.

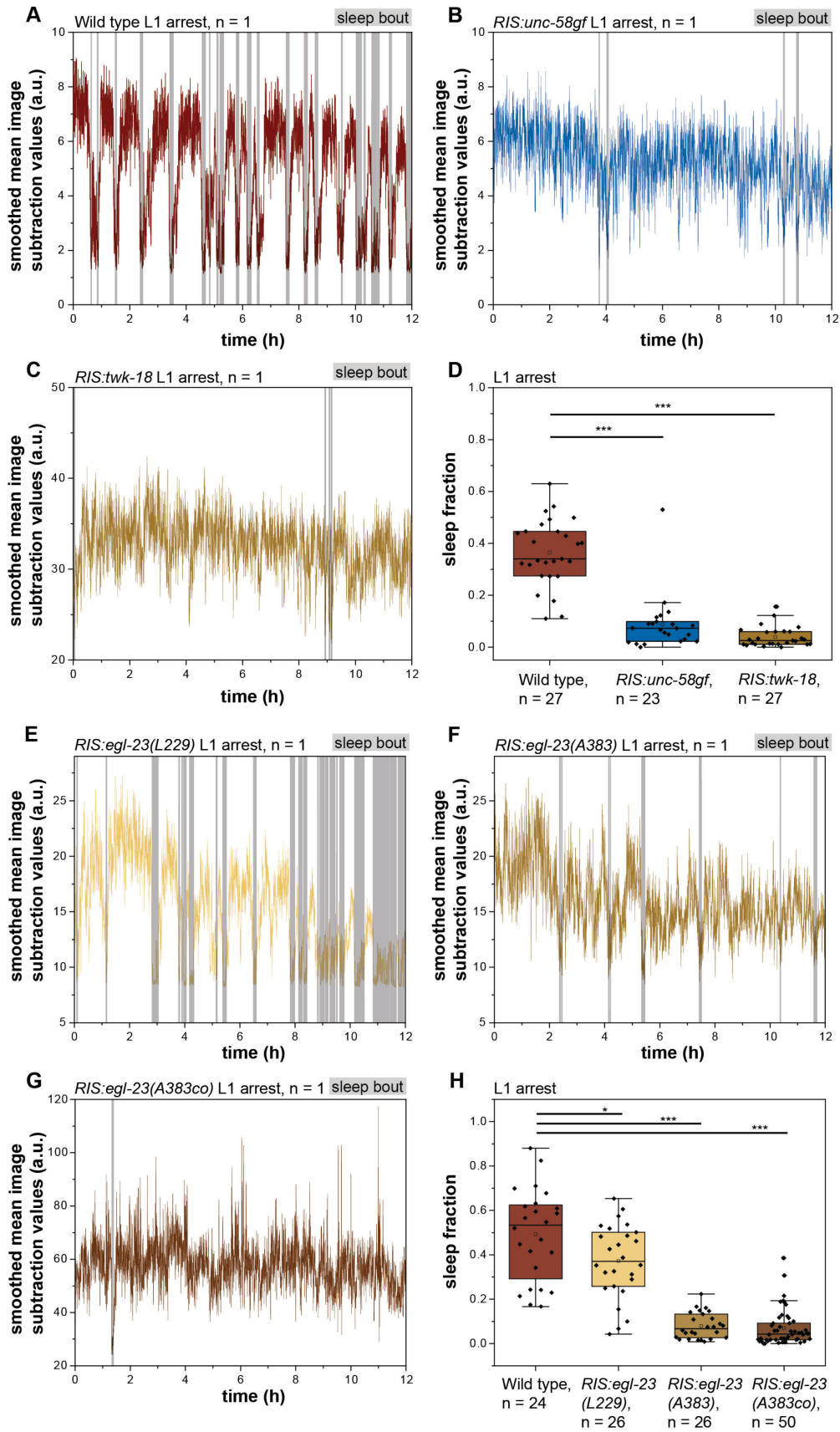


Figure 21. Constant RIS hyper- as well as depolarization cause decreased sleep in L1 arrested worms.

(A) Sample trace of the movement of a wild-type worm in L1 arrest. The worm cycles between wake and sleep bouts. (B) Sample trace of an *RIS:unc-58gf* worm in L1 arrest. The worm is mostly in wake bouts. (C) Sample trace of an *RIS:twk-18* worm in L1 arrest. The worm is mostly mobile and in wake bouts. (D) Quantification of the sleep fraction and a direct comparison to wild type. *RIS:unc-58gf* and *RIS:twk-18* worms, both show a highly significant reduction of sleep bouts. *** $p < 0.001$, Welch test. (E) Sample trace of an *RIS:egl-23(L229)* worm in L1 arrest. The worm is more awake but cycles between wake and sleep bouts. (F) Sample trace of an *RIS:egl-23(A383)* worm in L1 arrest. The worm is mostly in wake bouts and only has occasional sleep bouts. (G) Sample trace of an *RIS:egl-23(A383co)* worm in L1 arrest. The worm is awake for almost the entire 12 hours. (H) Worms that express the weaker EGL-23 variant (L229) only show a small reduction of sleep compared to wild type. Worms expressing a stronger variant of this channel as well as a codon-optimized version of the stronger variant have a highly reduced sleep fraction in L1 arrest. * $p < 0.05$, *** $p < 0.001$, Welch test.

While RIS plays the key role in regulating and inducing all types of sleep in *C. elegans* (8, 105, 106, 113), the upstream signaling pathways for sleep induction can vary. Next, I tested how de- or hyperpolarization of RIS changes the amount of developmentally regulated sleep in L1 lethargus. For this, I continuously imaged the different strains throughout lethargus through differential interference contrast imaging (DIC). The weak *RIS:egl-23(L229)* does not have a significantly changed amount of sleep. All other hyperpolarization strains do show a significant decrease of sleep compared to wild type (Figure 22A). A constant depolarization of RIS (*RIS:unc-58gf*) leads to a reduction of sleep of approximately 50% in lethargus (Figure 22B). One can see that for all tested strains the reduction of sleep compared to wild type is stronger in L1 arrest than lethargus. This points to lethargus being more strongly determined as a sleep-state through developmental regulation (102).

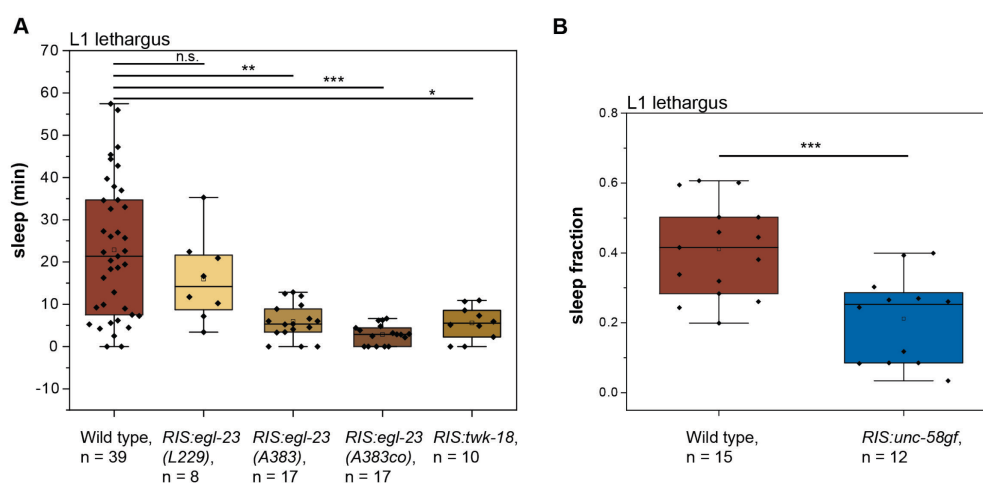


Figure 22. Ion-channels expressed in RIS influence the amount of sleep in lethargus.

(A) A weak constant hyperpolarization of RIS does not have an impact on the amount of sleep in lethargus. Worms in which RIS is strongly hyperpolarized sleep less than wild-type worms. * $p < 0.05$, ** $p < 0.01$, *** $p < 0.001$, Welch test. (B) A constant RIS depolarization leads to a reduction of sleep in lethargus. *** $p < 0.001$, Welch test.

4.3.4.3. Changing the potential of RIS impacts survival of arrested first larval stage worms

Sleep has been identified to act as anti-aging and lifespan prolonging in arrested first larval stage *C. elegans* (106). I could demonstrate in Publication II that long intervals of optogenetic inhibition of RIS lead to a premature death in the arrested first larval stage (151). With the newly designed tools in which the potential of RIS is constantly changed, one could investigate what effect constant hyper- or depolarization of this sleep neuron has on longevity. One would expect the RIS hyperpolarization strains to have a reduced lifespan. For the depolarization experiment the expectation is not that obvious. On the one hand, RIS depolarized worms show a reduced sleep behavior, so one might assume that this aspect should also lead to a reduction in longevity. On the other hand, it is not clear yet what constitutes the benefits of sleep. If only sleep behavior as immobility was responsible for the positive effects, there would not be the need to shut down the nervous system. It is possible that while a constant RIS depolarization causes a reduction in sleep behavior, perhaps still other cytoprotective mechanisms depending on FLP-11 release by RIS happen during wakefulness. In this case, the worms might have a lifespan comparable to wild-type worms or perhaps even longer.

The experiment was conducted in liquid M9 buffer at 25°C. Indeed, the RIS hyperpolarization strains have a highly reduced longevity, similar to *aptf-1(gk794)* mutants. Interestingly, RIS depolarization led to a significant longevity extension (Figure 23). This points to the idea that activation of RIS and perhaps release of the neuropeptide FLP-11 could be part of a protective pathway that contributes to sleep benefits.

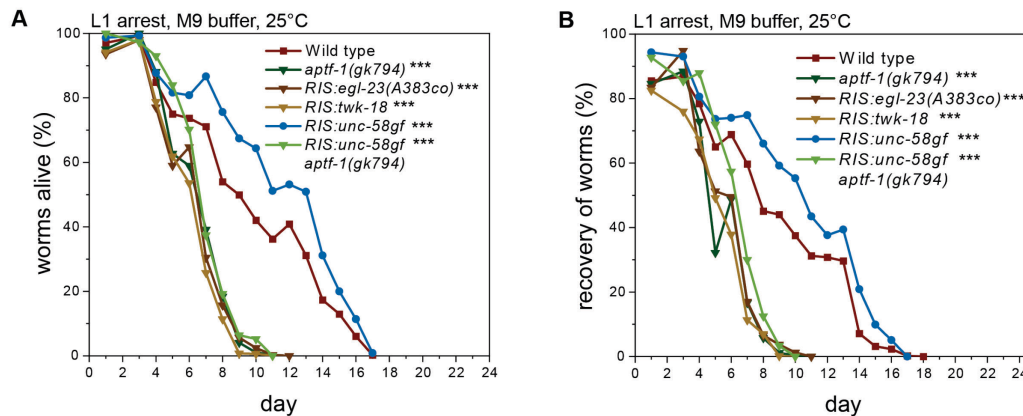


Figure 23. Changes in RIS activity influence the lifespan of *C. elegans* in L1 arrest.

(A) RIS hyperpolarization leads to a reduced lifespan similarly to worms under genetic sleep deprivation. In contrast, constant RIS depolarization leads to a prolonged lifespan compared to wild type. This graph includes data from two replicates for the *RIS:unc-58gf*, *aptf-1(gk794)* strain and three replicates for all other strains. *** $p < 0.001$, Fisher's exact test on day 7. p -values were corrected for multiple comparisons with the Benjamini-Hochberg procedure. (B) RIS hyperpolarization leads to a reduced recovery from the arrested first larval stage into the adult stage similarly to *aptf-1(gk794)* mutants. In contrast, constant RIS depolarization leads to an increased recovery compared to wild type. This graph includes data from two replicates for the *RIS:unc-58gf*, *aptf-1(gk794)* strain and three replicates for all other strains. *** $p < 0.001$, Fisher's exact test on day 7. p -values were corrected for multiple comparisons with the Benjamini-Hochberg procedure.

4.3.4.4. Activity of the nervous system is wake-like in constantly RIS activated worms

The previous experiments show that the same behavior, in this case a reduced amount of sleep, can have diverging effects on longevity depending on the cause for this behavior. If immobility does not constitute the benefits of sleep, what else does? Previous research has linked neural excitation to lifespan. It was shown that inhibition of neural excitation prolongs longevity (161). I hence wanted to test the overall neuronal activity in the RIS depolarization strain. For this, I calcium imaged L1 arrested worms expressing *rab-3p::GCaMP* and *arrd-4p::GCaMP*. I treated all neurons in the head as a single large neuron and investigated how their activity levels changed over time. Wild-type worms showed a decreased activity during sleep bouts whereas *RIS:unc58gf* worms and *RIS:unc-58gf*, *aptf-1(gk794)* worms had less obvious neuronal activity changes (Figure 24A). A sleep bout detection analysis confirmed that RIS depolarized worms (*RIS:unc58gf*) sleep less than wild type in L1 arrest. However, worms

expressing *RIS:unc58gf* in the *aptf-1(gk794)* background, in which RIS is non-functional, sleep even less (Figure 24B).

To investigate if a change in neural activity might underlie longevity phenotypes dependent on sleep and RIS in L1 arrest, first, the overall neuronal activity was investigated. Averaging the neuronal activity for each animal interestingly shows that shorter lived *RIS:unc-58gf, aptf-1(gk794)* mutants have an average increase in neuronal activity of approximately 17% compared to wild type (Figure 24C). This again points to a more dampened nervous system being beneficial for survival as has been described before (161). However, there is no significant difference between the wild-type and the constantly RIS depolarized strain (*RIS:unc-58gf*) which could account for their lifespan difference. Therefore, other mechanisms must contribute to the life-prolonging effects of RIS depolarization.

To understand overall neuronal changes during wake and sleep bouts, mean intensities were calculated for all worms for both states. For all averaged wake and sleep bout intensities, one can see that there are two distinct neuronal states for the wild type. The wild type has a higher neuronal activity during wake bouts versus sleep bouts (Figure 24D). While RIS depolarized worms (*RIS:unc-58gf*) also show a significant decrease in neuronal intensities during sleep compared to wake, it is less pronounced than in wild-type worms. There were almost no detected sleep bouts for *RIS:unc-58gf, aptf-1(gk794)* worms. However, in the very few detected sleep bouts, the neuronal activity is not changed compared to wake bouts in this strain. The sleep bout detection analysis was optimized for the wild type and the results point to the few detected sleep bouts in *RIS:unc-58gf, aptf-1(gk794)* being false positives. Anyways, the mean intensities during wake bouts of both mutant strains were not significantly different from the wild type even though one could see small trends with the RIS depolarization strain (*RIS:unc-58gf*) having a 2% reduction and the *RIS:unc-58gf, aptf-1(gk794)* strain having a 9% increase in mean neuronal intensities compared to wild-type intensities. Strikingly, the mean wake intensities of the RIS depolarization strain (*RIS:unc-58gf*) were significantly reduced compared to the double *RIS:unc-58gf, aptf-1(gk794)* strain. It is possible that perhaps a more precise experimental set-up could detect neural activity differences during wake bouts for all strains. Anyways, the mean intensities during sleep bouts vary for all strains and are hence mostly responsible for the overall neuronal dampening in

wild type and constantly RIS depolarized worms. All three strains have a significant reduction in speed during the detected sleep bouts (Figure 24E).

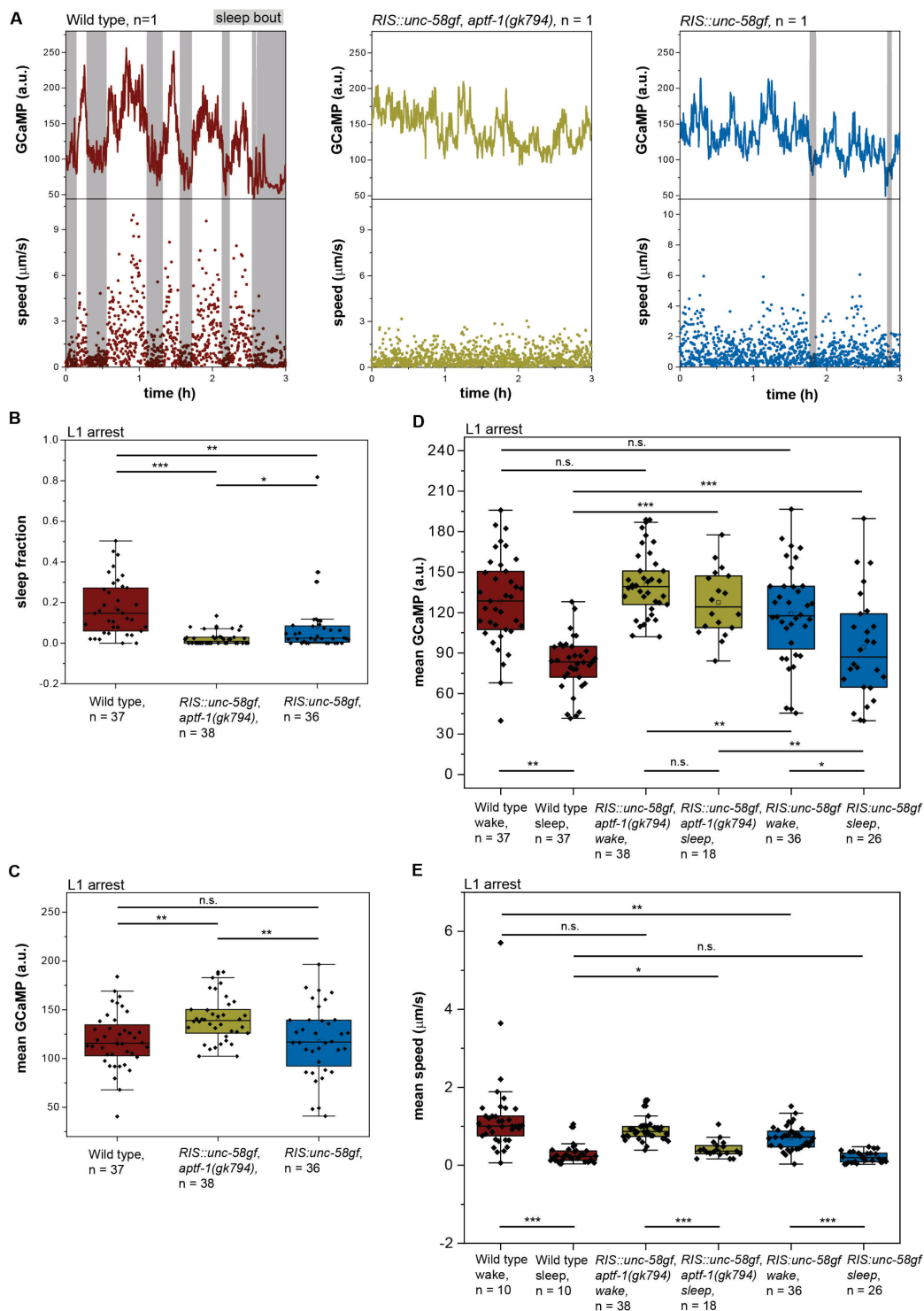


Figure 24. A lack of sleep bouts leads to an overall neuronal activity increase in worms in the *aptf-1(gk794)* background.

(A) Sample traces of the speeds and neuronal activities of a wild-type worm, a constantly RIS depolarized worm and a *RIS::unc-58gf, aptf-1(gk794)* worm in L1 arrest.

(B) Constantly RIS depolarized worms have a strong reduction in sleep compared to wild type. There is almost no detectable sleep in an *aptf-1(gk794)* background. * $p < 0.05$, ** $p < 0.01$, *** $p < 0.001$, Welch test. (C) *RIS:unc-58gf, aptf-1(gk794)* mutants have an increased overall neuronal activity. ** $p < 0.01$, Welch test. (D) All three strains have comparable neuronal activities during wakefulness. There are differences in neuronal activity in detected sleep bouts. * $p < 0.05$, ** $p < 0.01$, *** $p < 0.001$, Welch test for comparisons between different strains and Wilcoxon signed rank test for comparisons between the same strain. (E) All strains have a reduced speed during detected sleep bouts. * $p < 0.05$, ** $p < 0.01$, *** $p < 0.001$, Welch test for comparisons between different strains and Wilcoxon signed rank test for comparisons between the same strain.

4.3.4.5. RIM peaks wild-type-like in constantly RIS depolarized worms

The previous pan-neuronal analysis gives a good overview of overall neuronal changes. However, it had been shown before that sleep does not necessarily modulate all neurons. Previous research has for example identified the elevated arousal threshold in sleeping adult *C. elegans* to be determined by neuromodulation of interneurons whereas sensory neurons stayed unaffected (162). An important interneuron, which has been characterized in Publication I to be a key regulator of RIS (114), is RIM. I was next interested to see how the activity of RIM changes in constantly RIS depolarized worms upon 48h of starvation in L1 arrest. From the pan-neuronal experiment I developed the hypothesis that RIM should behave similarly to wild-type wake states. I imaged GCaMP and mKate fluorescence intensities in RIM by expressing the fluorophores with the *tdc-1* promoter. The GCaMP intensities were then normalized for expression by dividing over the mKate intensities. Wild-type worms show RIM peaks throughout wake bouts but not during sleep bouts (Figure 25A, B). Double *RIS:unc-58gf, aptf-1(gk794)* mutants show many RIM peaks throughout L1 arrest (Figure 25A). Single *RIS:unc-58gf* mutants do not show RIM peaks during their few sleep bouts but throughout wake bouts (Figure 25A, C). The sleep fraction was again calculated to control for a potential silencing. As in the pan-neuronal experiment, *RIS:unc-58gf* as well as double *RIS:unc-58gf, aptf-1(gk794)* animals have a strong reduction in sleep compared to the wild type so that silencing can be excluded (Figure 25D). The RIM peaks were quantified to allow for a comparison between the different strains. First, I investigated the total number of RIM peaks per worm throughout the filmed three hours. The RIS depolarization strain did not differ to the wild type in number of peaks. However, the double *RIS:unc-58gf, aptf-1(gk794)* worms had a significant increase in

RIM peaks (Figure 25E). This might be due to the extended time in wake as double *RIS:unc-58gf, aptf-1(gk794)* do not really sleep. To account for that aspect I next compared the mean RIM peak frequencies only during wake bouts. Here, there is again no significant difference between wild type and the RIS depolarization strain. However, worms in the *aptf-1(gk794)* background have increased peak frequencies of 161% during wake bouts (Figure 25F). Logically, the next quantification compared the peak amplitude. Again, wild type and the RIS depolarization strain have no significant difference but interestingly the double *RIS:unc-58gf, aptf-1(gk794)* has a 41% decreased mean peak amplitude (Figure 25G). Worms in the *aptf-1(gk794)* background without functional RIS seem to have more frequent peaks of smaller amplitudes. To compare overall RIM activity I multiplied the peak frequency by the peak amplitude. There was no significant difference for the product (Figure 25H). Concluding, constantly RIS depolarized worms behave similarly to wake wild-type worms. Both non-wild-type strains have reduced amounts of sleep but varying nervous system responses. The intention of neuronal characterization was to characterize the RIS depolarization strain (*RIS:unc-58gf*) as wake- or sleep-like. The results suggest that the nervous system behaves wake-like in accordance to the worms' mobility. Interestingly, double *RIS:unc-58gf, aptf-1(gk794)* mutants, which were originally filmed as control, show a strong phenotype of the nervous system compared to wild type.

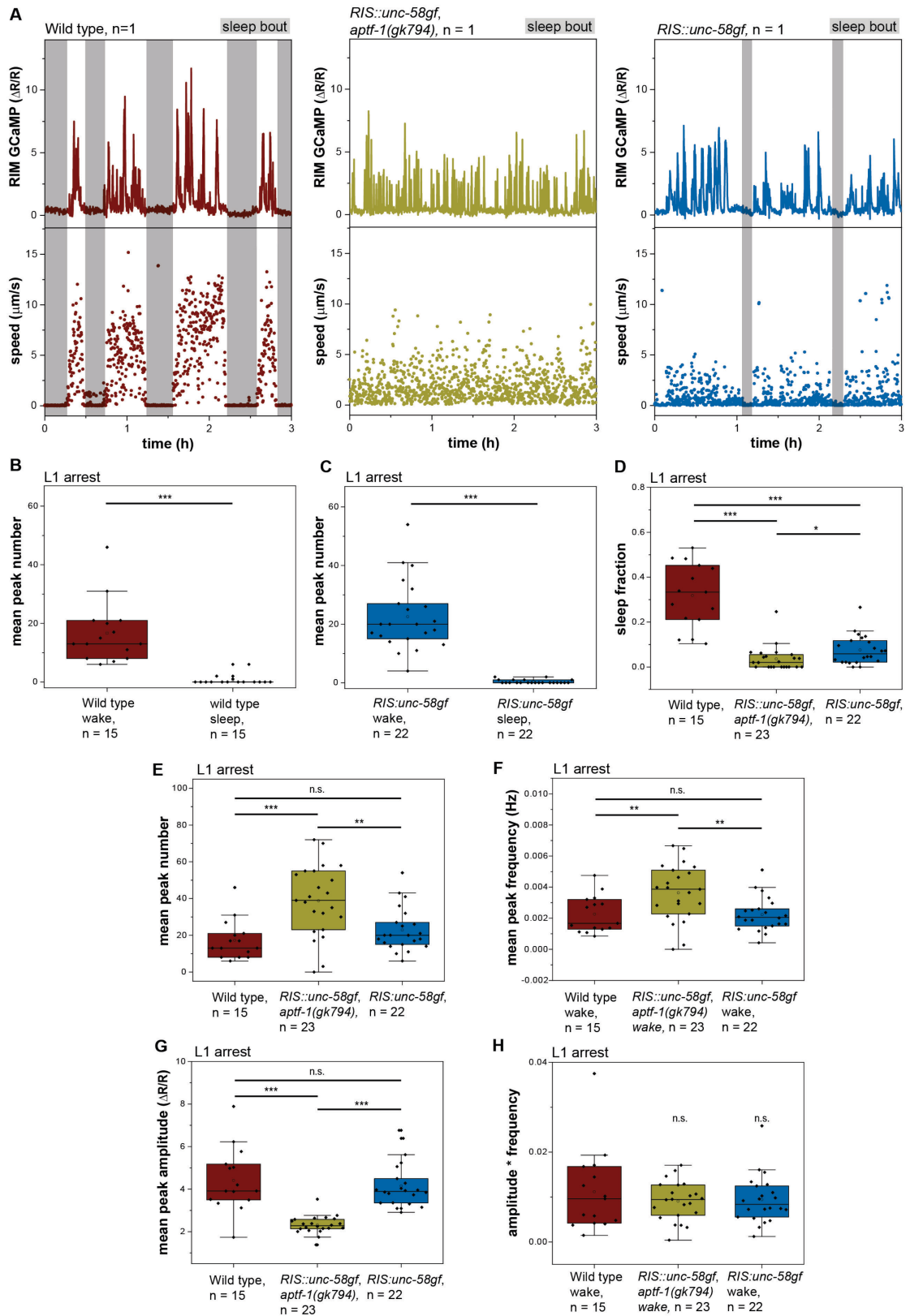


Figure 25. RIM peaks more frequently but with less amplitude in an *aptf-1(gk794)* background in L1 arrest.

(A) Sample traces of the speeds and RIM activities of a wild-type worm, a constantly RIS depolarized worm (*RIS::unc-58gf*) and an *RIS::unc-58gf*, *aptf-1(gk794)* worm in L1 arrest. (B-C) Wild type and RIS depolarized worms have RIM peaks during wake but

not during motion bouts. *** $p < 0.001$, Wilcoxon signed rank test. (D) Constantly RIS depolarized worms (*RIS:unc-58gf*) have a strong reduction in sleep compared to wild type. There is almost no detectable sleep in an *aptf-1(gk794)* background. * $p < 0.05$, *** $p < 0.001$, Welch test. (E) *RIS:unc-58gf, aptf-1(gk794)* mutants have more RIM peaks throughout L1 arrest. ** $p < 0.01$, *** $p < 0.001$, Welch test. (F) *RIS:unc-58gf, aptf-1(gk794)* mutants have an increased mean peak frequency. ** $p < 0.01$, Welch test. (G) *RIS:unc-58gf, aptf-1(gk794)* mutants have decreased mean peak amplitude, *** $p < 0.001$, Welch test. (H) Multiplication of the peak frequency and amplitude gives similar results for the different strains. n.s. $p > 0.05$, Welch test.

5. Discussion and Outlook

5.1. Command interneurons regulate RIS activity and homeostasis

Previous studies have characterized a wake-sleep flip-flop switch. In this switch, wake-promoting neurons inhibit sleep-promoting neurons and vice versa (41, 42). However, how exactly the switch is turned from wake to sleep had not been understood. We could identify formerly known wake-active neurons that are sleep-promoting and required to induce sleep in *C. elegans*. Interneurons PVC and RIM from the locomotion circuit regulate the activity of the sleep neuron RIS and sleep homeostasis in lethargus. During the wake-state, these neurons do not activate RIS in order to induce sleep. Instead, PVC is forward and RIM backward locomotion inducing. However, during lethargus the properties of interneurons change and reverse and forward circuits can act in concert to activate RIS for sleep induction. This is important in that it illustrates how the switch from wake to sleep is turned in *C. elegans*. We could show that the wake-sleep flip-flop switch model needs to be extended with wake-active, sleep-promoting neurons that activate sleep-active neurons to turn the switch from wake to sleep. In *C. elegans* this additional component are interneurons PVC and RIM but brain regions of equivalent function might perhaps also be found in other sleeping organisms. However, an upstream signal needs to be present in order to modulate command interneuron properties and allow for sleep induction. In lethargus, this signal is most likely a developmental cue, which could act directly on command interneurons or more thinkable on their upstream neurons. As a next step, one could optogenetically screen through upstream neurons that might regulate PVC and RIM during lethargus in order to answer this question. Furthermore, one should investigate how PVC can activate RIS. Which neurotransmitters or peptides are important for the activation of RIS by PVC? While we were able to find that RIM activates RIS via glutamate and inhibits RIS through tyramine and FLP-18, this information is still lacking for the PVC to RIS connection. Many neuropeptides and neurotransmitters are expressed in PVC. Primary experiments revealed that the neuropeptides FLP-10 and FLP-20 and the arthropod pigment dispersing factor homolog PDF-1 might be important for the regulation of RIS

by PVC (personal communication with Dr. Elisabeth Maluck). However, for more certainty a thorough screen would have to be conducted.

I could show that the command interneurons are not only regulators of sleep in first larval stage lethargus, but they are additionally important for starvation-induced sleep in L1 arrest. This suggests that the overall neuronal circuitry for RIS regulation could be invariable for different sleep triggers or at least for sleep during the first larval state. However, upstream pathways acting on this interneuron circuit differ since sleep in lethargus is regulated by the developmental gene *lin-42* (107, 112) and starvation induced sleep in L1 arrest is regulated by insulin-like signaling (163).

Since submission and publication of our neuronal circuit for sleep regulation, the connectome of *C. elegans* was revised (93, 164). Additional RIS upstream neurons were identified and might also play a role in RIS and sleep regulation. The RIB second-layer interneurons are the most promising candidates, as RIB and RIM neurons seem to be the only RIS presynaptic neurons with stable connections onto RIS throughout development. Other neurons that have recently been found to be upstream of RIS are, for example, the SMD motor neurons, the sensory neurons OLL and FLP and the polymodal neuron AVL (motor and interneuron) (93, 164). The improved recent connectome, including the finding of dynamic synaptic changes throughout development, as well as our characterization of SDQL to be an additional activator of RIS, all support the idea that the neuronal network gets remodeled throughout development and the neuronal circuit for sleep induction might differ in older developmental stages. We could identify the sleep-regulating circuit for the first larval stage. However, how this circuit is remodeled during later larval stages or the adult worm needs further investigation.

In conclusion, sleep induction is much more complex than the previously proposed flip-flop switch between wake- and sleep-promoting neurons. We could add the missing component of wake-promoting sleep-inducing neurons to the model for *C. elegans*. Since sleep is evolutionary conserved, it is likely that this is a key regulatory aspect, which could also exist in higher animals such as mammals.

5.2. The OptoGenBox

With the OptoGenBox I implemented a stand-alone device for long-term optogenetic experiments. Amongst other features, the box allows for a precise long-term environmental control. Additionally, different light protocols can run in parallel, which allows for high throughput experiments. The OptoGenBox is currently the only device to account for all previously mentioned aspects and is a lot cheaper than alternative microscopic set-ups that could be used for single long-term experiments.

I conducted three different proof-of-principle experiments. First, an escape assay showed that ASH-activated worms display an escape response as anticipated. Next, I investigated what effects an optogenetic increase in arousal and sleep deprivation have on the survival of *C. elegans*. As expected, sleep deprivation and an increase in arousal lead to a reduction of longevity. These proof-of-principle experiments show that the OptoGenBox is functional.

I could demonstrate with the lifespan assays that optogenetic long-term inhibition of the sleep neuron RIS caused a significant reduction in survival. However, what would be the longevity of worms in which there is long-term optogenetic sleep induction via RIS activation? This could easily be tested by expressing a red-shifted channelrhodopsin (ReaChR) in RIS and by utilizing the OptoGenBox. It is a very interesting experiment in that it is not clear if optogenetic RIS activation and sleep induction could further increase the longevity or if the wild type is already optimized in that regard.

While in my publication I only tested how an increase in arousal and sleep-deprivation affect the worms' survival, the OptoGenBox could be utilized for many other problems. Egg-laying behavior can for example be triggered in adult worms by optogenetic activation of the HSN neurons (165). Specific locomotion directions can be controlled optogenetically since optogenetic activation of RIM induces reverse locomotion (114, 166) whereas activation of PVC causes a forward movement (114, 167). One can see that the OptoGenBox presents the option to answer many questions in regards to long-term behavioral changes. Currently, the device has only been tested with *C. elegans*. It

is however thinkable that other small organisms such as *Drosophila* larvae could furthermore get controlled through the device.

5.3. No found evidence for the synaptic homeostasis hypothesis or sleep improving health in arrested first larval stage *C. elegans*

Several functions of sleep such as sleep counteracting aging have already been characterized in *C. elegans* (106). However, the existence of some benefits that could be attributed to sleep in higher organisms has yet to be identified in worms. The synaptic homeostasis hypothesis is a well-established hypothesis for higher order animals such as mammals and considers sleep to be the price for memory (148). *C. elegans* might have a simple nervous system but they are able to learn and form memories (168). For this reason, I was curious to test if the synaptic homeostasis hypothesis also holds in *C. elegans*. Unfortunately, neither pre- nor post-synaptic marker imaging gave any evidence for synaptic homeostasis in *C. elegans*. However, I only tested specific subsets of neurons and it is possible that synapses of other neurons potentiate according to the synaptic homeostasis hypothesis. The utilized pre-synaptic marker was expressed in mechanosensory neurons and the post-synaptic marker in GLR-1 (AMPA receptor) expressing neurons. These neurons were chosen based on previous findings of glutamatergic AMPA receptors expressing according to the synaptic homeostasis hypothesis in the rat cerebral cortex and hippocampus (79). Additionally, the arrested first larval stage might not have been the ideal developmental stage for testing and perhaps phenotypes could be observed in other stages. Non-sleeping mutants have a decreased longevity in L1 arrest (106). Hence, sleep seems to be of very high relevance for L1 arrested *C. elegans*, which is why this state was chosen for experimentation.

A habituation assay was conducted to compare habituation responses and memory formation between non-sleeping *aptf-1(gk794)* mutants and wild-type worms. Following the argumentation of the synaptic homeostasis hypothesis, one would expect non-sleeping worms to have a worse memory. However, there was no observed difference between wild-type worms and *aptf-1(gk794)* mutants. While sleep did not seem to have an impact on memory formation and dishabituation, age did. Young adult worms were able to generate a memory of at least 15min whereas old adult worms had dishabituated at that time point. This age-dependent cognitive decline is consistent with

previous studies (169). Summarizing, the here tested habituation assay could not support sleep to be beneficial for memory. However, only a very specific memory was tested in adult worms and it is possible that other learning assays or testing memory in larvae might generate different results.

While the here presented experiments do not prove the absence of synaptic homeostasis as a function of sleep in *C. elegans*, the lack of evidence thereof could suggest that other sleep functions might be of higher relevance in the worms. One could speculate that synaptic homeostasis might be a higher order function of sleep that is only of importance in animals with more complex nervous systems. Hence, maintenance of synaptic homeostasis might not be the primary reason for why animals sleep but rather an added-on function to sleep. This idea is of course highly speculative and further research is needed.

To test for other functions of sleep in *C. elegans* I conducted different health span experiments. Neither recovery from coldness nor pumping rates were affected by genetic sleep deprivation. It is actually very interesting to observe that many physiological processes are independent of sleep in *C. elegans*. To find additional positive functions of sleep one might need to investigate further.

5.4. Ion channels expressed in RIS allow for behavioral manipulations and the discovery of pathways for sleep benefits

RIS functions as a single sleep neuron in *C. elegans* (8, 113). Manipulating the activity state of RIS allows for behavioral control. With the here newly invented and characterized strains, I was able to generate worms with constant RIS de- or hyperpolarization.

A constant RIS hyperpolarization led to a reduction in sleep and shortened lifespan in arrested first larval stage animals. These results were as expected since it has previously been reported that sleep deprivation decreases longevity (106, 151). The *RIS:twk-18* as well as the *RIS:egl23(A383co)* strain had approximately 10.6% of wild-type sleep amounts in L1 arrest. Additionally, their longevity did not differ from each other. Hence, both strains present potent tools for the investigation of effects and pathways of sleep-loss. The newly generated strains have an advantage over already established non-

sleeping *aptf-1(gk794)* worms in that they are more specific for RIS. APTF-1 is expressed in the neurons RIB and AIB and of course the sleep neuron RIS. Additionally, APTF-1 is a transcription factor that might not only be required for the transcription of *flp-11* but probably also for other genes. While both new RIS hyperpolarization strains function as anticipated, RIS calcium imaging is more difficult in *RIS:egl23(A383co)* worms as the GCaMP signal was only very faintly expressed. This might hint that the tool works more efficiently. Regardless, the *RIS:twk-18* strain is to be preferred for experiments to image RIS activity.

The different *RIS:egl-23* strains cause sleep deprivation of varying strengths. This result is very promising in that it opens up the possibility to conduct dose-response experiments of sleep deprivation. Previously, these dose-response experiments could only be done through, for example, varying the time or intensity of light for optogenetic stimulation or varying the duration or strength of mechanical taps (114). Now, for the first time it is possible to investigate this dose-response through genetic manipulations of varying strengths. A strong or entire loss of sleep has for example been shown to shorten longevity in L1 arrest. However, how longevity changes when there is only a partial and weaker loss of sleep remains unclear. The *RIS:egl-23(L229)* strain sleeps approximately 75% of wild type in L1 arrest. Whether this strain also has a small decrease in longevity compared to wild type needs to be investigated. Longevity and the amount of sleep might be directly correlated but it's also possible that a weak reduction in sleep does not cause premature death or even an extreme premature death similar to complete loss of sleep. This is a very interesting point, which would be worth investigating further in the future. Similar experiments including a dose-response of sleep deprivation are conceivable, for example, regarding aging markers as sleep-less *aptf-1(gk794)* worms have been shown to age quicker than wild type (106).

The *RIS:unc-58gf* strain was designed to allow for a constant RIS depolarization and the here presented experiments show that the design was successful. Interestingly, a constant RIS depolarization does not lead to an increase but a reduction of sleep behavior. RIS activation causes release of the sleep-inducing neuropeptide FLP-11. One possible explanation for the reduced amount of sleep is that neurons or other cells expressing FLP-11 receptors might get desensitized to the constant availability of FLP-11. Hence, they might simply get used to an FLP-11 oversupply and behave as if there

was no FLP-11. In this case, the animal would be in a wake state the entire time. However, if desensitization of the entire nervous system really happened, one would not expect benefits for longevity. Therefore, some molecular pathways that are perhaps independent of direct RIS downstream neurons must still respond to the constant FLP-11 supply. As a second theory, one could hypothesize that FLP-11 cannot be transcribed or translated quickly enough for sleep induction. With a constant release of FLP-11, the transcription might be lacking behind so that the actually released amounts of FLP-11 are too little to activate downstream pathways. Of course, also here, this can only partially be true, as some protective pathways would still need to be activated to account for the longevity extension. These theories would of course need further investigation. To test if FLP-11 is the determining factor for the loss of sleep and longevity extension phenotypes, one could, for example, overexpress FLP-11 and see how the worms start behaving. One could also genetically encode a tagged GFP to FLP-11 and compare intensities and locations between wild type and the RIS depolarization strain. The results would give insights into a quantification of FLP-11 levels, which would directly point towards one theory.

Ideally, one would identify pathways downstream of RIS activity that are directly responsible for 1) immobility as sleep behavior and 2) life-prolonging benefits of sleep. This strain is groundbreaking in that it for the first time can uncouple these two pathways. Discovering these two molecular pathways is of course no trivial task but FLP-11 and its targets present a good starting point.

To confirm the results of the RIS depolarization strain one could investigate neuronal long-term optogenetic activation of RIS using the OptoGenBox. One would expect a reduction in sleep as consequence of long-term optogenetic activation and prolonged longevity.

Furthermore, a characterization of the exact neuronal state would give further evidence whether the RIS depolarization strain is constantly awake from a neuronal activity point of view and if nervous system properties contribute to longevity phenotypes. The pan-neuronal and RIM experiments were a first step into that direction. In these experiments, it looks like the RIS depolarized worms are mostly awake as the nervous system intensity of the RIS depolarization strain during wake is similar to wake

intensities of wild-type worms. Quantification of the RIM peaks supports that the RIS depolarization strain behaves wake-like. However, it would be interesting to further quantify individual neurons. It was described in a recent preprint that sleep in adult *C. elegans* does not alter sensory neuron activity but instead activity of the interneuron AVA (162). It is possible that also in L1 arrest the properties of only some neurons as for example AVA get altered in the RIS depolarization strain. To further investigate individual neuronal changes in the *RIS:unc-58gf* strain, calcium imaging of command interneurons should be the next step. Additionally, single-cell resolved pan-neuronal imaging would present an ideal method to screen for neurons that respond to constant RIS depolarization.

While a constant RIS depolarization has benefits for longevity in the arrested first larval stage, it must have some downsides that explain that this strain did not evolutionary develop into the wild type. Perhaps, the benefits only appear in stages of extreme stress such as L1 arrest but during the regular development the worms might have disadvantages that reduce their fertility. This is another point worth investigating in the future.

To summarize, all newly generated strains expressing ion-channels in RIS function by either de- or hyperpolarizing RIS as anticipated. The RIS depolarization strain is extremely interesting in that it challenges common beliefs about the coupling of sleep benefits and immobility. Here, further investigation is necessary. All strains could be useful for the identification of molecular pathways downstream of the sleep neuron RIS in *C. elegans*.

5.5. Pan-neuronal imaging to investigate the regulation and benefits of sleep

Pan-neuronal imaging is a recent and still developing method that allows the investigation of complex neuronal responses (126, 134, 170). Throughout this PhD thesis, I conducted several pan-neuronal experiments. By treating the neurons in the head as a large single neuron I was able to show how sleep (Figure 12) and also the sleep neuron RIS directly (Figure 13) turn off the nervous system. Furthermore, I could compare the neuronal intensities between different worm strains (Figure 24). These

experiments already give very insightful results. However, to fully utilize the potential of pan-neuronal imaging, a single-cell analysis would have to be conducted. Furthermore, optogenetics has yet to be combined with single-cell pan-neuronal imaging. It is challenging in that most single-cell pan-neuronal imaging requires the use of several lasers of different wavelengths, which interferes with optogenetic tools. This problem could be overcome by utilizing a pan-neuronal strain that only requires one wavelength for imaging. Regardless, it would especially be interesting to see how exactly RIS turns off the nervous system by optogenetically activating RIS and calcium imaging all neurons.

5.6. Conclusion

In this PhD thesis, I solve the main neuronal circuit for sleep regulation in *C. elegans*, present a novel device - the OptoGenBox - to conduct optogenetic long-term experiments and I am able to uncouple longevity benefits of sleep from the sleep behavior immobility. Of course, the here presented findings are just pieces to the puzzle that is sleep. However, the depicted pieces are very important in that they further improve our understanding of how sleep is regulated and also address why organisms sleep. *C. elegans* is an ideal model organism for sleep research that allows for these key findings. The demonstrated results are likely also transferable to higher order organisms as sleep is evolutionary conserved.

6. Appendix

6.1. Sequences of CRISPR strains generated by Sunybiotec

PHX1433: *flp-11(syb1433[flp-11-SL2-egl-23cDNA(A383V)-linker-mKate2])X*

>flp-11b-SL2(gp2)-egl-23(n601)-linker(GSGSGSGSG)-mKate2(two introns)

ctatttagTGCGGAGAAACGTGCCATGCGGAACGCCTTGGTTTCGATTTGGAAGAGCTAGTGGTG
 GAATGAGAAATGCTCTCGTTAGATTTCGAAAGAGGTCTCCATTGGACGAGGAAGACTTTGCT
 CCAGAGAGCCCACTCCAGGAAAACGGAACGGTGCCCCACAACCATTGgtaagttgtctaaattttct
 tccgcttttgccttgcctcatgtctcttattttgctttgcagttcgctttggccgatccggtcaactc gaccacatgcacgacctttgtcactctcagAA
 GCTCAAGTTCGCCAACAAACAAGTAATGACCGAGGACGACCGTCTTCTGCTCGAACAACTCCT
 GCGACGAATTCATCATTAAgctgtctcatcctactttcacctagtaactgctgtcttaaatctatgctctctttagatctaaattttccta
 gaagctfacaagatataaatggtctcttcaataaagggtgtatatttattcatttgaatctgcaattcctcgttttgcgagttatataacctccaatttct
 ttctattgtattttcaacttcaatttcaatcaaggaaactgctcaacgcatcATGAAGCTCACGTTGAAGAAATCCGTATTCT
 CAAGGGATAAACATATCTTGCAAAGGCGACACCACTATTCTGTTCACTTTCTAATGATAGTA
 AGTGTGGGTGCCTACGCAATATTGGAGCACTTGTAAATGAGAAGTCTTGAATCGAGAAGTGT
 CACAAGTATTGAAAAGAAGACGGATGTTACAGAAAGACATGTTAATTTGACTAATTTTCAAC
 ATCCACCAACTCCAATCACATTAGAGCAAAGACATCGACGGAGACGCAGACATAATGAGAC
 AGCTTTGGAAGACCATTGTCTGAAAAATTATCCAGAGAAAAACGTGCAGCAGCGCATATC
 ATGAGAAGTCGAAAATGCGTTATCAGTGTGATAAAGAAAAATGTCAAGCATGGAATGTTTCA
 TTGACACTCTCGAGAGAAGCTCGTAAAAGCACTCGATGAATGTTACCACGTGGCAGTTGAA
 CATAATACTCATGTGAATCATGTACTTTTTCACGAATAGTAAGGAAGAAGTGGAGTCAAGTGG
 GGAAGAAGCAGAAGAAGATGTTTCCGAATGGTCAATTTATGGACTCGTGTGTTGTTGCATTCA
 CTGTTATTACGACGATTGGATACGGAACGTGGCACCTCGAACATTTGGTGGCCGCTATTT
 GTCATTGGTTATGGTCTAATTGGTATTCCGTTTACACTGCTGGCAATTGCAGATCTCGAAAA
 TTCATATCAGAAATGATGGTGGAGGCGAAAAAGTTTTGTAGGAAAAACCTGGAAAAAACTCA
 AAAAAAGCGTGGAACCCGAATTTCAATTCGCGCAAAGGATCTTCAAATACGGATATTGAGGA
 GAAAAATATTGGATAATGAGAAAAATCGAAAAATGAGCCGAAACTTCAGAAGTATCAGAAGA
 AGAAGACGATTTGACAGAGACAGAAGCCACGTCACTTTTCAATTTATTTTGGTTTATATCGC
 ATTTGGAGGGTTCATGTTAGCTGCTTATGAACCTGATATGGACTTTTCAAAGCGGTCTACTT
 TAATTTTGTGACATTGACATCAATTGGTCTGGGAGATATTGTACCGAGAAGTGAAACCTATA
 TGCTCATTACAATAGTCTACATTGCAATTGGTCTTGCTCTTACCACAATTGCCATTGAAATCG
 CCGTAGATGCATTGAAGAAGCTGCATTATTTTGGAAAGAAAAATCGAAAAATGTTGGAAATGT
 GGCTATATGGTTTGGAGGAAAGAAAATTACAATGAAAGCACTGGTCAAAAACCTCGGTGAC
 CAGTTCAATCTTCCAACCTACCGTAGTCAAGAATTTGAATTTGGATCATTTTGTGGATCAAGC
 GATTAAGTGGAGGAAGGAGAGATTGAGACACTCAGACCCGCCCTTATGAGCCACCGTCT
 GATCGATTTGAAGCTGAATTCGCTGATGAACCAGAAATGTGAATGGATCCGTGATCCGACTCC
 AACTCCACCCCATCACCTCAACCGGTTTATCGTCTTCCATCTCCAAAACAGTTACACCGG
 AACCTCTACCAAGTCCAACAATAACTGATGTATCACTTGCATTGCAACACCATCACCTGAA
 GAATCGGATGATGATCAAGAACTAATTTCCCATCACCTGAACCGAGTCCAGTTGAGAGCC
 AACTCCACCACCGCCTCCACGGGAGCCAACACCTCGTGAGCCAACTCCTGAGCCAGAGCCA
 GTTCGAGAGCCGACGCCTCCACCTCCGCCACCTGCCAAGCCCCGTCCACTGACTGCCGCTGA
 AATCGCGGCTCAAAAACGCAAAGCGTACAGCGAAGAAGCATGGCGTCGATACCAAGAATAC
 CAGAACAATGGAAGAAGTTCCGTCAAACCTCAGAAAACTCCCGCACCATCTGGAGCCTTA
 CATCAGGGGCATCAACATCAAAAACCGTCTGGAACATCACCGGAAAGTGGAGCCGGAGTATG
 TACTGGACCATCAACAAGGAGTCAATCAATAACATCAGTTGCATCTGGAAGACATCAAGA
 AGTGCAACACCGGAAAGCAAGAAATCATCACATTTGAGTGGCTCATCGAGAAGAGAAAGCG
 GTGAAAAAGGATCCGGATCCGGATCCGGATCCGGAATGTCCGAGTCTATCAAGGAGAACAT
 GCACATGAAGCTCTACATGGAGGGAACCGTCAACAACCACTTCAAGTGCACCTCCGAG
 GGAGAGGGAAAGCCATACGAGGGAACCCAAACCATGCGTATCAAAGtaagtttaaacatatataactaacta
 acctgatttttaattttcagGCCGTCGAGGGAGGACCACTCCCATTCGCTTCGACATCCTCGCCACCT
 CCTTCATGTACGGATCCAAGACCTTCATCAACCACACCCAAGGAATCCCAGACTTCTTCAAG
 CAATCCTTCCAGAGGGATTACCTGGGAGCGTGTACCACCTACGAGGACGGAGGAGTCC
 TCACCGCCACCAAGACACCTCCCTCCAAGACGGATGCCTCATCTACAACGTCAAGATCCGT
 GGAGTCAACTTCCCATCCAACGACCAGTCATGCAAAAAGAAGACCCTCGGATGGGAGGCCT
 CCACCGAGACCCTTACCCAGCCGACGGAGGACTCGAGGGACGTGCCGACATGGCCCTCAA

GCTCGTCGGAGGAGGACACCTCATCTGCAACCTCAAGGtaagtttaaacatgattttactaactaactaatctgattttaa
 ttttcagACCACCTACCGTTCCAAGAAGCCAGCCAAGAACCTCAAGATGCCAGGAGTCTACTACG
 TCGACCGTCGTCTCGAGCGTATCAAGGAGGCCGACAAGGAGACCTACGTTCGAGCAACACGA
 GGTCGCCGTCGCCCGTTACTGCGACCTCCCATCCAAGCTCGGACACCGTTAAaatcatatgttttctct
 ctcaactctcttttttc

PHX1445: *aptf-1(gk794)II*; *flp-11(syb1445[flp-11-SL2-unc-58(L428F)-linker*
mKate2])X

>flp-11b-SL2(gpd-2)-unc-58(e665)-linker(GSGSGSGSG)-mKate2(two introns)

TGGAAGAGCTAGTGGTGAATGAGAAATGCTCTCGTTAGATTTCGAAAGAGGTCTCCATTG
 GACGAGGAAGACTTTGCTCCAGAGAGCCACTCCAGGGAAAACGGAACGGTGGCCACAAAC
 CATTGtaagttgtcttaaaattttctccgcttttgcctttgcttcatgtgtcgtttatttgccttgcagttcgtttggccgatccggteaactcgacca
 catgcacgacctttgtcgactctttagAAGCTCAAGTTCGCCAACAACAAGTAATGACCGAGGACGACCGTCT
 TTCTGCTCGAACAACCTCTGCGACGAATTCATCATTAAgctgtctcactcactttcactagtaactgcttcttaaa
 atctatgcttctttagatctaaaaatftctagaagcttacaagtataaaatggctctctcaataaagggtgtatatttattcattgaatctgccatttcc
 tcgcttttgcgagttatataacctccaatfttcttctattgtatttcaacttcaatfttaattcaggaaactgctcaacgcacATGGCTCCACTG
 ACTGTGAAAAGCTCACCTCCAAAAGGCAAAAGGAATATCAAAAATTTTCGGAGAAAAAAG
 AAGCAGCCACCACGACTCAACCGTATTCTGCTGCATGGCCTCCGAAAGTGTCCGAGAGT
 CTCTGATCCAAGTTGATCCATTGGCCGCTGCACCTTGCACATCAGGCTCGAAAGACAAATAGT
 GTGCCAGCTGTCTCGAGAACTCCACTGCTTCTACAGTTCACTCCTTTTCGGACCACCTCTCAGT
 GCGTATCATGTGACAGCTCGGTGGGAAGGTGCAAATATCAATTCACAATCAGCATTGCTCGA
 TGCAGATGATGGAGCTACAGTTATCACAGATACCATCAAAGATGACCAAGATGATAAAGAA
 CAAAAAGCTGCCCGCAACAGACTGTCAAATACATCAAATACTTACACCTCACGTGATCTT
 GGTGTGAGTGTAAATTGGATATTTATGCTTGGGAGCTTGGATACTCATGTTACTGGAAACAA
 GGACGGAACCTTCTGCCAGATCCAAAAAAGTGTGAGGTTAACAAATTTGATGTCAAACCTTC
 ACTGCCGAAAGTTGGAAGATGCTCAATAATGCTCAACACGGGGTTAGTAATATGGATGAAG
 GTGAATGGGCTGCAACATTTTCGAGAATGGATGGTACGAGTATCAGAAACAGTGGACGATAG
 GAGACCTATACGACGTGAATTAACCGGCCTGATGACTTATCAAATATGCATAATAAATGG
 ACATTTCCAACCTGCAATATTATATGTTCTCACTGTGTTAACTACTTGCGGTTATGGAGAAGTA
 TCTGTGACACAGACGTCGGAAAGGTTTTCTCAGTAGCATTTCGCGCTTGTGGTATACCACTT
 ATGTTCCATAACAGCTGCCGATATTGGTAAATTTTTATCTGAAACATTACTCCAGTTTGTGAGC
 TTTTGGAAATCGAAGTGTCCGAAAAGTGAAGCAATGGATGAGTCGTATTTCGTCACGGCAGGA
 GAAAGTCATTACAATCAACGGGTGGTCCCAACGATACTCTCGATATTCTTGGTGTGACGGA
 ACTGAAGAGAACTTTGGTTCCCAATAGGTGCATATGTATCATGATTTTGCATATATTGCTC
 AATTGGGTCTGCCATGTTTATCACATGGGAAAGAAGTGGTCTTTCATTCATGCGTTTCATTT
 TGGTTTCAATTTGATTGTAACAGTCCGACTCGGAGATATCGTTGTGACTGATTACATATTTTT
 ATCACTTATCGTTGCATTTGTGATAGTTGGTITTTCCGTAAGTACCATGTGCGTGGATCTTGC
 GTCCACACATCTCAAGGCGTACTTCACCAGAATTCACTACTTTGGTCGAGCAAAACGATTCT
 TAGGAATGAGTGAGGAACTCAAAGAAATCGTTGCTTTACTGGGGCGATGCGACGGA AAAA
 AGGCGGTAAGTTACATGGAATGATGTGCGAGACTTCTTGATAACGAACACTCCGCGATCGA
 CCTTTTGAACCTCATGAGCTTCTGATGAAGCTCAGATTTATTGACGAAACATCTTCTGGAATG
 TCTACAATCCGTCACAATTCCTTCCAGTCAGATTTTTTCCGAGAATCAGAGTACATCCGAAG
 AGTGGCTGCGCTGAGGCCAGAACAGCCAGCATATTTGGATCCGGATCCGGATCCGGATCC
 GGAATGTCCGAGCTCATCAAGGAGAACATGCACATGAAGCTCTACATGGAGGGAACCGTCA
 ACAACCACCACTTCAAGTGCACCTCCGAGGGAGAGGGAAAAGCCATACGAGGGAACCCAAAC
 CATGCGTATCAAAGtaagtttaaacatataataactaactaaccctgatttttaaatcttcagGCCGTCGAGGGAGGACCACT
 CCCATTTCGCTTCGACATCCTCGCCACCTCCTTCATGTACGGATCCAAGACCTTCATCAACCA
 CACCAAGGAATCCAGACTTCTTCAAGCAATCCTTCCAGAGGGATTACCTGGGAGCGTG
 TCACCACCTACGAGGACGGAGGAGTCTCACCAGCCACCAAGACACCTCCCTCCAAGACGG
 ATGCCTCATCTACAACGTCAAGATCCGTGGAGTCAACTTCCCATCCAACGGACCAGTCATGC
 AAAAGAAGACCCTCGGATGGGAGGCCTCCACCAGACCCTTACCAGCCGACGGAGGACT
 CGAGGGACGTGCCGACATGGCCCTCAAGCTCGTCGGAGGAGGACACCTCATCTGCAACCTC
 AAGtaagtttaaacatgattttactaactaactaatctgatttttaaatcttcagACCACCTACCGTTCCAAGAAGCCAGCCAAG
 AACCTCAAGATGCCAGGAGTCTACTACGTTCGACCGTCGTCTCGAGCGTATCAAGGAGGCCG
 ACAAGGAGACCTACGTTCGAGCAACACGAGGTCGCCGTCGCCCGTTACTGCGACCTCCCATCC
 AAGCTCGGACACCGTTAAaatcatatgttttctctcaactctcttttttc

PHX1464: *flp-11*(*syb1464*[*flp-11-SL2-egl-23cDNA(L229N)-linker-mKate2*])X

>*flp-11b-SL2(gpd-2)-egl-23(L229N)-linker(GSGSGSGS)-mKate2(two introns)*

ctattgtagTGC GGAGAAACGTGCCATGCGGAACGCCTTGGTTCGATTTGGAAGAGCTAGTGGTG
 GAATGAGAAATGCTCTCGTTAGATTTCGGAAAAGAGGTCTCCATTGGACGAGGAAGACTTTGCT
 CCAGAGAGCCCACTCCAGGGAAAACGGAACGGTGCCCCACAACCATTGgtaagttgtcttaaaatftttct
 tccgcttttgcctttgcttcatgtgtcgtttattttgctttgcagttcgtttggccgatccggtaactcgaccacatgcacgacctttgtcgactctcagAA
 GCTCAAGTTCGCCAACAAACAAGTAATGACCGAGGACGACCGTCTTCTGCTCGAACAACTCCT
 GCGACGAATTCATCATTAAGctgtctcatctactttcacctagtttaactgcttcttaaaatctatgcttctcttagtatctaaatfttccta
 gaagcttacaagatataaaatgctcttctcaataaagggttatatttattcatcttattgaatcgccatttctctgttttgcgagtttatatacctccaattttc
 ttctattgtattttcaacttctaattttaattcagggaaactgcttcaacgcatcATGAAGCTCACGTTGAAGAAATCCGTATTCT
 CAAGGGATAAACATATCTTGCAAAAAGGCGACACCACTATTTCGTTCACTTTCTAATGATAGTA
 AGTGTGGGTGCCTACGCAATATTTGGAGCACTTGTAATGAGAAGTCTTGAATCGAGAAGTGT
 CACAAGTATTGAAAAGAAGACGGATGTTACAGAAAGACATGTTAATTTGACTAATTTTCAAC
 ATCCACCAACTCCAATCACATTAGAGCAAAGACATCGACGGAGACGCAGACATAATGAGAC
 AGCTTTGGAAGACCATTGTCTGAAAAATTATCCAGAGAAAAACGTGCAGCAGCGCATATC
 ATGAGAAGTCGAAAATGCGTTATCAGTGTGATAAAGAAAAATGTCAAGCATGGAATGTTTCAT
 TTGACACTCTCGACGAGAAGCTCGTAAAAGCACTCGATGAATGTTACCACGTGGCAGTTGAA
 CATAATACTCATGTGAATCATGTACTTTTACGAATAGTAAGGAAGAAGTGGAGTCAGTTGG
 GGAAGAAGCAGAAGAAGATGTTCCGAATGGTCATTTATGGACTCGTTGTTGTTGCATTCA
 CTGTTATTACGACGATTGGATACGGAAACGTGGCACCTCGAACATTTGGTGGCCGCTATTI
 GTCATTGGTTATGGTCTAATTGGTATTCCGTTTACAAAACCTGGCAATTGCAGATCTCGGAAA
 ATTCATATCAGAAAATGATGGTGGAGGGCGAAAAAGTTTTTGTAGGAAAACCTGGAAAAAACTC
 AAAAAAGCGTGGAACCCGAATTTTCATTCGCGCAAAGGATCTTTCAAATACGGATATTGAGG
 AGAAAAATATTGGATAATGAGAAAAATCGAAAAATGAGCCGGAACCTTCAGAAAGTATCAGAAG
 AAGAAGACGATTTGACAGAGACAGAAGCCACGTCACTTTTCATTTTATTTTGGTTTATATC
 GCATTTGGAGGGTTCATGTTAGCTGCTTATGAACCTGATATGGACTTTTCAAAGCGGTCTAC
 TTTAATTTTGTGACATTGACATCAATTGGTCTGGGAGATATTGTACCGAGAAGTGAAACCTA
 TATGCTCATTACAATAGTCTACATTGCAATTTGCTTGTCTTACCACAATTTGCCATTGAAAT
 CGCCGAGATGCATTGAAGAAGCTGCATTATTTTGGAAAGAAAAATCGAAAAATGCTTGGAAAT
 GTGGCTATATGGTTTGGAGGAAAGAAATTACAATGAAAGCACTGGTCAAAAACCTCGGTG
 ACCAGTTCAATCTTCCAACACTACCGTAGTCAAGAATTTGAATTTGGATCATTTTGTGGATCAA
 GCGATTAAGTGGAGGAAGGAGAGATTGAGACACTCAGACCGCCGCCTTATGAGCCACCGT
 CTGATCGATTTGAAGCTGAATTCGCTGATGAACCAGAAATGTGAATGGATCCGTGATCCGACT
 CCAACTCCACCCCATCACCTCAACCGGTTTATCGTCTTCCATCTCCAAAACAGTTACACCG
 GAACCTCTACCAAGTCCAACAATAACTGATGTATCACTTTCGATTGCAACACCATCACCTGA
 AGAATCGGATGATGATCAAGAACTAATTCTCCATCACCTGAACCGAGTCCAGTTTCGAGAGC
 CAACTCCACCACCGCCTCCACGGGAGCCAAACACCTCGTGAGCCAACCTCCTGAGCCAGAGCC
 AGTTTCGAGAGCCGACGCTCCACCTCCGCCACCTGCCAAGCCTCCGCTCCACTGACTGCCGCTG
 AAATCGCGGCTCAAAAACGCAAAGCGTACAGCGAAGAAGCATGGCGTCGATACCAAGAAT
 ACCAGAAACAATGGAAGAAGTTCGTCAAAACCTCAGAAAACCTCCCGCACCATCTGGAGCCTC
 TACATCAGGGGCATCAACATCAAAACCGTCTGGAACATCACCGGAAAGTGGAGCCGGAGTA
 TGTACTGGACCATCAACAAGGAGTCAATCAATAACATCAGTTGCATCTGGAAAGACATCAA
 GAAGTGCAACACCGGAAAGCAAGAAATCATCACATTTGAGTGGCTCATCGAGAAGAGAAAG
 CGGTGGAAAAAGGATCCGGATCCGGATCCGGATCCGGAATGTCCGAGCTCATCAAGGAGAAC
 ATGCACATGAAGCTCTACATGGAGGGAACCGTCAACAACCACCACTTCAAGTGCACCTCCG
 AGGGAGAGGGAAAGCCATACGAGGGAACCCAAACCATGCGTATCAAGgtaagtttaaacatataataacta
 actaacctgattatttaatttcagGCCGTGAGGGAGGACCCTCCATTCGCCTTCGACATCCTCGCCAC
 CTCCTTCATGTACGGATCCAAGACCTTCATCAACCACACCCAAGGAATCCAGACTTCTTCA
 AGCAATCCTTCCAGAGGGATTACCTGGGAGCGTGTACCACCTACGAGGACGGAGGAGT
 CCTCACCGCCACCAAGACACCTCCCTCCAAGACGGATGCCTCATCTACAACGTCAAGATCC
 GTGGATCAACTTCCCATCCAACGGACCATGATGCAAAAAGAAGACCCCTCGGATGGAGGC
 CTCCACCGAGACCTCTACCCAGCCGACGGAGGACTCGAGGGACGTGCCGACATGGCCCTC
 AAGCTCGTCGAGGAGGACACCTCATCTGCAACCTCAAAGgtaagtttaaacatgattttactaactaactaactgatt
 aaatttcagACCACCTACCGTTCCAAGAAGCCAGCCAAGAACCTCAAGATGCCAGGAGTCTACTA
 CGTCGACCGTCGTCTCGAGCGTATCAAGGAGGCCGACAAGGAGACCTACGTCGAGCAACAC
 GAGGTCGCCGTCGCCGTTACTGCGACCTCCCATCCAAGCTCGGACACCGTTAAaaatcatatgtttt
 ctctctcacactctctttttc

PHX2146: *flp-11(syb2146[SL2::egl-23(n601)::linker(GSGSGSGS)::mKate2])X*

>flp-11b-SL2(gpd-2)-egl-23(n601)codon-optimized-linker(GSGSGSGS)-mKate2(two introns)

CGTTAGATTCGGAAAGAGGTCTCCATTGGACGAGGAAGACTTTGCTCCAGAGAGCCCCTCC
 AGGGAAAACGGAAACGGTGCCCCACAACCATTTGgtaagttgtcttaaattttctccgcttttgcctttgcttcatgtgctg
 ttttttgccttgcagttcgtttggccgatccggtaactcgaccacatgcacgacctttgtcgactctcagAAGCTCAAGTTCGCCAAC
 AACAAGTAATGACCGAGGACGACCGTCTTCTGCTCGAACAACCTCTGCGACGAATTCATCAT
 TAAgctgtctcatcctacttccactagtaactgctgtcttaaaatctatgcttctcttagtatctaaaattttcttagaagcttacaagtataaatgctc
 ttctcaataaaggtgtatatttattcatctattgaatctgccatttctcctgttttgcgagttatataacctccaattttcttattgtatttcaacttcaattt
 tcagggaactgcttcaacgcateATGAAGCTCACCTCAAGAAGTCCGTCTTCTCCCGTGACAAGCACAT
 CCTCCAAAAGGCCACCCACTCTTCGTCCACTTCTCATGATCGTCTCCGTCCGAGCCTACGC
 CATCTTCGGAGCCCTCGTCATGCGTTCCTCGAGTCCCGTACCGTACCTCCATCGAGAAGA
 AGACCGAGTCCACCGTCACGTCAACCTCACCAACTTCCAACACCCACCAACCCCAATC
 ACCCTCGAGCAACGTACCGTCCGTGTCGTCACAACGAGACCGCCCTCGAGGACCACT
 CTCCGAGAAGCTCTCCCGTGAGAAGCGTGCCGCCGCCACATCATGCGTTCCTGTAAGTGCG
 TCATCTCCGTTCATCAAGAAGATGTCCTCCATGGAGTGCTCCTTCGACACCCTCGACGAGAAG
 CTCGTCAAGGCCCTCGACGAGTGCTACCACGTGCGCGTCGAGCACAACCCACGTCAACCA
 CGTCTCTTACCAACTCCAAGGAGGAGGTGAGTCCGTCCGAGAGGAGGCCGAGGAGGAC
 GTCTCCGAGTGGTCTTTCATGGACTCCCTCCTCTTCGCCTTACCGTTCATCACCACCATCGGA
 TACGAAACGTGCCCCACGTACCTTCGGAGGACGTCTCTTCGTCATCGGATACGGACTCAT
 CGGAATCCCATTCACCTCCTCGCCATCGCCGACCTCGGAAAGTTCATCTCCGAGATGATGG
 TCGAGGCCAAGTCTTCTGCCGTAAGACCTGGAAGAAGCTCAAGAAGGCCTGGAACCCAAA
 CTTTCATCCGTGCCAAGGACCTCTCCAACACCGACATCGAGGAGAAGATCCTCGACAACGAG
 AAGATCGAGAACGAGCCAGAGACCTCCGAGGTCTCCGAGGAGGAGGACGACCTCACCAG
 ACCGAGGCCACCTCCCTCTTCATCCTCTTCCCTCGTCTACATCGCCTTCGGAGGATTTCATGCTC
 GCCGCCTACGAGCCAGACATGGACTTCTTCAAGGCCGTCTACTTCAACTTCGTACCCCTCAC
 CTCCATCGGACTCGGAGACATCGTCCACGTTCCGAGACCTACATGCTCATCACCATCGTCT
 ACATCGCCATCGGACTCGCCCTCACCACCATCGCCATCGAGATCGCCGTCGACGCCCTCAAG
 AAGTCCACTACTTCGGACGTAAGATCGAGAACGTTCGAAACGTTCGCCATCTGGTTCGGAG
 GAAAGAAGATCACCATGAAGGCCCTCGTCAAGAACCTCGGAGACCAATTCACCTCCCAAC
 CACCGTTCGTAAGAACCTCAACCTCGACACTTCGTTCGACCAAGCCATCAAGGTTCGAGGAG
 GGAGAGATCGAGACCCTCCGTCCACCACCATACGAGCCACCATCCGACCGTTTCGAGGCCG
 AGTTCGCCGACGAGCCAGAGTGGAGTGGATCCGTGACCCAACCCCAACCCACCCACCATC
 CCCACAACAGTCTACCGTCTCCATCCCCAAAGCCAGTCAACCCAGAGCCACTCCCATCCC
 CAACCATCACCGAGTCTCCCTCGCCATCGCCACCCCATCCCCAGAGGAGTCCGACGACGAC
 CAAGAGTCACTCCTCCATCCCCAGAGCCATCCCCAGTCCGTGAGCCAACCCACCCACCCAC
 ACCAGTTCGAGCCAACCCACGTGAGCCAACCCAGAGCCAGAGCCAGTCCGTGAGCCAACC
 CCACCACCACCACCAGCCAAGCCACGTCCACTACCGCCGCCGAGATCGCCGCCAAA
 AGCGTAAGGCCTACTCCGAGGAGGCCGTCGTTACCAAGAGTACCAAAAAGCAATGGAA
 GAAGTTCGTCAAACCCAAAAGACCCAGCCCCATCCGGAGCCTCCACCTCCGGAGCCTCCA
 CCTCCAAGCCATCCGAAACCTCCCCAGAGTCCGGAGCCGGAGTCTGCACCGGACCATCCACC
 CGTTCCCAATCCATCACCTCCGTGCTCCGAAAGACCTCCCGTTCGCCACCCAGAGTC
 CAAGAAGTCTCCACCTCTCCGGATCCTCCCGTTCGTGAGTCCGGAGGAAAGGGATCCGGAT
 CCGGATCCGGATCCGGAATGTCCGAGCTCATCAAGGAGAACATGCACATGAAGCTCTACAT
 GGAGGGAACCGTCAACAACCACCACTTCAAGTGCACCTCCGAGGGAGAGGGAAAGCCATAC
 GAGGGAACCCAAACCATGCGTATCAAGgtaagtttaacatatataactaactaacctgattttaaattttcagGCCGTC
 GAGGGAGGACCACTCCCATTCGCCTTCGACATCCTCGCCACCTCCTTCATGTACGGATCCAA
 GACCTTCATCAACCACACCCAAGGAATCCAGACTTCTTCAAGCAATCCTTCCCAGAGGGAT
 TCACCTGGGAGCGTGTACACCACTACGAGGACGGAGGAGTCCACCGCCACCCAAGACAC
 CTCCCTCCAAGACGGATGCCTCATCTACAACGTCAAGATCCGTGGAGTCAACTTCCCATCCA
 ACGGACCAGTCATGCAAAAAGAAGACCCTCGGATGGGAGGCCCTCACCGAGACCCTCTACCC
 AGCCGACGGAGGACTCGAGGGACGTGCCGACATGGCCCTCAAGCTCGTCCGAGGAGGACAC
 CTCATCTGCAACCTCAAGgtaagtttaacatgatttactaactaactaatctgatttaaattttcagACCACCTACCGTTCCA
 AGAAGCCAGCCAAGAACCTCAAGATGCCAGGAGTCTACTACGTGACCGTTCGTCTCGAGCG
 TATCAAGGAGGCCGACAAGGAGACCTACGTGAGCAACACGAGGTCCCGTCCGCCGTTAC
 TGCGACCTCCCATCCAAGCTCGGACACCGTTAAaaatcatatgtttttctctctcactctctttttc

PHX2193: *flp-11(syb2193[flp-11b-SL2(gpd-2)-mKate2-linker-tw-18(e1913)])X*

>flp-11b- SL2(gpd-2)-mKate2(two introns)-linker(GSGSGSGS)- twk-18(e1913)(one intron)

gtaagttgtcttaaaatcttccgctttttgcctttgcttcatgtgtcgtttatcttgccttgcagttcgtttggccgatccggcaactcgaccacatgcacga
ccttttgcgactcttcagAAGCTCAAGTTCGCCAACAAACAAGTAATGACCGAGGACGACCGTCTTCTGC
TCGAACAACCTCTGCGACGAATTCATCATTAAGctgtctcatctactttcacctagtaactgcttcttaaaatctatgcttc
tcttagtatctaaaatctcctagaagcttacaagtataaaatggctcttctcaataaaaggtgtatatttattcatcttattgaatctgccatttctcgttttgcg
agttatatacctccaatcttcttctattgtatttcaacttctaatttaattcagggaactgctcaacgcataaaaATGTCCGAGCTCATCA
AGGAGAACATGCACATGAAGCTCTACATGGAGGGAACCGTCAACAACCACCTTCAAGTG
CACCTCCGAGGGAGAGGGAAAGCCATACGAGGGAAACCAACCATGCGTATCAAGgtaagttta
acatataataactaactaacctgattattfaaatttcagGCCGTCGAGGGAGGACCACTCCATTCGCCTTCGACATC
CTCGCCACCTCCTTCATGTACGGATCCAAGACCTTCATCAACCACACCAAGGAATCCCAGA
CTTTCAAGCAATCCTTCCCAGAGGGATTACCTGGGAGCGTGTACCACCTACGAGGACG
GAGGATCCCTCACCGCAACCAAGACACTCCCTCCAAGACGGATGCCTCATCTACAACGTC
AAGATCCGTGGAGTCAACTTCCCATCCAACGGACCAGTCATGCAAAAAGAAGACCCTCGGAT
GGGAGGCCTCCACCGAGACCCTTACCCAGCCGACGGAGGACTCGAGGGACGTGCCGACAT
GGCCCTCAAGCTCGTCGGAGGAGGACACCTCATCTGCAACCTCAAAGtaagtttaaacatgatttactaacta
actaatctgatttaaatcttcagACCACCTACCGTTCGAAGAAGCCAGCCAAGAACCTCAAGATGCCAGGA
GTCTACTACGTCGACCGTCGTCTCGAGCGTATCAAGGAGGCCGACAAGGAGACCTACGTCG
AGCAACACGAGGTCGCCGTCGCCCGTTACTGCGACCTCCCATCCAAGCTCGGACACCGTGGA
TCCGGATCCGGATCCGGATCCGGAATGGCCATCGTCGCCCAAGGAGTCTCCACCATCCTCAC
CACCTTCCAAAAGACCTTCAAGGGACTCCTCCCCTCATCATCCTCGTCGCCTACACCCTCCT
CGGAGCCTGGATCTTCTGGATGATCGAGGGAGAGAACGAGCGTGAGATGCTCATCGAGCAA
CAAAAGGAGCGTGACGAGCTCATCCGTCGTACCGTCTACAAGATCAACCAACTCCAAATCA
AGCGTCAACGTCGTCTCATGACCGCCGAGGAGGAGTACAACCGTACCGCAAGGTCTCAC
CACCTTCCAAGAGACCCTCGGAATCGTCCCAGCCGACATGGACAAGGACATCCACTGGACC
TTCCTCGGATCCATCTTACTGTCATGACCGTCTACACCACCATCGGATACGGAAACATCGT
CCCAGGAACCGGATGGGGACGTTTTCGCCACCATCCTCTACGCCTTCATCGGAATCCCCTCA
CCGTCCTCTCCCTTACTGCCTCGACTCCCTCTTCGCCAAGGGATGCAAGATGCTCTGGCGTT
TCTTCTCAAGTCCACCCGTGTCTCTCCAAGGACCTCTCCAACAAGATCTCCGAGGCCGCC
GACAACATCGAGGAGGGAACCAACCGCCATCACCCATCCGCCGAGAAAGtaagtttaaacagttcggtag
taactaacatacatatttaaatcttcagACCGAGAACAACGACGACGACCTCCTCTCCTTCCAATCTCCGGAC
TCCTCCTCATCACCGTCATCTGGGTCATCTTCTGCGCCGTCCTCTCACCTTCTCGAGGAGT
GGGACTTCGGAACCTCCCTTACTTACCCTCATCTCCTTACCACCATCGGATTCGGAGACA
TCCTCCCATCCGACTACGACTTCATGCCAATCGTGGAGTCTCCTCCTCATCGGACTCTCCC
TCGTCTCACCGTCATGACCCTCATCCAACAACAATAATCGAGGCCCTCGCCTCCGGAATGAAG
GACAACATCGACCAAGAGTACGCCCGTGCCTCAACGAGGCCCGTGAGGACGGAGAGGTCCG
ACGAGCACGTCGACCCAGAGGAGGACCCAGAGAACAACAAGAAGTCTTCGACGCCGTCAT
CTCCCATGAACTGGTCCAAGCGTGGACTTACTACCTCCTCCCAGACTCCCAAAAGAAGG
AGCTCGCAAGCAATCCGAGAAGAAGATGGGACGTAAGTCCATCAAGATCCAAACCGACAA
CGACCTCCTCGAGACCCTCATCCGTGAGGAGATCCTCAAGGCCGAGCTCAACAACGAGATG
CACAAGTACACCGCCCCACGTTCTTCCCACCAACCAAGCTCGTCTACTCCGACGTCCGTGA
GAAGGAGGTCCCAATCGAGGTCGTCCGTGTGAGCACTTCAACCACGGAAACGAGGACTAC
CTCGAGCACGACATCTAAaatcatatgttttctctctcacactctctttttc

6.2. Recurrently used MATLAB scripts

6.2.1. Extract individual neuron intensities

This script can also be used to extract intensities from several neurons that are treated as a single large neuron. Thresholds need to be adjusted accordingly. The script requires 4 input parameters and returns the normalized intensity and speed values. It furthermore saves intensities and speed values as text files.

```
function [bgsubtraction1, speed] =
highestintensitysingleworm(cutoutlength, thresh, pixelsignal, time)
%input parameters are the length of the cutout square that includes
%the signal and background, the threshold for what is recognized as
%signal vs.background, the number of pixel from the square that are
%taken as signal and the time between frames in seconds
%[s,v] = highestintensitysingleworm(18,500,100,3); for flp-11::GCaMP
% and PVC:ReaChR

if ~mod(cutoutlength,2)
    error('first input argument needs to be even')
end
%first red in files
name = '*HBR2420.tif'; %change name here if necessary
tifffiles = dir(name);
    for kf = 1:length(tifffiles)
        images = imread(tifffiles(kf).name, 1); %read in images
        halfwidth = cutoutlength/2;
        square2 = [];

        %use threshold to create binary from image
        length_worm = length(images)/4;
        for k = 1:4
            for p = 1:4
                worm = images((k*length_worm-length_worm+1):k*length_worm,
(p*length_worm-length_worm+1):p*length_worm);
                mask(:, :) = worm < thresh;
                imagestack = worm;
                imagestack(mask) = 0;
                bw_image = (imagestack > 0);
                % find largest centroid and center of mass
                L = bwlabel(bw_image);
                s_1 = regionprops(L, 'area', 'centroid');
                area_vector1 = [s_1.Area];
                [tmp, idx] = max(area_vector1);
                if ~isempty(idx)
                    centroids(kf, :, 4*k-4+p) = s(idx(1)).Centroid; %change index if you
                    want second largest blob
                    if ~mod(kf,300) %control if signal is identified correctly
                        figure; imagesc(worm)
                        hold on;
                        plot(centroids(kf,1,4*k-4+p),centroids(kf,2,4*k-4+p),'*', 'color','r')
                        title('found intensity')
                    end

                %check if cut out frame is in image, otherwise shift
                xmaxpix = size(worm,1)-1;
```

Appendix

```
ymaxpix = size(worm,2)-1;

if round(centroids(kf,1,4*k-4+p)) < halfwidth+1
    centroids(kf,1,4*k-4+p) = halfwidth+1;
end
if round(centroids(kf,1,4*k-4+p))+halfwidth > xmaxpix
    centroids(kf,1,4*k-4+p) = xmaxpix-halfwidth;
end

if round(centroids(kf,2,4*k-4+p)) < halfwidth+1
    centroids(kf,2,4*k-4+p) = halfwidth+1;
end
if round(centroids(kf,2,4*k-4+p))+halfwidth > ymaxpix
    centroids(kf,2,4*k-4+p) = ymaxpix-halfwidth;
end

%cut out square around signal
square = worm(((round(centroids(kf,2,4*k-4+p))-
halfwidth):(round(centroids(kf,2,4*k-
4+p))+halfwidth)), ((round(centroids(kf,1,4*k-4+p))-
halfwidth):(round(centroids(kf,1,4*k-4+p))+halfwidth)));

%rearrange matrix into array
num = size(square,1);
allvalues = [];
for l= 1:num
    allvalues = [allvalues, square(l,:)];
end

%sort for highest intensities - defined in input how many intensities
are the signal
%the other intensities are the background
sortint = sort(allvalues);
signallval = sortint(end:-1:(end-pixelsignal));
signallmean = mean(signallval);
backgroundlval = sortint(1:(end-(pixelsignal+1)));
backgroundlmean = mean(backgroundlval);
bgsubtraction1(kf,4*k-4+p) = signallmean-backgroundlmean;
    else
        centroids(kf, :,4*k-4+p) = [nan nan];
        bgsubtraction1(kf,4*k-4+p) = nan;
    end
end
end
end

%calculate speed from the position of the highest intensity value
deltay = zeros(kf-1,1);
deltax = zeros(kf-1,1);
speed = zeros(kf-1,1);

for u=1:16
    for l = 1:(length(centroids)-1)
        deltay(l,u) = centroids((l+1),2,u)-centroids(l,2,u);
        deltax(l,u) = centroids((l+1),1,u)-centroids(l,1,u);
        speed(l,u) = 1.6*sqrt(deltax(l,u)^2+deltay(l,u)^2)/time; %already
included camera pixel conversion
    end
    bouts(:,u) = boutdetection(speed(:,u),18,0.1);
end
end

%take out positions without worms
pos_withoutworm = isnan(speed(1,:));
```

```

    speed(:,pos_withoutworm) = [];
    bgsubtraction1(:,pos_withoutworm) =[];
    bouts(:,pos_withoutworm)=[];
save('200429_HBR2420_GCaMP_intensity.txt', 'bgsubtraction1','-ascii');
save('200429_HBR2420_speed.txt', 'speed','-ascii'); %change filenames
save('200429_HBR2420_bouts.txt', 'bouts','-ascii'); %here
end

```

6.2.2. Bout detection

This script requires a speed vector, a minimum bout length threshold and a normalized maximum speed threshold as input.

```

function q = boutdetection(speed, timethresh, speedthresh)

speedsmooth = smooth(speed,50);
normspeed = (speedsmooth-min(speedsmooth)) ./ (max(speedsmooth) -
min(speedsmooth));
%normspeed = smooth(speed,50);
for u = 1:length(normspeed)
if normspeed(u) < speedthresh
    u;
q(u) = 1;
else
q(u)=0;
end
end

boutstarts = [];
boutends = [];
for n = 1:(length(q)-1)
    if q(n) == 0 & q(n+1) == 1
        boutstarts = [boutstarts, n+1];
    end
    if q(n) == 1 & q(n+1) == 0;
        boutends = [boutends, n];
    end
end
if length(boutstarts) < length(boutends)
    boutstarts = [1, boutstarts];
else if length(boutstarts) > length(boutends)
    boutends = [boutends, length(normspeed)];
end
end

for k = 1:size(boutstarts,2)
    boutlength(k) = boutends(k)-boutstarts(k);
    if boutlength(k) < timethresh
        q(boutstarts(k):boutends(k)) = 0;
    end
end
end
figure; plot(normspeed)
hold on
plot(q./2)
end

```

6.2.3. Calculation of the direction of movement from the wormtracker data

```
% this program reads in dat files for the noses and centroids
% generated by the worm tracker. it then matches the files and
% detects the direction of movement

% the dat files have columns in the following order:
% frame no; nose x; nose y; tail x; tail y; centroid x; centroid % y;
nose speed; centroid speed

close all
clear all

nose_files = dir('*Nose.dat');

direction = zeros(1420,size(nose_files,1));
for i = 1:size(nose_files,1)
    data_nose = importdata(nose_files(i).name);
    correct_data_nose = data_nose.data(1:1420,:);
    nose_x = correct_data_nose(:,2);
    nose_y = correct_data_nose(:,3);
    centroid_x = correct_data_nose(:,4);
    centroid_y = correct_data_nose(:,5);

    for j = 1:(size(nose_x)-1)
        dist_noseA_centroidB(j) = sqrt((nose_x(j)-
        centroid_x(j+1))^2+(nose_y(j)-centroid_y(j+1))^2);
        dist_noseB_centroidA(j) = sqrt((nose_x(j+1)-
        centroid_x(j))^2+(nose_y(j+1)-centroid_y(j))^2);

        if dist_noseA_centroidB(j) < dist_noseB_centroidA(j)
            direction(j,i) = 1;
        else if dist_noseA_centroidB(j) > dist_noseB_centroidA(j)
            direction(j,i) = -1;
        end
    end
end

all_direction = sum(direction,2);
end
```

6.2.4. Sleep bout alignment including sleep fraction and time in sleep

```
clear all; close all; clc

%first find files in directory
gcamp_files = dir('*intensity*.txt');
speed_files = dir('*speed*.txt');

%find length of lethargus files
%define how many seconds between frames
length_lethargus = 0;
for p=1:length(gcamp_files)
    read_files = textread(gcamp_files(p).name);
```

```

    time_between_frames = read_files(2,1);
    if length_lethargus < length(read_files)
        length_lethargus = length(read_files);
    end
end

% make nan matrices for lethargus files with correct size
gcamp = nan(length_lethargus,length(gcamp_files));
speed = nan(length_lethargus,length(gcamp_files));
bouts = nan(length_lethargus,length(gcamp_files));

%now read in files and detect sleep bouts
for i=1:length(gcamp_files)
    gcamp_read = textread(gcamp_files(i).name);
    gcamp(1:length(gcamp_read),i) = gcamp_read(:,2);
    speed_read = textread(speed_files(i).name);
    speed(1:length(speed_read),i) = speed_read(:,2);
    bouts(1:length(speed_read)-1,i) =
boutdetection(speed(1:length(speed_read)-1,i), 18, 0.1);
    clear gcamp_read
    clear speed_read
end

%now normalize gcamp
gcamp_sort = sort(gcamp);
gcamp_baseline = mean(gcamp_sort(61:80,:));
normalized_gcamp = (gcamp-gcamp_baseline)./gcamp_baseline;

%sleep fraction and sleep time in minutes for each animal

for u=1:size(bouts,2)
    nonan_len = length((bouts(~isnan(bouts(:,u))),u));
    sum_animal = nansum(bouts(:,u));
    sleep_fraction(u) = sum_animal/nonan_len;
    sleep_time(u) = sum_animal*time_between_frames/60;
    lethargus_time(u) = nonan_len*time_between_frames/60;
end

%bout alignment
framesperminute = 6;
timebeforesleep = 3;
timeaftersleep = 5;
boutstart = [];

    for i=1:size(bouts,2)
        for j=(timebeforesleep*framesperminute):(size(bouts,1)-
(timeaftersleep*framesperminute))
            if bouts(j,i) == 0 & bouts(j+1,i) == 1 &
~isnan(bouts(j+1+(timeaftersleep*framesperminute),i)) &
bouts((j-12):(j-1),i) == 0 & sum(bouts((j+1):(j+6),i))==6
                boutstart = [boutstart; [i , j+1]];
            end
        end
    end

signal =
zeros(size(boutstart,1),framesperminute*(timebeforesleep+timeaft

```

```
ersleep)+1);
    for k=1:size(boutstart,1)
        animal = (boutstart(k,1));
        datapoint = boutstart(k,2);

        signal(k,:) = gcamp((datapoint-
            (timebeforesleep*framesperminute)):(datapoint+(timeaftersleep*fr
            amesperminute)), animal);
        velocity(k,:) = speed((datapoint-
            (timebeforesleep*framesperminute)):(datapoint+(timeaftersleep*fr
            amesperminute)), animal);
        sleep(k,:) = bouts((datapoint-
            (timebeforesleep*framesperminute)):(datapoint+(timeaftersleep*fr
            amesperminute)), animal);
    end

    bout_base = mean(signal(:,1:18),2);
    normalized_signal = (signal-bout_base)./bout_base;
    meansignal = nanmean(normalized_signal);
    meanvelocity = 5*nanmean(velocity);
    errorvelocity = nanstd(velocity)/sqrt(length(boutstart))
    errorsignal = nanstd(normalized_signal)/sqrt(length(boutstart));
    figure; errorbar(meansignal,errorsignal); figure;
    errorbar(meanvelocity, errorvelocity);
```


References

1. N. Gravett *et al.*, Inactivity/sleep in two wild free-roaming African elephant matriarchs - Does large body size make elephants the shortest mammalian sleepers? *PLoS One.* **12**(3): e0171903. (2017), doi:10.1371/journal.pone.0171903.
2. J. M. Siegel, Clues to the functions of mammalian sleep. *Nature.* **437**, 1264–71 (2005), doi:10.1038/nature04285.
3. S. S. Campbell, I. Tobler, Animal sleep: A review of sleep duration across phylogeny. *Neurosci. Biobehav. Rev.* **8**(3), 269–300 (1984).
4. H. Bringmann, Genetic sleep deprivation: using sleep mutants to study sleep functions. *EMBO Rep.* **20**(3), e46807 (2019), doi:10.15252/embr.201846807.
5. N. Stavropoulos, M. W. Young, Insomniac and cullin-3 regulate sleep and wakefulness in drosophila. *Neuron.* **72**(6), 964–976 (2011), doi:10.1016/j.neuron.2011.12.003.
6. T. Yokogawa *et al.*, Characterization of sleep in zebrafish and insomnia in hypocretin receptor mutants. *PLoS Biol.* **5**(10): e277. (2007), doi:10.1371/journal.pbio.0050277.
7. C. Cirelli, G. Tononi, Is sleep essential? *PLoS Biol.* **6** (8): e216 (2008), doi:10.1371/journal.pbio.0060216.
8. H. Bringmann, Sleep-active neurons: Conserved motors of sleep. *Genetics.* **208**(4), 1279–1289 (2018), doi:10.1534/genetics.117.300521.
9. M. H. Schmidt, The energy allocation function of sleep: A unifying theory of sleep, torpor, and continuous wakefulness. *Neurosci. Biobehav. Rev.* **47**, 122–153 (2014), doi:10.1016/j.neubiorev.2014.08.001.
10. A. A. Borbély, S. Daan, A. Wirz-Justice, T. Deboer, The two-process model of sleep regulation: A reappraisal. *J. Sleep Res.* **25**(2), 131–143 (2016). doi:10.1111/jsr.12371.
11. J. M. Krueger, M. G. Frank, J. P. Wisor, S. Roy, Sleep function: Toward elucidating an enigma. *Sleep Med. Rev.* **28**, 46–54 (2016), doi:10.1016/j.smrv.2015.08.005.
12. B. P. Tu, S. L. McKnight, Metabolic cycles as an underlying basis of biological oscillations. *Nat. Rev. Mol. Cell Biol.* **7**(9), 696–701 (2006), doi:10.1038/nrm1980.
13. J. Mellor, The molecular basis of metabolic cycles and their relationship to circadian rhythms. *Nat. Struct. Mol. Biol.* **23**(12), 1035–1044 (2016), doi:10.1038/nsmb.3311.
14. L. Xie *et al.*, Sleep drives metabolite clearance from the adult brain. *Science.* **342**(6156), 373–377 (2013). doi:10.1126/science.1241224.
15. A. J. Hill, R. Mansfield, J. M. N. G. Lopez, D. M. Raizen, C. Van Buskirk, Cellular stress induces a protective sleep-like state in *C. elegans*. *Curr. Biol.* **24**(20), 2399–2405 (2014), doi:10.1016/j.cub.2014.08.040.
16. J. H. Benington, H. Craig Heller, Restoration of brain energy metabolism as the function of sleep. *Prog. Neurobiol.* **45**(4), 347–360 (1995), doi:10.1016/0301-0082(94)00057-O.
17. D. Zada, I. Bronshtein, T. Lerer-Goldshtein, Y. Garini, L. Appelbaum, Sleep increases chromosome dynamics to enable reduction of accumulating DNA damage in single neurons. *Nat. Commun.* **10**(1), 895 (2019), doi:10.1038/s41467-019-08806-w.

18. M. Bellesi, D. Bushey, M. Chini, G. Tononi, C. Cirelli, Contribution of sleep to the repair of neuronal DNA double-strand breaks: Evidence from flies and mice. *Sci. Rep.* **6**, 36804 (2016), doi:10.1038/srep36804.
19. A. P. Vorster, J. Born, Sleep and memory in mammals, birds and invertebrates. *Neurosci. Biobehav. Rev.* **50**, 103-119 (2015), doi:10.1016/j.neubiorev.2014.09.020.
20. L. De Vivo *et al.*, Ultrastructural evidence for synaptic scaling across the wake/sleep cycle. *Science.* **355**(6324), 507-510 (2017), doi:10.1126/science.aah5982.
21. J. Seibt *et al.*, Protein synthesis during sleep consolidates cortical plasticity in vivo. *Curr. Biol.* **22**(8), 676-682 (2012), doi:10.1016/j.cub.2012.02.016.
22. G. H. Diering *et al.*, Homer1a drives homeostatic scaling-down of excitatory synapses during sleep. *Science.* **355**(6324), 511-515 (2017), doi:10.1126/science.aai8355.
23. Y. Dudai, A. Karni, J. Born, The Consolidation and Transformation of Memory. *Neuron.* **88**(1), 20-32 (2015), doi:10.1016/j.neuron.2015.09.004.
24. U. Wagner, S. Gais, H. Haider, R. Verleger, J. Born, Sleep inspires insight. *Nature.* **427**(6972), 352-355 (2004), doi:10.1038/nature02223.
25. C. L. Drake, T. Roehrs, T. Roth, Insomnia causes, consequences, and therapeutics: An overview. *Depress. Anxiety.* **18**(4), 163-176 (2003), doi:10.1002/da.10151.
26. M. Irwin, Why Sleep is Important for Health: A Psychoneuroimmunology Perspective. *Annu Rev Psychol.* **66**, 143-172 (2015), doi:10.1146/annurev-psych-010213-115205.
27. K. L. Knutson, K. Spiegel, P. Penev, E. Van Cauter, The metabolic consequences of sleep deprivation. *Sleep Med. Rev.* **11**(3), 163-178 (2007), doi:10.1016/j.smrv.2007.01.002.
28. G. N. Pires, A. G. Bezerra, S. Tufik, M. L. Andersen, Effects of acute sleep deprivation on state anxiety levels: a systematic review and meta-analysis. *Sleep Med.* **24**, 109-118 (2016), doi:10.1016/j.sleep.2016.07.019.
29. A. L. Loomis, E. N. Harvey, G. A. Hobart, Cerebral states during sleep, as studied by human brain potentials. *J. Exp. Psychol.* **21**(2), 127-144 (1937), doi:10.1037/h0057431.
30. I. G. Campbell, EEG recording and analysis for sleep research. *Curr. Protoc. Neurosci.* Chapter 10 (2009), doi:10.1002/0471142301.ns1002s49.
31. A. F. Jackson, D. J. Bolger, The neurophysiological bases of EEG and EEG measurement: A review for the rest of us. *Psychophysiology.* **51**(11), 1061-1071 (2014), doi:10.1111/psyp.12283.
32. E. Aserinsky, N. Kleitman, Regularly occurring periods of eye motility, and concomitant phenomena, during sleep. *Science.* **118**(3062), 273-274 (1953), doi:10.1126/science.118.3062.273.
33. J. Peever, P. M. Fuller, The Biology of REM Sleep. *Curr. Biol.* **27**(22), R1237-R1248 (2017), doi:10.1016/j.cub.2017.10.026.
34. D. J. Dijk, Regulation and functional correlates of slow wave sleep. *J. Clin. Sleep Med.* **5**(2 Suppl), S6-S15 (2009), doi:10.5664/jcsm.5.2s.s6.
35. D. Léger *et al.*, Slow-wave sleep: From the cell to the clinic. *Sleep Med. Rev.* **41**, 113-132 (2018), doi:10.1016/j.smrv.2018.01.008.
36. T. E. Scammell, E. Arrigoni, J. O. Lipton, Neural Circuitry of Wakefulness and Sleep. *Neuron.* **93**(4), 747-765 (2017), doi:10.1016/j.neuron.2017.01.014.

37. H. R. Colten, B. M. Altevogt, *Sleep disorders and sleep deprivation: An unmet public health problem*. National Academies Press (US). Chapter Sleep Physiology, 33-54 (2006).
38. K. S. Chen *et al.*, A Hypothalamic Switch for REM and Non-REM Sleep. *Neuron*. **97**(5), 1168-1176.e4. (2018), doi:10.1016/j.neuron.2018.02.005.
39. M. H. Silber *et al.*, The visual scoring of sleep in adults. *J. Clin. Sleep Med.* **3**(5) (2007), doi:10.5664/jcsm.26814.
40. C. B. Saper, T. E. Scammell, J. Lu, Hypothalamic regulation of sleep and circadian rhythms. *Nature*. **437**(7063), 1257-1263 (2005), doi:10.1038/nature04284.
41. C. B. Saper, P. M. Fuller, N. P. Pedersen, J. Lu, T. E. Scammell, Sleep State Switching. *Neuron*. **68**(6), 1023-1042 (2010), doi:10.1016/j.neuron.2010.11.032.
42. P. M. Fuller, J. J. Gooley, C. B. Saper, Neurobiology of the sleep-wake cycle: Sleep architecture, circadian regulation, and regulatory feedback. *J. Biol. Rhythms*. **21**(6), 482-493 (2006), doi:10.1177/0748730406294627.
43. A. Chen *et al.*, QRFP and its receptors regulate locomotor activity and sleep in zebrafish. *J. Neurosci.* **36**(6), 1823-1840 (2016), doi:10.1523/JNEUROSCI.2579-15.2016.
44. G. Artiushin, A. Sehgal, The *Drosophila* circuitry of sleep-wake regulation. *Curr. Opin. Neurobiol.* **44**, 243-250 (2017), doi:10.1016/j.conb.2017.03.004.
45. W. J. Joiner, A. Crocker, B. H. White, A. Sehgal, Sleep in *Drosophila* is regulated by adult mushroom bodies. *Nature*. **441**(7094), 757-760 (2006), doi:10.1038/nature04811.
46. D. Sitaraman *et al.*, Propagation of Homeostatic Sleep Signals by Segregated Synaptic Microcircuits of the *Drosophila* Mushroom Body. *Curr. Biol.* **25**(22), 2915-2927 (2015), doi:10.1016/j.cub.2015.09.017.
47. P. R. Haynes, B. L. Christmann, L. C. Griffith, A single pair of neurons links sleep to memory consolidation in *Drosophila melanogaster*. *Elife*. **4**, e03868 (2015), doi:10.7554/eLife.03868.
48. K. Foltenyi, R. J. Greenspan, J. W. Newport, Activation of EGFR and ERK by rhomboid signaling regulates the consolidation and maintenance of sleep in *Drosophila*. *Nat. Neurosci.* **10**(9), 1160-1167 (2007), doi:10.1038/nn1957.
49. J. M. Donlea, M. S. Thimgan, Y. Suzuki, L. Gottschalk, P. J. Shaw, Inducing sleep by remote control facilitates memory consolidation in *Drosophila*. *Science*. **332**(6037), 1571-1576 (2011), doi:10.1126/science.1202249.
50. Q. Liu, S. Liu, L. Kodama, M. R. Driscoll, M. N. Wu, Two dopaminergic neurons signal to the dorsal fan-shaped body to promote wakefulness in *Drosophila*. *Curr. Biol.* **22**(22), 2114-2123 (2012), doi:10.1016/j.cub.2012.09.008.
51. R. Y. Moore, V. B. Eichler, Loss of a circadian adrenal corticosterone rhythm following suprachiasmatic lesions in the rat. *Brain Res.* **42**(1), 201-206 (1972), doi:10.1016/0006-8993(72)90054-6.
52. M. R. Ralph, R. G. Foster, F. C. Davis, M. Menaker, Transplanted suprachiasmatic nucleus determines circadian period. *Science*. **247**(4945), 975-978 (1990), doi:10.1126/science.2305266.
53. A. Balsalobre, F. Damiola, U. Schibler, A serum shock induces circadian gene expression in mammalian tissue culture cells. *Cell* **93**(6), 929-937 (1998), doi:10.1016/S0092-8674(00)81199-X.
54. G. Tosini, M. Menaker, Circadian rhythms in cultured mammalian retina. *Science*. **272**(5260), 419-421 (1996), doi:10.1126/science.272.5260.419.

55. S. Yamazaki *et al.*, Resetting central and peripheral circadian oscillators in transgenic rats. *Science*. **288**(5466), 682-685 (2000), doi:10.1126/science.288.5466.682.
56. E. D. Buhr, J. S. Takahashi, Molecular components of the mammalian circadian clock. *Handb. Exp. Pharmacol.* (2013), doi:10.1007/978-3-642-25950-0-1.
57. J. F. Duffy, C. A. Czeisler, Effect of Light on Human Circadian Physiology. *Sleep Med. Clin.* **4**(2), 165-177 (2009), doi:10.1016/j.jsmc.2009.01.004.
58. R. J. Nelson, I. Zucker, Absence of extraocular photoreception in diurnal and nocturnal rodents exposed to direct sunlight. *Comp. Biochem. Physiol. -- Part A Physiol.* (1981), doi:10.1016/0300-9629(81)90651-4.
59. F. G. Do Amaral, J. Cipolla-Neto, A brief review about melatonin, a pineal hormone. *Arch. Endocrinol. Metab.* **62**(4), 472-479 (2018), doi:10.20945/2359-3997000000066.
60. I. V. Zhdanova, H. J. Lynch, R. J. Wurtman, Melatonin: A Sleep-Promoting Hormone. *Sleep* **20**(10), 899-907 (1997).
61. R. Sharma, P. Sahota, M. M. Thakkar, Melatonin promotes sleep in mice by inhibiting orexin neurons in the perifornical lateral hypothalamus. *J. Pineal Res.* **65**(2), e12498 (2018), doi:10.1111/jpi.12498.
62. N. Gekakis *et al.*, Role of the CLOCK protein in the mammalian circadian mechanism. *Science*. **280**(5369), 1564-1569 (1998), doi:10.1126/science.280.5369.1564.
63. J. B. Hogenesch, Y. Z. Gu, S. Jain, C. A. Bradfield, The basic-helix-loop-helix-PAS orphan MOP3 forms transcriptionally active complexes with circadian and hypoxia factors. *Proc. Natl. Acad. Sci. U. S. A.* **95**(10), 5474-5479 (1998), doi:10.1073/pnas.95.10.5474.
64. E. A. Griffin, D. Staknis, C. J. Weitz, Light-independent role of CRY1 and CRY2 in the mammalian circadian clock. *Science*. **286**(5440), 768-771 (1999), doi:10.1126/science.286.5440.768.
65. A. M. Sangoram *et al.*, Mammalian circadian autoregulatory loop: A timeless ortholog and mPer1 interact and negatively regulate CLOCK-BMAL1-induced transcription. *Neuron* **21**(5), 1101-1113 (1998), doi:10.1016/S0896-6273(00)80627-3.
66. T. Porkka-Heiskanen, Sleep homeostasis. *Curr. Opin. Neurobiol.* **23**(5), 799-805 (2013), doi:10.1016/j.conb.2013.02.010.
67. T. Gallopin *et al.*, The endogenous somnogen adenosine excites a subset of sleep-promoting neurons via A2A receptors in the ventrolateral preoptic nucleus. *Neuroscience*. **134**(4), 1377-1390 (2005).
68. T. Porkka-Heiskanen *et al.*, Adenosine: A mediator of the sleep-inducing effects of prolonged wakefulness. *Science*. **276**(5316), 1265-1268 (1997), doi:10.1126/science.276.5316.1265.
69. T. Porkka-Heiskanen, L. Alanko, A. Kalinchuk, D. Stenberg, Adenosine and sleep. *Sleep Med. Rev.* **6**(4), 321-332 (2002), doi:10.1053/smr.2001.0201.
70. H. P. Landolt, Sleep homeostasis: A role for adenosine in humans? *Biochem. Pharmacol.* **75**(11), 2070-2079 (2008), doi:10.1016/j.bcp.2008.02.024.
71. S. Morairty, D. Rainnie, R. McCarley, R. Greene, Disinhibition of ventrolateral preoptic area sleep-active neurons by adenosine: A new mechanism for sleep promotion. *Neuroscience*. **123**(2), 451-457 (2004), doi:10.1016/j.neuroscience.2003.08.066.

72. M. M. Halassa *et al.*, Astrocytic Modulation of Sleep Homeostasis and Cognitive Consequences of Sleep Loss. *Neuron*. **61**(2), 213-219 (2009), doi:10.1016/j.neuron.2008.11.024.
73. M. G. Frank, Astroglial regulation of sleep homeostasis. *Curr. Opin. Neurobiol.* **23**(5), 812-818 (2013), doi:10.1016/j.conb.2013.02.009.
74. E. Reimund, The free radical flux theory of sleep. *Med. Hypotheses*. **43**(4), 231-233 (1994), doi:10.1016/0306-9877(94)90071-X.
75. V. V. Vyazovskiy, K. D. Harris, Sleep and the single neuron: The role of global slow oscillations in individual cell rest. *Nat. Rev. Neurosci.* **14**(6), 443-451 (2013), doi:10.1038/nrn3494.
76. M. T. Scharf, N. Naidoo, J. E. Zimmerman, A. I. Pack, The energy hypothesis of sleep revisited. *Prog. Neurobiol.* **86**(3), 264-280 (2008), doi:10.1016/j.pneurobio.2008.08.003.
77. J. J. Grubbs, L. E. Lopes, A. M. van der Linden, D. M. Raizen, A salt-induced kinase is required for the metabolic regulation of sleep. *PLOS Biol.* **18**(4), e3000220 (2020), doi:10.1371/journal.pbio.3000220.
78. G. Tononi, C. Cirelli, Sleep and synaptic homeostasis: A hypothesis. *Brain Res. Bull.* **62**(2), 143-150 (2003), doi:10.1016/j.brainresbull.2003.09.004.
79. V. V. Vyazovskiy, C. Cirelli, M. Pfister-Genskow, U. Faraguna, G. Tononi, Molecular and electrophysiological evidence for net synaptic potentiation in wake and depression in sleep. *Nat. Neurosci.* **11**(2), 200-208 (2008), doi:10.1038/nn2035.
80. R. A. Ankeny, The natural history of *Caenorhabditis elegans* research. *Nat. Rev. Genet.* **2**(6), 474-479 (2001).
81. M. A. Félix, C. Braendle, The natural history of *Caenorhabditis elegans*. *Curr. Biol.* **20**(22), R965-R969 (2010), doi:10.1016/j.cub.2010.09.050.
82. S. Brenner, The genetics of *Caenorhabditis elegans*. *Genetics*. **77**(1), 71-94 (1974).
83. B. Goldstein, Sydney Brenner on the genetics of *Caenorhabditis elegans*. *Genetics*. **204**(1), 1-2 (2016), doi:10.1534/genetics.116.194084.
84. Z. F. Altun, D. H. Hall, Introduction. *WormAtlas* (2009), doi:10.3908/wormatlas.1.1.
85. J. E. Sulston, H. R. Horvitz, Post-embryonic cell lineages of the nematode, *Caenorhabditis elegans*. *Dev. Biol.* **56**(1), 110-156 (1977), doi:10.1016/0012-1606(77)90158-0.
86. J. E. Sulston, E. Schierenberg, J. G. White, J. N. Thomson, The embryonic cell lineage of the nematode *Caenorhabditis elegans*. *Dev. Biol.* **100**(1), 64-119 (1983), doi:10.1016/0012-1606(83)90201-4.
87. C. H. Lai, C. Y. Chou, L. Y. Ch'ang, C. S. Liu, W. C. Lin, Identification of novel human genes evolutionarily conserved in *Caenorhabditis elegans* by comparative proteomics. *Genome Res.* **10**(5), 703-713 (2000), doi:10.1101/gr.10.5.703.
88. R. Lints, D. H. Hall, WormAtlas Male Handbook - Neuronal Support Cells - Overview. *WormAtlas* (2005), doi:10.3908/wormatlas.2.9.
89. Z. Altun, D. Hall, Handbook - Nervous System General Description. *WormAtlas*. (2011), doi:10.3908/wormatlas.1.18.
90. M. Leyssen, B. A. Hassan, A fruitfly's guide to keeping the brain wired. *EMBO Rep.* **8**(1), 46-50 (2007), doi:10.1038/sj.embor.7400869.
91. S. Herculano-Houzel, The human brain in numbers: A linearly scaled-up primate brain. *Front. Hum. Neurosci.* **3**, 31 (2009),

- doi:10.3389/neuro.09.031.2009.
92. J. G. White, E. Southgate, J. N. Thomson, S. Brenner, The Structure of the Nervous System of the Nematode *Caenorhabditis elegans*. *Philos. Trans. R. Soc. B Biol. Sci.* **314**, 1–340 (1986).
 93. S. J. Cook *et al.*, Whole-animal connectomes of both *Caenorhabditis elegans* sexes. *Nature*. **571**(7763), 63–71 (2019), doi:10.1038/s41586-019-1352-7.
 94. M. Seung, S., Chklovskii, The *C. elegans* connectome. *connectome* (2011), (available at <http://connectomethebook.com/?portfolio=the-c-elegans-connectome>).
 95. J. Y. Cho, P. W. Sternberg, Multilevel modulation of a sensory motor circuit during *C. elegans* sleep and arousal. *Cell*. **156**(1-2), 249–260 (2014), doi:10.1016/j.cell.2013.11.036.
 96. H. K. DeBardeleben, L. E. Lopes, M. P. Nessel, D. M. Raizen, Stress-induced sleep after exposure to ultraviolet light is promoted by p53 in *caenorhabditis elegans*. *Genetics*. **207**(2), 571–582 (2017), doi:10.1534/genetics.117.300070.
 97. R. D. Nath, E. S. Chow, H. Wang, E. M. Schwarz, P. W. Sternberg, *C. elegans* Stress-Induced Sleep Emerges from the Collective Action of Multiple Neuropeptides. *Curr. Biol.* **26**(18), 2446–2455 (2016), doi:10.1016/j.cub.2016.07.048.
 98. M. D. Nelson *et al.*, FMRFamide-like FLP-13 Neuropeptides Promote Quiescence following Heat Stress in *Caenorhabditis elegans*. *Curr. Biol.* **24**(20), 2406–2410 (2014), doi:10.1016/j.cub.2014.08.037.
 99. S. Skora, F. Mende, M. Zimmer, Energy Scarcity Promotes a Brain-wide Sleep State Modulated by Insulin Signaling in *C. elegans*. *Cell Rep.* **22**(4), 953–966 (2018), doi:10.1016/j.celrep.2017.12.091.
 100. T. Gallagher, Y.-J. You, Falling asleep after a big meal: Neuronal regulation of satiety. *Worm*. **3**, e27938 (2014), doi:10.4161/worm.27938.
 101. M. Hyun *et al.*, Fat Metabolism Regulates Satiety Behavior in *C. elegans*. *Sci. Rep.* **6**, 24841 (2016), doi:10.1038/srep24841.
 102. M. D. Nelson, D. M. Raizen, A sleep state during *C. elegans* development. *Curr. Opin. Neurobiol.* **23**(5), 824–830 (2013), doi:10.1016/j.conb.2013.02.015.
 103. M. Olmedo, M. Merrow, M. Geibel, Sleeping Beauty? Developmental Timing, Sleep, and the Circadian Clock in *Caenorhabditis elegans*. *Adv. Genet.* **97**, 43–80 (2017), doi:10.1016/bs.adgen.2017.05.001.
 104. C. Van Buskirk, P. W. Sternberg, Epidermal growth factor signaling induces behavioral quiescence in *Caenorhabditis elegans*. *Nat. Neurosci.* **10**(10), 1300–1307 (2007), doi:10.1038/nn1981.
 105. J. Konietzka *et al.*, Epidermal Growth Factor Signaling Promotes Sleep through a Combined Series and Parallel Neural Circuit. *Curr. Biol.* **30**(1), 1–16.e13 (2020), doi:10.1016/j.cub.2019.10.048.
 106. Y. Wu, F. Masurat, J. Preis, H. Bringmann, Sleep Counteracts Aging Phenotypes to Survive Starvation-Induced Developmental Arrest in *C. elegans*. *Curr. Biol.* **28**(22), 3610–3624.e8 (2018), doi:10.1016/j.cub.2018.10.009.
 107. M. Jeon, H. F. Gardner, E. A. Miller, J. Deshler, A. E. Rougvie, Similarity of the *C. elegans* developmental timing protein LIN-42 to circadian rhythm proteins. *Science*. **286**(5442), 1141–1146 (1999), doi:10.1126/science.286.5442.1141.
 108. R. N. Singh, J. E. Sulston, Some Observations on Moulting in *Caenorhabditis Elegans*. *Nematologica*. **24**(1), 63–71 (1978), doi:10.1163/187529278X00074.

109. S. Iwanir *et al.*, The Microarchitecture of *C. elegans* Behavior during Lethargus: Homeostatic Bout Dynamics, a Typical Body Posture, and Regulation by a Central Neuron. *Sleep*. **36**(3), 385-395 (2013), doi:10.5665/sleep.2456.
110. M. D. Nelson *et al.*, The neuropeptide NLP-22 regulates a sleep-like state in *Caenorhabditis elegans*. *Nat. Commun.* **4**, 2846 (2013), doi:10.1038/ncomms3846.
111. M. Turek, H. Bringmann, Gene expression changes of *Caenorhabditis elegans* larvae during molting and sleep-like lethargus. *PLoS One*. **9**(11), e113269 (2014), doi:10.1371/journal.pone.0113269.
112. D. M. Raizen *et al.*, Lethargus is a *Caenorhabditis elegans* sleep-like state. *Nature*. **451**(7178), 569–572 (2008), doi:10.1038/nature06535.
113. M. Turek, I. Lewandrowski, H. Bringmann, An AP2 transcription factor is required for a sleep-active neuron to induce sleep-like quiescence in *C. elegans*. *Curr. Biol.* **23**(22), 2215–2223 (2013), doi:10.1016/j.cub.2013.09.028.
114. E. Maluck *et al.*, A wake-active locomotion circuit depolarizes a sleep-active neuron to switch on sleep. *PLOS Biol.* **18**(2), e3000361 (2020) doi:10.1371/journal.pbio.3000361.
115. M. Turek, J. Besseling, J.-P. Spies, S. König, H. Bringmann, Sleep-active neuron specification and sleep induction require FLP-11 neuropeptides to systemically induce sleep. *Elife*. **5**, e12499 (2016), doi:10.7554/eLife.12499.
116. WormAtlas. *Choice Rev. Online* (2008), doi:10.5860/choice.46-0292.
117. L. Fenno, O. Yizhar, K. Deisseroth, The Development and Application of Optogenetics. *Annu. Rev. Neurosci.* **34**, 389-412 (2011), doi:10.1146/annurev-neuro-061010-113817.
118. G. Nagel *et al.*, Channelrhodopsin-1: A light-gated proton channel in green algae. *Science*. **296**(5577), 2395-2398 (2002), doi:10.1126/science.1072068.
119. G. Nagel *et al.*, Channelrhodopsin-2, a directly light-gated cation-selective membrane channel. *Proc. Natl. Acad. Sci. U. S. A.* **100**(24), 13940-13945 (2003), doi:10.1073/pnas.1936192100.
120. X. Han *et al.*, A High-Light Sensitivity Optical Neural Silencer: Development and Application to Optogenetic Control of Non-Human Primate Cortex. *Front. Syst. Neurosci.* **5**, 18 (2011), doi:10.3389/fnsys.2011.00018.
121. S. J. Husson, A. Gottschalk, A. M. Leifer, Optogenetic manipulation of neural activity in *C. elegans*: From synapse to circuits and behaviour. *Biol. Cell*. **105**(6), 235-250 (2013), doi:10.1111/boc.201200069.
122. C. Schmitt, C. Schultheis, S. J. Husson, J. F. Liewald, A. Gottschalk, Specific Expression of Channelrhodopsin-2 in Single Neurons of *Caenorhabditis elegans*. *PLoS One*. **7**(8), e43164 (2012), doi:10.1371/journal.pone.0043164.
123. J. Y. Lin, P. M. Knutsen, A. Muller, D. Kleinfeld, R. Y. Tsien, ReaChR: A red-shifted variant of channelrhodopsin enables deep transcranial optogenetic excitation. *Nat. Neurosci.* **16**(10), 1499-1508 (2013), doi:10.1038/nn.3502.
124. A. Okazaki, Y. Sudo, S. Takagi, Optical silencing of *c. elegans* cells with arch proton pump. *PLoS One*. **7**(5), e35370 (2012), doi:10.1371/journal.pone.0035370.
125. N. F. Trojanowski, D. M. Raizen, Call it Worm Sleep. *Trends Neurosci.* **39**(2), 54-62 (2016), doi:10.1016/j.tins.2015.12.005.
126. J. P. Nguyen *et al.*, Whole-brain calcium imaging with cellular resolution in freely behaving *Caenorhabditis elegans*. *Proc. Natl. Acad. Sci. U. S. A.* **113**(8), e1074-e1081 (2016), doi:10.1073/pnas.1507110112.

127. N. Pokala, Q. Liu, A. Gordus, C. I. Bargmann, Inducible and titratable silencing of *Caenorhabditis elegans* neurons in vivo with histamine-gated chloride channels. *Proc. Natl. Acad. Sci. U. S. A.* **111**(7), 2770-2775 (2014), doi:10.1073/pnas.1400615111.
128. C. Rongo, C. W. Whitfield, A. Rodal, K. Stuart K, J. M. Kaplan, LIN-10 is a shared component of the polarized protein localization pathways in neurons and epithelia. *Cell.* **94**(6), 751-759 (1998), doi:10.1016/S0092-8674(00)81734-1.
129. J. C. Campbell, L. F. Polan-Couillard, I. D. Chin-Sang, W. G. Bendena, NPR-9, a Galanin-Like G-Protein Coupled Receptor, and GLR-1 Regulate Interneuronal Circuitry Underlying Multisensory Integration of Environmental Cues in *Caenorhabditis elegans*. *PLoS Genet.* **12**(5), e1006050 (2016), doi:10.1371/journal.pgen.1006050.
130. A. Bounoutas, Q. Zheng, M. L. Nonet, M. Chalfie, mec-15 encodes an F-box protein required for touch receptor neuron mechanosensation, synapse formation and development. *Genetics.* **183**(2), 607-4SI (2009), doi:10.1534/genetics.109.105726.
131. E. Yemini *et al.*, NeuroPAL: A Neuronal Polychromatic Atlas of Landmarks for Whole-Brain Imaging in *C. elegans*; *bioRxiv*, 676312 (2019), doi:10.1101/676312.
132. S. Nagy, Y. C. Huang, M. J. Alkema, D. Biron, *Caenorhabditis elegans* exhibit a coupling between the defecation motor program and directed locomotion. *Sci. Rep.* **5**, 17174 (2015), doi:10.1038/srep17174.
133. Y. Zheng, P. J. Brockie, J. E. Mellem, D. M. Madsen, A. V. Maricq, Neuronal control of locomotion in *C. elegans* is modified by a dominant mutation in the GLR-1 ionotropic glutamate receptor. *Neuron.* **24**(2), 347-361 (1999), doi:10.1016/S0896-6273(00)80849-1.
134. S. Kato *et al.*, Global Brain Dynamics Embed the Motor Command Sequence of *Caenorhabditis elegans*. *Cell.* **163**(3), 656-669 (2015), doi:10.1016/j.cell.2015.09.034.
135. Invitrogen, Gateway ® Technology A universal technology to clone DNA sequences for functional analysis and expression in multiple systems – User Manual. (2003).
136. T. Wilm, P. Demel, H. U. Koop, H. Schnabel, R. Schnabel, Ballistic transformation of *Caenorhabditis elegans*. *Gene.* **229**, 31–35 (1999), doi:10.1016/s0378-1119(99)00043-8.
137. V. Praitis, E. Casey, D. Collar, J. Austin, Creation of low-copy integrated transgenic lines in *Caenorhabditis elegans*. *Genetics.* **157**(3), 1217–1226 (2001).
138. O. Hobert, Classical genetic methods. *Wormb. Online Rev. C. Elegans Biol.* (2013), doi:10.1895/wormbook.1.1.
139. M. Turek, J. Besseling, H. Bringmann, Agarose Microchambers for Long-term Calcium Imaging of *Caenorhabditis elegans*. *J Vis Exp*, e52742 (2015), doi:10.3791/52742.
140. H. Bringmann, Agarose hydrogel microcompartments for imaging sleep- and wake-like behavior and nervous system development in *Caenorhabditis elegans* larvae. *J. Neurosci. Methods.* **201**(1), 78–88 (2011), doi:10.1016/j.jneumeth.2011.07.013.
141. S. Nagy, D. M. Raizen, D. Biron, Measurements of behavioral quiescence in *Caenorhabditis elegans*. *Methods.* **68**(3), 500–507 (2014), doi:10.1016/j.ymeth.2014.03.009.

142. B. Urmersbach, J. Besseling, J. P. Spies, H. Bringmann, Automated analysis of sleep control via a single neuron active at sleep onset in *C. elegans*. *Genesis*. **54**(4), 212-219 (2016), doi:10.1002/dvg.22924.
143. M. Chalfie, A. C. Hart, C. H. Rankin, M. B. Goodman, Assaying mechanosensation. *WormBook* (2014), doi:10.1895/wormbook.1.172.1.
144. P. J. Brockie, J. E. Mellem, T. Hills, D. M. Madsen, A. V. Maricq, The *C. elegans* glutamate receptor subunit NMR-1 is required for slow NMDA-activated currents that regulate reversal frequency during locomotion. *Neuron*. **31**(4), 617-630 (2001), doi:10.1016/S0896-6273(01)00394-4.
145. M. Chalfie *et al.*, The neural circuit for touch sensitivity in *Caenorhabditis elegans*. *J. Neurosci.* **5**(4), 956-964 (1985), doi:10.1523/JNEUROSCI.05-04-00956.1985.
146. A. L. A. Nichols, T. Eichler, R. Latham, M. Zimmer, A global brain state underlies *C. Elegans* sleep behavior. *Science*. **356**(6344), eaam6851 (2017), doi:10.1126/science.aam6851.
147. C. G. Silva-García *et al.*, Single-copy knock-in loci for defined gene expression in *caenorhabditis elegans*. *G3 Genes, Genomes, Genet.* **9**(7),2195-2198 (2019), doi:10.1534/g3.119.400314.
148. G. Tononi, C. Cirelli, Sleep function and synaptic homeostasis. *Sleep Med. Rev.* **10**(1), 49-62 (2006), doi:10.1016/j.smrv.2005.05.002.
149. G. Tononi, C. Cirelli, Sleep and the Price of Plasticity: From Synaptic and Cellular Homeostasis to Memory Consolidation and Integration. *Neuron*. **81**(1), 12-34 (2014), doi:10.1016/j.neuron.2013.12.025.
150. A. Nere, A. Hashmi, C. Cirelli, G. Tononi, Sleep-dependent synaptic down-selection (I): Modeling the benefits of sleep on memory consolidation and integration. *Front. Neurol.* **4**, 143 (2013), doi:10.3389/fneur.2013.00143.
151. I. Busack, F. Jordan, P. Sapir, H. Bringmann, The OptoGenBox – a device for long-term optogenetics in *C. elegans*. *J. Neurogenet.*, 1–9 (2020), doi:10.1080/01677063.2020.1776709.
152. J. K. Rose, K. R. Kaun, S. H. Chen, C. H. Rankin, GLR-1, a Non-NMDA Glutamate Receptor Homolog, Is Critical for Long-Term Memory in *Caenorhabditis elegans*. *J. Neurosci.* **23**(29), 9595-9599 (2003), doi:10.1523/jneurosci.23-29-09595.2003.
153. C. D. O. Beck, C. H. Rankin, Effects of aging on habituation in the nematode *Caenorhabditis elegans*. *Behav. Processes.* **28**(3), 145-163 (1993), doi:10.1016/0376-6357(93)90088-9.
154. B. Rasch, J. Born, About sleep's role in memory. *Physiol. Rev.* **93**(2), 681-766 (2013), doi:10.1152/physrev.00032.2012.
155. J. J. Collins, C. Huang, S. Hughes, K. Kornfeld, The measurement and analysis of age-related changes in *Caenorhabditis elegans*. *WormBook* (2008), doi:10.1895/wormbook.1.137.1.
156. S. A. Keith, F. R. G. Amrit, R. Ratnappan, A. Ghazi, The *C. elegans* healthspan and stress-resistance assay toolkit. *Methods.* **68**(3), 476-486 (2014), doi:10.1016/j.ymeth.2014.04.003.
157. H. E. H. Park, Y. Jung, S. J. V. Lee, Survival assays using *Caenorhabditis elegans*. *Mol. Cells.* **40**(2), 90-99 (2017), doi:10.14348/molcells.2017.0017.
158. L. Salkoff *et al.*, Potassium channels in *C. elegans*. *WormBook* (2005), doi:10.1895/wormbook.1.42.1.

159. I. Ben Soussia *et al.*, Mutation of a single residue promotes gating of vertebrate and invertebrate two-pore domain potassium channels. *Nat. Commun.* **10**(1), 787 (2019), doi:10.1038/s41467-019-08710-3.
160. S. Redemann *et al.*, Codon adaptation-based control of protein expression in *C. elegans*. *Nat. Methods.* **8**(3), 250-252 (2011), doi:10.1038/nmeth.1565.
161. J. M. Zullo *et al.*, Regulation of lifespan by neural excitation and REST. *Nature.* **574**(7778), 359-364 (2019), doi:10.1038/s41586-019-1647-8.
162. D. E. Lawler *et al.*, Automated analysis of sleep in adult *C. elegans* with closed-loop assessment of state-dependent neural activity. *bioRxiv*, 791764 (2019), doi:10.1101/791764.
163. R. J. Driver, A. L. Lamb, A. J. Wyner, D. M. Raizen, DAF-16/FOXO regulates homeostasis of essential sleep-like behavior during larval transitions in *C. elegans*. *Curr. Biol.* **23**(6), 501-506 (2013), doi:10.1016/j.cub.2013.02.009.
164. D. Witvliet *et al.*, Connectomes across development reveal principles of brain maturation in *C. elegans*. *bioRxiv*, 2020.04.30.066209, doi:10.1101/2020.04.30.066209.
165. J. C. Brewer, A. C. Olson, K. M. Collins, M. R. Koelle, Serotonin and neuropeptides are both released by the HSN command neuron to initiate *C. elegans* egg laying. *PLoS Genet.* **15**(1), e1007896 (2019), doi:10.1371/journal.pgen.1007896.
166. Z. V. Guo, A. C. Hart, S. Ramanathan, Optical interrogation of neural circuits in *Caenorhabditis elegans*. *Nat. Methods.* **6**(12), 891-896 (2009), doi:10.1038/nmeth.1397.
167. S. J. Husson *et al.*, Optogenetic analysis of a nociceptor neuron and network reveals ion channels acting downstream of primary sensors. *Curr. Biol.* **22**(9), 743-752 (2012), doi:10.1016/j.cub.2012.02.066.
168. H. Sasakura, I. Mori, Behavioral plasticity, learning, and memory in *C. elegans*. *Curr. Opin. Neurobiol.* **23**(1), 92-99 (2013), doi:10.1016/j.conb.2012.09.005.
169. R. N. Arey, C. T. Murphy, Conserved regulators of cognitive aging: From worms to humans. *Behav. Brain Res.* **322**, 299-310 (2017), doi:10.1016/j.bbr.2016.06.035.
170. T. Schrödel, R. Prevedel, K. Aumayr, M. Zimmer, A. Vaziri, Brain-wide 3D imaging of neuronal activity in *Caenorhabditis elegans* with sculpted light. *Nat. Methods.* **10**(10), 1013-1020 (2013), doi:10.1038/nmeth.2637.